Danilo Pani *Editor*

Innovative Technologies and Signal Processing in Perinatal Medicine

Volume 2

Springer

Innovative Technologies and Signal Processing in Perinatal Medicine

Danilo Pani
Editor

Innovative Technologies and Signal Processing in Perinatal Medicine

Volume 2

Springer

Editor
Danilo Pani
Department of Electrical and Electronic
Engineering
University of Cagliari
Cagliari, Italy

ISBN 978-3-031-32624-0 ISBN 978-3-031-32625-7 (eBook)
https://doi.org/10.1007/978-3-031-32625-7

This Springer imprint is published by the registered company Springer Nature Switzerland AG
The registered company address is: Gewerbestrasse 11, 6330 Cham, Switzerland

Paper in this product is recyclable.

Foreword

The perinatal period represents the most critical time in our life, where even tiny problems can lead to severe, life-lasting consequences. Indeed, after the "miracle" of conception, the complex pathway leading to the delivery of a healthy baby undergoes continuous threats, whose timely detection and understanding is key to take effective countermeasures. Technological advances and innovations hold the potential to make the difference for both mothers and newborns. I have over 20 years of research experience in biomedical signal analysis, and pregnancy monitoring has always represented one of my leading interests, motivated by the challenges and the relevance of this fascinating research field.

I have known Dr. Danilo Pani of the University of Cagliari for over 10 years, and I have had the pleasure to see him grow as a major scientist fostering technological advances in the field of perinatal monitoring. This is not only because of his important research activities, but also because of his unique ability to connect and bring together leading scientists in the field. Danilo lives and works in one of the most beautiful regions in Italy, Sardinia. To be honest, this may have also played a role in his ability to bring together many international researchers, motivating them to come over and contribute to the first International Summer School on Technologies and Signal Processing in Perinatal Medicine in 2018.

Due to the COVID-19 pandemic, the second edition of this school in 2021 had to be held online. Yet, Danilo was again able to motivate many important contributions from major researchers in the field of perinatology. Moreover, the same as for the first edition of the school, he has made the great effort to collect and integrate all these contributions in this special book, which establishes a solid basis supporting future advances in the field. In line with the spirit of his school, this book can also play an important educational role to form the new generations of young scientists who will advance the field in the future to come.

Indeed, the book covers several aspects in the area of perinatal technology, collecting contributions from major, experienced scientists in the field. The assessment of the fetal and newborn brain development, along with measurements of the fetal cardiac function, are further complemented with a presentation of the state of the art in the assessment of the fetal condition through cardiotocography and fetal

electrocardiography, where information-theoretic principles can provide important avenues and opportunities for the interpretation of the signals.

Technologies for effective neonatal resuscitation are also presented, paving the way for the discussion of ethical and legal aspects related to perinatology. Especially in this field, awareness of these aspects is key for the successful introduction of technological innovations. As a result, the present book not only represents an invaluable reference supporting future technological advances in the field, but it also contributes to guide toward a careful consideration of all the relevant aspects that are crucial for the clinical translation and uptake of technological innovations in perinatology.

Based on the extensive experience of Dr. Pani in this research area, along with the contributions of eminent scientists in the field of perinatology, as also evidenced by their publication track record in highly ranked scientific journals, this book provides a unique presentation of the state of the art in perinatology, and an invaluable tool supporting and motivating future developments in the field. It should definitely be on the desk of both young and experienced scientists developing new technologies and signal processing methods for improving perinatal healthcare.

Biomedical Diagnostics Research Laboratory, Massimo Mischi
Electrical Engineering Department,
Eindhoven University of Technology,
Eindhoven, the Netherlands

Preface

The perinatal period ranges from the third trimester of pregnancy up to one month after birth. It is a critical phase, as some problems arising during this period can affect the entire life of the newborn. Even if this represents a quite broad field from the medical perspective, involving several specializations, for biomedical engineers this is a quite tight research niche characterized by high barriers. From a purely technical perspective, this issue is due to the intrinsic problems with the measurand accessibility and the disproportion between the small fetal signals and the stronger maternal interferences. From a broader bioengineering perspective, this is also due to both the peculiarities of fetal physiopathology, which evolves and changes during gestation, and the lack of knowledge of the underpinnings behind some clinical outcomes, particularly in labor. All these challenges require biomedical engineers to provide support in developing a deep understanding of medical and physiological aspects, and to sharpen signal processing, artificial intelligence, and data mining weapons, in order to conceive innovative solutions for the open issues.

Baring this in mind, in 2018 I ignited a series of educational events, realized thanks to the collaboration and the financial contribution of the Autonomous Region of Sardinia and Sardegna Ricerche, in the wonderful framework of Sardinia, with the aim to present both the fundamentals needed to start moving some steps in the field, and the advanced (applied) techniques. The International Summer School on Technologies and Signal Processing in Perinatal Medicine (TSPPM2018) and then the second edition in 2021 (TSPPM2021) were conceived to create a multidisciplinary environment with both clinical and engineering outlines, for young researchers approaching this research niche or already active in it. This successful event also contributed to establishing a strong network of researchers from all over the world, including world-recognized top scientists and research groups. A first book collecting several book chapters inspired by the lectures presented during the TSPPM2018 was already published by Springer Nature with a positive impact. Following the success of the first volume, *Innovative Technologies and Signal Processing in Perinatal Medicine – Volume 2* covers other important topics presented at TSPPM2021, and more.

Although many excellent books exist in the field of biomedical signal processing, machine learning, medicine, etc., no one expressly targets this specific area in a way that the aforementioned barriers could be reduced, if not destroyed. For this purpose, all the experts and scientists who participated in the production of this unique collection were asked to consider an engineering target, either new to this exciting topic, or with some previous experience, up to really advanced skills. The result is a stimulating reading with a rich bibliography and a clear didactic intention, including medical, legal, and engineering chapters. In particular, the first three chapters are dedicated to the presentation of the gynecologist's, neonatologist's, and coroner's perspective of perinatal medicine, with an inspiring representation of the potentialities and opportunities for technological innovation in the field. A profound chapter on the legal issues associated with medical liability tackles the double-edged sword of technology in medicine, not only in terms of sensible data protection but also in terms of potentialities and criticalities of artificial intelligence and telemedicine systems. Then, three technical chapters cover methods and technologies for fetal monitoring and diagnosis, i.e., non-invasive techniques for neurodevelopment assessment, study of myocardial performance by Doppler ultrasound, and principles and technologies for fetal electrocardiography. A deep dive into the information processing for the solution of specific problems is then presented, with further four chapters dealing with non-linear time-frequency techniques for non-invasive fetal electrocardiography, fundamentals of information theory for the analysis of fetal heart rate variability, its analysis with Gaussian processes, and the estimation of the fetal state by signal processing and machine learning from such signals. In the end, as data availability is an important barrier for producing relevant research in the field, and considering the difficulty in obtaining fetal monitoring data, the closing chapter reviews the most important datasets for fetal electrocardiography, providing some hints also for phonocardiography and cardiotocography.

Starting the International Summer School on Technologies and Signal Processing in Perinatal Medicine series, and collecting the chapters in this second volume, was difficult but I think the result deserved the lavished efforts. I sincerely thank all the authors for their excellent work and for being part of this adventure. It is a great honor for me to present to you the *Innovative Technologies and Signal Processing in Perinatal Medicine book, Volume 2*.

Cagliari, Italy Danilo Pani

Contents

Fetal Growth Monitoring and Issues: The Intrauterine Monitoring of Middle Cerebral Artery and Its Role in Neuronal Development of the Newborn 1
Silvia Visentin, Stefania Carli, Federica Sartor, Ignazio D'Errico, and Erich Cosmi

2020 Guidelines on Neonatal Resuscitation: What Can Be of Interest to an Engineer? 11
Daniele Trevisanuto and Viraraghavan Vadakkencherry Ramaswamy

A Conundrum Waiting for Clinical, Technical, and Medico-Legal Solutions: Looking for the "Perfect Biomarker" of Perinatal Asphyxia ... 21
Alberto Chighine, R. Fratini, E. d'Aloja, and M. Nioi

Medical Liability Issues (and Beyond) Resulting from the Use of New Technologies 31
Massimo Farina and Alessia Palladino

Noninvasive Techniques to Assess the Development of the Fetal Brain and Nervous System 71
Amna Samjeed and Ahsan H. Khandoker

Antepartum Noninvasive Evaluation of Fetal Myocardial Performance from Continuous Doppler Signals and Its Research Potential 97
Ahsan H. Khandoker and Amna Samjeed

Principles of Fetal Electrocardiography 121
Rik Vullings

Modern Signal Processing Tools for Fetal Electrocardiogram Extraction from Single-Channel Transabdominal Maternal Electrocardiogram 149
Pei-Chun Su and Hau-Tieng Wu

Information Theory and Fetal Heart Rate Variability Analysis 171
Massimo W. Rivolta

Fetal Heart Rate Analysis with Gaussian Processes 189
Guanchao Feng, J. Gerald Quirk, Cassandra Heiselman, and Petar M. Djurić

Intrapartum Cardiotocography Feature Detection and Fetal State Estimation Using Signal Processing and Machine Learning 207
Philip A. Warrick

Open Data: Valuable Resources and Opportunities for the Researchers in Fetal Cardiac Monitoring 221
Giulia Baldazzi and Danilo Pani

Index 241

Fetal Growth Monitoring and Issues: The Intrauterine Monitoring of Middle Cerebral Artery and Its Role in Neuronal Development of the Newborn

Silvia Visentin, Stefania Carli, Federica Sartor, Ignazio D'Errico, and Erich Cosmi

1 Fetal Growth Restriction

Fetal growth restriction (FGR) represents a very common pathology of pregnancy in which the fetus, due to maternal, fetal, or placental causes, is unable to fully develop its growth potential. It is a leading cause of perinatal–neonatal morbidity and mortality, and occurs in approximately 1–3% to 10% of pregnancies. Possible perinatal problems include perinatal asphyxia, difficult cardiopulmonary transition after birth, meconium aspiration, and persistent pulmonary hypertension. In addition, FGR infants are at higher risk of immediate postnatal complications, such as hypothermia, hypoglycemia, polycythemia, jaundice, feeding difficulties, necrotizing enterocolitis, and late-onset sepsis [1]. Furthermore, changes in the fetal nutritional environment, prenatal programming, and postnatal catch-up growth in FGR infants lead to long-term adverse consequences such as neurodevelopmental impairment, increased risk of cardiovascular disease, and metabolic syndrome that span over a lifetime [2–4]. Contributing to long-term chronic diseases, perinatal issues continue to be a challenging problem for clinicians despite advances in both obstetric and neonatal care.

Fetal growth restriction can result from multiple causes, such as genetic, epigenetic, environment, hormonal regulation, maternal vascular disorders, and their potential interaction. It represents multiple global health concerns, through infancy, with neurodevelopmental, growth and metabolic issues, to the onset of puberty and

S. Visentin (✉) · S. Carli · F. Sartor · E. Cosmi
Department of Woman's and Child's Health, Obstetrical and Gynecological Clinic, Padova University, Padova, Italy
e-mail: silvia.visentin.1@unipd.it; stefania.carli@studenti.unipd.it; erich.cosmi@unipd.it

I. D'Errico
Neuroradiology Unit, University Hospital, Padova, Italy
e-mail: ignazio.derrico@aopd.veneto.it

D. Pani (ed.), *Innovative Technologies and Signal Processing in Perinatal Medicine*, https://doi.org/10.1007/978-3-031-32625-7_1

later in life, with elevated risks of cardiovascular, metabolic, renal, and neurological diseases [5].

Barker's hypothesis, according to which a condition of undernutrition in utero and during childhood can modify the structure, physiology, and metabolism of the body, has been confirmed in several cohort and geographical studies. The principle that the maternal nutritional, hormonal, and metabolic "environment" can permanently program the structure and physiology of their offspring is now an accepted concept. This is the manifestation of the more general "phenomenon of developmental plasticity," fundamental from an evolutionary point of view, for which the same genotype can rise to several phenotypes with different development morphologies, in response to the different environmental conditions that may occur [6].

The first evidence for the association between developmental plasticity and chronic adult disease came from studies showing that people with coronary artery disease, type 2 diabetes, stroke, or hypertension tended to have low birth weight as a result of either constitutional structure or slowed fetal growth, as well as accelerated weight and body mass index gain early in development [7, 8].

Why should fetal responses to undernutrition in utero lead to the development of hypertension or other disorders? The answer is that, according to the "theory of survival," a blood-sparing phenomenon, such as in the brain or in the heart, would lead to a reduction in other peripheral body parts, such as the kidney or liver [9].

From a pathophysiological point of view, fetal growth restriction is based on placental insufficiency, which is a vascular disorder, due to inadequate trophoblastic invasion of the maternal spiral arteries. Chronic vasoconstriction in the placental district will consequently determine an increase in resistance at the level of the umbilical artery, which will manifest itself as a decrease in the speed of end diastole in the umbilical artery, which in turn can come to cancel itself and, in some cases, have a flow inversion. To protect the noble organs, the fetus therefore tends to centralize the blood circulation toward the heart, the central nervous system, and the adrenal glands, subtracting it from the renal and splanchnic circulation.

If we consider the pulsatility index as

$$(\text{End systolic velocity} - \text{End diastolic velocity})/\text{Average velocity}$$

it is easy to understand how cerebral vasodilatation with an increase in end diastolic velocity therefore leads to a reduction in the pulsatility index of the middle cerebral artery. Monitoring of fetal cardiovascular function with Doppler ultrasound is, indeed, an essential part of the clinical care of such fetuses. The clinical standards for fetal surveillance and timely delivery are the umbilical artery, middle cerebral artery (MCA), and ductus venosus.

The umbilical artery is the most easily sampled fetal vessel and is an expression of the placental function on the fetal side. The parameter commonly used to evaluate fetal velocimetry in the umbilical area is the pulsatility index (PI): normal values in the third trimester are around 0.9 while higher indices are an expression of the "brain-sparing effect" aimed at adjusting the oxygenation of fetal cerebral,

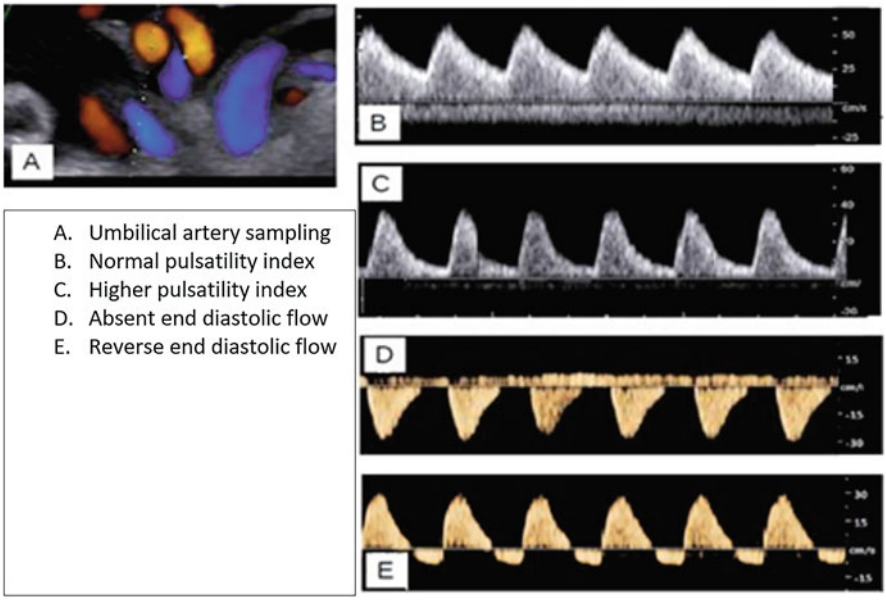

Fig. 1 Different waves in umbilical artery. (Source: SIEOG, Early IUGR, 2018, Editeam). (**a**) Umbilical artery sampling. (**b**) Normal pulsatility index. (**c**) Higher pulsatility index. (**d**) Absent end diastolic flow. (**e**) Reverse end diastolic flow

adrenal, and cardiac tissues in response to the chronic hypoxic stimulus. When the compensation mechanism is exhausted, umbilical velocimetry shows absent end diastolic flow (absent end diastolic flow [AED]) or inverted (reversed end diastolic flow [REDF]) expression of a high risk of prenatal mortality [13]. However, it should be remembered that the velocimetry alterations of the umbilical artery appear only in a late phase of fetal distress and centralization of the circulation [13] (Fig. 1).

The ductus venosus (DV), indeed, is a vessel present during fetal life that connects the intra-abdominal portion of the umbilical vein to the left section of the inferior vena cava, just below the diaphragm. Ultrasonographically, the vessel is identified by visualizing this connection with two-dimensional imaging or in a longitudinal mid-sagittal scan of the fetal trunk or finally in a transverse scan through the upper abdomen. By identifying with the use of color flow mapping the presence of high velocity at the level of the narrow entrance of the DV, it is certain that the vessel has been identified and therefore the correct sampling site to perform Doppler measurements [13]. Waveforms are usually triphasic; however, biphasic waves and nonpulsatile recordings may still be encountered. Velocities are relatively high (between 55 and 90 cm/sec) throughout the second half of pregnancy [13]. It is an expression of the pressure in right atrium, so if we identify the absent or reverse of a wave in ductus venous, it represents a high pressure in the right district of the heart, expression of heart failure (Fig. 2).

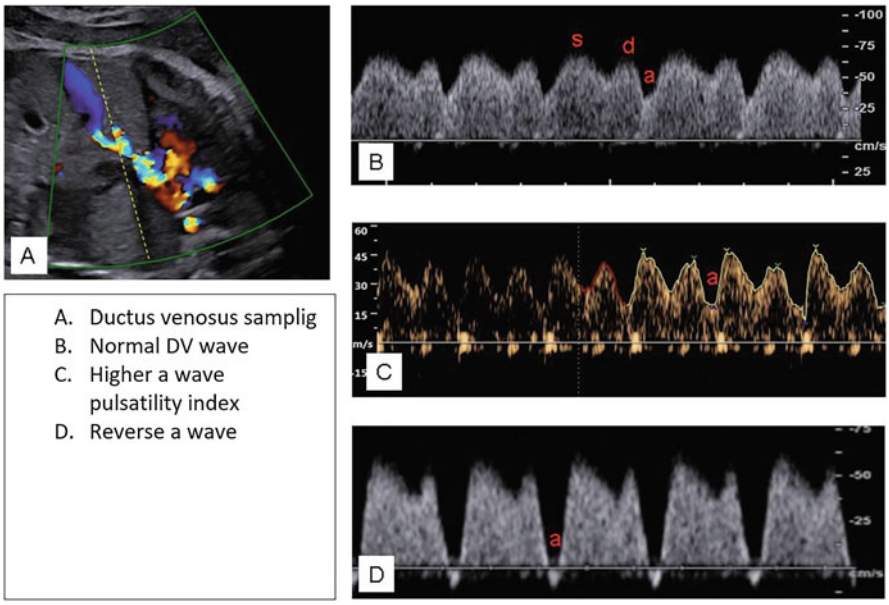

Fig. 2 Different types of DV waves. (Source: Sieog, Early IUGR, 2018, Editeam). (**a**). Ductus venosus samplig. (**b**) Normal DV wave. (**c**) Higher a wave pulsatility index. (**d**) Reverse a wave

In the end, in accordance with International Society of Ultrasound in Obstetrics and Gynecology (ISUOG) guidelines and Italian Society of Ultrasound in Obstetrics and Gynecology (SIEOG) guidelines, the middle cerebral artery (MCA) can be visualized with Doppler technique at the level of the axial scan of the fetal brain, including the thalami and the wings of the sphenoid bone. Sampling of the middle cerebral artery must take place at the level of the proximal third of the vessel, in proximity to the point of origin from the internal carotid artery, as the peak systolic velocity decreases as one moves away from the origin of the vessel. It is also important to avoid excessive pressure on the fetal head, and recording of at least three consecutive flow waves is necessary. The peak systolic velocity corresponds to the fastest velocity among the recorded waves. The normal values of the pulsatility index and peak systolic velocity vary according to the gestational age [13].

All these parameters appear to be very important for obstetric management, and, while the PI DV appears to be fundamental for the obstetric decisions of the early FGR, the PI MCA is instead decisive in the decisions for the management of childbirth after the 32nd week of gestation, in those which are defined as late FGR fetuses.

MCA Doppler, in particular, is considered a surrogate for fetal hypoxemia, and its value in predicting neurological damage in preterm and term FGR is going on [10]. Increased impedance in the umbilical artery and reduced impedance in cerebral blood flow are considered “early” changes of uteroplacental insufficiency. The

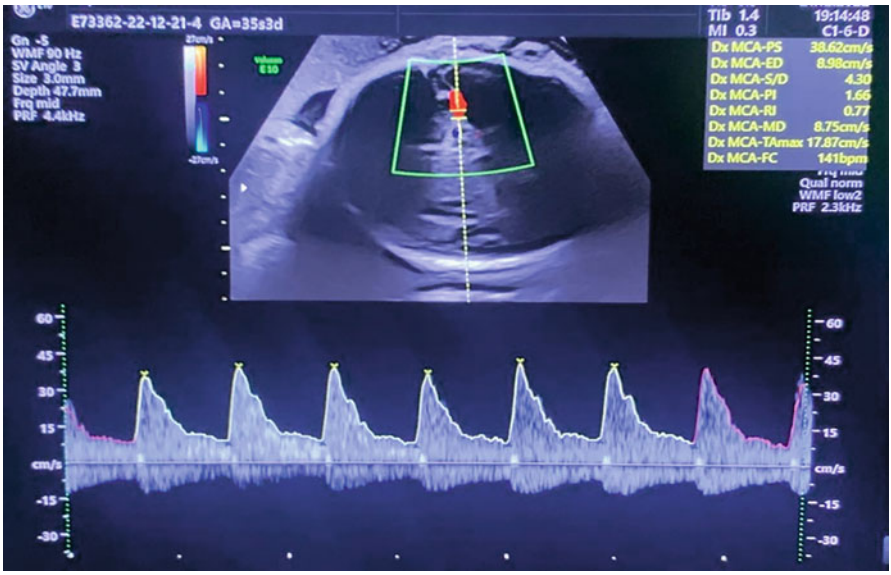

Fig. 3 Example of MCA sampling

cerebral redistribution has traditionally been regarded as a protective autoregulatory mechanism and is referred to as "brain sparing." Animal models demonstrate that hypoxia in the fetus leads to redistribution of blood to the brain, heart, and adrenals [11]. Preferential delivery of nutrients and oxygen to the brain is achieved through vasodilatation of the cerebral vasculature by chemoreceptors and baroreceptors. Fetal hypoxemia is associated with a reduction in the middle cerebral artery pulsatility index [12] (Fig. 3).

2 FGR and Neurodevelopment

Individuals who had FGR experience a range of poorer developmental outcomes, encompassing cognitive, socioemotional, and behavioral domains, compared with individuals who were born appropriate for gestational age [14]. Regarding cognitive outcomes, gold standard measures include IQ, mental quotient, and cognitive developmental quotient, which are all concise indicators of general cognitive functioning. Previous systematic reviews and meta-analyses [15] have investigated the association between FGR and such cognitive outcomes. However, some key issues remain undefined, such as the potential differences between preterm and term-born children who had FGR and between children who had FGR and those who were small for gestational age, a different type of intrauterine restriction fetus. In addition to the known risks of prematurity, chronic hypoxia also contributes to the risk

of ultrasound-detected cranial abnormalities, such as intraventricular hemorrhage and periventricular leukomalacia [16]. These have a strong association with later neurodevelopmental and visual impairments, above all below the 28th gestational week. Moreover, accumulating evidence suggests that cerebral redistribution may be associated with an increased risk of adverse neurodevelopmental outcomes, particularly neonatal motor and state organization, and lower communication and problem-solving scores at 2 years of age. Cerebral redistribution in preterm small fetuses was associated with an increased risk of abnormal psychomotor development at 1 year of age [17].

Doppler studies in FGR fetuses suggest that an increase in frontal lobe perfusion occurs first, detected by changes in the anterior cerebral artery. This is followed by changes in the MCA, which supplies the basal ganglia and influences motor function [18]. MCA Doppler changes correlate with a relative decrease in blood flow to the frontal areas in favor of the basal ganglia [19]. As MCA changes are thought to indicate an advanced stage of brain sparing, it is possible that the impact on cognitive function through abnormal frontal lobe perfusion has already occurred by the time that MCA changes are detected. This redistribution of fetal blood flow in FGR fetuses is also associated with reduced brain volume at term by a three-dimensional approach [20]. It is unknown at what point following cerebral redistribution in FGR fetuses cerebral compromise may lead to a greater risk of neurodevelopmental sequelae.

The result of a recent systematic review showed that, considering term-born FGR children had significantly lower cognitive scores compared with those with appropriate for age, similar to preterm children, underlining the importance of identifying those children at risk of developing cognitive sequelae as early as possible, monitoring their development, and effectively intervening if and when needed to strengthen their cognitive profile are needed [21].

3 Functional Magnetic Resonance Imaging

Human brain development is a finely orchestrated process that relies on the sequential execution of genetic programs, complex cellular interactions, and the formation and resolution of transient organs [22]. The protracted telencephalon maturation and the evolutionary expansion of the neocortex are prerequisites for our intellectual capacity [23], and many highly developed cognitive abilities are linked to features that are unique to humans [24]. In contrast to our knowledge on brain circuit formation and histogenesis from postmortem studies and functional examinations in early childhood [25], to date, we have only a limited understanding of emerging neural activity during human fetal development. The fetal to neonatal period is a critical stage in brain development since rapid neurodevelopmental processes establish key functional neural circuits.

Although myelination mainly occurs postnatally, we were able to demonstrate that functional connections develop first in the occipital and temporal areas at

around the 25th gestational week, whereas the frontal lobe connectivity evolves later.

Fetal magnetic resonance imaging (MRI) is an important diagnostic tool for the assessment of fetal brain development and pathologies. In FGR disease, MRI conventional sequences can demonstrate restricted fetal brain growth, delayed cortical gyration, or focal ischemic or hemorrhagic lesions.

Functional brain networks and microstructural abnormalities are not detectable by conventional MRI sequences but can be identified by functional magnetic resonance imaging (fMRI).

The development of functional magnetic resonance imaging (fMRI) revolutionized the field of cognitive neuroscience. The technique permitted researchers to infer human brain activity at rest or during any given task, detecting changes in cerebral blood flow or the movement of water molecules, and mapping white matter tracts, the large nerve fiber bundles connecting brain regions.

The possibility to use these methods in utero gives an unprecedented look at the developing brain.

Several studies were performed on preterm and term fetuses (from 32 to 140 fetuses, at different gestational age) to deepen this aspect.

Probably, human fetal brain has modular organization and modules overlap functional systems observed postnatally. Age-related differences between younger (<31 gestational weeks) and older (≥31 gestational weeks) fetuses demonstrate that brain modularity decreases, and connectivity of the posterior cingulate to other brain networks becomes more negative, with advancing gestational age. By mimicking functional principles observed postnatally, these results support early emerging capacity for information processing in the human fetal brain [26, 27].

The application of fRMN on FGR fetuses, with or without brain sparing, could permit us to investigate the connection among neurodevelopment dysfunction in later life, vascular distribution, neuronal network, and the cerebral area more involved in the restriction disease [28, 29].

In conclusion, FGR disease represents the leading cause of morbidity and mortality, and a risk factor for adult later disease, as hypertension, diabetes, stroke, and neurological disease.

In utero, the Doppler of the main fetal vessels represents a fundamental technical aid useful for diagnostic purposes and in the management of FGR fetuses. The sampling of the umbilical artery allows for verification of the presence of placental insufficiency and the venous duct in the presence of heart failure in early FGR, also useful for the timing of delivery. Nowadays, MCA sampling is still an evolving field of investigation. From an initial sign of cerebral redistribution, it currently represents one of the reference vessels in the management of late FGR. The correlation between neurodevelopment at 2 years and cerebral vasodilatation, and therefore altered vascularization and secondary damage from cerebral reperfusion, can be investigated by means of investigations such as functional magnetic resonance, in order to “map” the different cerebral territories.

References

1. A. Rosenberg, The IUGR newborn. Semin. Perinatol. **32**(3), 219–224 (2008)
2. S. Longo, L. Bollani, L. Decembrino, et al., Short-term and long-term sequelae in intrauterine growth retardation (IUGR). J. Matern. Fetal Neonatal Med. **26**(3), 222–225 (2013)
3. A.K. Von Beckerath, M. Kollmann, C. Rotky-Fast, et al., Perinatal complications and long-term neurodevelopmental outcome of infants with intrauterine growth restriction. Am. J. Obstet. Gynecol. **208**(2), 130.e1–130.e6 (2013)
4. V. Zanardo, S. Visentin, D. Trevisanuto, et al., Fetal aortic wall thickness: a marker of hypertension in IUGR children? Hypertens. Res. **36**(5), 440–443 (2013)
5. E. Giabicani, A. Pham, F. Brioude, D. Mitanchez, I. Netchine, et al., *Diagnosis and Management of Postnatal Fetal Growth Restriction* (Elsevier, 2018)
6. D.J.P. Barker, The origins of the developmental origins theory. J. Intern. Med. **261**, 412–417.7 (2007)
7. W. Young, J.W. Gofman, R. Tandy, N. Malamud, E.S.G. Waters, The quantification of atherosclerosis, III: the extent of correlation of degrees of atherosclerosis within and between the coronary and cerebral vascular beds. Am. J. Cardiol. **6**, 300–308 (1960)
8. M.I. Chimowitz, E.F. Lafranchise, A.J. Furlan, K. Dorosti, L. Paranadi, G.J. Beck, Evaluation of coexistent carotid and coronary disease in combined angiography. J. Stroke Cerebrovasc. Dis. **1**, 89–93 (1991)
9. M. Hughson et al., Glomerular number and size in autopsy kidneys: the relationship to birthweight. Kidney Int. **63**, 2113–2122 (2003)
10. A.A. Baschat, U. Gembruch, R.M. Viscardi, L. Gortner, C.R. Harman, Antenatal prediction of intraventricular hemorrhage in fetal growth restriction: what is the role of Doppler? Ultrasound Obstet. Gynecol. **19**, 334–339 (2002)
11. B.S. Richardson, A.D. Bocking, Metabolic and circulatory adaptations to chronic hypoxia in the fetus. Comp. Biochem. Physiol. A Mol. Integr. Physiol. **119**, 717–723 (1998)
12. S. Vyas, K.H. Nicolaides, S. Bower, S. Campbell, Middle cerebral artery flow velocity waveforms in fetal hypoxaemia. Br. J. Obstet. Gynaecol. **97**, 797–803 (1990)
13. ISUOG Practice Guidelines (updated), Use of Doppler velocimetry in obstetrics. Ultrasound Obstet. Gynecol. Published online in Wiley Online Library (wileyonlinelibrary.com) (2021). https://doi.org/10.1002/uog.23698
14. Murray E, Fernandes M, Fazel M, Kennedy SH, Villar J, Stein A. Differential effect of intrauterine growth restriction on childhood neurodevelopment: a systematic review. BJOG. 2015;122(8):1062–1072
15. Chen J, Chen P, Bo T, Luo K. Cognitive and behavioral outcomes of intrauterine growth restriction school-age children. Pediatrics. 2016;137(4):e20153868
16. N.F. Padilla-Gomes, G. Enriquez, R. Acosta-Rojas, J. Perapoch, E. Hernandez-Andrade, E. Gratacos, Prevalence of neonatal ultrasound brain lesions in premature infants with and without intrauterine growth restriction. Acta Paediatr. **96**, 1582–1587 (2007)
17. R.K. Morris, R. Say, S.C. Robson, J. Kleijnen, K.S. Khan, Systematic review and meta-analysis of middle cerebral artery Doppler to predict perinatal wellbeing. Eur. J. Obstet. Gynecol. Reprod. Biol. **165**, 141–155 (2012)
18. H. Figueroa-Diesel, E. Hernandez-Andrade, R. Acosta-Rojas, L. Cabero, E. Gratacos, Doppler changes in the main fetal brain arteries at different stages of hemodynamic adaptation in severe intrauterine growth restriction. Ultrasound Obstet. Gynecol. **30**, 297–302 (2007)
19. E. Hernandez-Andrade, H. Figueroa-Diesel, T. Jansson, H. Rangel-Nava, E. Gratacos, Changes in regional fetal cerebral blood flow perfusion in relation to hemodynamic deterioration in severely growth-restricted fetuses. Ultrasound Obstet. Gynecol. **32**, 71–76 (2008)
20. J. Maunu, E. Ekholm, R. Parkkola, P. Palo, H. Rikalainen, H. Lapinleimu, L. Haataja, L. Lehtonen, THE PIPARI STUDY GROUP, Antenatal Doppler measurements and early brain injury in very low birth weight infants. J. Pediatr. **150**, 51–56 (2007)

21. C. Sacchi, C. Marino, C. Nosarti, A. Vieno, S. Visentin, A. Simonelli, Association of Intrauterine Growth Restriction and Small for gestational age status with childhood cognitive outcomes. A systematic review and meta-analysis. JAMA Pediatr. **174**(8), 772–781 (2020)
22. I. Kostovic, M. Judas, The development of the subplate and thalamo- cortical connections in the human foetal brain. Acta Paediatr. **99**, 1119–1127 (2010)
23. T.M. Preuss, The cognitive neuroscience of human uniqueness, in *The Cognitive Neurosciences*, ed. by M.S. Gazzaniga, (MIT Press, Cambridge, MA, 2009), pp. 49–64
24. A.M. Fjell, L.T. Westlye, I. Amlien, C.K. Tamnes, H. Grydeland, A. Engvig, et al., High-expanding cortical regions in human development and evolution are related to higher intellectual abilities. Cereb. Cortex **25**(1), 26–34 (2015)
25. M. Judas, G. Sedmak, I. Kostovic, The significance of the subplate for evolution and developmental plasticity of the human brain. Front. Hum. Neurosci. **7**, 423 (2013)
26. F. Neubert, R. Mars, A. Thomas, J. Sallet, M.S. Rushworth, Comparison of human ventral frontal cortex areas for cognitive control and language with areas in monkey frontal cortex. Neuron **81**, 700–713 (2014)
27. S. Mueller, D. Wang, M.D. Fox, B.T. Yeo, J. Sepulcre, M.R. Sabuncu, et al., Individual variability in functional connectivity architecture of the human brain. Neuron **77**, 586–595 (2013)
28. A. Jakab, E. Schwartz, G. Kasprian, G.M. Gruber, D. Prayer, V. Schöpf, G. Langs, Fetal functional imaging portrays heterogeneous development of emerging human brain networks. Front. Hum. Neurosci. **8**, 852 (2014)
29. M.E. Thomason, J.A. Brown, M.T. Dassanayake, R. Shastri, H.A. Marusak, E. Hernandez-Andrade, L. Yeo, S. Mody, S. Berman, S.S. Hassan, R. Romero, Intrinsic functional brain architecture derived from graph theoretical analysis in the human fetus. PLoS One **9**(5), e94423 (2014)

2020 Guidelines on Neonatal Resuscitation: What Can Be of Interest to an Engineer?

Daniele Trevisanuto and Viraraghavan Vadakkencherry Ramaswamy

1 Introduction

Approximately 5–10% of newborn infants need some assistance (such as neutral positioning, stimulation, airway suctioning) immediately after birth. About 3–5% may need face mask positive pressure ventilation (PPV), and approximately 1% could require PPV through an endotracheal tube. Only a small proportion of neonates (about 0.1%) might require advanced resuscitation such as chest compression and medication [1–3]. In Europe, there were approximately 4.24 million births in 2018. It means that around 4,00,000 neonates might have required stimulation to initiate breathing immediately after birth, about 2,00,000 could have received bag and mask ventilation, and less than 50,000 advanced resuscitation. Intrapartum-related complications such as birth asphyxia account for a quarter of neonatal mortality and are responsible for about 600–700 thousand deaths per year worldwide [4].

In high-resource settings, around 45–50% of infants with moderate or severe hypoxic-ischemic encephalopathy who undergo therapeutic hypothermia either die or have long-term neurodevelopmental impairment [5]. Henceforth, prevention of perinatal asphyxia and management of asphyxiated neonates immediately after birth is crucial to reduce neonatal mortality and prevent long-term neurodevelopmental adverse consequences.

The 1st edition of the Neonatal Resuscitation Program (NRP) Textbook was published 35 years ago and the last edition (8th) in 2021 [6]. The NRP Textbook

D. Trevisanuto (✉)
Department of Woman and Child Health, University Hospital of Padua, Padua, Italy
e-mail: daniele.trevisanuto@unipd.it

V. V. Ramaswamy
Department of Neonatology, Ankura Hospital for Women and Children, Hyderabad, India

D. Pani (ed.), *Innovative Technologies and Signal Processing in Perinatal Medicine*, https://doi.org/10.1007/978-3-031-32625-7_2

is a practical guide based on the American Heart Association (AHA) & American Academic Pediatrics (AAP) Guidelines on Neonatal Resuscitation that have been published every 5 years since 2000 [7].

The European Guidelines on Neonatal Resuscitation have been regularly published by the Neonatal Task Force of the European Resuscitation Council (ERC) [8]. The Guidelines on Neonatal Resuscitation of different countries or continents across the globe are mainly based on the Consensus on Science and Treatment Recommendations (CoSTR) published by the Neonatal Task Force (NTF) of the International Liaison Committee on Resuscitation (ILCOR), which includes a group of expert members on neonatal resuscitation from different countries. The ILCOR NTF does a continuous revision of the latest literature on newborn resuscitation based on a structured approach as suggested by the Grading of Recommendations, Assessment, Development and Evaluation (GRADE) working group [9].

2 Guidelines 2020: Key Points and Knowledge Gaps

Maintaining normothermia soon after birth in preterm infants is one of the key strategies to improve their outcomes as hypothermia at neonatal intensive care unit (NICU) admission has been shown to be associated with an increased risk of mortality and other adverse outcomes such sepsis [10, 11]. A Canadian cohort study showed that there was a U-shaped relationship between temperature at NICU admission and major adverse neonatal outcomes such as mortality, severe neurological injury, severe retinopathy of prematurity, neonatal enterocolitis, and bronchopulmonary dysplasia in very preterm infants [12]. Similar results were reported by Cavallin et al. in preterm and term infants born in a low-resource setting [13]. International guidelines for neonatal resuscitation suggest several interventions to prevent thermal loss at birth in very preterm infants, such as adequate delivery suite room temperature, use of infant warmers, plastic bags or wraps, and preheated mattresses, caps, and heated humidified gases for resuscitation [7, 8]. Despite the implementation of these interventions, a certain proportion of very preterm infants are still hypothermic at the time of NICU admission, suggesting that in addition to these, further interventions are to be researched [14].

Physiologically, there are four mechanisms of heat loss (conduction, convection, radiation, and evaporation), all of which should be taken into consideration while planning any research and development of equipment that could be used for the prevention of hypothermia in neonates immediately after birth [15]. The combination of the aforementioned interventions has been shown to be most effective. However, the weightage of each of these interventions on the final outcome remains unknown [8, 9, 15, 16]. For example, setting the thermal power of the infant warmers differs among the different companies [17]. In addition, a previous study suggests that the use of a servo-controlled system does not improve the incidence of normothermia in neonates at NICU admission [18]. While the quantum of heat output delivered by a servo-controlled warmer would depend upon the neonate's body temperature, the

manual mode delivers 100% heat output irrespective of the neonate's temperature. It is to be noted that frequent unwrapping to measure the temperature would reduce the effectiveness of the plastic bag or wrap. In addition, though the use of a combination of interventions has been shown to be effective in preventing hypothermia, these interventions are also associated with the adverse outcome of hyperthermia [6]. Similar to hypothermia, hyperthermia has also been shown to be associated with adverse outcomes [6]. There remains a gap in knowledge as to how effectively the temperature of the neonate be monitored continuously without unwrapping the plastic bag or wrap till the neonate is stabilized in the delivery room and hence avoid hypothermia or hyperthermia. Research related to continuous monitoring of temperature of neonates wrapped in a plastic bag or a wrap is a potential area of interest.

Identifying a rapid and reliable method to measure the newborn's heart rate is of vital importance during neonatal resuscitation [6–9]. In the past few years, there have been many technological advancements in improving the evaluation of the heart rate during the first minutes of life. Johnson et al. have described 10 modalities (e.g., photoplethysmography, Doppler ultrasound, digital stethoscope, capacitive sensors, piezoelectric transducer sensors, and electrocardiography) for the assessment of heart rate in neonates immediately after birth [19]. Compared to photoplethysmography, other modalities such as electrocardiography (ECG) have been shown to detect heart rate earlier in a neonate immediately after birth [19]. However, it still remains contentious as to which among these approaches is the most effective one. Furthermore, many of these modalities are costly, a major bottleneck in low-resource settings. Hence, cost-effective innovations related to rapid assessment of a newborn's heart rate immediately after birth are encouraged. Finally, some of these such as an ECG might detect heart rate when there is no significant cardiac activity and no peripheral pulse felt, referred to as pulseless electrical activity (PEA) [19]. PEA needs immediate resuscitation, and use of modalities such as ECG might result in delaying the therapy. Though an algorithmic approach might be useful in diagnosing PEA, how to diagnose this entity with ECG alone or that incorporated with other technology is an area that requires further research.

Avoiding both hypoxia and hyperoxia in a newly born infant is of critical importance. Oxygen concentrations provided to neonates at birth are based on saturation targets derived from healthy neonates [6–9]. The fraction of inspired oxygen (FiO_2) that is delivered to a neonate is usually adjusted manually to achieve the target peripheral oxygen saturation levels at various time points after birth. This approach usually is not very efficacious in maintaining the peripheral saturation levels within the desired range. A new technology referred to as closed-loop automated oxygen control system has been shown to be of benefit in NICUs [20]. This technology automatically changes the FiO_2 delivered based on the neonates of the peripheral oxygen saturation. Whether this technology could be implemented in the delivery room is a topic of potential research. In addition to the monitoring of the peripheral oxygen saturation that is recommended, cerebral near-infrared spectroscopy (NIRS) is an emerging technology that might guide oxygen saturation

at tissue level in the brain [21]. Though NIRS might be of huge potential, Vesoulis et al. pointed out the deficiencies of NIRS such as the lack of standardization in device application, methods of recording, and ways to correct artifacts [22]. Addressing these are areas of scientific research that might have a major bearing on the use of NIRS in neonatal resuscitation.

Effective PPV and respiratory support are the most important interventions during neonatal resuscitation and stabilization [6]. PPV may be provided by using a T-piece resuscitator, a self-inflating bag (SIB), or a flow-inflating bag. While a T-piece resuscitator provides the required peak inspiratory pressure (PIP) as desired by the health personnel while providing PPV, the PIP delivered by a SIB can be widely variable [6]. It is to be noted that while the use of high PIP can result in lung injury, low PIP results in under-ventilation and hence ineffective resuscitation. Furthermore, T-piece resuscitator provides adequate positive end expiratory pressure (PEEP), which keeps the lung alveoli open; a SIB even with the use of a PEEP valve may not provide the desired PEEP. A recent ILCOR review and meta-analysis showed that the use of a T-piece resuscitator was more effective in reducing the incidence of bronchopulmonary dysplasia in very preterm infants compared to a self-inflating bag, but the other outcomes evaluated (survival, NICU admission, and pneumothorax) were similar between the two groups [23]. Where the resources are available, the use of a T-piece resuscitator is the preferred modality for administering PPV at birth, but it is important to be aware of the fact that the devices available in the market have varying performances [24]. Clinical implications due to these differences need to be evaluated in future clinical studies [25]. Furthermore, using T-piece resuscitator requires a compressed source of gas and oxygen that are major bottlenecks in low-resource settings. Low-cost devices that could incorporate these into a T-piece resuscitator could have a major impact in low-resource settings and hence is another field where research and development is required.

Interfaces for administering PPV include face mask, laryngeal mask, and endotracheal tube [6–9]. The laryngeal mask might be a more effective interface in providing PPV at birth than the face mask. Furthermore, it has a shorter learning curve and is less invasive compared to an endotracheal tube [26, 27]. The designs and characteristics of laryngeal mask have improved over the past few decades. The third-generation laryngeal mask includes a video camera that improves the ease of its use further [28]. Unfortunately, this model is available only in adult sizes, but there is a great deal of interest in including these advancements in neonatal models as well.

European guidelines recommend supporting spontaneously breathing preterm infants with continuous positive airway pressure (CPAP) of at least 6 cm H_2O via a nasal mask or a nasal prong immediately after birth [29]; however, the most effective interface for administering noninvasive respiratory support in the delivery room still remains unclear (Fig. 1).

Respiratory function monitoring (RFM) is a tool recently introduced in newborn resuscitation. It gives continuous information on ventilation parameters, including inspiratory and expiratory tidal volumes, leakages around the interface, delivered positive end expiratory pressure and peak inspiratory pressure, and the PPV rate

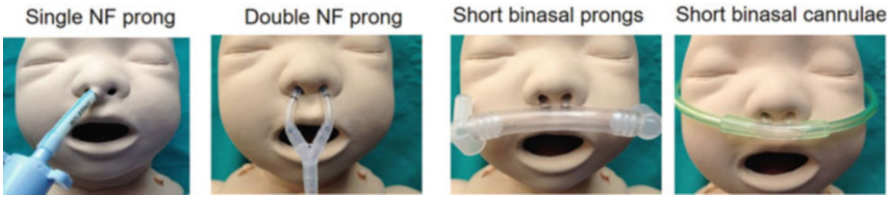

Fig. 1 Different interfaces for administering noninvasive respiratory support at birth

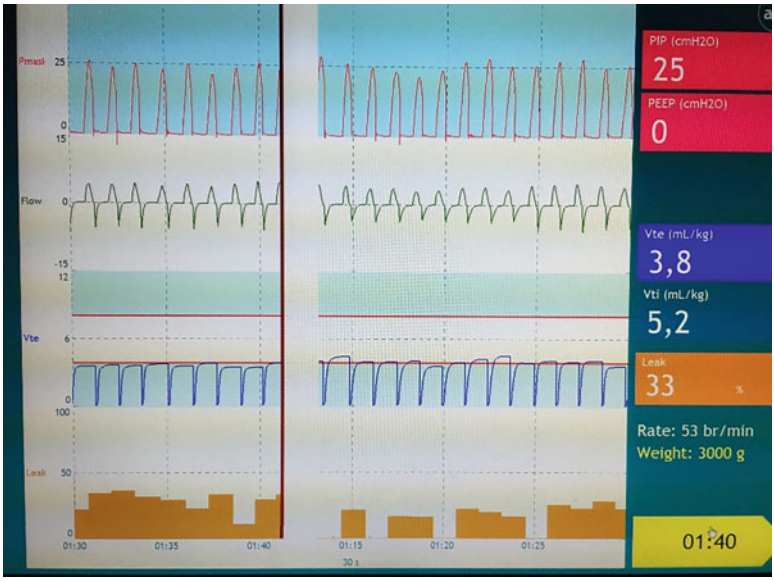

Fig. 2 Information obtained from the respiratory function monitoring

provided by the health personnel (Fig. 2). These data help the healthcare providers to adjust and optimize the effectiveness of PPV. A recent systematic review and meta-analysis showed that the use of an RFM was associated with a significant reduction of any brain injury and intraventricular hemorrhage (all grades) during face mask ventilation of preterm infants at birth [30]. However, there are some aspects that need further research such as ways of displaying data that could be easily interpreted, ideal position of the monitor among the other technologies used during neonatal resuscitation, and types of alarms that could be incorporated into the RFM. Another important aspect is related to developing a cost-effective RFM.

Delayed cord clamping (DCC) (for at least 1 minute) is recommended in preterm and term infants who do not need resuscitation at birth [6–9]. A recent meta-analysis showed that DCC was associated with a reduction in requirement of blood transfusions and mortality compared to immediate cord clamping in preterm infants [31]. Despite the 2020 guidelines on neonatal resuscitation stating that "for term

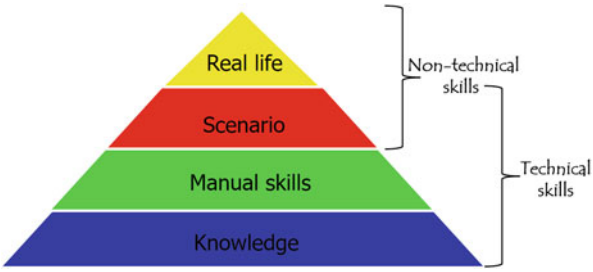

Fig. 3 Pyramid of education on neonatal resuscitation

and preterm infants who require resuscitation at birth, there is insufficient evidence to recommend early cord clamping versus delayed cord clamping," [7] there are ongoing studies aiming to assess the impact of resuscitation at mother's bedside with an intact umbilical cord [32]. For this purpose, innovations related to emergency trolleys that are equipped with sophisticated technologies that could ensure the maintenance of normal temperature, monitoring of oxygen saturation, and heart rate have been developed [32]. This is another promising area of interest for clinical engineers. In addition, a new staff organization with the involvement of all perinatal staff members will be necessary during the procedure [33].

Effective education is crucial for those involved in neonatal resuscitation. Educational programs include training the health personnel in progressive steps of resuscitation, which in turn needs different skills that could be technical as well as nontechnical (Fig. 3). For example, the use of high-fidelity manikins that may provide realistic feedback to the trainees could improve the effectiveness of the educational program [34, 35]. Virtual reality is another emerging technique of simulation that has been recognized as an effective educational tool in training [36, 37]. Finally, the use of the telemedicine that uses sophisticated video cameras might have an enormous potential for training purpose as well as real-time monitoring of neonatal resuscitation in rural areas where additional help of an expert in guiding the healthcare provider is a rarity [38].

3 Conclusions

The past few decades have seen new and sophisticated technologies that have been introduced in the delivery room for resuscitation and monitoring of neonates immediately after birth. The utility and positive impact of some of these innovations on clinical outcomes of neonates have already been confirmed and are included in the armamentarium of neonatologists. Other technologies, though promising, need further evaluation in large clinical trials. A strict collaboration between clinical engineers and healthcare providers in the innovation of other promising technologies may not only improve antenatal, perinatal, and postnatal monitoring and outcomes

of the fetuses/neonates, it would also enhance the technical and nontechnical skills of healthcare staff involved in neonatal resuscitation.

References

1. M.H. Wyckoff, J. Wyllie, K. Aziz, et al., Neonatal Life Support Collaborators, Neonatal life support: 2020 International consensus on cardiopulmonary resuscitation and emergency cardiovascular care science with treatment recommendations. Circulation **142**(16 suppl 1), S185–S221 (2020)
2. J. Madar, C.C. Roehr, S. Ainsworth, H. Ersdal, C. Morley, M. Rüdiger, C. Skåre, T. Szczapa, A. Te Pas, D. Trevisanuto, B. Urlesberger, D. Wilkinson, J.P. Wyllie, European resuscitation council guidelines 2021: newborn resuscitation and support of transition of infants at birth. Resuscitation **161**, 291–326 (2021)
3. J.M. Perlman, R. Risser, Cardiopulmonary resuscitation in the deliveryroom. Associated clinical events. Arch. Pediatr. Adolesc. Med. **149**(1), 20–25 (1995)
4. Levels & Trends in Child Mortality. Report 2020. UNICEF, WHO, World Bank Group. https://www.unicef.org/reports/levels-and-trends-child-mortality-report-2020. Last access 8 Oct 2022
5. E.J. Molloy, M. El-Dib, S.E. Juul, M. Benders, F. Gonzalez, C. Bearer, Y.W. Wu, N.J. Robertson, T. Hurley, A. Branagan, C. Michael Cotten, S. Tan, A. Laptook, T. Austin, K. Mohammad, E. Rogers, K. Luyt, S. Bonifacio, J.S. Soul, A.J. Gunn, Newborn Brain Society Guidelines and Publications Committee, Neuroprotective therapies in the NICU in term infants: present and future. Pediatr. Res. (2022). https://doi.org/10.1038/s41390-022-02295-2. Epub ahead of print
6. American Heart Association and American Academy of Pediatrics, *Textbook of Neonatal Resuscitation*, 8th edn. (2021)
7. K. Aziz, H.C. Lee, M.B. Escobedo, et al., Part 5: neonatal resuscitation: 2020 American Heart Association guidelines for cardiopulmonary resuscitation and emergency cardiovascular care. Circulation **142**(16_suppl_2), S524–S550 (2020)
8. J. Madar, C.C. Roehr, S. Ainsworth, et al., European resuscitation council guidelines 2021: newborn resuscitation and support of transition of infants at birth. Resuscitation **161**, 291–326 (2021)
9. M.H. Wyckoff, J. Wyllie, K. Aziz, et al., Neonatal Life Support Collaborators, Neonatal Life Support 2020 International consensus on cardiopulmonary resuscitation and emergency cardiovascular care science with treatment recommendations. Resuscitation **156**, A156–A187 (2020)
10. D. Trevisanuto, G. Sedin, Thermal homeostasis and clinical management, in *Neonatology. A Practical Approach to Neonatal Diseases*, ed. by G. Buonocore, R. Bracci, M. Weindling, (Springer Ed, 2016)
11. K. Lunze, D.E. Bloom, D.T. Jamison, D.H. Hamer, The global burden of neonatal hypothermia: systematic review of a major challenge for newborn survival. BMC Med. **11**, 24 (2013)
12. Y. Lyu, P.S. Shah, X.Y. Ye, R. Warre, B. Piedboeuf, A. Deshpandey, M. Dunn, S.K. Lee, Canadian Neonatal Network, Association between admission temperature and mortality and major morbidity in preterm infants born at fewer than 33 weeks' gestation. JAMA Pediatr. **169**(4), e150277 (2015)
13. F. Cavallin, S. Calgaro, V. Brugnolaro, O.M. Wingi, A.R. Muhelo, L. Da Dalt, D. Pizzol, G. Putoto, D. Trevisanuto, Non-linear association between admission temperature and neonatal mortality in a low-resource setting. Sci. Rep. **10**(1), 20800 (2020)
14. E. Wilson, R.F. Maier, M. Norman, B. Misselwitz, E.A. Howell, J. Zeitlin, A.K. Bonamy, Effective Perinatal Intensive Care in Europe (EPICE) Research Group, Admission hypothermia in very preterm infants and neonatal mortality and morbidity. J. Pediatr. **175**, 61–67.e4 (2016)

15. D. Trevisanuto, D. Testoni, M.F.B. de Almeida, Maintaining normothermia: why and how? Semin. Fetal Neonatal Med. **23**(5), 333–339 (2018)
16. V.V. Ramaswamy, M.F. de Almeida, J.A. Dawson, D. Trevisanuto, F.L. Nakwa, C.O. Kamlin, S. Hosono, M.H. Wyckoff, H.G. Liley, International Liaison Committee on Resuscitation Neonatal Life Support Task Force, Maintaining normal temperature immediately after birth in late preterm and term infants: a systematic review and meta-analysis. Resuscitation **180**, 81–98 (2022)
17. D. Trevisanuto, I. Coretti, N. Doglioni, A. Udilano, F. Cavallin, V. Zanardo, Effective temperature under radiant infant warmer: does the device make a difference? Resuscitation **82**(6), 720–723 (2011)
18. F. Cavallin, N. Doglioni, A. Allodi, N. Battajon, S. Vedovato, L. Capasso, E. Gitto, N. Laforgia, G. Paviotti, M.G. Capretti, C. Gizzi, P.E. Villani, P. Biban, S. Pratesi, G. Lista, F. Ciralli, M. Soffiati, A. Staffler, E. Baraldi, D. Trevisanuto, Servo COntrol for PReterm Infants (SCOPRI) Trial Group, Thermal management with and without servo-controlled system in preterm infants immediately after birth: a multicentre, randomised controlled study. Arch. Dis. Child. Fetal Neonatal Ed. **106**(6), 572–577 (2021)
19. P.A. Johnson, G.M. Schmölzer, Heart rate assessment during neonatal resuscitation. Healthcare (Basel) **8**(1), 43 (2020). https://doi.org/10.3390/healthcare8010043
20. S. Sturrock, E. Williams, T. Dassios, A. Greenough, Closed loop automated oxygen control in neonates-a review. Acta Paediatr. **109**(5), 914–922 (2020). https://doi.org/10.1111/apa.15089
21. A.A. Garvey, E.M. Dempsey, Applications of near infrared spectroscopy in the neonate. Curr. Opin. Pediatr. **30**(2), 209–215 (2018)
22. Z.A. Vesoulis, J.P. Mintzer, V.Y. Chock, Neonatal NIRS monitoring: recommendations for data capture and review of analytics. J. Perinatol. **41**(4), 675–688 (2021)
23. D. Trevisanuto, C.C. Roehr, P.G. Davis, G.M. Schmölzer, M.H. Wyckoff, H.G. Liley, Y. Rabi, G.M. Weiner, International Liaison Committee on Resuscitation Neonatal Life Support Task Force, Devices for administering ventilation at birth: a systematic review. Pediatrics **148**(1), e2021050174 (2021)
24. M. Hinder, A. McEwan, T. Drevhammer, S. Donaldson, M.B. Tracy, T-piece resuscitators: how do they compare? Arch. Dis. Child. Fetal Neonatal Ed. **104**(2), F122–F127 (2019)
25. S. Donaldsson, T. Drevhammar, L. Taittonen, S. Klemming, B. Jonsson, Initial stabilisation of preterm infants: a new resuscitation system with low imposed work of breathing for use with face mask or nasal prongs. Arch. Dis. Child. Fetal Neonatal Ed. **102**(3), F203–F207 (2017)
26. S.C. Bansal, S. Caoci, E. Dempsey, D. Trevisanuto, C.C. Roehr, The laryngeal mask airway and its use in neonatal resuscitation: a critical review of where we are in 2017/2018. Neonatology **113**(2), 152–161 (2018)
27. N.K. Yamada, C.J. McKinlay, B.H. Quek, G.M. Schmölzer, M.H. Wyckoff, H.G. Liley, Y. Rabi, G.M. Weiner, Supraglottic airways compared with face masks for neonatal resuscitation: a systematic review. Pediatrics **150**, e2022056568 (2022). https://doi.org/10.1542/peds.2022-056568. Epub ahead of print. PMID: 35948789
28. A.A.J. Van Zundert, C.M. Kumar, T.C.R.V. Van Zundert, S.P. Gatt, J.J. Pandit, The case for a 3rd generation supraglottic airway device facilitating direct vision placement. J. Clin. Monit. Comput. **35**(2), 217–224 (2021)
29. D.G. Sweet, V. Carnielli, G. Greisen, M. Hallman, E. Ozek, A. Te Pas, R. Plavka, C.C. Roehr, O.D. Saugstad, U. Simeoni, C.P. Speer, M. Vento, G.H.A. Visser, H.L. Halliday, European consensus guidelines on the management of respiratory distress syndrome - 2019 update. Neonatology **115**(4), 432–450 (2019)
30. S.M. de Medeiros, A. Mangat, G.R. Polglase, G.Z. Sarrato, P.G. Davis, G.M. Schmölzer, Respiratory function monitoring to improve the outcomes following neonatal resuscitation: a systematic review and meta-analysis. Arch. Dis. Child. Fetal Neonatal Ed. **107**(6), 589–596 (2022)
31. H. Rabe, G.M. Gyte, J.L. Diaz-Rossello, L. Duley, Effect of timing of umbilical cord clamping and other strategies to influence placental transfusion at preterm birth on maternal and infant outcomes. Cochrane Database Syst. Rev. **9**, CD003248 (2019)

32. R. Knol, E. Brouwer, T. van den Akker, P.L.J. DeKoninck, E. Lopriore, W. Onland, M.J. Vermeulen, M.E. van den Akker-van Marle, L. van Bodegom-Vos, W.P. de Boode, A.H. van Kaam, I.K.M. Reiss, G.R. Polglase, G.J. Hutten, S.A. Prins, E.E.M. Mulder, C.V. Hulzebos, S.J. van Sambeeck, M.E. van der Putten, I.A. Zonnenberg, S.B. Hooper, A.B. Te Pas, Physiological-based cord clamping in very preterm infants: the Aeration, Breathing, Clamping 3 (ABC3) trial-study protocol for a multicentre randomised controlled trial. Trials **23**(1), 838 (2022)
33. R. Usha Devi, S. Mangalabharathi, V. Prakash, S. Thanigainathan, S. Shobha, Delivery room care and neonatal resuscitation while on intact placental circulation: an open-label, single-arm study. J. Perinatol. **41**(7), 1558–1565 (2021)
34. D.M. Campbell, T. Barozzino, M. Farrugia, M. Sgro, High-fidelity simulation in neonatal resuscitation. Paediatr. Child Health **14**(1), 19–23 (2009)
35. J. Haynes, P. Bjorland, Ø. Gomo, A. Ushakova, S. Rettedal, J. Perlman, H. Ersdal, Novel neonatal simulator provides high-fidelity ventilation training comparable to real-life newborn ventilation. Children (Basel) **8**(10), 940 (2021)
36. S.Y. Yang, Y.H. Oh, The effects of neonatal resuscitation gamification program using immersive virtual reality: a quasi-experimental study. Nurse Educ. Today **117**, 105464 (2022)
37. J. Williams, D. Jones, R. Walker, Consideration of using virtual reality for teaching neonatal resuscitation to midwifery students. Nurse Educ. Pract. **31**, 126–129 (2018)
38. K. McCauley, B.L. Kreofsky, T. Suhr, J.L. Fang, Developing a newborn resuscitation telemedicine program: a follow-up study comparing two technologies. Telemed. J. E Health **26**(5), 589–596 (2020)

A Conundrum Waiting for Clinical, Technical, and Medico-Legal Solutions: Looking for the "Perfect Biomarker" of Perinatal Asphyxia

Alberto Chighine, R. Fratini, E. d'Aloja, and M. Nioi

1 Introduction

Perinatal asphyxia (PA) remains despite important advances happening in the last few decades in the perinatal care, a serious condition that carries still significant mortality and morbidity.

PA is an event that occurs at a frequency of 1–6 for every 1000 live births in countries with high levels of socioeconomic development and at higher rate in less developed ones. Moreover, PA has been shown to be, after preterm birth (28%) and severe infections (26%), the third most common cause of neonatal death (23%). Asphyxial or hypoxic injuries may virtually involve every organ of the body, but hypoxic-ischemic encephalopathy (HIE) is the most investigated clinical condition, due to the occurrence of the most serious sequelae [1]. The HIE has an incidence ranging from 0.5 to 2 every 1000 live births, being a frequent cause of death and severe disability in survivors [2] representing a high personal and social burden for babies, families, and even for hospital and physicians.

From the medical legal point of view, HIE results to be the most common birth injury claim, mainly based on the allegation that a foreseeable intrapartum asphyxial event must be considered responsible for serious long-term neurological sequelae. The average indemnity payment is close to one million dollars, with economic values in Italy up to several million euros. The compensation reaches this high economic settlement due to the need, from a civil law point of view, to restore – from

A. Chighine (✉)
Department of Medical Sciences and Public Health, University of Cagliari, Cittadella Universitaria di Monserrato, Cagliari, Italy
e-mail: alberto.chighine@unica.it

R. Fratini · E. d'Aloja · M. Nioi
Cagliari University, Department of Medical Sciences and Public Health, Cagliari, Italy

D. Pani (ed.), *Innovative Technologies and Signal Processing in Perinatal Medicine*, https://doi.org/10.1007/978-3-031-32625-7_3

the economic side – the loss of all the "normal biological functions" in a newborn who will bear this handicap for his/her entire life [3].

Although not frequent in the neonatal scenario, this issue directly involves most of the health professionals working in the peripartum field, having been one-third of pediatricians and quite all the obstetricians involved in such a claim.

Scientific debate in the courtroom among consultants generally deals with personal opinions about the presence or the absence of early signs of fetal intrapartum hypoxia–ischemia, which – whenever adequately identified, evaluated, and prevented by physicians – could have prevented the lengthening of the fetal hypoxia/anoxia and the resulting cerebral damage [4].

It is well known to all the expert witnesses who are used to testify in court – on both sides, plaintiff or defendant – that the main issue to be addressed in this context is the evidence of the causal relationship between an intrapartum asphyxial event and the neonatal brain damage with a special focus on the timing of injury's onset (see report "Overview of the 2015 American Congress of Obstetricians and Gynaecologists' Survey on Professional Liability"; https://protectpatientsnow.org/wp-content/uploads/2016/02/2015PLSurveyNationalSummary11315.pdf; last access January 2023). This issue could be addressed, and in part solved, by means of good and validated biomarkers, either as damage or outcome ones, of time-related asphyxial phenomena.

The widespread applied criteria proposed by the Task Force convened by the ACOG and the AAP are still insufficient to positively confirm, while being of some help in rejecting, such a relationship (see report "Neonatal encephalopathy and neurologic outcome" available at https://www.acog.org/clinical/clinical-guidance/task-force-report/articles/2014/neonatal-encephalopathy-and-neurologic-outcome, last access January 2023).

The delicate balance between the right of the plaintiff to be compensated for an unjust damage due to a malpractice of the treating physician and the right of the physician to be absolved of a misconduct whenever the damage is not related to his/her behavior needs new tools.

"Omic" sciences seem to have the ability to give an in-depth representation of biological phenomena leading from a healthy and normal fetal brain to a damaged and not fully functional newborn brain, so as to depict peculiar biological features useful to discriminate between "inner" causes of damage from the "outer" ones, clearly related to the medical misconduct.

Clinicians are eager to have among their paraphernalia an easy tool – something that may be employed at bedside, possibly giving an on-off answer – to unravel the complexity of metabolic network in asphyxia. But up to now, this issue is better addressed by a multibiomarker approach. The combination of different parameters, each one able to explain a single aspect of the complex picture of all the clinical and humoral modifications, on the same biofluid or from different biological sources (such as blood, CSF, and urine) may help the physician to piece together the metabolic pathways that have been, simultaneously or continuously, activated or deactivated as a direct or indirect consequence of the abrupt shortage of oxygen.

This overall view may pave the path not only to the identification of markers of damage and/or of outcome, but even to the creation of new protective pharmaceutical means to reduce or eliminate the evolution of neurological damage from transient to permanent.

A multibiomarker diagnostic panel may result in an effective and sensitive tool to assess brain injury and increase diagnostic accuracy [5]. In this perspective, nervous cell–specific markers (e.g., GFAP, S100B, VEGF for astrocyte and microglia; NSE, UCHLI, BDNF, Activin A for neuron; MBP for myelin sheath, and MAP2 for dendrites) are already available to clearly identify the nervous component (single type of cells and/or structure of central nervous system) eventually damaged by hypoxia–ischemia, and the analysis of these markers released by suffering cells into the blood, singularly or as a whole, may help to unravel the phenomenon, giving a unified picture of this composite. It is clear that these serum protein markers could be helpful only to confirm the existence of a CNS damage and to let hypothesize its extension, with a very limited – if null – value in prediction and primary prevention of damage.

2 The Genetics/Genomics Perspective

First among the "omics sciences," both from a physiological and chronological point of view, is genomics and, even if not properly an "-omic" science, genetics.

In the last years, a growing body of evidence has underlined that a large number of individuals with cerebral palsy have potentially clinically relevant genomic findings. This awareness generated a sound discussion concerning the issue of whether the clinical diagnosis of cerebral palsy should be revised in light of genetic findings. The term cerebral palsy may be defined as agnostic compared with underlying etiology. There are many known and, ever more, unknown genetic and environmental risk factors and causal pathways that may be responsible or may influence in a positive or negative way the clinical outcome of a hypoxic-ischemic insult to the neonatal brain. As previously stated, current data suggest that well-defined severe acute intrapartum hypoxia using international criteria may account for only a minority of cases of cerebral palsy in high-income countries. Accumulating evidence shows that a potential genetic etiology can be identified in between 10% and 30% of individuals with cerebral palsy because of both de novo and inherited genetic variants, more commonly among children without recognized environmental risk factors. Some of these identified genetic variants, such as TUBA1A and L1CAM, have been found in genes that have been previously implicated in several neurodevelopmental disorders [6]. This evidence, although not to be considered as a unique causative *noxa*, has raised clinical questions as to whether these individuals, after a confirmatory molecular diagnosis of a genetic "mutation," has to be still classified from a nosographic point of view, affected by cerebral palsy [7]. These questions, devoid of an actual clinical and medical interest, have a relevant importance in a medico-legal context. If an alternative, and well-

documented, cause of newborn cerebral damage may be identified in a claim, the preponderance of evidence – mainly applied in several civil law systems (as in the Italian one) – may be in favor of the defendant, suggesting in the developing of the disease a predominant role of the genetic heritage more than that of medical conduct.

Recent studies have implicated several other genetic factors as contributors or causes of CP, including single-nucleotide variants/polymorphisms (SNVs/SNPs) and copy number variants (CNVs). In these studies, recurrent likely pathogenic CNVs were identified, such as a 2p25.3 and 22q11.2 deletions, duplications, and even Xp monosomy. All these analyses share common limitations mainly characterized by the small sample sizes – due to the relative rarity of this clinical entity – the lack of robust statistical methods, and the paucity of well-matched controls. An international collaborative publication [8] addressed several of these limitations, reporting the largest trio-based cohort to date using a rigorously statistical approach supported by mechanistic and biological validations. Models obtained so far showed a capacity to predict between 27 and 124 genes likely contribute to CP through a de novo mechanism. Although the increased number of trios that underwent the genetic analysis, the cohort has still to be considered limited and an exponential rise of contributing genes is expected with the ongoing number of trios sequenced.

Despite the considerable advances made in this field, the relative contribution of both environmental and genetic causal factors remains unclear and undetermined. It has been hypothesized that different mutations in the same gene may lead to either degenerative or developmental phenotypes, reflecting different effects on cellular biology [9], but no clear relationship between these mutations and cerebral palsy has been so far identified. A common genetic backbone shared by different neurological entities may be foreseen but, due to the partial overlapping of clinical presentations and genetic heritage, its diagnostic value in a sound differential diagnosis is still far to come.

Genomics, or to better say a sound genetic analysis, may become in a near future an irreplaceable approach in the classification of perinatal asphyxia, being able to discriminate sound events related to exogenous causes – including professional ones – from events mainly ascribable to an endogenous *noxa* in which the final effect on newborn health may not be avoided, whatever the professional conduct was.

If so, genomics and genetic markers even if they will never be able to be predictive neither of damage nor of outcome, weakening their potential use in perinatal routine, may find an intriguing role in the medico-legal context.

3 Proteomics

Proteomics seem to be among all the “omics” sciences the less promising in this scenario due to the nature of its biological substrate, which is mainly represented by constitutive proteins of the newborn brain. If so, the biological specimen may be

collected only postmortem or in the few cases in which a brain biopsy is needed for clinical or diagnostic purposes. So far, the application of the proteomics approach to the perinatal asphyxia has been limited to animal models, and more focused on the investigation of post-insult modification and mechanisms of damage than on its diagnostic/prognostic value.

Using a proteomic approach to identify proteins involved in the formation of hypoxic-ischemic brain injuries could provide insight into the potential mechanisms of neuronal dysfunction and apoptosis associated with the insult while few or no information may be gained so as to address the causes of damage or the outcomes of the pathological picture.

To identify the proteins involved in the mechanisms of hypoxic-ischemic brain injury, some authors chose two-dimensional difference gel electrophoresis (2D-DIGE) as the preferred analytical method. This approach enables a global comparison of proteins of healthy tissue against those from hypoxic-ischemic tissue of rat brains on the same gel. Using a global 2D-DIGE analysis, essential proteins affected by perinatal HI were identified. Among the regulated proteins, calcineurin A, coronin-1A, and GFAP are involved in the most detrimental processes following HI, for example, apoptosis and inflammation, suggesting a potential key regulator role in the onset and in the development of perinatal HI [10]. If genetics/genomics have gained space in the comprehension of individual substrate in damaging mechanism, proteomics is still one step backward. Even if pathological changes have been described (such as the ones here reported), their clinical use is still limited to brain cadaveric samples and these markers seem not suitable for clinical purposes.

In a recent systematic review, a wide list of proteins is detectable in CSF as a consequence of an asphyxial insult. All these proteins are related to noninflammatory pathways activated as an adaptive response of the newborn brain or as a direct manifestation of the permanent damage to nervous structures, lying in three major categories (namely, cell adhesion and proliferation, oxidants and antioxidants, and cell damage). Starting from a very large number of putative biomarkers, authors ended with a few promising biomarkers (creatine kinase, xanthine oxidase, vascular endothelial growth factor, and neuron-specific enolase, superoxide dismutase, and malondialdehyde), which are mainly related to the degree of damage more than to its mechanism or to differential diagnosis (often failing to discriminate between damage and normal individuals) [11].

As stated before, in a wider meaning of the term proteomics, the identification and quantification of cerebral-related proteins in circulating biofluids (mainly cerebrospinal fluid and blood) may be an indirect sign of damage to specific cells and structure of the newborn brain. Whenever the comparison of identified proteins has been extended among different groups – such as normal control versus asphyxiated newborn, Sarnat II vs. Sarnat III newborn, newborn survived to asphyxia vs. dead one, and so on – the result showed a low level of reproducibility, sensibility, and accuracy. Although very interesting as investigative tools, all the aforementioned protein markers failed to show a diagnostic capacity in the clinical routine.

4 Transcriptomic

Micro-RNA analysis and metabolomics seem to be up to now the two more promising approaches. In the last few years, microRNAs (miRNAs) have become of interest to many researchers due to their important role in post-transcriptional control and deep evolutionary history. miRNAs are evolutionarily preserved short non-coding RNA molecules made up of 19–22 nucleotides that are involved in the regulation of gene expression [12]. In the CNS, miRNAs have been known to influence varying stages of neurodevelopment, including cell differentiation, proliferation, and synaptogenesis [13].

Despite this, the role of miRNAs in newborns with HIE remains largely unknown due to limited research in this field, being mainly focused on a class of them known as hypoxamiRs (such as miR-21, -210, -335, -137, and -376c) [14]. These miRNAs are involved in the biological response to hypoxia, modulating individual cellular response to lowering level of oxygen. For this reason, being a common pathway in the adaptation to decreasing level of available oxygen at a cellular level, they are involved in a physiological response common to several clinical conditions (ranging from cardiac ischemia to cancer up to perinatal asphyxia), not owning the requested feature to be brain specific. Moreover, miRNAs can not only be present within cells but can also circulate freely extracellularly within exosomes and act on other distant cells [15].

Their preeminent role in the regulation of physiological response to hypoxia and the ability to pass the blood–brain barrier, due to their small size, make them suitable as promising therapeutical agents so as to modulate the pathological response to hypoxic insult.

However, the role of miRNAs in newborns with HIE still remains largely unknown. One of the main limitations is that the newborn brain is still developing, and it may be very likely that the expression of several miRNAs in a neonate's brain may be the expression of a normal developmental phenomenon more than a direct consequence of pathological condition such as HIE. Moreover, miRNA expression may rapidly change with temporal and spatial differences related to developmental stages, anatomical areas of the CNS, and functional activities [16]. Therefore, miRNAs can be expressed differently in neuronal precursors and stem cells through their various stages of differentiation up to mature neurons [17]. Finally, they can have dual effects due to their presence in one cell type to suppress expression and to their absence in another cell at a different time point, allowing a genetic expression.

An atlas of miRNAs involved in normal brain development is available [18]. The investigation of miRNA in the context of PA has shown up- and downregulation of blood miRNAs, especially the ones specific to the mechanism of cellular death and of neuroinflammation.

To date, there are only a few published studies studying the expression of miRNA in human neonatal HIE [19].

Looney and colleagues have shown that miR-374a is downregulated in the umbilical cord blood of infants with HIE and suggested a possible pathway for miR-

374a, involving activin-A through its receptor AVCR2B [20]. Subsequently, Wang and colleagues have also selectively studied miR-210 and miR-374a in umbilical cord blood and shown their combined potential role as a biomarker for severity and prognosis of HIE [21]. A study on maternal blood has shown miR-20b and miR-21 to be related to fetal hypoxia during labor [22]. The additional studies vary from in vivo rat and piglet animal models to cell cultures under various hypoxic-ischemic conditions. None of the above studies have highlighted any specific miRNA as a highly reliable and reproducible biomarker or a therapeutic target in HIE in neonates [18].

The investigation of miRNA in the context of PA has shown up−/downregulation of blood miRNA. Interestingly, miRNAs are specific to the mechanism of cellular death and of neuroinflammation. In the last few years, a growing interest in miRNA-374a and miR-210 has been shown by two of the more active research groups in this field. In Garberg et al., the authors have tried to characterize the temporal expression of selected circulating miRNAs in a clinically relevant piglet model of neonatal HI. A total of 13 anesthetized newborn piglets were randomized into a control group and a transient global HI group, the latter achieved by ventilation with 8% oxygen until the occurrence of severe acidosis and/or hypotension. Blood samples were withdrawn at predetermined time points, and on this specimen, the expression of miRNAs was measured. miR-374a and miRNA 210 rapidly increased (in the first 30 minutes) during HI and went back to baseline values in a 10 h time window. The authors stated that miR-374a and miR-210 are important regulators in their animal model of neonatal HI and could be used as biomarkers in this context, having also shown a correlation to increased serum lactate and cerebral damage [23].

For the first time in a proposed biomarker context, these results were partially confirmed in an exploratory setting of human beings by Murray et al., showing a good correlation of increased level of miR374-a with HIE, although with an opposite trend if compared with the animal model (downregulated) [24]. To further validate these results, Murray investigated a larger group of neonates (validation cohort), confirming the results obtained within the discovery cohort [25].

Due to their clear and well-defined – although not always organ-specific – functional activities, some of the miRNAs, either circulating or tissue-specific, may find a role in the diagnosis of perinatal hypoxia both as damage and outcome markers. Collaborative studies and a very strict design of experiment are needed before implementing this tool into the clinical activities.

5 Metabolomics

Metabolomics, by the analysis of the end products of the entire metabolic network of the individual, may be of some help in gaining a wide spectrum of information from individual profiles. In the last few years, much attention has been devoted to the use of metabolomics for the simultaneous identification and quantification of low-molecular-weight metabolites present in a biological fluid or tissue and for

monitoring the modifications induced by a pathological condition [26, 27]. For this reason, a polymorphic syndrome such as PA represents a perfect candidate to be investigated by this approach. One of the major advantages offered by this technique is the ability of metabolomics to describe a biological phenomenon through the concurrent movement of a plenitude of metabolites that are the final products of the response of a living organism to a well-defined noxa, such as hypoxia. Moreover, the dynamic representation of the alterations of individual metabolomics profiles may help address several clinical aspects, such as early PA diagnosis, differentiation of PA versus HIE, response to pharmacological or TH treatments, and, possibly, the prediction of early and late neurodevelopmental outcomes.

Metabolomics studies based on the use of different analytical platforms (nuclear magnetic resonance spectroscopy and mass spectrometry coupled with gas- or liquid-chromatography) have been performed to investigate PA in both animal models and humans.

These metabolomics studies were mainly performed on several animal models [28] due to the very low incidence of this disease and ethical reasons, although some studies on human newborns have been performed [2]. Each biological matrix gives a different snapshot of the metabolic status of the individual under study; blood – both cord and newborn ones – and CSF metabolomic modifications provide real-time monitoring of the acute hypoxic condition, while urinary modifications are delayed and depend on the renal function and the individual clearance of the metabolites. Nonetheless, urine is the only biofluid that can be safely (and ethically) withdrawn in human newborns [29, 30]. To better compare results coming from these approaches, several reviews have been so far published and readers are referred to them [31–34].

Once a metabolomic profile or a set of specific biomarkers will be validated, future clinical implications could be the development of appropriate kits for the metabolomic analysis of newborn biofluids to be used at the bedside for early diagnosis and outcome prediction. Among the latter, the possibility in the field of neonatology to use urinary samples to monitor the time-related modifications of a metabolomic profile may guarantee an early and noninvasive harvesting of biofluids (first post-birth urine), a precocious insight into the severity of the hypoxic insult and into the possible outcome, and a snapshot of metabolic modifications prior, during, and after the therapeutical hypothermia.

With the advent of “omics” techniques, the main interest of both biological and clinical research has rapidly moved from the “ideal biomarker” of damage/outcome to a biological signature/ phenotype related to the injury’s biological network. Although the chase of a set of biomarkers or of a metabolomics phenotype seems to be promising, the goal is still “elusive” [35, 36]. Nowadays a holistic approach to this clinical conundrum seems the best and the only choice to unravel the complexity of the biological cascade blooming from the original noxa.

As a matter of fact, the huge amount of genomics, transcriptomics, and metabolomics data so far published has not been able to generate a validated profile or a set of biomarkers to be implemented in everyday clinical routine.

As previously stated by our group, as the promising and intriguing results stemming from “omics” research in perinatal asphyxia show, the need for the right

profile, from the right biological samples, at the right time, and in the right patient, is still under scrutiny [28].

References

1. R. Antonucci, A. Porcella, M.D. Pilloni, Perinatal asphyxia in the term newborn. J. Pediatr. Neonatal Individualized Med. (JPNIM) **3**, e030269 (2014)
2. E. Locci, A. Noto, M. Puddu, et al., A longitudinal 1H-NMR metabolomics analysis of urine from newborns with hypoxic-ischemic encephalopathy undergoing hypothermia therapy. Clinical and medical legal insights. PLoS One **13**, e0194267 (2018)
3. S.M. Donn, M.L. Chiswick, J.M. Fanaroff, Medico-legal implications of hypoxic-ischemic birth injury. Semin. Fetal Neonatal Med. **19**, 317–321 (2014)
4. S.M. Donn, G.N. McAbee, *Medicolegal Issues in Paediatrics*, 7th edn. (AAP, Illinois, 2012), pp. 58–59
5. E.M. Graham, I. Burd, A.D. Everett, et al., Blood biomarkers for evaluation of perinatal encephalopathy. Front. Pharmacol. **7**, 196 (2016)
6. G. McMichael, M.N. Bainbridge, E. Haan, et al., Whole-exome sequencing points to considerable genetic heterogeneity of cerebral palsy. Mol. Psychiatry **20**, 176–182 (2015)
7. A.H. MacLennan, S. Lewis, A. Moreno-De-Luca, et al., Genetic or other causation should not change the clinical diagnosis of cerebral palsy. J. Child Neurol. **34**, 472–476 (2019)
8. S.C. Jin, S.A. Lewis, S. Bakhtiari, et al., Mutations disrupting neuritogenesis genes confer risk for cerebral palsy. Nat. Genet. **52**, 1046–1056 (2020)
9. S.A. Lewis, S. Shetty, B.A. Wilson, et al., Insights from genetic studies of cerebral palsy. Front. Neurol. **11**, 625428 (2021)
10. K. Rosenkranz, C. May, C. Meier, et al., Proteomic analysis of alterations induced by perinatal hypoxic−ischemic brain injury. J. Proteome Res. **11**, 5794–5803 (2012)
11. Z. Shi, K. Luo, S. Deol, et al., A systematic review of noninflammatory cerebrospinal fluid biomarkers for clinical outcome in neonates with perinatal hypoxic brain injury that could be biologically significant. J. Neurosci. Res. **100**, 2154–2173 (2022)
12. D.P. Bartel, MicroRNAs: target recognition and regulatory functions. Cell **136**, 215–233 (2009)
13. D. Motti, J.L. Bixby, V.P. Lemmon, MicroRNAs and neuronal development. Semin. Fetal Neonatal Med. **17**, 347–352 (2012)
14. E.S. Peeples, MicroRNA therapeutic targets in neonatal hypoxic-ischemic brain injury: a narrative review. Pediatr. Res. (2022). https://doi.org/10.1038/s41390-022-02196-4
15. M. Fabbri, TLRs as miRNA receptors. Cancer Res. **72**, 6333–6337 (2012)
16. B. Ason, D.K. Darnell, B. Wittbrodt, et al., Differences in vertebrate microRNA expression. Proc. Natl. Acad. Sci. U. S. A. **103**, 14385–14389 (2006)
17. M. Kapsimali, W.P. Kloosterman, E. de Bruijn, et al., MicroRNAs show a wide diversity of expression profiles in the developing and mature central nervous system. Genome Biol. **8**, R173 (2007)
18. V. Ponnusamy, P.K. Yip, The role of microRNAs in newborn brain development and hypoxic ischaemic encephalopathy. Neuropharmacology **149**, 55–65 (2019)
19. V. Ponnusamy, O. Kapellou, E. Yip, et al., A study of microRNAs from dried blood spots in newborns after perinatal asphyxia: a simple and feasible biosampling method. Pediatr. Res. **79**, 799–805 (2016)
20. A.M. Looney, C.E. Ahearne, B. Hallberg, et al., Downstream mRNA target analysis in neonatal hypoxic-ischaemic encephalopathy identifies novel marker of severe injury: a proof of concept paper. Mol. Neurobiol. **54**, 8420–8428 (2017)

21. Z. Wang, Y. Liu, M. Shao, et al., Combined prediction of miR-210 and miR-374a for severity and prognosis of hypoxic-ischemic encephalopathy. Brain Behav. **8**, e00835 (2017)
22. C.L. Whitehead, W.T. Teh, S.P. Walker, et al., Circulating MicroRNAs in maternal blood as potential biomarkers for fetal hypoxia in-utero. PLoS One **8**, e78487 (2013)
23. H.T. Garberg, M.U. Huun, L.O. Baumbusch, et al., Temporal profile of circulating microRNAs after global hypoxia-ischemia in newborn piglets. Neonatology **111**, 133–139 (2017)
24. A.M. Looney, B.H. Walsh, G. Moloney, et al., Downregulation of umbilical cord blood levels of miR-374a in neonatal hypoxic ischemic encephalopathy. J. Pediatr. **167**, 269–73.e2 (2015)
25. M.P. O'Sullivan, A.M. Looney, G.M. Moloney, et al., Validation of altered umbilical cord blood MicroRNA expression in neonatal hypoxic-ischemic encephalopathy. JAMA Neurol. **76**, 333–341 (2019)
26. E. Locci, M. Stocchero, R. Gottardo, et al., Comparative use of aqueous humour ^{1}H NMR metabolomics and potassium concentration for PMI estimation in an animal model. Int. J. Legal Med. **135**, 845–852 (2021)
27. E. Locci, A. Chighine, A. Noto, et al., Metabolomics improves the histopathological diagnosis of asphyxial deaths: an animal proof-of-concept model. Sci. Rep. **11**, 10102 (2021)
28. E. Locci, G. Bazzano, R. Demontis, et al., Exploring perinatal asphyxia by metabolomics. Meta **10**, 141 (2020)
29. J.D. Piñeiro-Ramos, M.M. Cascant, A. Núñez-Ramiro, et al., Noninvasive monitoring of evolving urinary metabolic patterns in neonatal encephalopathy. Pediatr. Res. **91**, 598–605 (2022)
30. E. Valerio, V. Mardegan, M. Stocchero, et al., Urinary metabotypes of newborns with perinatal asphyxia undergoing therapeutic hypothermia. PLoS One **17**, e0273175 (2022)
31. C. Fattuoni, F. Palmas, A. Noto, et al., Perinatal asphyxia: a review from a metabolomics perspective. Molecules **20**, 7000–7016 (2015)
32. M.J. Debuf, K. Carkeek, F. Piersigilli, A metabolomic approach in search of neurobiomarkers of perinatal asphyxia: a review of the current literature. Front. Pediatr. **9**, 674585 (2021)
33. N.M. Denihan, J.A. Kirwan, B.H. Walsh, et al., Untargeted metabolomic analysis and pathway discovery in perinatal asphyxia and hypoxic-ischaemic encephalopathy. J. Cereb. Blood Flow Metab. **39**, 147–162 (2019)
34. D.S. O'Boyle, W.B. Dunn, D. O'Neill, et al., Improvement in the prediction of neonatal hypoxic-ischemic encephalopathy with the integration of umbilical cord metabolites and current clinical makers. J. Pediatr. **229**, 175–181.e1 (2021)
35. D.M. Murray, Biomarkers in neonatal hypoxic-ischemic encephalopathy - review of the literature to date and future directions for research, in *Handbook of Clinical Neurology*, ed. by L.S. de Vries, H.C. Glass, (Elsevier, Amsterdam, 2019), pp. 281–293
36. D.M. Ferriero, S.L. Bonifacio, The search continues for the elusive biomarkers of neonatal brain injury. J. Pediatr. **164**, 438–440 (2014)

Medical Liability Issues (and Beyond) Resulting from the Use of New Technologies

Massimo Farina and Alessia Palladino

1 Toward the Evolution of Medical Liability Legal Framework

Technological developments in healthcare have given rise to an earnest appeal, as well as a strong legal debate toward the most appropriate regulatory system. Academics have been debating toward the need to address a new regulatory framework by also revising the traditional legal categories.

On the one hand, the use of new technologies in the medical sector has forced a re-examination of the traditional healthcare relationship between the doctor and the patient.

On the other hand, technology has given birth to new legal subjects, potentially able to produce significant effects in the sphere of individuals. The greater or lesser autonomy of an artificial agent in the performance of a medical service is, for example, potentially capable of affecting the framework of liability, leading to

Massimo Farina is the author of the following sections: 1. Toward the evolution of medical liability legal framework; 1.1. Criminal liability in the medical field; 4. The advent of robotics and artificial intelligence in medicine; 5. Liability profiles of artificial agents; 8. Ethical evaluations. Alessia Palladino is the author of the following sections: 2. Telemedicine; 3. Medical devices; 6. Deontological issues; 7. Protection of personal health data; 9. Concluding remarks.

M. Farina (✉)
Department of Electrical and Electronic Engineering (DIEE), University of Cagliari, Cagliari, Italy
e-mail: m.farina@unica.it

A. Palladino
Suor Orsola Benincasa University, Napoli, Italy

D. Pani (ed.), *Innovative Technologies and Signal Processing in Perinatal Medicine*, https://doi.org/10.1007/978-3-031-32625-7_4

interruptions in the causal link between the conduct of the health professional and the damage caused to the patient.[1]

In order to meet this need for systematic adaptation, not a few clarifying efforts have been made by operators in the sector, also and above all with regard to the use of new technologies and artificial intelligence systems.[2]

Nonetheless, legal scholars are aware of the unstoppable process of technological evolution and digitization of health services, thus questioning it.[3]

Identifying and outlining a comprehensive regulatory framework in such a complex sector is constantly evolving as the health sector seems quite hard. As a matter of fact, more frequently the advent of technology makes the institutions unable to provide immediate answers due to the anachronistic legal framework, whose rules and legal concepts would need a more appropriate refreshing process. On this point, technical procedures – such as extensive interpretation and analogy – can aid the interpreter by bridging the gap in the law, as well as filling it by applying names provided for similar cases or similar matters.

However, whereas extensive interpretation and analogy are allowed in civil law,[4] this is not possible in criminal law,[5] which only consents to an extensive interpretation.[6]

---

[1]Lior, A. (2020). The AI accident network: Artificial intelligence liability meets network theory. In Tulane Law Review (vol. 95) p. 1103 ff. available at https://advance.lexis.com/api/document?collection=analytical-materials&id=urn:contentItem:63B8-YDY1-F30T-B47G-00000-00&context=1516831

[2]These include, for instance, the Guidelines established by the European Commission on Artificial Intelligence (https://ec.europa.eu/commission/presscorner/detail/en/IP_18_3362), the Ethical Charter for Artificial Intelligence signed in Rome on February 28, 2020, by the Italian government, the Vatican City, Microsoft, IBM, and FAO (https://www.repubblica.it/tecnologia/2020/02/28/news/pav_governo_microsoft_ibm_e_fao_firmano_la_carta_etica_per_l_intelligenza_artificiale-249799549/), and the recent document by Italian Superior Council of Health – Section V on Artificial Intelligence Systems as a Diagnostic Support Tool, year 2021 (https://www.salute.gov.it/imgs/C_17_pubblicazioni_3218_allegato.pdf).

[3]Topol, E. (2019). Deep medicine: how artificial intelligence can make healthcare human again. Hachette UK, p. 95: "We can build these models, but we don't know how they work. We already accept black boxes in medicine. For example, electroconvulsive therapy is highly effective for severe depression, but we have no idea how it works. [...] As patients we willingly accept this human type of black box, so long as we feel better or have good outcomes".

[4]See, Art. 12 by preliminary provisions of Italian civil code: "In applying the law, no other meaning may be attributed to it than that made manifest by the proper meaning of the words according to their connection and the intention of the legislature. If a dispute cannot be decided by a specific provision, regard shall be had to the provisions governing similar cases or similar matters; if the case still remains doubtful, it shall be decided according to the general principles of the legal system of the state". See also Rosa F. (2020) The Use of IT Tools and Artificial Intelligence in the Health Sector: The Patient as a Vulnerable Subject. In European Journal of Privacy Law & Technologies (vol. 2), p. 224–240.

[5]See, art. 14 preliminary provisions of Italian civil code: "Criminal laws and laws that make exceptions to general rules or other laws do not apply beyond the cases and times considered therein", in accordance with principle of legality enshrined in Article 25, par. II of Italian Republican Constitution.

[6]However, it is not always easy to distinguish extensive interpretation from analogy in practice; indeed, sometimes the risk is that extensive interpretation turns into a mechanism circumventing the prohibition of analogical application.

Hence, the legal vacuum related to the phenomenon under analysis is destined, at least for the time being, to affect the activity of doctrine and jurisprudence, which are also called upon to question the limits of their interpretative activity.

Moreover, medical liability has always been at the center of numerous doctrinal and jurisprudential debates.

Originally, the Italian legal scenario upon civil liability degree entirely depended on the role of the medical professional[7]: a freelance doctor would be considered liable for breach of contract, while a doctor employed by a facility was liable for noncontractual liability under Article 2043 of the Civil Code.[8]

This was due to the hospitalization of the patient in the healthcare facility, which automatically entailed the conclusion of a work contract between patient and facility and never between patient and doctor.[9] In this perspective, the doctor was merely an organ through which the hospital or nursing home entered into the contract with the patient.

This opinion was later superseded by a revirement of the Courts of Cassation that led to a re-qualification in terms of contractual liability for the medical practitioner (pursuant to Article 1218 of the Civil Code). This was due to the so-called principle of "organic identification" of the medical employee into the structure. In this regard, any damage caused by the doctor was charged only by the structure, placing the doctor's conduct exclusively in the area of risk of the healthcare company.

As a result, all the issues dealing with the distribution of the burden of proof, the degree of fault, and the limitation period have suffered a change. Thus, a more typical and favorable legal framework has occurred for the injured party of contractual obligations.

As a matter of fact, whereas contractual liability comes into force, the patient only has to prove the existence of the contract, the nonperformance determining the pathology, and the damage complained. The doctor (or the healthcare facility), on the other hand, is called upon to prove that he/she performed the service with diligence, thus having no causal impact on the occurrence of the damage.

At a later stage, given the continued absence of a constraining negotiation, a new theory emerged that succeeded in granting a more solid foundation to the contractual liability paradigm, named "qualified social contact."[10]

---

[7] Stanzione P. and Zambrano V. (1998), Attività sanitaria e responsabilità civile, Giuffrè, p. 505 ff.; Toscano M. (1996), Il difetto di organizzazione: una nuova ipotesi di responsabilità?. In Responsabilità civile e previdenza, p. 389 ff.

[8] Art. 2043 Italian civil code (Compensation for unlawful acts) provides the general norm for tort liability. However, starting from 1999, the Italian Supreme Court (with ruling n. 589/1999), through the recourse to the fictio iuris of the so-called "contatto sociale" between the physician and the patient, deemed such liability as a contractual one, thus applying the relevant legal regime, more favorable to the patient. On behalf of the healthcare provider, it used to be invoked the application of art. 2236 Italian civil code, limiting the liability of the practitioner to the event of her malice or gross negligence, but only for cases requiring the solution of technical issues of particular difficulty.

[9] Italian Supreme Court of Cassation, judgment no. 2428/1990 and judgement no. 2750/1998.

[10] Italian Supreme Court of Cassation, judgment no. 589/1999.

As far debated in the legal scenario, social contact is generally understood to mean that the de facto relationship capable of generating mutual reliance of the parties involved, to which specific duties of protection and cooperation are bound, aimed at safeguarding a specific legal asset.

Liability arising from qualified social contact is thus in a particular form of civil liability that disregards the existence of a contract, when a particular social relationship exists between the parties involved that is considered by the legal system as capable of determining specific behavioral duties.[11]

The doctor–patient relationship represents a concrete example of this relationship: regardless of the existence of a contract, an obligation to protect the right to health is incumbent on the health professional.

Social contact between doctor and patient is a qualified relationship that occurs not only at the time of taking charge of the patient, but also in purely fortuitous and informal cases, such as in the event of therapeutic statements made by the doctor during a casual encounter.[12]

All these developments have thus defined a process of "contractualization in forced stages" of medical liability, culminating in four important Italian Supreme Court pronouncements dating back to 2004.[13]

However, given the liability paradigm more favorable to the injured party, the exponential increase in litigation initiated by patients and the consequent spread of defensive medicine attitudes on the part of medical practitioners soon forced greater clarity on the age-old problem of the medical liability regime.

Defensive medicine means the conduct of doctors who, in order to protect themselves from possible litigation, prescribe a huge amount – even unnecessary – diagnostic or therapeutic interventions (so-called positive defensive medicine)

[11]For a more detailed examination of the subject, see Venosta, F. (2021). "Contatto sociale" e affidamento (vol. 173). Giuffrè.; Ronga G. (2007), Le varie ipotesi di responsabilità cosiddetta da contatto sociale, in L. Viola (ed.), La responsabilità civile ed. il danno (vol. 1) Halley; Rossi S. (2010), Contatto sociale (fonte di obbligazione), in Digesto delle discipline privatistiche, civ sec., V update appendix, Utet; F. Claris Appiani F. (2015), Contatto sociale (responsabilità da), in Ridare, Giuffrè; Gazzoni F. (2016), Obbligazioni e contratti, ed. XVII., Edizioni Scientifiche Italiane.

[12]Amidei Andrea, Savini Nicci Mario, La responsabilità civile del medico 'strutturato' in Giurisprudenza italiana, 2021, fasc. 2, pp. 468–472.

[13]Italian Supreme Court of Cassation, judgments no. 4400/2004, no. 9471/2004; no. 10297/2004 and no. 11488/2004. Before, see also the judgments of the Italian Supreme Court of Cassation (United Sections) were expressed, according to which "the complex and atypical relationship that is established between the clinic and the patient (in this case: a pregnant woman), even if the latter chooses a treating doctor from outside the health care, facility, is not limited to the mere provision of services of a hospitality nature (provision of board and lodging), but consists in the provision of auxiliary medical and paramedical personnel and the provision of medicines and all necessary equipment, even in view of any complications': judgement n. 9556/2002. In Giustizia Civile 2003, p. 2196 ff.

or refrain from taking care of the patient at all (so-called negative defensive medicine).[14]

With the primary intention of curbing these risks arising from the spread of unsuitable medical practices, Law Decree No 158 of September 13, 2012 (also known as the Balduzzi Decree), was thus issued.[15]

Although first commentators believed that with the introduction of the aforesaid decree the legislator would have consciously intended to bring medical liability within the regime of civil liability, the subsequent jurisprudence of legitimacy returned to the subject and opted for the permanence of the regime of contractual liability from qualified social contact of the healthcare professional.[16] Even after the Balduzzi Decree, therefore, the medical liability scheme continued to be that, already consolidated in jurisprudence, of qualified social contact.[17]

---

[14]Marchisio E. (2020), Evoluzione della responsabilità civile medica e medicina 'difensiva'. In Rivista di diritto civile, (fasc. 1) p. 189–220; Sudiero F. (2020), La giurisprudenza, la 'medicina difensiva' ed. il ruolo del sindaco. In Il Nuovo Diritto delle Società (vol. 1), p. 29–49; Iannone R. F. (2019), La nuova responsabilità sanitaria: rilievi critici alla luce dei primi pronunciati delle Corti. In Danno e responsabilità (vol. 2) p. 287 ff. On the subject, see the following jurisprudential collection: Italian Supreme Court of Cassation, judgments: no. 577/2008; no. 28187/2017; no. 8770/2017; no. 18392/2017; no. 16601/2017. In Danno e Responsabilità, 2019 (vol. 2) p. 283–292; Granelli C. (2018), Il fenomeno della medicina difensiva e la legge di riforma della responsabilità sanitaria. In Responsabilità civile e previdenza (vol. 2) p. 410–444.

[15]Italian Decree-Law no. 158, September 1, 2012, containing Urgent provisions to promote the development of the country by means of a higher level of health protection, converted with amendments into Law no. 189, November 8, 2012. See generally Giulio Ponzanelli (2016), La responsabilita medica: dal primato della giurisprudenza alla disciplina legislativa. In Danno e Responsabilità (vol. 8–9) p. 819 ff. See also Cupelli C. (2017), Il perimetro applicativo della legge Balduzzi: aperture giurisprudenziali 'vs.' restrizioni normative?. In Processo penale e giustizia (Vol. 7:1) p. 196–204.

[16]In this regard, it is worth mentioning the principle expressed by Italian Supreme Court of Cassation, judgments, no. 4030/2013 following the enactment of law decree no. 158, September 13, 2012: "The matter of civil liability follows its own consolidated rules, and not only for the civil liability of the doctor, but also for the so-called contractual liability of the doctor and the healthcare facility due to social contact".

[17]Franciosi L. M. (2018), The New Italian Regime for Healthcare Liability and the Role of Clinical Practice Guidelines: A Dialogue among Legal Formants. In Journal of Civil Law Studies (vol. 11:2), p. 371–414. The author underlined that "the 2017 Law was to reduce defensive medicine, thus benefiting patients. In particular, the 2017 Law intended to address the topics of medical malpractice, defensive medicine and safety of patients introducing a more favorable regime of professional liability for the healthcare providers, both from the civil law and the criminal law perspective, focused on a new and more detailed role for Clinical Practice Guidelines (CPGs). In its original intention, it should have redressed some gaps and limits of the Balduzzi Law on the one hand, and, it should have decreased defensive medicine and healthcare liability on the other hand, by providing judges with clearer and more favorable rules and standard of behavior for healthcare professionals. In spite of several positive aspects, the 2017 Law did not reach its ambitious goal, in particular because of the limits of the new regime for criminal liability". See also Granelli C. (2016), La medicina difensiva in Italia. In Responsabilità Civile e Previdenza, p. 22–39); Manna A. (2014), Medicina difensiva e diritto penale. Tra legalità e diritto alla salute, Pisa University Press; Roiati A. (2012), Medicina difensiva e colpa professionale medica in diritto penale. Tra teoria e prassi giurisprudenziale, Giuffrè.

In the regulatory framework thus described, Law No. 24 of March 8, 2017 (also known as the Gelli reform,)[18] finally intervened with disruptive effect, eliminating all doubts and definitively overcoming the previous jurisprudential orientations on physician liability.[19]

Without prejudice to the contractual liability of the healthcare facility, whether public or private, the Gelli reform brought the doctor's liability back under the umbrella of noncontractual liability pursuant to Article 2043 of the Civil Code, except when the patient has chosen by contract the doctor from whom to receive healthcare services.[20]

In the first case (contractual liability), the rules on the burden of proof have radically changed: the patient is called upon to prove all the constituent elements

[18]Italian Law No. 24, March 8, 2017 (so-called Gelli reform), provisions on the safety of care and the assisted person, as well as on the professional liability of healthcare professionals. For a further discussion of the Gelli reform, see Acconciaioco B., Altomare M., Dimonte G., Fiorella R. Petronelli M., Quartarella A, Raeli V., Santoro P. (2019), La nuova responsabilità medica. Profili civili, penali, amministrativi e assicurativi, in Acconciaioco B., Dimonte G. (eds.), Duepuntozero, pp. 23–42.

[19]Alpa G. (2017), Ars interpretandi e responsabilità sanitaria a seguito della nuova legge Bianco-Gelli. In Contrato e Impresa, p. 728–732. Besides the liability of the physician, it used to be affirmed that the contractual liability of the healthcare institution (public and/or private) due to the atypical contract, expressly or implicitly entered into force between the patient and the institution. In light of its peculiarities, the medical malpractice used to be deemed by some commentators and tribunals as a subsystem of civil liability. See, out of many, Granelli C. (2018), Il fenomeno della medicina difensiva e la legge di riforma della responsabilità sanitaria. In Responsabilità civile e previdenza (vol. 83:2), p. 410–444); De Matteis R. (1995), La responsabilita medica: un sottosistema della responsabilità civile, Cedam; Roppo V. (1993), La responsabilita civile dell'impresa nel settore dei servizi innovativi. In Contratto e Impresa, p. 891–894. According to other scholars, though speaking of system would raise conceptual issues, medical malpractice should nevertheless be intended as a special regime comparable to that of tort liability; see, also, Alpa G. (2017), From the Physician to the Team, to the Healthcare Setting, to the System. In Law and medicine. Current topics in a German and Italian Perspective, Botta C. & Armbrister C. eds., Edizioni Scientifiche Italiane.

[20]On this point, see Article 7 of Italian Law No. 24, March 8, 2017: "1. The public or private health or social care facility that, in the performance of its obligation, makes use of the work of health professionals, even if chosen by the patient and even though they are not employees of the facility itself, is liable under Articles 1218 and 1228 of the Civil Code, for their conduct malicious or negligent. 2. The provision referred to in paragraph 1 shall also apply to the health care services carried out under the regime of free profession intramurary profession or within the framework of experimental and clinical research or under an agreement with the National Health Service National Health Service as well as through telemedicine. 3. The health care practitioner referred to in paragraphs 1 and 2 shall be liable for his or her actions pursuant to Article 2043 of the Italian Civil Code, unless he has acted in the performance of obligation contractual obligation undertaken with the patient. The court, in determination of damages, shall take into account the conduct of the health care practitioner pursuant to Article 5 of this Law and Article 590-sexies of the Italian Criminal Code, introduced by Article 6 of this Law. [. . .]". See, also, Ponzanelli G. (2017), Medical Malpractice: la Legge Bianco Gelli. Una Premessa. In Danno e Responsabilità (vol. 3), p. 268–270.

of the tort, that is, the breach of contract, the subjective element (willful misconduct or fault), the harmful event, and the causal link between conduct and damage.[21]

In the second case, on the other hand, two types of contractual relationship have been distinguished[22]: the first occurs between the patient and the hospital (or nursing home) and, the other, between the patient and the doctor. However, these responsibilities may be concurrent according to the general principle inferable from Article 2055 of the Civil Code, which regulates joint and several liability for damage attributable to more than one person.

1.1 Criminal Liability in the Medical Field

The liability of the healthcare professional[23] has been constituting the focus of numerous regulatory developments and heated doctrinal and jurisprudential debates.[24]

With particular reference to the subject of medical malpractice, in origin only the conduct of a doctor who lacked the minimum level of professionalism and experience – required for a medical professional – was considered to be criminally relevant,[25] without therefore distinguishing between forms and degrees of guilt.[26] This benevolent attitude toward the medical profession was justified by the fact that, since it was impossible to foresee exhaustive treatment mechanisms, an error of judgment was always considered possible.[27]

---

[21] For more information, see: Munaro L. (2018), Responsabilità sanitaria, in Martini F., Rodolfi M. (eds.), Responsabilità civile, Giuffrè, pp. 1–17.

[22] On this point, authors such as Richard Epstein, who tend to be unfavorable to state intervention in private relationships, have argued that a recourse to the scheme of contractual liability could easily obviate many problems related to medical malpractice. For a more detailed discussion, see Epstein, R. A. (2000). Managed Care Liability. In Civil Justice Forum (Vol. 39). Manhattan Institute.

[23] Term introduced by Italian Law No. 24, March 8, 2017, which extended the scope of the reform to all professions involving the exercise of a health activity, including, for example, also the nurse, pharmacist or psychologist, with the sole exclusion of healthcare professionals and persons exercising the auxiliary arts of the health professions (such as the masseur, optician, or dental technician).

[24] Di Marzo C. (2012), Medical malpractice: the Italian experience. In Chicago-Kent Law Review (Vol. 87:1), p. 54–77; Lorè C. and Martini P. (1998), Sulla responsabilità penale degli amministratori di strutture sanitarie. In Rivista italiana di medicina legale, p. 403 ff.

[25] Bilancetti M. (2017), Profili penalistici della L. 8 marzo 2017 n. 24. In Rivista italiana di medicina legale e del diritto in campo sanitario (vol. 3) p. 999–1014.

[26] See on this point the opinion of Siracusano F. (1997), Ancora sulla responsabilità colposa del medico: analisi della giurisprudenza sulle forme e i gradi della colpa. In Cassazione Penale. p. 2904 and, even earlier, that of Grasso G. (1979), La responsabilità penale dell'attività medico-chirurgica: orientamenti giurisprudenziali sul 'grado' della colpa. In Rivista italiana di medicina legale, p. 82.

[27] E. Battaglini E. (1953), La colpa professionale dei sanitari, in Giustizia penale (vol. 2) p. 506.

Subsequently, since the lack of other normative references, part of the doctrine sanctioned the liability of the doctor for malice or gross negligence in the case of activities requiring the resolution of particularly complex technical problems, thus extending the scope of Article 2236[28] of the Civil Code to criminal law.

The application of this article in criminal law has in fact been the subject of much discussion[29]: on the one hand, admitting its application would in fact have entailed a violation of the principle of completeness and non-hetero-integrability of criminal law; on the other hand, not admitting it would have led to the consequence that, in the cases described by the rule, the same act would have caused the doctor's criminal liability and, absurdly, his nonliability in civil law.[30]

Actually, the major legal literature held that the applicability of Article 2236 of the Civil Code was to be limited to the concept of malpractice: every time, due to particular circumstances (e.g., technical difficulties), the highest degree of expertise could not be required, at least the highest degree of diligence and prudence could be expected of the doctor. Consequently, professional misconduct, when contested in terms of negligence and imprudence, had to be determined according to the normal criteria of culpable imputation, thus also taking into account average and slight negligence.[31]

In this scenario, the criteria of Article 2236 of the Civil Code were used as a rule of experience in the assessment of the doctor's malpractice,[32] whereas in other cases reference had to be made to the traditional criteria for ascertaining liability under Article 43 of the Criminal Code,[33] with reference to the assessment of the psychological element of the agent (malice, negligence, intent).

[28]Article 2236 of Italian Civil Code states: "If the service involves the solution of problems of special difficulty, the service provider shall not be liable for damages, except in the case of wilful misconduct or gross negligence".

[29]Blaiotta R., (2000) Causality and fault in the medical profession between probability and certainty. In Cassazione penale p. 1188 ff.

[30]Crespi A. (1960), Il grado della colpa nella responsabilità professionale del medico chirurgo. In Scuola Positiva, p. 488.

[31]Siracusano F. (1997), Ancora sulla responsabilità colposa del medico: analisi della giurisprudenza sulle forme e i gradi della colpa. In Cassazione penale, p. 2904. Medium and slight negligence are distinguished in particular from gross negligence, which occurs when the doctor acts with extraordinary and inexcusable imprudence, without observing even the most elementary degree of diligence.

[32]See Italian Supreme Court of Cassation, judgments no. 14446/1990 and no. 39592/2007.

[33]Pursuant to the Italian Criminal Code, art. 43, psychological element of the crime shall be "intentional, or according to intention, when the harmful or dangerous event, which is the result of the action or omission and on which the law makes the existence of the crime depend, is foreseen and intended by the agent as a consequence of his action or omission; preterintentional, or beyond intent, when a more serious harmful or dangerous event results from the action or omission than that intended by the agent; negligent, or against intention, when the event, even if foreseen, is not intended by the agent and occurs due to negligence or recklessness or inexperience, or due to failure to comply with laws, regulations, orders or discipline". The distinction between intentional and negligent offenses, established by this article for felonies, also applies to misdemeanors, whenever for these the criminal law makes any legal effect dependent on this distinction'.

In this context, guidelines were increasingly affirmed as a useful tool aimed at formalizing and proceduralizing the precautionary rules that the doctor is called upon to follow. Once the failure to comply with the guidelines had been ascertained as determining the damaging event, medical negligence was not as a rule ruled out since it could only be considered in a liberating sense when the patient's overall condition was such as to make the damaging event itself inevitable, and therefore attributable to chance.[34]

Faced, however, with a jurisprudential panorama that had become increasingly severe in terms of punishable medical malpractice,[35] Law Decree No. 158 of September 13, 2012 (Balduzzi Decree),[36] was issued, designed to regulate the limits of the liability of healthcare professionals, without prejudice, however, to the use of the rule set forth in Article 2236 of the Civil Code in the criminal sphere as well,[37] in the case of issues of particular technical-scientific difficulty.[38]

In a nutshell, the Balduzzi Decree became significant under two different aspects. At first glance, it introduced the distinction between slight and gross negligence for the affirmation or exclusion of criminal liability. Secondly, it also enhanced the role of Clinical Practice Guidelines (hereinafter, "CPGs").[39]

In particular, Article 3 of the Balduzzi Decree, as amended at the time of its conversion, excepts the liability for slight negligence on the part of the doctor

[34]In this sense, see Italian Supreme Court of Cassation, judgments no. 16328/2011and no. 39592/2007.

[35]Maggese D. (2002), Probabilità scientifica e nesso di causalità, tra lesione personale ed. intervento chirurgico. In Danno e Responsabilita, (Vol. 6:1), p. 72; Fiori A. (1991), Il criterio di probabilità nella valutazione medico-legale del nesso causale. In Rivista italiana di medicina legale, (vol. 13), p. 29–42.

[36]For an in-depth analysis of the reform, see see Bona M. (2013), La responsabilità medica civile e penale dopo il Decreto Balduzzi, Maggioli, 2013; Poli P.F. (2013), Legge Balduzzi tra problemi aperti e possibili soluzioni interpretative: alcune considerazioni. In Diritto Penale Contemporaneo, (vol. 4), p. 86–98.

[37]Crespi A. (1955), La responsabilità penale nel trattamento medico-chirurgico con esito infausto, Priulla; ID (1992), I recenti orientamenti giurisprudenziali nell'accertamento della colpa professionale del medico chirurgo: evoluzione o involuzione?. In Rivista italiana di medicina legale, (vol. 4), p. 29–42.

[38]Bartoli R. (2018), Riforma Gelli-Bianco e sezioni unite non placano il tormento: una proposta per limitare la colpa medica. In Diritto penale contemporaneo (vol. 5) p. 233 ff.; Basile f. (2017), Itinerario giurisprudenziale sulla responsabilità medica colposa tra art. 2236 c.c. e legge Balduzzi (aspettando la riforma della riforma). In Diritto penale contemporaneo (vol. 2) p. 159 ff.; Bilancetti M. (2003), La responsabilità penale per colpa professionale medica è destinata a ridimensionarsi anche in Italia?. In Giurisprudenza italiana, p. 1982 ff.

[39]Scoletta M. (2013), Rispetto delle linee guida e non punibilita della colpa lieve dell'operatore sanitario: la norma penale di favore al giudizio della Corte costituzionale. In penalecontemporaneo.it; See also Di Landro A. R. (2012), Dalle linee guida e dai protocolli all'individualizzazione della colpa penale nel settore sanitario. Misura oggettiva e soggettiva della malpractice, Giappichelli. For critical remarks about the role of good clinical practices within malpractice trials (in particular when invoked by the defendant in a criminal judgment), see D'Alessandro F. (2017), La responsabilità penale del sanitario alla luce della riforma Gelli-Bianco. In Diritto penale e processo (vol. 5) p. 572–578.

whereas the professional had complied with the guidelines and best clinical and healthcare practices, in the event that the event that had occurred was not otherwise configurable in terms of a crime or, in any case, was attributable to negligent, imprudent, or reckless conduct on the part of the doctor.[40]

In such cases, the obligation to pay compensation pursuant to Article 2043 of the Civil Code remained in place, but the judge, in determining the damage, was called upon to take into account the conduct of the sanitary practitioner. At the same time, reliance was also placed on the guidelines and good practices accredited by the scientific community, thereby implicitly recognizing that compliance with them would exempt the doctor from criminal liability for minor negligence.[41]

Lastly, the Gelli reform returned to the issue of fault and compliance with guidelines,[42] reformulating new regulations on culpable liability for death or personal injury in healthcare and repealing the former extra-codice regulations.[43]

In particular, Article 6 of Law March 8, 2017, no. 24 – which specifically deals with criminal liability of healthcare providers – introduced the current Article 590-sexies of the Italian Criminal Code, entitled "Culpable liability for death or personal injury in healthcare," which provided that "if the adverse event has occurred due to malpractice, punishability is excluded when the recommendations provided for by the guidelines as defined and published by law have been complied with,[44] or,

[40]For a more in-depth analysis, see Brusco C. (2013), Linee guida, protocolli e regole deontologiche. Le modifiche introdotte dal c.d. Decreto Balduzzi. In Diritto Penale Contemporaneo, (vol. 4), p. 51–72. See also Antonella M. (2019), La causa di impunità re-introdotta dalla legge Gelli-Bianco in materia di colpa medica. Le Sezioni Unite recuperano la colpa lieve come requisito intrinseco alla norma. In Rivista italiana di medicina legale e del diritto in campo sanitario (vol. 2), p. 533–551; Provera A. (2019), 'Omnis definitio in iure ..' La responsabilità medica e la problematica distinzione tra i tipi di colpa generica. In Rivista italiana di medicina legale e del diritto in campo sanitario (vol. 4), p. 1355–1366; Schiavo M. (2019), La persistente imprevedibilità delle pronunce sulla colpa medica a due anni dall'entrata in vigore della legge Gelli-Bianco. In Diritto penale contemporaneo (vol. 5) p. 5–30.

[41]Pardolesi R. (2017), Chi (vince e chi) perde nella riforma della responsabilita sanitaria. In Danno e Responsabilita (vol. 3), p. 261–264; Pavich G. (2017), La responsabilità penale dell'esercente la professione sanitaria: cosa cambia con la legge Gelli-Bianco. In Cassazione Penale (vol. 7–8), p. 2961 (the Author expresses critical remarks about the distinction between different kinds of liability).

[42]Di Landro A. (2018), Colpa medica, linee guida e buone pratiche. Spunti di riflessione comparatistici. Dalle Sez. un. 'Mariotti' alle esperienze angloamericane 2018. In Archivio penale (vol. 2), p. 403–422; Gatta G. (2017): Colpa e responsabilità medica: il decreto Balduzzi va in soffitta e approda in G.U. la legge 'Gelli-Bianco'. In penalecontemporaneo.it; Iadecola G. (2013), Brevi note in tema di colpa medica dopo la c.d. legge Balduzzi. In Rivista italiana di medicina legale e del diritto in campo sanitario, p. 549 ff.; Grosso S. (2013), I profili di interesse penalistico del 'decreto Balduzzi' (D.L. 158/2012, conv. in L. 189/2012): un'indagine sui delicati rapporti tra linee-guida e colpa grave. In Legislazione penale, p. 543 ff.

[43]For an in-depth discussion, see, Romano B. (2018), La responsabilità penale dell'esercente della professione sanitaria tra antichi dubbi e nuovi problemi, In penalecontemporaneo.it.

[44]With a view to implementing the Gelli reform and the public system of accreditation introduced by article 5, the Ministry of Health has published a list of 293 scientific societies and associations of health professions authorized to produce guidelines. This list is updated

in the absence thereof, the so-called clinical-assistance best practices, provided, however, that the said recommendations provided for by the aforesaid guidelines are appropriate with respect to the specificity of the case in question". However, this is without prejudice to the subsequent Article 7 of Law No. 24 of March 8, 2017, which establishes the civil liability of the health profession under Article 2043 of the Civil Code.

Conversely, therefore, negligence and imprudence always determine the existence of the liability of the doctor, even where his conduct complies with the guidelines.

This reconstruction,[45] following a heated debate in the Criminal Section IV of the Court of Cassation,[46] was confirmed in 2018 by the United Sections,[47] which held that Article 590-sexies of the Criminal Code identified a cause of non-punishability in the technical sense, operating only in the case in which the healthcare professional had identified and adopted the appropriate guidelines for the concrete case and was slightly negligent due to inexperience in the implementation phase of the recommendations provided for by the same. This is not the case, on the other hand, in the event of negligence due to imprudence or negligence, when the service is not regulated by guidelines or best practices, or when the same have been identified by the professional in an inadequate manner or, again, in the event of gross negligence due to malpractice in the implementation phase. In all these cases, there is criminal liability of the health professional.[48]

---

every 2 years. See, Cupelli C. (2018), L'art. 590-sexies c.p. nelle motivazioni delle sezioni unite: un'interpretazione 'costituzionalmente conforme' dell'imperizia medica (ancora) punibile. In penalecontemporaneo.it; Di Landro A. (2013), Le novità normative in tema di colpa penale (L. 189, c.d. 'Balduzzi'). Le indicazioni del diritto comparato. In Rivista italiana di medicina legale e del diritto in campo sanitario, p. 833 ff.

[45]For a more recent riconstruction, see Basile F., Poli P. (2022), La responsabilità per 'colpa medica' a cinque anni dalla legge Gelli-Bianco. In Diritto penale contemporaneo (vol 1) p. 79 ff.

[46]See, on the one hand, the reconstruction first made by Italian Supreme Court of Cassation, judgment no. 28187/2017 and, on the other hand, that made by the judgment no. 50078/2017. See also Alagna R. (2018), Le colpa penale del medico dinanzi alle Sezioni Unite: innovazioni, incertezze e perplessità. In Responsabilità civile e previdenza, (vol. 3) p. 888–899; Di Giovine O. (2018), A proposito delle Sezioni Unite della Corte di Cassazione 'Mariotti' sulla colpa medica e a margine del libro di Matteo Caputo su 'Colpa medica e sicurezza delle cure. In Rivista italiana di medicina legale e del diritto in campo sanitario (vol. 3) p. 837–866.

[47]Italian Supreme Court of Cassation, judgment no. 8770/2018. For further details, see Abukar Hayo A., La presunzione di non colpevolezza di cui alla legge Gelli-Bianco non può essere assoluta. In Cassazione penale, 2020 (vol. 6) p. 2546–2554; Caletti G. (2019), La Cassazione alle prese con il 'post-Mariotti': precisazioni 'metodologiche' in tema di prova scientifica, linee guida e apprezzamento della responsabilità penale del sanitario. In Rivista italiana di medicina legale e del diritto in campo sanitario (vol. 1) p. 289–301.

[48]Ferrara S. D., Viel G. and Boscolo-Berto R. (2013), Present and future for medical malpractice, responsibility and liability. In Ferrara S. D., Boscolo-Berto R. and Viel G. (eds.), Malpractice and Medical Liability. European state of the art and Guidelines, Springer-Verlag, p. 3–9.

Therefore, in the hypothesis of negligence or recklessness, the cause of non-punishment will not operate, whereas the mere acknowledgment of the existence of guidelines relevant to the specific case does not imply that their violation automatically gives rise to negligence due to malpractice.

The United Sections therefore recognized the suitability and validity of the clinical guidelines to constitute a guide for the disoriented healthcare worker, especially in relation to the most dangerous activities; nevertheless, the Court also held that the benefit provided for by Article 590-sexies of Italian Criminal Code cannot be pegged to automatisms. "It is not, in fact, a 'shield' against any liability, their effectiveness and preceptive force being, in any case, dependent on the demonstrated 'suitability' to the specifics of the concrete case (Article 5), which is also the appreciation that remains, for the health professional, the means by which to recover autonomy in the performance of his professional talents and, for the community, that to see the risk of bureaucratic flattening dissolved. From which would re-emerge the danger for the safety of care and the risk of 'defensive medicine', in a negative vortex destined to feed itself."[49]

In more recent times, the use of new technologies in healthcare has stimulated questions that have once again tested the resilience of our penal system.[50] Indeed, current innovations aim to perform complex tasks previously only performed by human beings in an increasingly autonomous manner.

In such a scenario, one wonders whether technology is really destined to create new subjects of law liable to criminal liability.[51]

Starting from the concept of the personality of criminal liability expressed in Article 27 of the Constitution, a more traditionalist reasoning would probably lead to the view that machina delinquere non potest.[52] If this were not the case, recognizing criminal liability in the hands of nonhuman subjects would mean having to redefine all the concepts of subjective capacity, action, and culpability.

At the same time, however, we are witnessing an effective personalization of machines that, although not human, are now concretely endowed with a significant degree of autonomy of action.

[49]Thus, also Italian Supreme Court of Cassation, judgment no. 8770/2018. Bartoli R. (2011), I costi 'economico-penalistici' della medicina difensiva. In Rivista italiana di medicina legale, p. 1107 ff.

[50]For an in-depth study of the topic, see Ubertis G. (2020), Artificial intelligence, criminal justice, meaningful human control. In Diritto pena le Contemporaneo (vol. 4), p. 74–88; Basile F. (2019), Artificial intelligence and criminal law: four possible paths of enquiry. In Diritto Penale e Uomo (vol. 10) p. 1–33 and Borsari R. (2019), Intelligenza Artificiale e responsabilità penale: prime considerazioni. In Media Laws, Vol. 3, p. 262–268.

[51]Feola A., Mariano V., Marsella L. T. (2015), Medical Liability: The Current State of Italian Legislation. In European Journal of Health Law 22, no. 4, p. 347–358.

[52]Cappellini A. (2018), 'Machina delinquere non potest'? Brevi appunti su intelligenza artificiale e responsabilità penale Relazione al Convegno 'Il ragionamento giuridico nell'era dell'intelligenza artificiale'. In Criminalia: Annuario di scienze penalistiche, ETS, p. 499–520, available at https://discrimen.it/wp-content/uploads/Cappellini-Machina-delinquere-non-potest.pdf

In the difficulty of determining specific criteria regarding the autonomy of machine liability, three possible solutions can be drawn: (i) prohibiting the total autonomy of such systems with the consequent renunciation of their benefits, (ii) identifying an area of permissible risk in their use, or (iii) recognizing real forms of liability in technological innovations.

2 Telemedicine

With the recent advent of new models of remote care, medical liability is an ever-expanding legal scheme.[53]

With a view to the development of a more efficient system, technological innovation could in fact avoid (or even solve) different problems linked to lower levels of care and caution than those established by law. In other words, the use of medical devices and artificial agents in healthcare could simplify medical activity, making it more accessible and, in some cases, reduce the risk of error linked to the human factor.[54]

In recent years, mainly due to the spread of the Covid-19 pandemic,[55] there has been a gradual increase in attention to numerous online medical assistance projects.[56] Evidence is the spread of teleconsultation practices, that is, medical apps, social networks, and chatbots that can generate answers on the health status of the patient-user, monitor him/her, and provide him/her with consultations. An example of this is the Italian portal Pagine Mediche,[57] a digital health platform that connects doctors and registered patients, or the chatbot created by the Ministry of Health as part of the telemedicine project "Ti Video Visito",[58] created as a free support service for pandemic health management and capable of guaranteeing remote therapeutic-assistance services.

These are useful instruments that are currently unregulated. For this reason, they raise legal challenges and concerns.

[53] Botrugno C. (2014), A right for telemedicine: analysis of a regulatory complex in the making, in Politica del diritto (vol. 4) p. 639–668.

[54] Fennell M. L. (2008), The New Medical Technologies and the Organizations of Medical Science and Treatment. In Health Services Research, (vol. 43), p. 1–9. World Health Organization (2010), Telemedicine: opportunities and developments in member states. In http://apps.who.int/iris/bitstream/handle/10665/44497/9789241564144_eng.pdf?sequence=1&isallowed=y

[55] Wrinkle R. B. (2022), Telemedicine across Borders: Entrenched Issues Exposed by COVID-19. In Georgia Journal of International and Comparative Law (vol. 50) no. 2, p. 563–597.

[56] They quickly demonstrated how remote healthcare can be useful in reducing the risk of infection, especially considering the high number of healthcare personnel who died after contracting the virus. To discover more about telemedicine, see McMenamin, J. P. (1998). Telemedicine. International Legal Practitioner, (vol. 23:3), 88–89.

[57] For more information, please consult the official portal https://www.paginemediche.it/

[58] For more information, please consult the initiative's website https://tivideovisito.it/

Such a reorganization of the healthcare system has, moreover, already begun to have important repercussions in terms of the redistribution of responsibility and conflicts in cases of malpractice.[59]

Using the World Health Organization's definition (WHO), telemedicine consists of "the delivery of health services when distance is a critical factor, whereby it is necessary to use information and telecommunication technologies for the purpose of exchanging information useful in the diagnosis, treatment and prevention of diseases to ensure continuous information to health care providers and to support research and evaluation of care".[60]

Its roots can be probably traced back to the 1960s to the first medical care experiments carried out by the National Aeronautics and Space Administration (NASA) for astronauts on orbital missions.[61]

The formal coining of the term, however, can be attributed to Thomas Bird, who in the 1970s first used the word telemedicine to refer to "the practice of medicine without the usual physical confrontation between doctor and patient, using an interactive multimedia communication system."[62]

In today's doctor–patient relationship, telemedicine cannot replace traditional healthcare provision, but only complement and enhance it, increasingly shifting the focus of the doctor's intervention from the hospital to the patient's home.[63]

[59] Amendolagine V. (2021), La responsabilità professionale dell'equipe sanitaria derivante da medical malpractice in Danno e responsabilità (vol. 4) p. 517 ff; Amidei A. (2021), Le responsabilità, per fatto proprio e degli ausiliari, della struttura sanitaria. In Giurisprudenza italiana (vol. 2) pp. 463–468.

[60] Telemedicine was so defined by the World Health Organization in the report A health telematics policy in support of WHO's health-for-all strategy for global health development: report of the WHO Group Consultation on Health Telematics, Geneva, 11–16, December 1997. See, also, Parrott C. M. (2017), Talking Telemedicine and Terminology: The South Carolina Telemedicine Act. In South Carolina Law Review (vol. 68) no. 4, p. 665–688. Parrott Creasie M. (2017), Talking Telemedicine and Terminology: The South Carolina Telemedicine Act. In South Carolina Law Review (Vol. 68: 4) p. 665–688. The Author states that (p. 677) "Telemedicine's popularity skyrocketed in the 1960s–1970s when organizations like NASA, the Department of Defense, and the U.S. Health and Human Services Department began funding research to develop the practice. Currently, over half of all hospitals in the United States use some form of telemedicine, and patient access can be as simple as downloading an app on to their smartphones". See also Kerry A. Kearney and Celia M. Santander (2001), Telemedicine: Evolving into Cybherspace. In Health Lawyer 13, no. 3, p. 28–32.

[61] In fact, the NASA program called Integrated Medical and Behavioral Laboratories and Measurement Systems dates back to 1964. Its aim was to monitor the biometric data of orbiting astronauts and provide remote support in the event of a medical emergency.

[62] Bird K. T. (1975), Telemedicine; concept and practice. In Bashshur R. L., Armstrong P. A. and Youssef Z. I. (eds.), Telemedicine: Explorations in the Use of Telecommunications in Health Care, Illinois.

[63] Botrugno C. (2021) Telemedicina e diritto alla salute in carcere: stato dell'arte, rischi e opportunità. In BioLaw Journal – Rivista di Biodiritto (vol. 3) p. 401–414.

According to the European Commission, which expressed itself on this point in its Communication No. 233 of April 25, 2018,[64] telemedicine could help a virtuous development of the Member States' health and care systems, alleviating numerous problems through digital responses capable of increasing patients' well-being and generally improving the level of efficiency with which healthcare services are delivered.

However, there are several challenges facing healthcare systems today: cost containment, staff shortages, an aging population, the presence of multiple diseases or chronic conditions in patients, as well as the spread of noncommunicable but preventable diseases caused by risk factors such as alcohol, tobacco, and obesity.

From being a potential instrument for improving and integrating the healthcare level, telemedicine is thus beginning to be seen as a useful solution to the economic-management problems of healthcare facilities, as well as an evolution of traditional care mechanisms. On this point, suffice it to think of the innumerable potentials for making better use of patients' health data, facilitating doctor–patient communication and developing a personalized healthcare system.

Already in the early 2000s the development of the remote care modality prompted the European institutions, and in particular the Commission,[65] to urge the Member States to adopt common strategies for the development of telemedicine. This is also with a view to contributing to the economy and, above all, to containing public and private health expenditure. More recently, the European programs "Horizon2020"[66] and "Horizon Europe"[67] have been activated in an attempt to further promote its development.

Taking a step back in time, in Italy, the National e-Care Observatory was set up in 2007 with the aim of encouraging access to technology in the health sector and promoting the effectiveness of the services provided by the National Health

[64] Communication from the Commission to the European Parliament, the Council, the European Economic and Social Committee and the Committee of the Regions on the digital transformation of health and care in the digital single market, empowering citizens and creating a healthier society April 25, 2018, No 233, Brussels. See also Standing Committee of European Doctors (2002), 'The practice of tele-medicine in Europe: analysis, problems and CPME recommendations', 2002 M/027. See Callens S. (2003), Telemedicine and European Law. In Medicine and Law (vol. 22), no. 4, p. 733–742. The author stated that "A Directive of the European Union was first published in 2000, which dealt with telemedicine as part of its provisions. This ECommerce Directive, as it became known, was subjected to further study which revealed some problems relative to the practice of telemedicine. Among the subjects discussed in this paper are those of privacy, data protection, free movement of services, the impact of electronic communication and ethical issues".

[65] Also as part of the Digital Agenda in the implementation of the "Europe2020" plan, a specific action was planned with the clear objective of spreading telemedicine services among the Member States by the year 2020.

[66] For more information, see https://ec.europa.eu/programmes/horizon2020/sites/horizon2020/files/H2020_EN_KI0213413UTN.pdf

[67] For more information, see https://ec.europa.eu/info/research-and-innovation/funding/funding-opportunities/funding-programmes-and-open-calls/horizon-europe_en

System (NHS). In the meantime, several national strategies aimed at enhancing and increasing the quality of telemedicine services have been launched. These include the Ministry of Health's E-Health Information Strategy of 2008 and the National Guidelines prepared by the working group within the Consiglio Superiore della Sanità set up in 2011 to support the systematic use of telemedicine in the National Health Service.

The latter, in its latest version of August 11, 2020, still stands as the main national regulatory reference in the field of telemedicine, defined as a mechanism for "the provision of healthcare services through the use of innovative technologies, in particular Information and Communication Technologies (ICT), in situations where the health professional and the patient (or two professionals) are not in the same location. Telemedicine involves the secure transmission of medical information and data in the form of text, sound, images, or other forms necessary for the prevention, diagnosis, treatment and subsequent follow-up of patients."[68]

Despite the fact, however, that Italy ranks among the first countries in the world in terms of the use of digital technologies by health professionals,[69] there are several reasons why this model of care has not yet managed to take off completely. These include the partial reluctance to digitalization on the part of some doctors and citizens, also due to the lack of well-defined fee schedules for professional fees and, above all, the fear of dehumanization of care activities.[70] Not least, of course, is the absence of a well-defined regulatory framework.

In the latter respect, the use of telemedicine applications has made necessary to analyze the liability of the medical professional and the manufacturer of the medical devices; moreover, it is important to discuss the doctor's liability in the context of telemedicine.[71]

With reference to this last case, given the existence of a legal loophole, the legal debate has firstly pointed out that, even in the physical absence of the doctor, the

[68] See Paragraph 2 of Telemedicine. National Guidelines, Ministry of Health, July 10, 2012, available at https://www.salute.gov.it/imgs/C_17_pubblicazioni_2129_allegato.pdf

[69] See the sixth edition of the Philips future health index, Report Italy, year 2021. This report, especially in the wake of the Covid-19 pandemic, looked at how healthcare leaders are responding to modern healthcare needs and demands.

[70] On this point, there are numerous reflections in the literature. See, Shortliffe E. H., The evolution of electronic medical records, in Academic Medicine (vol. 74:4) pp. 414–419; Bauer K.A. (2021), Home-based telemedicine: a survey of ethical issues. In Cambridge Quarterly of Health Care Ethics (vol. 10:2) p. 137–173; Fleming D.A., Edison K.E. and Pak H. (2009), Telehealth Ethics. In Telemedicine and e-Health (vol. 8) pp. 797–803. The opinion of a psychiatrist interviewed in May C., Gask L., Atkinson T., Ellis N., Mair F. and Esmail A., Resisting and promoting new technologies in clinical practice: the case of telepsychiatry. In Social Science & Medicine (vol. 52:12) p. 1897: "I don't know how therapy can help the person if they are asked to talk to a machine [...] I believe that patients are already in a state of psychological stress, so asking them to talk to a camera is dehumanising".

[71] D'Angiolella R. (2009), Responsabilità e telemedicina. In Rassegna di diritto civile (vol. 4) p. 921–950.

liability of the professional continues to be personal[72]; thus, the concept of mere presence has to be distinguished from that of the personality of the service as set out in Article 2232 of the Civil Code.[73]

However, in such particular cases, including the use of instruments that are not established in medical practice, the majority doctrine and jurisprudence stated the applicability of the aforementioned Article 2236 of the Civil Code, with the consequent mitigation, or even exclusion, of the doctor's liability except in the case of malice or gross negligence, with the burden of proof being placed on the injured party.[74]

In all these cases, there is therefore an allocation of risk to the patient who consensually decides to undergo that type of treatment; this is the reason why the provision of an informed consent that is geared to a true representation of all the risks and benefits of the individual intervention becomes essential.

On this point, the Italian Federation of Family Physicians (FIMMG) has encouraged the issuing of a self-regulation code for telemedicine services, specifying that the latter cannot be proposed as the only diagnostic modality and that the patient must always feel free to accept it or not in a conscious and informed manner.[75]

The case of telemedicine services rendered by several medical (or paramedical) figures is far more problematic.

Jurisprudence holds that the doctor responsible for treatment must also be liable for the willful or negligent acts of all those with whom he has a coordinating relationship, without there being any division of causality.[76]

This duty of knowledge on the part of the coordinator is, however, mitigated by a general principle of reliance whereby each professional must be able to rely on the diligent performance of the service by each member of the team.

In this landscape still partly dominated by uncertainty, the aforementioned National Guidelines on Telemedicine therefore continue to be the main point of reference within our legal system.

---

[72]Tarasco A. L. (2010), La telemedicina per lo sviluppo della sanità del Mezzogiorno: una introduzione giuridica. In Rivista giuridica del Mezzogiorno (vol. 4) p. 16 ff.; Nardone A. (2005), Tutela della salute e nuove tecnologie. La telemedicina, Jovene, p. 127 ff.

[73]Article 2232 of Italian Civil Code provides in particular that the service provider must personally perform the task he has taken on, with substitutes and auxiliaries under his own responsibility only where the collaboration of others is permitted by contract or custom and is not incompatible with the object of the service. See Leanza C. (2020), La telemedicina: profili civilistici di responsabilità. In Rassegna di diritto farmaceutico e della salute (vol. 3), p. 531–538; Botrugno C. (2014), La diffusione dei modelli di cura a distanza: verso un 'diritto alla telesalute'?. In BioLaw Journal – Rivista di BioDiritto (Vol. 1) p. 17.

[74]In this sense, see Italian Supreme Court of Cassation, judgments no. 15857/2010 and no. 2428/1990.

[75]Amidei A. (2021), Consenso informato e risarcimento del danno per omessa informazione. In Giurisprudenza italiana (vol. 2) p. 495–501; Liberali B. (2021), Le nuove dimensioni del consenso informato: quali limiti materiali e temporali?. In BioLaw Journal (vol. 3) p. 505–519.

[76]In this sense, see Italian Supreme Court of Cassation, judgments no. 8826/2007 and no. 2285/1999.

3 Medical Devices

On the basis of the definition contained in Article 1 of Legislative Decree No. 46 of February 24, 1997,[77] medical device means any instrument, apparatus, implant, substance, or other product, including any computer software used for its operation, which, used alone or in combination with the practitioner's activity, is intended to be used in the medical sector for diagnostic and therapeutic purposes and, therefore, for the purposes of prevention, diagnosis, care, and treatment of the patient.[78]

From a historical-normative point of view,[79] in Italy, the first relevant intervention was marked by Royal Decree No. 1265 of July 27, 1934 (so-called Consolidated Law on Health),[80] which extended the control of the national authorities to medical-surgical devices other than medicines, immediately subjecting their marketing to stricter rules. Considered, in fact, to be capable of generating risks in the event of deviation from the rules of the market, these devices, although at the time very different from the current ones, had to be registered on a list kept by the Ministry of the Interior, which was also responsible for health matters at the time. The inclusion of devices in this list meant that a special authorization had to be obtained to market the product.

Then, starting in the 1980s, with the adoption of Presidential Decree No 128 of March 13, 1986,[81] while maintaining the authorization regime previously adopted, it was decided to go a step further and provide medical device manufacturers with more transparent conditions for granting authorizations.

At the same time, in Europe, the first steps were being taken toward the technical harmonization of disciplines through a system based on the distinction into families and risk categories.[82]

[77] Legislative Decree no. 46 of February 24, 1997, implementing Directive 93/42/EEC concerning medical devices, amended by Legislative Decree no. 37 of January 25, 2010. See in particular article 1, par. II, lett. (a).

[78] As clarified by the Court of Justice of the European Union in its judgment of November 22, 2010, in Case C-219/11, Brain Products GmbH v. BioSemi VOF, published in O.J.E.U. January 26, 2013, no. C26/8, for a device to be considered medical, it is not sufficient that it be used in a medical context, but it is necessary that it be specifically used for health protection purposes. See, in this regard, Veale J. R (1980), Characterization of Medical Devices. In Food, Drug, Cosmetic Law Journal (vol. 35) no. 10, p. 588–593.

[79] Parziale A. (2021), Le 'chiocciole di Bobek': il principio europeo di non-discriminazione tra assicurazione, responsabilità civile e dispositivi medici. In Danno e responsabilità (vol. 2) p. 199–206.

[80] Royal Decree no. 1265 of July 27, 1934, Approval of the Consolidated Law on Health Laws.

[81] Presidential Decree no. 128 of March 13, 1986, entitled Regulations for the implementation of the rules referred to in Article 189 of the Consolidated Text of Health Laws, approved by Royal Decree no. 1265 of July 27, 1934, and subsequent amendments, concerning the production and trade of medical-surgical aids.

[82] In particular, the Council Resolution of May 7, 1985, on a new approach to technical harmonization and standardization, published in the Official Journal of the European Communities June 4, 1985, no. C/136/1; Council Directive 90/385/EEC of June 20, 1990, on the approximation

This process of speeding up the authorization system culminated with the enactment of Directive 2007/47/EC.[83]

The entire European discipline was finally transposed into the Italian legal system with the aforementioned Legislative Decree No. 46 of February 24, 1997, as amended by Legislative Decree No. 37 of January 25, 2010, which provided for today's mechanism of ex ante self-certification of devices by manufacturers and, at the same time, the ex post supervisory power duty on the correct application of the discipline by the Ministry of Health in agreement with the Ministry of Economic Development.[84]

The detailed regulations analyzed so far must, however, be supplemented with the provisions of Legislative Decree No. 206 of September 6, 2005 (also known as the Consumer Code),[85] that set of rules dictated to regulate and protect the interests and rights of consumers,[86] considered to be the weaker parties in buying and selling relationships. These rules are also applicable to healthcare devices since they fall within the concept of "product" as defined by the Consumer Code, as "movable property, even if incorporated into other movable or immovable property".[87]

In particular, in the case of damage resulting from the use of a defective device,[88] the Consumer Code provides for the strict liability[89] of the manufacturer,[90] with

of the laws of the Member States relating to active implantable medical devices, published in the Official Journal of the European Communities, July 20, 1990, no. L189/17; Council Directive 93/42/EEC of June 14, 1993, concerning medical devices; Directive 98/34/EC of the European Parliament and of the Council of June 22, 1998, laying down a procedure for the provision of information in the field of technical standards and regulations. See Kingham R. F. (1992), Regulation of Medical Devices in the European Community. In Food and Drug Law Journal (vol. 47) no. 5, p. 563–570.

[83]Directive 2007/47/EC of the European Parliament and of the Council of September 5, 2007, amending Council Directive 90/385/EEC on the approximation of the laws of the Member States relating to active implantable medical devices, Council Directive 93/42/EEC concerning medical devices, and Directive 98/8/EC concerning the placing of biocidal products on the market.

[84]See Article 17, Italian Legislative Decree no. 46 of February 24, 1997.

[85]Italian Legislative Decree no. 206 of September 6, 2005, as last amended by Italian Law of December 23, 2021, n. 238. For a European perspective, see Passarelli G. (2020), Legal aspects of the path towards a true EU medical devices innovation. In Le nuove leggi civili commentate, (vol. 2) p. 305–324.

[86]In particular, the current Article 3, par. 1, lett. (a) of the Italian Consumer Code defines the consumer (or user) as "a natural person acting for purposes which are outside his trade, business, craft or profession". By contrast, the subsequent lett. (c) defines the professional as "the natural person or legal entity acting in the exercise of its entrepreneurial, commercial, craft or professional activity, or an intermediary thereof".

[87]See, Art. 115, par. 1 of the Italian Consumer Code.

[88]For a definition of a defective product, see Article 117 of the Italian Consumer Code.

[89]See, Article 114 of the Italian Consumer Code.

[90]Under Article 115, para. 2-bis, this means "the manufacturer of the finished product or of a component thereof, the producer of the raw material, as well as, in the case of agricultural products of the soil and in the case of those of breeding, fishing and hunting, the farmer, breeder, fisherman and hunter respectively".

an extension of liability in some cases also to the manufacturer of one or more components of the device and, in others, even to the manufacturer of the raw materials used.

While the injured party is required to prove the defect in the product, the damage suffered and the causal link,[91] the producer will instead be released by proving that the defect that caused the damage did not exist at the time the product was purchased.[92]

Moreover, due to the continuous technological development in the healthcare sector, the regulatory framework is today continuously being enriched. At the same time, there is a growing interest on the part of the European institutions in improving safety and creating an increasingly clear and innovation-friendly regulatory framework.

Examples of this are Regulation (EU) No 745/2017[93] and Regulation (EU) No 746/2017[94] on medical devices and in vitro diagnostic medical devices, the application of which was, however, postponed giving priority to the fight against the Covid-19 pandemic, an extraordinary event that has made the importance of the essential, if not vital, use of medical devices more evident than ever. Significant innovations include the introduction of a European bank (Eudamed) for greater traceability of products,[95] a more detailed definition of the obligations and responsibilities of medical professionals, and a mechanism for post-market surveillance of devices (post-market clinical follow-up [PMCF]).

Thus, while important steps are being taken to allow new innovative technologies to enter the health sector, there are still many concerns about their complete reliability and accuracy. Any errors, in fact, could not only have consequences in terms of the allocation of resources allocated to healthcare, but also serious repercussions on the individual's very life.

[91] See, Art. 120, par. 1, Italian Consumer Code.

[92] See, Art. 120, par. 2, Italian Consumer Code.

[93] Regulation (EU) No. 745/2017 of the European Parliament and of the Council of April 5, 2017, on medical devices, amending Directive 2001/83/EC, Regulation (EC) No. 178/2002 and Regulation (EC) No. 1223/2009 and repealing Council Directives 90/385/EEC and 92/42/EEC.

[94] Regulation (EU) No 746/2017 of the European Parliament and of the Council of April 5, 2017, on in vitro diagnostic medical devices and repealing Directive 98/79/EC and Commission Decision 2010/227/EU.

[95] At present, Eudamed is only used on a voluntary basis by some companies in the Member States. Passarelli G. (2018), Responsabilità civile e dispositivi medici difettosi. In Rassegna di diritto civile, (vol. 2), p. 559–592.

4 The Advent of Robotics and Artificial Intelligence in Medicine

The drive toward innovation in the medical field is such intense that it has ushered in a true technological revolution.

Practitioners have been interfacing with new systems capable of significantly modifying not only treatment pathways but also the practitioner's own decision-making mechanisms.

The frequent use of artificial intelligence in medicine constitutes an exemplary field, such as virtual assistants providing automated responses to patients or interpreting laboratory tests, and the use of robots[96] in surgery, rehabilitation procedures or tele-monitoring.

Moreover, in everyday life, the use of self-health devices capable of detecting vital health data such as heart rate, oxygen volume, and body temperature (so-called "wearable devices," such as smart watches) is becoming increasingly common.

Uncontrolled and ungoverned use of artificial agents can, however, entails considerable risks due to the absence of scientific validation or control in the processed data, or in the presence of discriminatory mechanisms (even unintentionally) introduced when programming the algorithms.

Another issue concerns the protection of personal data: artificial intelligence feeds on an enormous amount of data.[97] In most cases, we can also talk about personal data, pursuant to Regulation (EU) No. 679/2016[98] (also known as GDPR) must be observed.

[96] As defined by the Robotic Institute of America, (RIA), "a robot is a multifunctional, reprogrammable manipulator designed to move materials, parts, tools, or specialised devices through variable programmed motions to perform a variety of tasks. A robot also acquires information from the environment and moves intelligently accordingly". These are therefore machines capable of autonomously performing functions of interaction with the outside world by performing certain tasks on the basis of programmed external impulses.

[97] The Economist, The World's most valuable resource is no longer oil, but data, May 6, 2017.

[98] Regulation (EU) No 679/2016 of the European Parliament and of the Council of April 27, 2016, on the protection of individuals with regard to the processing of personal data and on the free movement of such data and repealing Directive 95/46/EC, published in OJEU 04.05.2016, L 119/1. See Lipari L. (2019), Privacy: dal Regolamento (UE) 2016/679 al d.lgs. n.101/2018. In diritto.it (February 7), arguing that: "the failure to give consent when data are processed for diagnosis and treatment (art. 2-septies of the Privacy Code amended by Legislative Decree no. 101/2018 in combination with art.9 GDPR)" would represent the transition ' "from a consensus-centric system to a system where it is necessary to first ask oneself and understand the reasons why the data are processed, and then evaluate, in light of the identified purpose, the basis of lawfulness of such processing". Available at https://www.diritto.it/privacy-dalregolamento-ue-2016-679-al-d-lgs-n-101-2018/; Finocchiaro G. (2017), Il nuovo Regolamento europeo sulla privacy e sulla protezione dei dati personali, Zanichelli, p. 101 ff.; see also Bolognini L., Pelino E. and Bistolfi C. (2016), Il Regolamento privacy europeo: commentario alla nuova disciplina sulla protezione dei dati personali, Giuffrè, p. 277 ff.

In fact, the regulation does not specifically take into account artificial intelligence applications and so-called big data, that is, mass data processing; nevertheless, there is no doubt that, where personal data relating to natural persons are processed, its principles must be respected.[99]

Prominent are the principles of lawfulness, fairness, and transparency laid down in Article 5, par. 1, lett. (a) GDPR.[100] In this respect, Chapter III of the Regulation, and in particular Article 12 of the GDPR, clarifies specific obligations on the data controller,[101] requiring it to take appropriate measures to provide the data subject with all the information referred to in Articles 13 and 14 of the GDPR and the notices referred to in Articles 15 to 22 and Article 34 of the GDPR in a concise, transparent, intelligible, and easily accessible form and in plain and intelligible language.[102]

Also relevant are all the other principles dictated by Article 5 of the GDPR and, in particular, the principles of purpose limitation,[103] data minimization,[104]

[99]For an in-depth discussion of the topic, see Pizzetti F. (2018), Artificial Intelligence, Data Protection and Regulation, Giappichelli and Pivatelli I., Privacy, security and ethics in the use of Big Data and Artificial Intelligence. In ICT Security Magazine, February 10, 2021.

[100]Article 5, Principles relating to processing of personal data, par. 1 "Personal data shall be: (a) processed lawfully, fairly and in a transparent manner in relation to the data subject ('lawfulness, fairness and transparency')".

[101]Pursuant to Article 12, par. 1, Reg EU 2016/679 (GDPR) "Transparent information, communication and modalities for the exercise of the rights of the data subject", The controller shall take appropriate measures to provide any information referred to in Articles 13 and 14 and any communication under Articles 15 to 22 and 34 relating to processing to the data subject in a concise, transparent, intelligible and easily accessible form, using clear and plain language, in particular for any information addressed specifically to a child. The information shall be provided in writing, or by other means, including, where appropriate, by electronic means. When requested by the data subject, the information may be provided orally, provided that the identity of the data subject is proven by other means.

[102]Serveto M. M. (2020), Exercising GDPR Data Subjects Rights: Empirical Research on the Right to Explanation of News Recommender Systems. In European Data Protection Law Review (vol. 6:4) p. 593–601. See also Art 29 Working Party, Guidelines on consent under Regulation 2016/679, last revised on April 10, 2018, WP259 rev.01.

[103]Article 5, GDPR, par. 1, lett. (b) "collected for specified, explicit and legitimate purposes and not further processed in a manner that is incompatible with those purposes; further processing for archiving purposes in the public interest, scientific or historical research purposes or statistical purposes shall, in accordance with Article 89(1), not be considered to be incompatible with the initial purposes ('purpose limitation')".

[104]Article 5, GDPR, par. 1, lett. (c) "adequate, relevant and limited to what is necessary in relation to the purposes for which they are processed ('data minimisation')".

accuracy,[105] storage limitation,[106] integrity and confidentiality,[107] and the accountability[108] of the data controller.

As for the existence of automated decision-making processes, without prejudice to the data subject's duty to provide information and right of access,[109] the data subject has the right not to be subject to a decision based solely on automated processing, including profiling, that produces legal effects on him/her (Article 22 GDPR).[110] The provision does not actually refer to automated decisions (as in the case of artificial intelligence), but only to making decisions by automated systems.

A further issue is then marked by the choice of who is to be identified as the data controller, an attribution that, as will be seen shortly, also has implications in terms of liability.[111]

In short, the development of artificial agents in medicine is certainly capable of offering new opportunities for protection, but at the same time it may expose patient-users to risky situations, such as the illicit instrumentalization of data, or even damage resulting from product malfunctioning. These innovations require a careful weighing up of the risks to the fundamental freedoms of the individual.[112]

[105] Article 5, GDPR, par. 1, lett. (d) "accurate and, where necessary, kept up to date; every reasonable step must be taken to ensure that personal data that are inaccurate, having regard to the purposes for which they are processed, are erased or rectified without delay ('accuracy')".

[106] Article 5, GDPR, par. 1, lett. (e) "kept in a form which permits identification of data subjects for no longer than is necessary for the purposes for which the personal data are processed; personal data may be stored for longer periods insofar as the personal data will be processed solely for archiving purposes in the public interest, scientific or historical research purposes or statistical purposes in accordance with Article 89(1) subject to implementation of the appropriate technical and organisational measures required by this Regulation in order to safeguard the rights and freedoms of the data subject ('storage limitation')".

[107] Article 5, GDPR, par. 1, lett. (f) "processed in a manner that ensures appropriate security of the personal data, including protection against unauthorised or unlawful processing and against accidental loss, destruction or damage, using appropriate technical or organisational measures ('integrity and confidentiality')".

[108] Article 5, GDPR, par. 2, "The controller shall be responsible for, and be able to demonstrate compliance with, paragraph 1 ('accountability')".

[109] See in particular Articles 13, par. 2, lett. (f) and art. 14, par. 2, lett. (g) of the GDPR with regard to duties of information and Article 15(I)(h) of the GDPR with regard to the data subject's right of access.

[110] Article 22, dedicated to automated individual decision-making, including profiling, stated that "The data subject shall have the right not to be subject to a decision based solely on automated processing, including profiling, which produces legal effects concerning him or her or similarly significantly affects him or her. 2. Paragraph 1 shall not apply if the decision: (a) is necessary for entering into, or performance of, a contract between the data subject and a data controller; (b) is authorised by Union or Member State law to which the controller is subject and which also lays down suitable measures to safeguard the data subject's rights and freedoms and legitimate interests; or (c) is based on the data subject's explicit consent".

[111] Finocchiaro G. (2020), Riflessioni su intelligenza artificiale e protezione dei dati personali. In Intelligenza artificiale. Il diritto, i diritti, l'etica, Ruffolo U. (eds), Giuffrè.

[112] Mariani L., Pegoraro R., Ruggiu D. (2019), Population health, Big Data and integrated systems. An ethical proposal, Piccin-Nuova Libraria.

The right to health is protected as a fundamental right under the Constitution, as also an expression of the right to human dignity.[113] Article 32 of the Italian Constitution states in particular: "The Republic protects health as a fundamental right of the individual and an interest of the community, and guarantees free care to the indigent. No one may be obliged to undergo any particular health treatment except by provision of law. The law may in no case violate the limits imposed by respect for the human person". As then reiterated by the Constitutional Court, "the balancing of constitutional values and the commensuration of objectives determined by existing resources cannot undermine the inalienable core of the right to health constitutionally protected as an inviolable value of human dignity".[114] Therefore, it is necessary at all costs to avoid those situations that, in the absence of protection, affect or prejudice the implementation of inviolable rights.

Despite these critical issues, however, for several years now the idea has been gaining ground that a development toward medical innovation is capable of leading concretely toward an improvement in the quality of the services provided.

In particular, the Ministry of Health has specified that "the activation of a pathway for the dissemination of the use of technology in health services based on telemedicine and teleassistance, electronic medical records, artificial intelligence technology platforms, point-of-care diagnostics, and platforms for patient empowerment for public health education is considered of fundamental importance".[115]

Given also the rapid spread, to direct the legislature to regulate these new forms of technology truly becomes a priority, also in order to prevent the interpretative and "regulatory" overload from once again affecting the work of judges.

[113]Luciani M. (2002), I diritti costituzionali tra Stato e regioni (a proposito dell'art. 117, comma 2, lett. (m), della Costituzione. In Sanità pubblica (vol. 12), P. 1025 ff. On the reasons for exclusive competence attribution to the Central Government, which could be exercised also in the transversal sectors, see Gallo C. E. (2002), La potestà legislativa regionale concorrente, i diritti fondamentali ed. i limiti alla discrezionalità del legislatore davanti alla Corte costituzionale. In Il Foro amministrativo – CdS, p. 2791 ff; Cavallo Perin R. (2016), L'organizzazione delle pubbliche amministrazioni e l'integrazione europea. In L'organizzazione delle pubbliche amministrazioni tra stato nazionale e integrazione europea, Cavallo R., Police A., Saitta F. (eds.), Firenze University Press, p. 3 ff.

[114]Italian Constitutional Court, judgment no. 509/2000.

[115]This is what the Ministry of Health specified in the 2021 Guidelines. For a more detailed discussion of the topic of digital transformation in healthcare, see, in particular, point 5.3 of Guidelines.

5 Liability Profiles of Artificial Agents

On the subject of the liability of artificial agents,[116] the literature is still divided between those who consider the need to introduce new legal categories and those who, on the other hand, believe that the phenomenon can be adapted to already established legal categories.[117]

In the absence of an ad hoc legal framework, it is inevitable to start from the already existing rules. Among the alternatives considered by the doctrine, we can consider in particular: vicarious liability of the owner,[118] liability of the agent,[119] and the already mentioned producer liability.[120]

Therefore, the distinction can be rooted within the ontological conception of an artificial agent[121]: against all, can a robot be held autonomously liability for its

[116] A brief overview can be provided by the Report from the Expert Group on Liability and New Technologies – New Technologies Formation, "liability for artificial intelligence and other emerging digital technologies," available at https://www.europarl.europa.eu/meetdocs/2014_2019/plmrep/COMMITTEES/JURI/DV/2020/01-09/AI-report_EN.pdf. By providing a general Overview of existing liability regimes (p. 15), it states that "The law of tort of EU Member States is largely non-harmonised, with the exception of product liability law under Directive 85/374/EC, some aspects of liability for infringing data protection law (Article 82 of the General Data Protection Regulation (GDPR), and liability for infringing competition law (Directive 2014/104/EU)".

[117] Bob Kocher & Zeke Emanuel (2019), Will Robots Replace Drs.?. In The Brookings Institute, https://www.brookings.edu/blog/usc-brookingsschaeffer-on-health-policy/2019/03/05/will-robots-replace-doctors/. See also Terry N. (2019), Of Regulating Healthcare AI and Robots. In Yale Journal of Law and Technology, (vol. 21:3), P. 144–147. As the Author observed, the American Medical Association (AMA) passed its first policy recommendations for Al in June 2018: see Press Release, Am. Med. Assn., AMA passes first policy recommendation on augmented intelligence (June 14, 2018), available at https://www.ama-assn.org/press-center/press-releases/ama-passes-firstpolicy-recommendations-augmented-intelligence. AMA position seems very interesting: thus, AMA policy preferred the phrase 'augmented intelligence'. Moreover, the Author concluded that (p. 137) "In a supporting document, the AMA noted that, in health care, a more appropriate term is 'augmented intelligence' (AI) because it reflects the enhanced capabilities of human clinical decision making when coupled with these computational methods and systems". Of course, that labelling hides a conclusion; that the physician, not the AI, will have primacy. "Artificial intelligence" is also viewed by some as threatening, perhaps explaining why Google now just uses the acronym "AI."

[118] Schaerer E., Kelley R. and Nicolescu M. (2009), Robots as animals: a framework for liability and responsibility in human-robot interactions, 18th IEE International Symposium on Robot and Human Interactive Communication.

[119] Mathias A., The Responsibility Gap: Ascribing Responsibility for the Actions of Learning Automata, in Ethics and Information Technology, fasc. 6, 2004, pp. 175 ff.

[120] Bertolini A., Robots and liability – Justifying a change in perspective, in F. Battaglia, J. Nida-Rümelin, N. Mukerji (eds.), Rethinking Responsibility in Science and Technology, Pisa University Press, 2014. See also Bruno S. and Divino S. (2020), Critical Considerations on Artificial Intelligence Liability: E-Personality Propositions. In Revista Eletronica Direito e Sociedade (vol. 8) no. 2, p. 193–214.

[121] Maddox T. M., Rumsfeld J. S. and Payne P. R. O. (2019), Questions for Artificial Intelligence in Health Care. In JAMA. (vol. 321:1) p. 31–32.

own actions? Besides, how should the responsibility of the health professional who uses it be declined? Think of an artificial intelligence device that misdiagnoses and, consequently, the doctor fails to administer the correct therapy, causing harm to the patient.[122]

In most cases, medical devices, even acting in autonomy, need to be controlled and validated since they have to provide precision services, carrying out corrective (but nevertheless complementary) actions toward human medical activity.[123]

In the case of artificial intelligence, the critical issues are not so much inherent in its computational capabilities, but more in its self-learning capacity (or machine-learning), which can create distortions in its functioning. The aim, therefore, is to be able to reassure users that, in the event of damage, there will still be compensation.[124]

Starting from the vicarious liability of the owner, reference must be made to Article 2051 of the Civil Code relating to damage caused by a thing in custody; the liberating proof of the custodian lies in the demonstration of having adopted all appropriate measures for the prevention of the harmful event.[125] The critical point, on the other hand, arises from the fact that, in order to justify an imputation to the custodian, it is necessary for him to have objective control over the property.[126] Can this be applied to an artificial intelligence system? And again, given that Article 2051 refers to damage that is caused directly by the artificial agent, what happens in the case of human intervention?

In line with this reasoning, alternative arguments have been developed, including references to Article 2052 of the Civil Code upon the custody of the animal[127] and Article 2048, para. II of the Civil Code on the liability of the tutor.[128]

According to these opinions, artificial intelligence could be compared, in the first case, to animals, with consequent liability of its owner or user and, in the second case, to that of a learning human being, with consequent liability of the one who imparted the teachings.

[122]Griffin F. (2021), Artificial Intelligence and Liability in Health Care. In Health Matrix: Journal of Law-Medicine (vol. 31) p. 65–106, available at https://ssrn.com/abstract=3850983

[123]Bambauer J. R. (2017), Dr. Robot. In 51 UC Davis Law Review 383, Arizona Legal Studies Discussion Paper No. 17–28, available at https://ssrn.com/abstract=3087983

[124]Finocchiaro G. (2019), Intelligenza Artificiale e protezione dei dati personali. In Giurisprudenza Italiana (vol. 7) p. 1676 ff.

[125]Article 2051 of Italian Civil Code states: “Everyone shall be liable for the damage caused by things in his custody, unless he proves unforeseeable circumstances”.

[126]Costanza M. (2019), L’Intelligenza Artificiale e gli stilemi della responsabilità civile. In Giurisprudenza Italiana (vol. 171:7) p. 1688 ff.

[127]Ruffolo U., Per i fondamenti di un diritto della robotica. In Intelligenza artificiale e responsabilità, Giuffré, p. 15 ff.

[128]Although this is a minority doctrine, see Santosuosso A., Boscarato C., Caroleo F. (2012), Robot e diritto: una prima ricognizione. In La nuova giurisprudenza civile commentata (vol. 28:8) p. 1–23.

Even these reconstructions, however, have not been without criticism. On the one hand, the substantial difference between animals and artificial intelligence: it can be set in their own instinctive behavior, which drive them to deflect their activities for which they are domesticated. On the other hand, it was emphasized that the instructions given to an algorithm has a far greater weight in determining behavior than that given to a human being.

According to other doctrine, Article 2050 of the Civil Code on the exercise of dangerous activities could apply,[129] with the consequent liability of the user of the artificial agent who fails to provide proof that he did everything possible to avoid the damage.[130] Even in this case, however, the tasks entrusted to artificial intelligence would seem to clash with the very concept of dangerous activity: more often, the artificial agent goes to make up for human failures of precision, as in the case of robots used in surgical operations.

Is it therefore possible to configure as a dangerous activity something capable of guaranteeing a higher level of precision? Not a few difficulties would then arise at the evidentiary level[131]: it would be difficult to determine the borderline between liability for the surgeon's malpractice under Article 2043 of the Civil Code and product-robot defect.

Lastly, the potential application of Article 2049 of the Civil Code has also been identified,[132] which, on the subject of the liability of masters and principals, establishes their liability "for damage caused by the wrongful act of their servants and committed in the exercise of the duties to which they are assigned." Whereas the artificial agent is considered to be the "employee" of the doctor, the damage caused would be attributable to the person who availed itself of his work. However, even in this case it is difficult to believe that an analogical extension of this institution could go beyond human conduct.

On the European scene, on the other hand, there have been interventions by institutions that have encouraged the adoption of specific sectoral rules, as well as aimed at considering an adaptive interpretation of already existing precepts as

[129] Article 2050 of Italian Civil Code: "Liability arising from exercise of dangerous activities. Whoever causes injury to another in the performance of an activity dangerous by its nature or by reason of the instrumentalities employed, is liable for damages, unless he proves that he has taken all suitable measures to avoid the injury". See Cardillo S. and Schaefer H. B. (2022), A Model for Europe? The Enhanced Level of Due Care in Article 2050 of the Italian Civil Code, A Theoretical and Empirical Study of its Content and Effects. Available at https://ssrn.com/abstract=4144092 and https://doi.org/10.2139/ssrn.4144092

[130] Comporti M. (2009), Fatti illeciti: le responsabilità oggettive. In Commentario Schlesinger, Giuffrè, p. 172 ff.

[131] Boscarato C. (2015), Robotics, Innovation and Law. In The challenge of Innovation Law, Pavia University Press, p. 233.

[132] Article 2049 of Italian Civil Code: "Liability or masters or employers. Masters and employers are liable for the damage caused by an unlawful act of their servants and employees in the exercise of the functions to which they are assigned".

a starting point.[133] In this regard, the Resolutions of the European Parliament of February 16, 2017,[134] and February 12, 2019,[135] become relevant. They standardize the regulation of aspects related to the use of artificial agents also in the health sector and Directive 85/374/EEC[136] on artificial intelligence and product liability.[137]

[133] Amidei A. (2017), Intelligent robotics and liability: profiles and evolutionary perspectives of the European regulatory framework. In U. Ruffolo (ed.), Intelligenza artificiale e responsabilità, Giuffrè, 2017, pp. 63 ff. Moreover, an important report published at the end of 2019 on the transformation of civil liability in the era of digitalization, called "Liability for Artificial Intelligence and other emerging digital technologies", by 'Expert Group on Liability and New Technologies – New Technologies Formation', appointed by the European Commission, available at https://www.europarl.europa.eu. For a detailed dialogue with this text, see, Barbosa M. M. (2020), O futuro da responsabilidade civil desafiada pela inteligência artificial: as dificuldades dos modelos tradicionais e caminhos de solução. In Revista de Direito da Responsabilidade (vol. 2) p. 280–326.

[134] European Parliament resolution of February 16, 2017, with recommendations to the Commission concerning civil law rules on robotics, published in OJEU 18.07.2018, No. C252/239. For a further investigation, see Navas, S. (2020). Robot Machines and Civil Liability. In M. Ebers & S. Navas (Eds.), Algorithms and Law, Cambridge University Press, p. 157–173. See also Sousa Antunes H. (2020), Civil Liability Applicable to Artificial Intelligence: A Preliminary Critique of the European Parliament Resolution of 2020, available at https://ssrn.com/abstract=3743242 or https://doi.org/10.2139/ssrn.3743242

[135] European Parliament resolution of February 12, 2019, on a comprehensive European industrial policy on robotics and artificial intelligence, available at https://eur-lex.europa.eu/legal-content/GA/TXT/?uri=CELEX:52019IP0081. Recital 72 states that "Notes the impact that AI has already had on wellbeing, prevention, diagnosis and research and its great potential for designing personalised care; considers that this ultimately leads to a more sustainable, efficient and outcome-based healthcare ecosystem". Compare in particular point no. 77 and 78: "(77). Stresses, however, that the existing system for the approval of medical devices may not be adequate for AI technologies; calls on the Commission to closely monitor progress on these technologies and to propose changes to the regulatory framework if necessary in order to establish the framework for determining the respective liability of the user (doctor/professional), the producer of the technological solution, and the healthcare facility offering the treatment; points out that legal liability for damage is a central issue in the health sector where the use of AI is concerned; stresses the need therefore to ensure that users will not be led invariably to back the diagnostic solution or treatment suggested by a technological instrument for fear of being sued for damages if, on the basis of their informed professional judgement, they were to reach conclusions that diverged even in part; (78). Calls on the Member States and the Commission to increase funding in health-related AI technologies in the public and private sectors; welcomes, in this context, the declaration of cooperation signed by 24 EU Member States and Norway with a view to boosting the impact of investments in AI at European level; calls on the Member States and the Commission to consider whether training programmes for medical and healthcare personnel should be updated and standardised on a Europe-wide basis so as to ensure high levels of expertise and a level playing field in the Member States as regards knowledge and use of the most advanced technological instruments in robotic surgery, biomedicine, and AI-based biomedical imaging". For a further information see Rodrigues R., Legal and human rights issues of AI: Gaps, challenges and vulnerabilities. In Journal of Responsible Technology (vol. 4) available at https://doi.org/10.1016/j.jrt.2020.100005

[136] Council Directive 85/374/EEC of July 25, 1985, on the approximation of the laws, regulations and administrative provisions of the Member States concerning liability for defective products.

[137] As a matter of fact, the European Resolution of 2017 paid greater attention to the effectiveness of the 1985 Directive. Thus, it is said that "whereas, as regards non-contractual liability, Directive

All these interventions, in parallel with the initiatives promoted by the European Commission,[138] while continuing to favor the use of new technologies, have expressed fears regarding the possible responsibility gap that could be created in the event of damage caused by the artificial agent. Therefore, they continue to recommend a "human–centric" approach, thus stopping the possibility of human control and intervention.[139]

However, as yet unregulated, several paths are suggested to fill "responsibility gaps."

Firstly, the European Parliament Resolution of February 16, 2017, proposes two alternative liability models: strict liability and the risk management approach.[140]

In the first case, which disregards the subjective element of culpability, it is only necessary to prove the damage suffered and the causal link, while in the second case it is necessary to focus on the role of the person who, depending on the case, is able to minimize the risk and deal with its negative impact. In other words, this second institute would make it possible to identify as liable the party causally closest to the malfunctioning product.

The regulation of product liability could then provide further indications on how to decline the liability of the parties involved. In particular, the regulatory contribution was provided by the aforementioned Directive 85/374/EEC, merged into the Italian Consumer Code,[141] which regulates compensation for damage caused by defective products according to the scheme of direct producer liability. According to this perspective, for example, the artificial intelligence algorithm would be considered as part of the product and the relative liability would be allocated to the person who devised the relative system.

85/374/EEC can cover only damage caused by a robot's manufacturing defects and on condition that the injured person is able to prove the actual damage, the defect in the product and the causal relationship between damage and defect, therefore strict liability or liability without fault framework may not be sufficient [...] notwithstanding the scope of Directive 85/374/EEC, the current legal framework would not be sufficient to cover the damage caused by the new generation of robots, insofar as they can be equipped with adaptive and learning abilities entailing a certain degree of unpredictability in their behaviour, since those robots would autonomously learn from their own variable experience and interact with their environment in a unique and unforeseeable manner".

[138] Communication from the Commission to the European Parliament, the Council, the European Economic and Social Committee and the Committee of the Regions of April 25, 2018, No 237, Artificial Intelligence for Europe, available at https://eur-lex.europa.eu/legal-content/EN/TXT/?uri=COM%3A2018%3A237%3AFIN

[139] This concept was also supported by the Ethics Guidelines for Trustworthy AI of April 8, 2019, developed by an expert group set up by the European Commission. See for further discussion, chapter 3, para. 8 of this monographs.

[140] See in particular points 53–55 of the aforementioned European Parliament Resolution of February 16, 2017.

[141] Decree of September 6, 2005, no. 206.

In a more radical sense, another approach has been taken, which sees the recognition of legal (or rather, electronic) personality to the most sophisticated robots capable of autonomous decision-making.[142]

However, this personality should only be conceived as a fictio aimed at the creation of patrimonial autonomy in such a way that the economic effects of liability are directly traced back to the machine, with consequent burden-sharing among those who have financed the associated assets through the creation of a special fund.[143]

Different solutions, therefore, can also be drawn in the European landscape.

Although the hope is to arrive at a regulated framework soon, given the importance of the topic, there is no lack of interpretative efforts to bring the phenomenon within the existing regulatory framework.

6 Deontological Issues

Thanks to their special features, robots and artificial intelligence algorithms might be destined to substitute the role of doctors in clinical reasoning and in determining therapeutic paths. Thus, it seems hard to imagine that the rules of ethics can be confined just to amoral and social ground.

In this regard, the current Italian Code of Medical Ethics defines a set of rules inspired by principles of medical ethics, committing the health professional to protecting health according to principles of dignity, decorum, independence, and quality of the profession.

The doctor has to know and respect the Code of Ethics to the extent that any noncompliance or violation, even if resulting from ignorance, constitutes a disciplinary offense, assessable according to the terms and procedures laid down by the medical professional order, which has the relevant (and autonomous) disciplinary power.

The codictic system now provides for a series of provisions relating to situations of deontological importance that constitute the most recurrent cases.

In terms of technological innovation, we speak in particular of telemedicine.

[142] Taddei Elmi G. (1995), I diritti dell'intelligenza artificiale, tra soggettività e valore: fantadiritto o ius condendum? in Lombardi Vallauri L. (ed.), Il meritevole di tutela, studi per una ricerca, Giuffrè, p. 685–711.

[143] Consequent also are the spin-offs in insurance terms, as already noted by Parliament in the aforementioned Resolution of February 16, 2017. See in particular point 57, where the Parliament "stresses that a possible solution to the problem of the complexity of attributing liability for damage caused by increasingly autonomous robots could be a compulsory insurance scheme, as is already the case, for example, with cars; it notes, however, that unlike the insurance scheme for motor vehicles, which covers human actions or errors, the insurance of robots should take into account all potential liabilities along the chain".

In the use of information and communication technologies in healthcare, Article 78 of the Code[144] requires compliance with the criteria of proportionality, appropriateness, effectiveness, and security, as well as with the rights of the personality and the application guidelines set out in the same Code of Ethics. In fact, the professional must respect the same principles that govern the use of any other instrument aimed at the exercise of the medical profession and avoid any distorted or illusory use, assuming deontological responsibility in the event of violations.

Although technology can in fact guarantee higher quality and efficiency in healthcare provision, a balancing act must always be performed in terms of cost and benefit to the patient.

Other duties relating to the use of IT tools in healthcare[145] include those of acquiring consent to process personal data, of confidentiality, and of eliminating all forms of discrimination.

Not of secondary importance is the level of accessibility of telemedicine, which, if not guaranteed equally, could lead to discriminatory effects.

In fact, despite the digital evolution, there is still a considerable segment of the population, mainly consisting of the elderly and functionally disabled, who have difficulties in using IT tools. Hence, the doctor must commit himself to working together to eliminate all forms of unequal treatment in the use of information technology, guaranteeing equal access to health services for all.

On the other hand, from the point of view of safety, the doctor must only use reliable systems aimed at the most appropriate management of the relationship with the patient, justifying the reasonableness of the individual choices of use on the basis of the clinical and scientific findings related to the concrete case. This also includes using specific procedures and simulation systems to protect patient safety.

The subject of computerization in the field of medical ethics is therefore a very delicate issue.

The health professionals should aim at exploiting technology to promote efficiency and personalization of services, but carrying out a balancing evaluation in terms of costs and benefits for the patient.

The current technological revolution caused by the advent of robots and artificial intelligence in medicine, however, seems to be a different matter altogether.

In fact, in the absence of a discipline to regulate these phenomena, in December 2021, the Federazione Nazionale Ordine Medici Chirurghi e Odontoiatri (FNOMCeO) (National Federation of the Order of Surgeons and Dentists) has decided on the imminent revision of the Italian Code of Medical Ethics.[146] The President of the Federation announced it, hoping for an indispensable update with

[144] Article 78, under the heading "information Technology", is specifically included in Title XVIII, the last title of the Italian Code of Medical Ethics, which is dedicated to "Computerisation and Healthcare Innovation".

[145] See the Application Guidelines attached to Article 78, Information Technology.

[146] See https://portale.fnomceo.it/nuovo-codice-per-medico-dell-oggi-e-del-domani-anelli-al-consiglio-nazionale-fnomceo/

a view to "combining our history, our ethical-deontological principles with the new requirements of a new role for the profession in a society that is completely different from that of the past".

Thus, a group of experts consisting of jurists, university professors of medical-scientific disciplines, and representatives of the professional orders of physicians and dentists began work in Rome in June 2022. The group began examining the principles and regulations that today govern the exercise of the medical profession to verify their appropriateness in light of the profound changes that have taken place on a cultural, social, and, above all, technological level.

7 Protection of Personal Health Data

The processing of personal data in the health sector is a prerequisite for an efficient system.[147] Indeed, the availability and use of health data are not only essential for treatment and care purposes, but also useful for secondary purposes such as research or, for example, the maintenance of Electronic Health Records.[148]

Health data, in fact, can be attributed both a function of aiding the patient's diagnostic-therapeutic pathway and a function of making the health system more efficient.

Similarly, the effective use of artificial agents in medicine is strongly linked to the use of significant amounts of data that, given their particular nature, requires levels of protection that are not reduced to a mere formal compliance with the rules on the subject, but are actually parameterized to the levels of risk and the specifics of the individual case.[149]

Without obscuring the advantages of the correct use of data, it is also necessary to analyze the critical aspects of data processing activities, under the aforementioned profile of the protection of personal data relating to individuals, as well as from the point of view of system security and confidentiality.[150]

[147] Artificial intelligence, robotics, privacy, and data protection. In Background document for the 38th international conference of data protection and privacy commissioner, at https://edps.europa.eu/sites/default/files/publication/16-10-19_marrakesh_ai_paper_en.pdf

[148] For more information, see https://www.fascicolosanitario.gov.it/. See also Rossi A. and Maceratini R. (2000), La cartella clinica elettronica. In Maceratini R. and Ricci F. (eds.), Il medico online – Manuale di informatica medica, Verduci; Fiaschi A., Fascicolo Sanitario Elettronico: i rischi per la data protection delle politiche di sanità integrata. In cybersecurity.it. (January 28, 2000).

[149] Galletta D. U., La Pubblica Amministrazione nell'era delle ICT: digital one-stop-shop and artificial intelligence at the service of transparency and citizens?, in Ciberspazio e Diritto, (vol. 3), pp. 319–336.

[150] For an in-depth study of the vast topic concerning the processing of personal data in the health sector, see the contributions by Iaselli M. (2020), La tutela dei dati personali in ambito sanitario, Giuffré; Tommasi N. and Vanoncini G. (2020), GDPR in sanità: una linea guida ragionata,

Pursuant to Regulation (EU) No 679/2016, data relating to health are afforded enhanced protection as they are likely to expose the data subject to forms of discrimination linked even to their mere disclosure. They are in fact included among the so-called "special categories of data" pursuant to Article 9 GDPR.

Health data is defined in Article 14, par. 1[151] and 15 of GDPR as data "relating to the physical or mental health of a person, including the provision of health care services, which disclose information relating to his or her state of health". Moreover, pursuant to Recital 35, health data includes all data that reveal information relating to the past, current, or future physical or mental health status of the data subject.

In fact, the boundaries of the concept of health data have been the subject of heated conflicts of interpretation. On this point, with Recommendation No. (97) 5,[152] the Council of Europe considered health data to be all data of a personal nature relating to a person's health, referring equally to data having a close and manifest link with health, as well as genetic data. The latter are in particular defined by Article 4(I)(13) GDPR as those personal data relating to the hereditary genetic characteristics of the data subject.

Biometric data, as defined in Article 4, par. 1, lett. 14 of GDPR, means data obtained by specific technical processing that enables or confirms the unambiguous identification of a subject, such as facial image or dactyloscopic data, are also likely to be linked to health status.[153]

Under Article 9 of the GDPR,[154] the processing of health data is generally prohibited, except in certain exceptional cases. As underlined by the legal scholars, the conditions of lawfulness that allow the processing of health data, as an exception to the general prohibition, can be traced to two categories: the first deals with the private sphere, while the second to the public sphere.[155]

Outsphera; Muià P. P. (2018), La tutela della privacy in ambito sanitario, Maggioli; Tarallo P. (2017), La tutela dei dati nel settore salute, EPC.

[151] Article 14, GDPR, Information to be provided where personal data have not been obtained from the data subject, stated that: "Where personal data have not been obtained from the data subject, the controller shall provide the data subject with the following information: (a) the identity and the contact details of the controller and, where applicable, of the controller's representative".

[152] Recommendation No. (97) 5 of the Council of Europe – Committee of Ministers to Member States of February 13, 1997, on health data protection.

[153] Pursuant to Article 4 GDPR, biometric data "means personal data resulting from specific technical processing relating to the physical, physiological or behavioural characteristics of a natural person, which allow or confirm the unique identification of that natural person, such as facial images or dactyloscopic data".

[154] Article 9 GDPR, Processing of special categories of personal data, stated that: "Processing of personal data revealing racial or ethnic origin, political opinions, religious or philosophical beliefs, or trade union membership, and the processing of genetic data, biometric data for the purpose of uniquely identifying a natural person, data concerning health or data concerning a natural person's sex life or sexual orientation shall be prohibited".

[155] On this point, see Melchionna S.- Cecamore F. (2019) Le nuove frontiere della sanità e della ricerca scientifica, in Panetta R. (ed.), Circulation and protection of personal data, between freedom

In particular, conditions for legitimacy are found in cases of processing necessary for "purposes of preventive medicine or occupational medicine, assessment of the employee's capacity for work, health or social diagnosis, care or treatment, or the management of health or social systems and services on the basis of Union or Member State law or in accordance with a contract with a health professional" (Article 9(II)(h)), or for "public interest in the area of public health, such as protection against serious cross-border threats to health or ensuring high standards of quality and safety of health care and social security" (Article 9(II)(h)). II(h)), or for "reasons of public interest in the area of public health, such as protection against serious cross-border threats to health or ensuring high standards of quality and safety of health care and of medicinal products and medical devices" (Article 9(II)(i)). The processing of health data is also allowed for the purposes of "archiving in the public interest, scientific or historical research or statistical purposes (...) on the basis of Union or national law" (Article 9(II)(j)) and when "necessary for reasons of public interest identified on the basis of Union or Member State law" (Article 9(II)(g)).

In addition to these conditions, each Member State may then introduce further conditions or provide for limitations.[156] In Italy, for example, Article 9 of Decree-Law No. 139 of October 8, 2021,[157] amended Article 2-sexies of Legislative Decree No. 196 of June 30, 2003[158] (also known as the Privacy Code), on the processing of special categories of personal data necessary for reasons of substantial public interest.

This attention paid by the Italian and European legislator to the protection of the rights of the data subject is based on the major interests at stake: on the one hand, the right to health and, on the other, the right to protect data relating to health. Since this

and market rules. Commentary on EU Regulation No. 679/2016 and Legislative Decree 101/2018, Giuffrè, p. 585 ff.

[156]Thus, also Article 9(IV) GDPR.

[157]Italian Decree-Law No.139 of October 8, 2021, containing urgent provisions on access to cultural, sporting and recreational activities, as well as on the organization of public administrations and on the protection of personal data, converted with amendments into Law No. 205 of December 3. In particular, Article 9 (V) stipulated that "Articles 2-ter(1), 2-sexies(1) and 58(1) and (2) of the code referred to in Legislative Decree No. 196 of 2003 [...], as amended by this Article, shall also apply to cases where legal provisions already in force stipulate that the types of data that may be processed, the operations that may be carried out, the relevant public interest ground, the purpose of the processing as well as the appropriate and specific measures to protect the fundamental rights of the data subject and his interests are laid down by one or more regulations".

[158]Italian Legislative Decree no. 196 of June 30, 2003, Personal Data Protection Code, containing provisions for the adaptation of the national system to Regulation (EU) no. 2016/679 of the European Parliament and of the Council of April 27, 2016, on the protection of individuals with regard to the processing of personal data and on the free movement of such data and repealing Directive 95/46/EC (title as amended by Article 1, co. I of Legislative Decree no. 101 of August 10, 2018).

relationship is liable to give rise to conflicting profiles, the legislator has preferred to strike a balance himself, dictating detailed rules on processing in the health sphere.

As for the use of digital tools in medicine, a last and no less important junction is determined by the necessary trust of citizens in the legitimacy of the processing of their personal data.

In this regard, Regulation (EU) No 679/2016 crystallizes two relevant cardinal principles: privacy by design and privacy by default (Article 25 GDPR[159]),[160] imposing, on the one hand, compliance with the principles and rules on the protection of personal data right from the design phase of each process (also at the level of technical and IT solutions) and, on the other hand, the adoption of technical and organizational measures to ensure that only the personal data necessary for each specific processing purpose are processed.

In a nutshell, the interaction between the health and digital world makes it more necessary than ever to strike a proper balance between technological development and the protection of personal data. Although, in fact, indissolubly linked, the right

[159]Article 25 GDPR, Data protection by design and by default, stated that: "1. Taking into account the state of the art, the cost of implementation and the nature, scope, context and purposes of processing as well as the risks of varying likelihood and severity for rights and freedoms of natural persons posed by the processing, the controller shall, both at the time of the determination of the means for processing and at the time of the processing itself, implement appropriate technical and organisational measures, such as pseudonymisation, which are designed to implement data-protection principles, such as data minimisation, in an effective manner and to integrate the necessary safeguards into the processing in order to meet the requirements of this Regulation and protect the rights of data subjects. 2. The controller shall implement appropriate technical and organisational measures for ensuring that, by default, only personal data which are necessary for each specific purpose of the processing are processed. That obligation applies to the amount of personal data collected, the extent of their processing, the period of their storage and their accessibility. In particular, such measures shall ensure that by default personal data are not made accessible without the individual's intervention to an indefinite number of natural persons. 3. An approved certification mechanism pursuant to Article 42 may be used as an element to demonstrate compliance with the requirements set out in paragraphs 1 and 2 of this Article". See Cortese B. (2013), La protezione dei dati di carattere personale nell'Unione europea dopo il trattato di Lisbona. In Diritto dell'unione Europea (vol. 2) p. 313 ff.

[160]Giannakakis J. E. (2017), Privacy by Design (PbD) and Transparency Requirements under the General Data Protection Regulation (GDPR) as Fraud Prevention Tools. In International Journal for the Data Protection Officer, Privacy Officer and Privacy Counsel (Vol. 1:2) p. 8–11. Calzolaio S. (2017), Privacy by design. Principi, dinamiche, ambizioni del nuovo Reg. Ue 2016/679. Commento a Reg. UE 2016/679. In federalismi.it (vol. 24) p. 21 ff; Véliz C. (2019), Medical Privacy and Big Data. In Philosophical Foundations of Medical Law, p. 306 ff; Vergottini G. and Carlo Bottari C. (2018), La sanità elettronica. Bononia University Press. Tsormpatzoudi P., Berendt B. and Coudert F (2016), Privacy by design: from research and policy to practice–the challenge of multi-disciplinarity. In Berendt B., Engel T., Ikonomou D., Le Métayer D., and Schiffner S. (Eds.), Privacy Technologies and Policy. Third Annual Privacy Forum, APF 2015. Luxembourg, October 7–8, 2015, Springer, p. 199–212. Stanzione M.G. (2016), Genesi ed. ambito di applicazione, in Sica S., D'Antonio V., Riccio G. M., La nuova disciplina europea della privacy, Wolters Kluver, p. 21 ff.

to health, technological development, and privacy show various conflict profiles due to the plurality of goods, values, and interests at stake, which cannot be disregarded.

8 Ethical Evaluations

To complete the scenario, there are several implications, and in some cases concerns, that the advent of artificial agents in healthcare has also brought in the ethical sphere.

To better understand its scope, we need only mention the example of Metroticket, developed in 2017 by the Transplant Centre of the National Cancer Institute of Milan and the University of Milan with the Transplant Centre of the Niguarda Hospital in Milan and the Sant'Orsola Malpighi Hospital in Bologna. Metroticket is an algorithm capable of predicting with a high percentage of long-term accuracy the positive or negative outcome of a liver transplant on the patient.[161]

On this point, there are innumerable and complicated evaluations that could be made in defining the priority criteria on the basis of which to favor one patient over another. It would be necessary to identify concrete and shared parameters of the value of life to choice who to favor. But how to carry out such an ethical assessment? What criteria should be used? The young age of an individual or who, for example, plays a certain role in a family context?

In 2019, following the issuance of the European Ethical Charter for the Use of Artificial Intelligence in Criminal Justice Systems and Related Fields,[162] the European Commission issued Communication No. 168 of April 8, 2019,[163] with some important ethical guidelines in order to guide the development and operation of artificial intelligence systems and to promote it internationally. In this measure, the European institution highlighted seven requirements for an artificial intelligence application to be considered trustworthy: (i) the need for human intervention and oversight, (ii) technical robustness and security of algorithms, (iii) confidentiality and governance of data, (iv) transparency and traceability, (v) consideration of diversity and nondiscrimination, (vi) protection of social and environmental well-

[161] For more information, see Mazzaferro V., Sposito C.,. Zhou J, Pinna A. D., L. De Carlis, J. Fan, M. Cescon, S. Di Sandro, H. Yi-Feng, A. Lauterio, M. Bongini and Cucchetti A., Metroticket 2.0 Model for Analysis of Competing Risks of Death After Liver Transplantation for Hepatocellular Carcinoma, in Gastroenterology, (vol. 154:1) pp. 128–139.

[162] European Ethical Charter for the Use of Artificial Intelligence in Criminal Justice Systems and Related Areas, adopted by the European Commission for the Efficiency of Justice (CEPEJ), December 3, 2018.

[163] Communication from the Commission to the European Parliament, the Council, the European Economic and Social Committee and the Committee of the Regions, Building trust in anthropocentric artificial intelligence, April 8, 2019, no 168.

being and, finally, (vii) accountability, understood as the provision of mechanisms capable of ensuring the responsibility of systems and their outputs.

The intervention of the Commission has, moreover, taken place against a European backdrop determined by multiple initiatives aimed at supporting a guarantor-friendly development of artificial intelligence applications, including the publication of a White Paper on Artificial Intelligence,[164] the establishment of a special Commission on AI at the European Parliament (AIDA),[165] and the passing of several Parliament resolutions regulating the phenomenon.[166]

The Resolution No. 2020/2012(INL) of October 20, 2020, is very clarifying. It proposes recommendations to the Commission concerning the framework for the ethical aspects of artificial intelligence, robotics and related technologies. The Parliament "considers that, without prejudice to sectoral legislation, an effective and harmonised regulatory framework based on Union law, the Charter and international human rights law, applicable in particular to high-risk technologies, is necessary in order to establish uniform standards across the Union and to effectively protect Union values" and that "any new regulatory framework on AI that includes legal obligations and ethical principles for the development, deployment and use of artificial intelligence robotics and related technologies should fully respect the Charter and accordingly respect human dignity, autonomy and self-determination of the individual, prevent harm, promote fairness, inclusiveness and transparency, eliminate bias and discrimination, including with regard to minorities and respect the principles of limiting negative external effects in the technologies used, of the explicability of the technologies and ensuring that the technologies serve people and are not intended to replace them or decide for them, with the ultimate aim of enhancing everyone's human well-being".[167]

With regard to the profile of ethical and social responsibility, the Parliament emphasized that "artificial intelligence, robotics and related technologies must be socially responsible and must contribute to finding solutions that protect and promote the fundamental rights and values of our society, in particular democracy, the rule of law plurality and independence of the media, objectivity and availability

[164] European Commission, White Paper on Artificial Intelligence – A European Approach to Excellence and Trust, February 19, 2020.

[165] Incorporated June 18, 2020, https://www.europarl.europa.eu/committees/it/aida/about

[166] European Parliament resolution of October 20, 2020, with recommendations to the Commission concerning the framework for the ethical aspects of artificial intelligence, robotics and related technologies, no. 2020/2012(INL); European Parliament resolution of October 20, 2020, with recommendations to the Commission on a liability regime for artificial intelligence, no. 2020/2014(INL); European Parliament resolution of October 20, 2020, on intellectual property rights for the development of artificial intelligence technologies, no. 2020/2015(INI).

[167] See, European Parliament Resolution of October 20th, 2020, with recommendations to the Commission regarding the framework for the ethical aspects of artificial intelligence, robotics and related technologies, No. 2020/2012(INL), paras. 1–2.

of information, health, economic prosperity, equality of opportunity, social and workers' rights, quality of education, protection of minors, cultural and linguistic diversity, gender equality, digital literacy, innovation, and creativity; recalls the need to ensure that the interests of all citizens, including those who are marginalized or in vulnerable situations, such as persons with disabilities, are given due consideration and represented".[168]

Without prejudice to the call for the creation of a well-defined legal framework, the European institutions have moved to devote special attention to the most dangerous technologies, such as those capable of self-learning, with the aim of generating greater trust in them on the part of the community and, at the same time, encouraging proposals for their ethical use.

Finally, the Proposal for a Regulation of April 21, 2021, No. 2021/0106 (COD)[169] concludes the legal framework. It is aimed at defining harmonized rules on artificial intelligence (also known as the Artificial Intelligence Act) and amending certain pieces of Union legislation.

9 Concluding Remarks

In conclusion, the impetuous advent of new technologies in healthcare is revolutionizing the entire way in which medical services are delivered by professionals, foreshadowing a gradual move away from human intervention in many dynamics of care.

On the one hand, there are countless advantages in terms of system efficiency that could result from this; on the other hand, there is also a pressing need to find a regulatory response to an ever-changing factual landscape.

Indeed, the use of artificial agents in medicine is certainly capable of guaranteeing an optimization of performance, contributing to the achievement of both scientifically and socially beneficial results. However, the same elements and techniques that fuel the socioeconomic benefits of new technologies also entail new risks or negative consequences for individuals or society.

This is why it is crucial for the health professional to have knowledge and familiarity with the technology and to be able to control its outcomes, but it is also necessary to raise society's awareness of innovation and understanding of its processes.

In this regard, it is necessary to initiate common strategies aimed at anticipating and controlling technological developments, but also at avoiding or limiting possible

[168] See, European Parliament resolution of October 20th, 2020, with recommendations to the Commission regarding the framework for the ethical aspects of artificial intelligence, robotics and related technologies, No. 2020/2012(INL), para. 38.

[169] See, Proposal for a Regulation of the European Parliament and of the Council of April 21, 2021, laying down harmonized rules on artificial intelligence (Artificial Intelligence Act) and amending certain acts of Union legislation, No. 2021/0106 (COD).

disastrous incidents, such as the definition of specific criteria for apportioning responsibility.

The goal is therefore to find a balanced regulatory approach to tackle the phenomenon quickly. At the moment, however, the interpretative reference to existing legal institutions, as well as the intervention of supranational authorities and case law, continues to be crucial.

Noninvasive Techniques to Assess the Development of the Fetal Brain and Nervous System

Amna Samjeed and Ahsan H. Khandoker

1 Introduction

To understand the highly complicated brain developmental process, it is essential to understand the structural changes during fetal brain development. Morphological changes of the brain from the fourth week of GA to the 40th week of GA are shown in Fig. 1. The human fetal brain originates with a simple tubular structure and eventually acquires the characteristics of an adult brain. Tiedemann et al. started studying the prenatal human brain in 1816. Then, a few neuroanatomists did some histology analysis to study the neural structures of the developing brain in detail [2].

Fetal brain development is a highly complex process. The fetal telencephalic wall is divided into five zones: (i) proliferative zone, (ii) intermediate zone, (iii) subplate zone, (iv) cortical zone, and (v) marginal zone [1]. As the gestation progresses, zonal change occurs. These are assessed quantitatively (thickness, volume) and qualitatively (histology). These zonal changes reflect neuronal migration, proliferation, differentiation, axonal ingrowth, and outgrowth (Fig. 2). All the structural components of the fetal brain develop toward the end of gestation.

A better understanding of fetal brain functional development is needed to detect brain and nervous system abnormalities [3]. Several MR fetal imaging/4D ultrasound techniques are available for neurological and brain assessment non-invasively. These techniques help assess brain morphology, the connection of neurons, functionality, metabolism, fetal motion, face expressions, and emotion-like behaviors [4]. At the same time, fetal brain activity can be identified using fMEG [5]. There are studies on fHRV that indirectly reflect the fetal nervous system [6]. These fHRV parameters can be measured using fMCG and NI-fECG. Variability

A. Samjeed (✉) · A. H. Khandoker
Department of Biomedical Engineering, Khalifa University, Abu Dhabi, UAE
e-mail: 100057584@ku.ac.ae; ahsan.khandoker@ku.ac.ae

D. Pani (ed.), *Innovative Technologies and Signal Processing in Perinatal Medicine*, https://doi.org/10.1007/978-3-031-32625-7_5

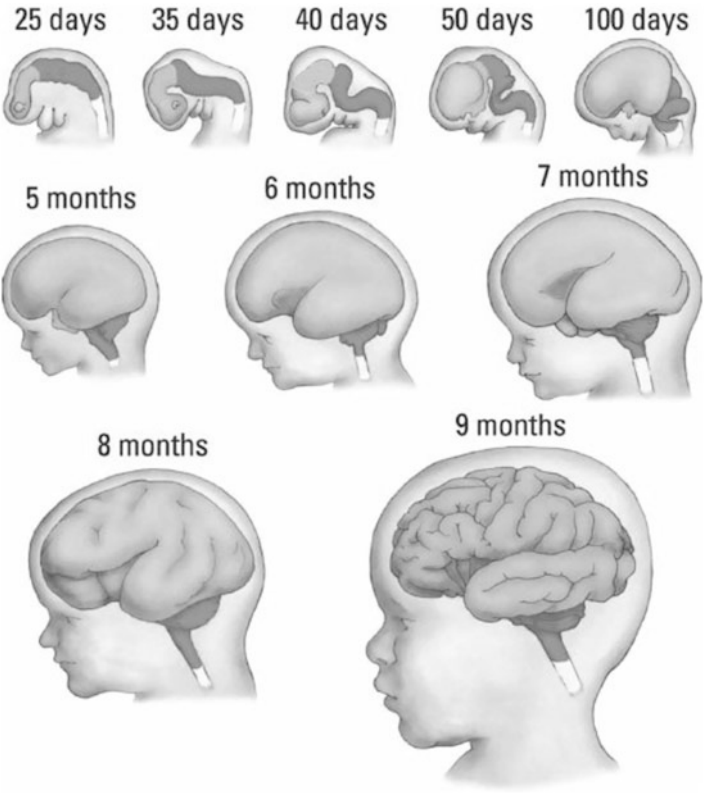

Fig. 1 Morphological changes of the fetal brain from 25 days of gestation to 40th week of gestation [1]

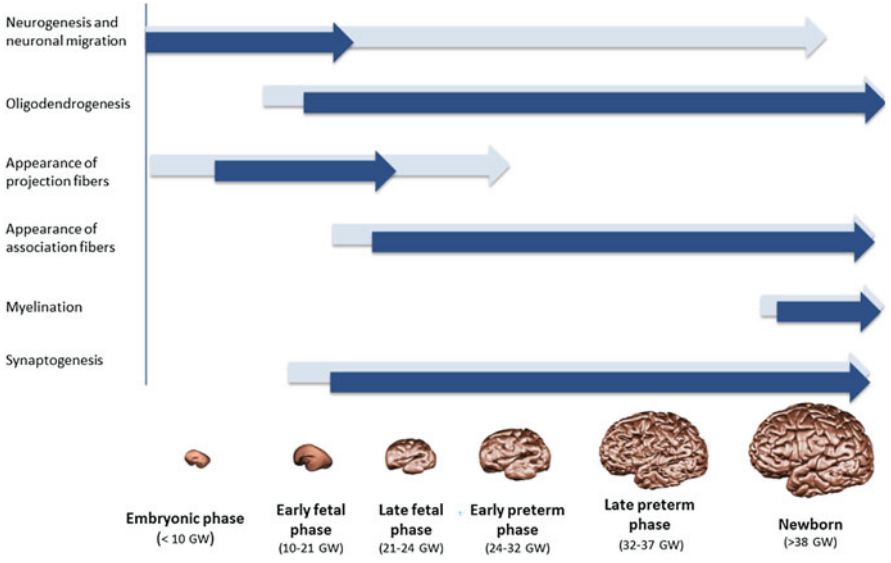

Fig. 2 The main neurogenic effects during fetal brain development [3]

in fHRV during different gestations measures sympathetic and parasympathetic activity reflecting autonomic nervous system (ANS) activity [7]. Along with that, the relationship between mHR and fHR also provides the functional status of ANS [8]. The fetus also shows four behavioral states: quiet sleep, quiet awake, active sleep, and active awake. The difference in the ratio of these states at other GA also represents fetal maturation.

This chapter reviews noninvasive techniques for analyzing fetal brain and neural development. This chapter discusses whether fetal imaging could give fetal behaviors and neurological assessment in utero rather than morphological changes/maturation. Also, it examines whether noninvasive signals could provide any information about fetal neurological development (Table 1).

2 Currently Available Noninvasive Techniques for Fetal Brain and Neurological Assessment

2.1 Fetal Magnetocardiography (FMCG)

Magneto cardiograms (MCGs) are body surface mappings that identify weak electrophysiological phenomena and cardiac magnetic fields utilizing SQUID sensors. The cardiac magnetic field was first identified and described by Baule and McFee in 1963. Throughout the long term, progress has been made in this field of MCGs, and it has emerged as a valuable diagnostic device with multichannel recordings.

Fetal heart rate variability (fHRV) indirectly indicates fetal well-being and autonomic nervous system development. fMCG is a noninvasive method for the detection of electrophysiology of the fetal heart. fMCG has a higher resolution compared to CTG and fECG. Signals obtained from the fetal heart using fMCG are exact, which helps assess PQRST complex alterations. Figure 3a represents the MCG experimental set-up and the dewar was positioned with its curvature above the fetal heart after sonographic localization without touching the maternal abdomen. A fetal MCG actocardiogram, or synchronized recording of FHR and fetal activity, facilitates the study of the relationship between FHR and fetal activity (Fig. 3b). Clearly, the large variations in the actogram are indicative of fetal body movements and are linked by the acceleration of the FHR. They also demonstrate small, rapid oscillations, which result from fetal breathing movements, observed in the middle of the tracing in the figure. There are studies using fMCG where the authors used different heart rate variability parameters to evaluate the maturation of the fetal autonomic nervous system.

Garner and group calculated six HRV parameters (complexity measures) and compared these parameters. These features are standard deviation (SD), hsEntropy, high spectral detrended fluctuation analysis (hsDFA), spectral multi-taper method (sMTM), Shannon entropy, sample entropy, and approximate entropy [10]. Of these, approximate entropy, sample entropy, and SD have the highest power for

Table 1 Description of the selected studies using noninvasive techniques described in the text

No	Author	Year	Gestation weeks	Fetus	Technique used	Parameters studied	Outcome
1	May [4]	2010	28–36	81	MCG	fHR, fHRV (RMSSD, SDNN, VLF, LF, HF)	Pregnant mothers with aerobic exercise showed lower fHR and higher fHRV. These fetuses showed improved autonomic tone and significant difference after 36 weeks of GA, especially in fetal active state.
2	Haddad [5]	2011	30–37	40	fMEG	Spectral edge frequency (SEF), continuous (CO), and discontinuous (DC) epochs	DC epochs are more common in quiet sleep compared to active sleep in early gestational periods. As gestation progresses, a decrease in DC epochs in quiet sleep was observed. DC patterns are replaced by CO patterns in late gestational age/near term. Higher SEF is also observed in late GA.
3	Hoyer [6]	2014	21–40	418	fMCG	FABAS based on HRV parameters (AMP, gMSE3, skew-ness,pNN5,VLFLLF, these patterns segmented w/o DC and basic)	FABAS could predict fetal maturation age accurately than conventional techniques. Improved FABAS after segmentation and behavioral state classification.
4	Brandle [7]	2015	24–41	55	fMCG	fHRV parameters (RMSSD,SDNN, SDNN/RMSSD ratio, PE)	During early gestation, the fetus showed two behavioral states: quiet (54.8%) and active state (41.6%). After 32 weeks of gestation, they identified three different behaviors, which are fetal quiet sleep state-1F (24%), active sleep-2F (65.4%), and active awake-4F (10.6%). Significant differences in fHRV parameters were observed in 1F and 4F. Decreased PE was observed with improved fetal activity These fHRV parameters could predict the ANS development.
5	Marzbanrad [8]	2015	16–41	65	NI-fECG	mRR and fRR, transfer entropy (TE)	After 26 weeks of gestation, TE significantly increased from mother to fetus. From mid to late gestation, the delay in transferring the message from mother to fetus decreased significantly. Fetal–mother coupling is an important marker of fetal well-being.

6	Thomason [9]	2015	24–38	38	fMRI	Functional connectivity (using CONN toolbox)	Long-range connections are stronger in older fetus. Different cerebral connectivity was observed.
7	Garner [10]	2016	16–42	11	fMCG	hsEntropy, approximate entropy (Ap entropy), sMTM, hsDFA, sample entropy (SampEn), standard deviation (SD), and the Shannon entropy	The Ap entropy, sample entropy, and SD parameters have higher statistical significance than others. The new complexity measures do not outperform Ap entropy.
8	Marzbanrad [11]	2017	16–47	87	NI-fECG	Cardiac valve intervals/timings (PEP, VET, VFT, ICT, EDT, IRT)	Cardiac valve interval could predict GA and fetal autonomic nervous system development. This method is less influenced by arrhythmias. VFT correlated with fHR ICT, EDT, VFT correlated with fRR.
9	Antsaklis [12]	2017	28–38	40	4D ultrasound	KANET test	Higher KANET score observed for nondiabetic group. Difference in fetal maturation could be observed using this score in diabetic and nondiabetic group.
10	Lobmaier [13]	2018	32–40	116	CTG	STV parameters, AAC and ADC using BPRSA method	AAC and ADC showed a significant difference between GDM and control group while conventional CTG results did not find any significant difference. The effect of GDM on fetal ANS could not be analyzed using conventional CTG technology.
11	AboEllail [14]	2018	30–40	111	4D ultrasound	Fetal facial expressions and its frequencies	Seven different fetal facial expressions were observed. They are yawning, mouthing, tongue expulsion, smiling, sucking, scowling, and blinking. Most recurrent expressions were mouthing followed by blinking. Recurrence of yawning reduced as the gestation progressed, which shows the controlled sleep and wake cycle pattern.

(continued)

Table 1 (continued)

No	Author	Year	Gestation weeks	Fetus	Technique used	Parameters studied	Outcome
12	Zollkau [15]	2019	18.8–40	185	fMCG	HRV parameters (mean HR, TP, VLF, LF, HF, IMF, SDNN, RMSSD, pNN5, pNN10, pNN20, AMP), DASS score	No significant maternal–fetal correlation in 1F state. Strong maternal–fetal correlation (HR) in 2F when GA $\geq$ 32. No correlation between maternal DASS score and fetal HR/HRV.
13	Chen [16]	2019	28–39	58	NI-fECG	Coupling index of FHR accelerations and UEMG signal (UFCI)	UFCI could predict SGA better.
14	Mori [17]	2019	28–35	81	4D ultrasound	Fetal facial expressions and its frequencies	There is no significant difference between fetal facial expressions in AGA, SGA, and FGR.
15	Wheelock [18]	2019	25–39	166	fMRI	Functional connectivity (using CONN toolbox), FC-GA correlations (enrichment analysis)	16 unique fetal networks identified.
16	Zavala [19]	2020	36–39	82	NI-fECG	fHR, SD, RMSSD	As gestation progresses, males have lower fHR and higher fHRV than females, specifically in the 2F state. Female fetus shows a mature pattern in the early period while male fetus shows the mature pattern in late period/near term.
17	Lobmaier [20]	2020	35.0–37.4	110	NI-fECG	mHR and fHR coupling, BPRSA index (FSI)	Decrease of fHR of fetus of stressed mothers. Increased FSI in fetus of stressed mothers.
18	Niepel [21]	2020	30–39	24	fMEG	Phase coherence and amplitude aspect of FSSR, MF of 27 Hz and 42 Hz, CF of 500 Hz, AM with modulation tone of 100%	Fetal ASSR could be evoked with MF of 27 Hz. Phase coherence is more advantageous than amplitude aspect. Significant positive stimulation was observed in the 2F behavioral state of the fetus.

19	Avci [22]	2020	28–39	40	fMEG	PSD with different frequency bands (alpha, delta, theta, beta), rPSD	Spontaneous brain activity in the fetus of a type I diabetic mother is significantly different from the control in all four bands. In contrast, the fetus with type 2 diabetes showed a significant difference only in alpha and beta bands. No significant difference between fetuses of type I and type 2 diabetes.
20	Lakhno [23]	2020	26–28	64	NI-fECG	HRV parameters (TP, VLF, LF,HF,LF/HF, SDNN,RMSSD,pNN5, Amo, SI)	TP, AMo, and SI were good predictors for predicting the fetal autonomic development.
21	Mannella [24]	2020	24–41	80	NI-fECG	HRV parameters time-domain (SDNN, RR mean, and RMSSD) and frequency-domain (HF, LF, and LF/HF), index of complexity (COSEN)	They found that mRR, LF, and HF increased with GA up to the 31st week, and after that, no dependency was observed. These parameters are found to be the markers of the fetal ANS maturation.
22	Li [25]	2020	24–40	148	fMRI	CNN using fMRI image	CNN could predict the fetal brain age using fMRI images. This could find an association between BOLD signal and fetal brain age.
23	Dirk Hoyer [26]	2021	24–41	547	CTG	HRV parameters (pNN5, ACst1, AMP, MSE3, skewness, VLF/LF, SDNN/RMSSD)	Compared CTG with fMCG and fECG. HRV parameters except for pNN5, ACst1 obtained from CTG were comparable with HRV parameters of fMCG and fECG. CTG did not represent a vagally modulated behavior.

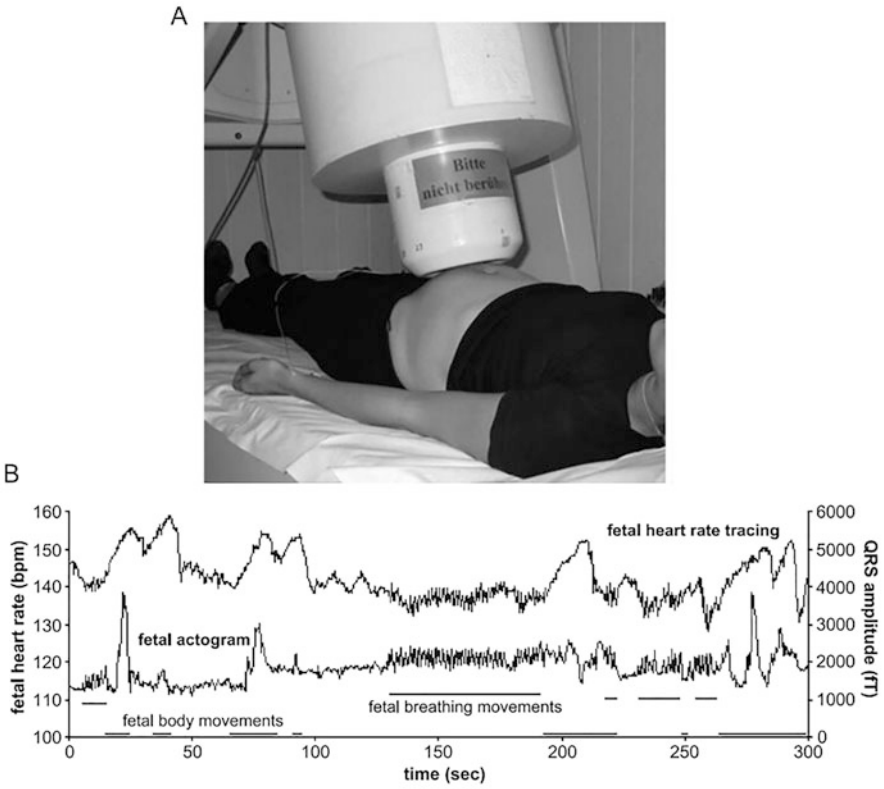

Fig. 3 (**a**) MCG system [27]; (**b**) fetal breathing and body movements captured by fMCG actocardiogram [28]

explaining gestational age. Among these, approximate entropy has the highest R^2 value. Approximate entropy, sample entropy, and SD have higher slopes than others. This implies that these three could classify the changes/maturation of fetuses over different gestational periods. They also concluded that nonlinear measures are more apt while characterizing the relation between individual HRV and gestational age [10].

Hoyer et al. developed the fetal autonomic brain age score (FABAS) for fetal maturation age prediction using different fHRV parameters. The parameters used are amplitude fluctuations (AMP), gradient multi-scale entropy (gMSE3), skewness, percentage of differences between adjacent NN intervals exceeding 5 ms (pNN5), and very low frequency/low frequency (VLF/LF). This FABAS could predict the fetal brain age in an unsegmented 30 min recording. They also fine-tuned the FABAS by including behavioral states (active sleep, quiet sleep). After segmentation based on behavioral conditions, a slight decline in the prediction was observed compared to an unsegmented recording. They mentioned that this slight decline

could be due to the 10 min recording used for segmented ones. But they could have validated this by doing an unsegmented 10 min recording. Further pattern segmentation based on acceleration (AC), decelerations (DC), and primary activity on quiet sleep showed more predictive dominance than the FABAS on unsegmented sections. They concluded that a detailed study on this pattern segmentation could detail fetal abnormality [6]. An increase in fetal HRV is associated with fetal neural maturation. These are related to the sympathetic and parasympathetic activity of the ANS [29].

Linda et al. compared the fetal autonomic development in exercising healthy pregnant mothers (doing aerobic exercise for at least 30 min) and nonexercising healthy pregnant mothers. They selected three different gestational periods: 28, 32, and 36 GA. They also included fetal active and quiet states for comparison. They observed that at 28 and 32 weeks of gestation there is no significant difference in fetal HR and HRV parameters in both behavioral states. But at 36 weeks of GA, significantly lower fetal HR and higher fetal HRV were observed in the active fetal state in the exercising group compared to the nonexercising one. This shows that regular exercise done by healthy pregnant mothers positively impacts fetal cardiac autonomic tone as the gestation progresses [4].

Zollkau et al. also showed a significant maternal–fetal HR/HRV correlation as the gestation advances ($\geq$32 GA) and during the active fetal state. There is no correlation observed in the fetal quiet sleep state. This study supports the study by Linda et al. Zollkau et al. also analyzed that maternal DASS score reflected in the maternal autonomic tone and had no effect on fetal autonomic tone. The DASS score obtained here was within the normal range. However, a DASS score outside this normal range might influence the fetal autonomic tone [15]. A detailed study on this is needed.

Brandle et al. observed only two behavioral states during early gestation, quiet (54.8%) and active state (41.6%). This represents a premature fetus. After 32 weeks of gestation, three different behavioral states were identified: quiet sleep-1F (24%), active sleep-2F (65.4%), and active awake-4F (10.6%). They observed a significant decrease in fetal HR from early gestation (24 weeks) to late gestation (35 weeks). As the gestation progressed, SDNN increased, but it was not statistically significant. Increased fetal activity can be concluded with increasing SDNN/RMSSD ratio and decreasing permutation entropy (PE) [7].

This technology can apply successfully in environments characterized by low or no noise. Most low magnetic field sensors can be tough to implement. They need shielded rooms. This issue explains why the use of MCG is yet to be adopted in many healthcare institutions. Moreover, this is an expensive instrument. So, hospitals must have adequate financial resources to implement this technology successfully.

2.2 *Functional Magnetic Resonance Imaging (fMRI)*

fMRI is considered a primary tool for fetal brain functional connectivity investigation. fMRI gives a better understanding of neurological functions and functional connectivity in adults and children. Functional development in the fetal brain has been explored using rs-fMRI and task-based fMRI methods. Both rs-fMRI and task-based fMRI use the same MRI hardware and image sequence. Both measure blood oxygen-dependent level (BOLD) signal. But rs-fMRI does not require controlled stimulus presentation like task-based fMRI. Hence, rs-MRI emerged as a new methodology for a better understanding of fetal neurological functions [30]. Figure 4a represents the MCG experimental set-up. A study by Thomason and colleagues was the first to use rs-fMRI to quantify cross-hemispheric connectivity in the human fetus as a function of age. The data collected in this study were the first to be collected at a field strength of 3.0 Teslas (T) for fetal fMRI (Fig. 4b).

fMRI distinguishes fetal brain activity using a reaction to different stimuli and depends on the BOLD effect. Based on fetal responses to various stimuli, there

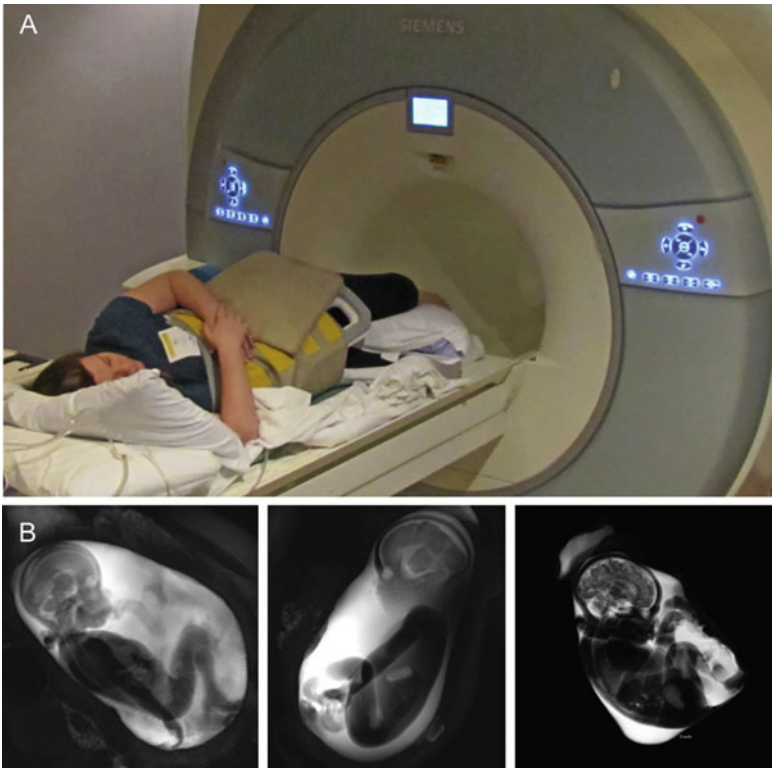

Fig. 4 (**a**) The fMRI facility; (**b**) the fetal images obtained through fMRI at three different gestational time points (28, 32, and 36 weeks – from left to right) [30]

will be an increment in neuronal development locally, leading to increased blood flow. This leads to an increase in blood volume and oxygenation. This eventually brings about an increased MR signal locally called BOLD difference/contrast. fMRI is done based on echo-planar imaging, and an fMRI signal is produced based on the distinction between oxygenated and deoxygenated hemoglobin. fMRI is profoundly delicate to differences in magnetic susceptibility. There have been restricted investigations utilizing fMRI to study the brain functions of embryos and neonates [31]. Fulford and the group found activation in the temporal lobe of 7–15 fetuses when a vibroacoustic stimulus (the sound level of 95–100 dB) was given utilizing earphones strapped to the maternal abdomen [32]. This group found activation in the frontal region of 4–8 fetuses when the visual stimulus was presented using a red LED cluster on the maternal abdomen. One fetus showed activation in some other parts, but none of the fetuses showed activation in the visual areas [33].

The hemodynamic response of adults is different from that of the fetus. This includes vascular control mechanisms, oxygen binding with hemoglobin, fMRI sensitivity, and brain activation. Any level of fetal movement will diminish the fMRI data quality. Even in the presence of fetal motion, suppose fMRI can produce a quantifiable amount of data, then this can obtain an exciting advancement in the field of fetal brain functionality. Figure 5 represents a resting-state network characterized by a lateral prefrontal and bilaterally medial activity pattern, which includes the

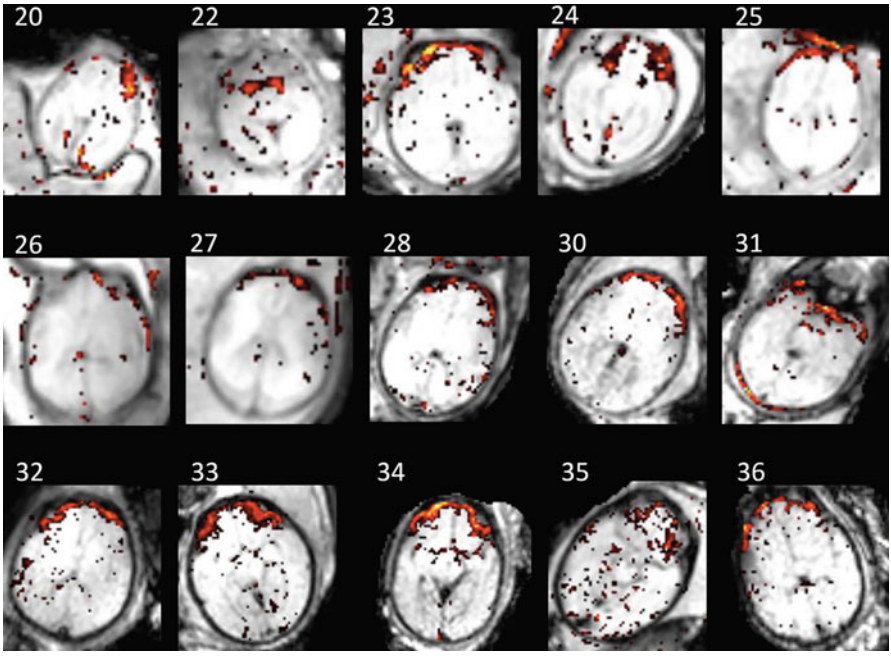

Fig. 5 Fetal brain functional images at different gestational weeks (20–36 weeks) [34]

frontopolar portions of the incompletely developed gyrus rectus and frontal gyrus in 15 subjects.

Thomson et al. identified the brain's primordial forms of visual, motor, temporal, and thalamic networks. They found new cerebral connectivity in the third trimester, like cortical–subcortical, cerebral–cerebellar, bilateral cross-hemispheric, and intra-hemispheric cortical structures. They also observed significant long-range connections in older fetuses compared to younger ones [9].

Wheelock and group used fMRI to study the fetus's functional connectivity and neural development in the uterus and learned whether functional connectivity development is sex-dependent. They used graph-theoretical community detection algorithms to detect prenatal functional connectivity (FC) brain networks. They identified 16 new unique fetal networks. They also observed a difference in functional connectivity GA correlation in male and female fetuses. Female fetuses showed long-range functional connectivity across gestation, especially between cortical and subcortical regions.

In contrast, males showed an FC-GA correlation between the ventral and dorsal parts of the prefrontal cortex (PFC) and cerebellum (CB). As GA increased, a change in functional connectivity was observed. Remarkable FC changes occurred in posterior cingulate cortex (PCC), superior frontal gyrus (SFG), and visual cortex connectivity between subcortical and cortical regions. They concluded that the fetal brain networks observed are the building blocks for neonatal, toddler, and adult brain networks [18].

Recently, Li et al. developed a novel CNN technique to predict fetal age using fMRI images. They compared their CNN-trained model with a gradient boosting machine (GBM), random forest (RF), and logistic regression. Their model achieved the best performance with an F1 score of 0.84 and an AUC of 0.91 [25].

Limitations of fMRI include high noise levels, difficulty obtaining the measuring space, and safety issues related to high magnetic fields and field gradients exposure. Aside from these, fMRI provides anatomical and functional information on the fetal brain.

2.3 Magnetoencephalography (MEG)

MEG was the primary technique to show the evoked responses in the neural framework and give a neural illustration of higher-order cognitive and sensory functions in the fetus. As the MEG technique has developed, increments in the number of channels used and utilization of post hoc algorithms produced improved detection rates and more precise outcomes. Most studies accomplishing complete fetal MEG information analyzed the functioning of auditory systems [30].

In 1985, Blum, Saling, and Bauer efficiently produced the first fetal evoked fields using an adult MEG system. The University of Arkansas for Medical Sciences installed the first equipment made exclusively for fetal and neonatal recordings in 2000 [35], a multichannel system known as SARA (Squid Array for Reproductive

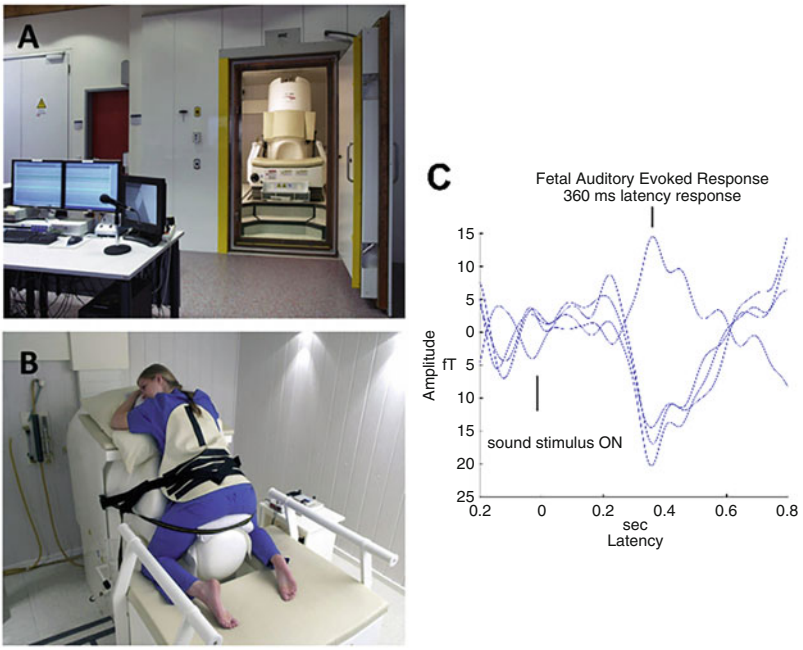

Fig. 6 (**a**) MEG instrument; (**b**) represents how a pregnant woman is positioned in the MEG system; (**c**) fetal auditory-evoked response [36]

Assessment). An illustration of the experimental setup and the positioning of the abdomen can be found in Fig. 6a, b. Eswaran et al. found that 80% of the fetuses showed auditory responses when pure tone stimuli were given. Those fetal responses happened at latencies around 200 ms after the stimulus began. Later, a latency reduction was observed as gestational age progressed (GA) [37]. These reduced latencies indicate highly developed responses from the fetal brain [38]. Using fMEG, the authors efficiently recorded fetal discriminative responses for different auditory stimuli and observed that the acoustic change identification functions even at the fetal stage. Draganova et al. observed that 60% of the fetuses (33–36 weeks GA) showed MMR [39]. In a recent study, MMR was observed in 66% of the fetuses (28 weeks GA) [40].

Higher-level process analysis is done based on the fetal response and latency period when an auditory stimulus is provided rapidly. Figure 6c represents a response obtained from a 33-week-old fetus at a latency of 360 ms. fMEG technology could successfully record rapid temporal processing (RTP). The later speech performance is based on this fast temporal processing (RTP) [41]. In addition, fetuses and younger newborns expressed a single reaction to the presented tone pair. This single reaction represents immature development in these early growth stages [42].

Haddad and group used fMEG to study spontaneous fetal patterns and their relationship with fetal behavioral state and GA. Fetal behavioral state detection was done using an echocardiogram, and data showed that most of the fetuses showed an active/quiet sleep state. This data confirms that sleep state is the most common fetal behavioral state. A more discontinuous pattern was observed at the early GA, and a gradual decrease was observed at the late GA. Before 35 weeks of GA, it is also observed that the DC pattern is predominant in quiet sleep compared to active sleep. As the GA progressed, a further decrease in the DC pattern was observed in quiet sleep. A significant increase in spectral edge frequency (SEF) was found in late GA compared to early GA. SEF was almost similar in quiet and active sleep states [5].

Niepel et al. are the first group to detect ASSR using MEG technology. They found that fetal auditory steady-state response (ASSR) could be evoked with a modulation frequency (MF) of 27 Hz. They also observed that the behavioral state 2F (active sleep) produced a significantly positive result than the 1F (quiet sleep) state. But they did not keep any significant change between different gestational ages [21].

Recently, Avci et al. analyzed the effect of gestational diabetes on fetal brain activity by comparing it with the control group. Compared to control, type 1 diabetes showed a significant difference in all the bands (alpha, theta, delta, beta), and type 2 diabetes showed a significant difference in two rounds (alpha and beta) only. These differences in fetal brain activity indicate slow neurological maturation [22].

A significant limitation of fMEG is that this cannot provide anatomical information directly. This technique requires additional imaging techniques like ultrasound. In addition, MEG has limited spatial resolution. So, it is challenging to decide the source of the recorded signal precisely. Nevertheless, direct evaluation of prenatal cortical development is possible using the fMEG method. Hence, it is a promising methodology, regardless of its limitations.

2.4 Noninvasive Fetal Electrocardiography (NI-FECG)

Compared to CTG, improved signal detection can be obtained using a fetal scalp electrode (FSE). In FSE, an electrode is applied directly to the fetus's scalp, which needs amniotic membrane rupture and dilation of the cervical area. This method provides an accurate measurement of fHR [43, 44]. But this way of fHR measurement is practical only in labor. Moreover, it is done only for high-risk pregnancy cases as the fetal scalp is delicate for electrode placement.

The NI-fECG monitoring technique is gaining more attention than CTG and FSE. This technique is done by putting electrodes on the abdomen surface of the pregnant woman and hence acquiring an fECG signal. Figure 7 illustrates the general steps followed to obtain electrophysiological data from a NI-fECG and process the signal to obtain FHR. NI-fECG monitoring using a Monica AN24 machine fitted to the maternal abdomen is capable of recording up to 20 hr. Pregnant mothers can easily handle this device without needing any experts – NI-fECG guarantees to evaluate the

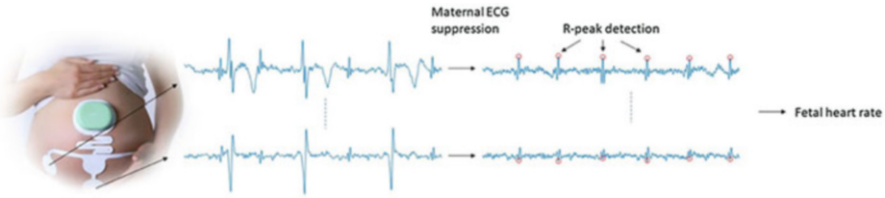

Fig. 7 Noninvasive FECG representation [45]

fHR rhythm and its patterns. Additionally, NI-fECG also provides fetal movement and fetal orientation details too [46]. NI-fECG conceivably offers a good quality of fHR data with these advances in contrast with existing observing modalities like CTG or FSE [47, 48]. NI-fECG could observe pregnant ladies with high body mass index (BMI) more efficiently and has the potential to decrease fHR and mHR confusion [49].

When a fetus experiences hypoxia, the cardiovascular system changes, which can be observed in fetal HRV; this change, by implication, influences the oxygenation and working of the central nervous system [50]. Therefore, the evaluation of fetal movement activity, uterine muscle contractions, and FHR variability plays a fundamental role in fetal well-being [51].

Marzbanrad et al. used transfer entropy (TE) to study the maternal–fetal correlation at different gestational ages and time delays. Compared to early gestation (16–25 weeks), maternal to fetal TE was significantly greater in mid (26–31 weeks) and late (32–41 weeks) gestational periods. Compared to mid-gestation, an increase in TE from mother to fetus was observed only in the fetal active state of late gestation and not in the quiet state of the same. As the gestation progressed from mid to late, information passing from the mother to the fetus was faster, indicating a more immediate fetal response and indirectly showing the fetus's maturation [8]. The same group did another study using fetal cardiac interval to estimate the GA and fetal autonomic development [11].

Zavala et al. studied the relationship between sex, fHR, and fHRV considering fetal behavioral states. It was observed that females have higher fHR and lower fHRV than males. Furthermore, they observed that in the 2F state males show lower fHR and higher fHRV. It is also observed that male fetuses show more mature patterns in the near term, while female fetuses show more mature patterns in early gestation [19].

Igor and the group have studied the difference in patterns of autonomic nervous regulation in fetal growth-restricted ones compared to normal ones (normal, w/o fetal distress, with fetal distress). They determined the total power and spectral components (VLF, LF, HF, and LF/HF ratio). They also calculated SDNN, RMSSD, pNN50, amplitude of mode (AMo), and stress index (SI). They observed a decrease in total power (TP) and elevation of AMo and SI in the fetal distress group. Fetal distress in fetal growth restriction (FGR) can be diagnosed using HRV and beat-to-

beat variations. Moreover, NI-FECG could support the detection well. This study concluded that good predictors of fetal deterioration are TP, Amo, and SI [23].

Kun Chen et al. were the first to study the long-term coupling between UEMG and fHR using a new wavelet-based approach. The coupling index (UFCI) could provide a strong relationship with gestational age. This performs better over other fHRV indices in predicting the small for gestational age (SGA) with an AUC of 0.88. These indicate that UFCI could help analyze SGA and sympathovagal regulation throughout the gestational period from the 28th week [16].

Paolo Mannella et al. extracted fHRV indexes related to ANS activity. fHRV indexes studied are RR interval, SDNN, RMSSD, corrected sample entropy (COSEN), low frequency (LF), high frequency (HF), and LF/HF. This study confirmed that NI-fECG could detect the parameters found to be the markers of fetal ANS maturation [24]. Lobmaier et al. analyzed the coupling between mHR and fHR using the bivariate phase-rectified signal averaging analysis (BPRSA) signal processing technique. They observed a decrease in mHR, reflecting the pattern of maternal breathing. At the same time, the control group's fHR remained the same while the stressed group's fHR decreased. This data indirectly shows the difference in the maturation of the sympathetic and parasympathetic systems. They also observed that the fetal stress index (FSI) was significantly higher in the stressed group. Thus, they concluded that FSI has more predictive power than cortisol in the context of fetal stress analysis [20].

The ability of the NI-FECG to successfully acquire and process these signals is dependent on an adequate number of electrodes. Furthermore, as maternal ECG will mask the fetal ECG, proper removal of maternal ECG is needed, highlighting a potential technological limitation [52].

2.5 4D Ultrasound

In the mid-1990s, the world accepted that 3D/4D ultrasound plays a significant role in fetal monitoring. This technology was first promoted by a French doctor, Bernard Benoit, who published 3D images of the fetus from the first trimester itself [53].

There are several studies for the fetal assessment or fetal brain maturation evaluation using fetal movements and facial expressions analyzed by 4D Ultrasound [54–56]. Kurjak et al. developed Kurjak Antenatal Neurological Test (KANET), a scoring system for fetal neurological assessment by assessing fetal facial expressions and movements [57].

The fetal facial expressions like blinking, yawning, smiling, mouthing, and sucking can be assessed using 4D ultrasound (Fig. 8) [59]. 4D ultrasound can also evaluate emotions like behavior and response to a stimulus [60]. A difference in fetal facial expression frequencies can be seen throughout the gestation. These frequency changes are an essential indicator of fetal brain maturation and well-being [61–63].

4D ultrasound can study a full range of facial movements from the 20th week of gestation onward [59]. Complex facial expressions can be seen from the 24th

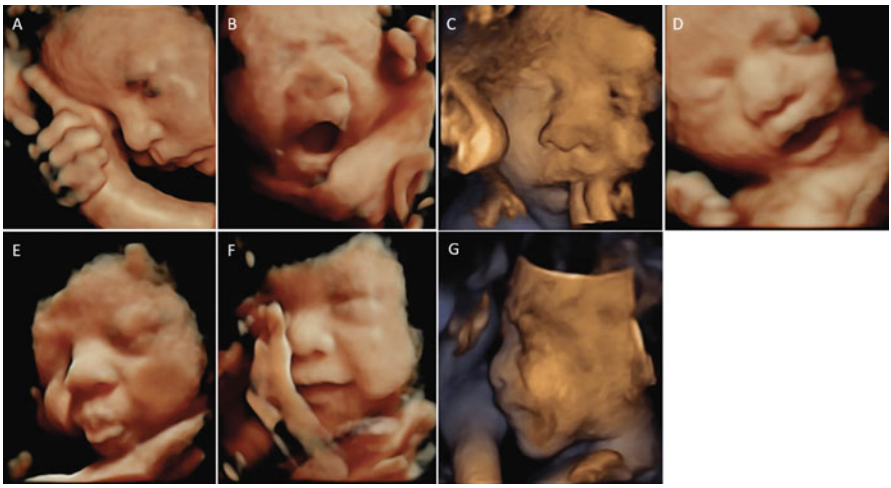

Fig. 8 Different fetal facial expressions and emotion-like behaviors: (**a**) eye blinking; (**b**) yawning; (**c**) finger-sucking; (**d**) mouthing movement; (**e**) tongue expulsion; (**f**) smiling; (**g**) sad. All these fetuses were in 28–34 weeks of gestation [58]

week onward with adipose tissue deposition [64]. As the gestation advances, an increase in spontaneous eye blinking is observed, which reflects the central dopamine system maturation [65–67]. Yawning indicates the development of brain stem and peripheral neuromuscular function. As the gestation progresses, changes in the frequency of yawning show the rhythmic control of sleep and wake timings [68]. Sufficient brain maturation is needed for in utero training of the fetus to do some vital postnatal movements like sucking [69]. After 35 weeks of gestation, nonrapid eye movements and mouthing movements simultaneously reflect the brain's maturation [70]. As the gestation progresses, a change in the frequency of tongue expulsion can be observed. This expression indicates the maturation of the auditory-motor system with its neural pathways [71]. The fetus used to show more complex facial expressions and express emotion-like behaviors in the third trimester. Fetuses show a smiley face in a relaxed state and a sad/frown face if they feel any discomfort or pain [72]. These emotion-like behaviors or expressions represent fetal consciousness.

Panagiotis Antsaklis et al. applied the KANET score to analyze the fetal neurological/brain maturation difference in diabetic and nondiabetic mothers. They observed that the KANET score was higher for the nondiabetic group. Based on the KANET score, the significant difference observed between the groups is in isolated eye blinking, finger movements, and facial alterations [12]. Four-dimensional ultrasound may be an essential modality in current and future research on fetal facial expressions and assist in evaluating fetal brain function.

AboEllail et al. analyzed the fetal face expressions in the third trimester and studied whether any change in frequency occurred as the brain developed. They

observed seven different facial expressions: yawning, mouthing, tongue expulsion, smiling, sucking, scowling, and blinking. The most recurrent expression was mouthing, followed by blinking in the third trimester (31–40 weeks). After 30 weeks, the recurrence of yawning was reduced. This reduction represents more rhythmic control of wake and sleep patterns. The frequency of other expressions also remained the same in the third trimester. They also observed the co-occurrence of mouthing and eye blinking, representing fetal brain maturation [14].

Mori et al. also studied the difference in fetal facial expression frequency in SGA, FGR, and AGA fetuses. In AGA fetuses, significantly higher mouthing expression was observed. In the SGA fetus, there was no significant difference between the facial expressions. Still, mouthing is the most frequent expression. In an FGR fetus, mouthing has a significantly higher recurrence than expressions like tongue expulsion, sucking, and scowling. Based on these results, it is concluded that fetal facial expressions cannot identify SGA and FGR [17].

4D ultrasound poses the same risk as 2D and 3D ultrasound because these all use the same wavelength frequency. Clinicians limit the exposure time to 30 minutes as this causes slight heating up of tissues. So, continuous monitoring is complex. Moreover, this is an expensive technique and requires experts to analyze the fetus.

2.6 Cardiotocography (CTG)

Dr. Konrad Hammacher first introduced the CTG instrument in the 1970s. CTG is used in clinics for the simultaneous assessment of uterine contractions and fetal heart rate monitoring noninvasively by placing the transducer on the mother's abdomen and invasively placing the transducer on the fetus during labor (Fig. 9) [73]. The significant features obtained from CTG regarding fetal well-being include baseline heart rate of fetus, variability in baseline, no of accelerations, and decelerations. As the gestation progresses, the fetal baseline heart rate reduces, showing fetal maturity. Fetal baseline heart rate reflects the ANS development. As the fetus develops, the parasympathetic system's maturation lowers the basal fetal heart rate, especially after 30 weeks [74]. Amplitude and frequency of accelerations are higher after 30 weeks of GA [75]. Frequent heart rate decelerations usually occur in preterm fetuses compared to term fetuses [76]. Reduced baseline variability could be observed in the immature and preterm fetus [77].

Fetal monitoring using CTG can be done from the 20th week of gestation itself [78]. Even though CTG is widely used clinically, it has low specificity due to evaluator variability [79]. To overcome this, computerized CTG technology was introduced, which has recently been used to identify an abnormality in fHRP using artificial intelligence methods [80]. This developed CTG-artificial intelligence-based system could detect the normal and intrauterine growth restriction (IUGR) fetus [81].

Spyridou et al. compared the fetus of smoker mothers with healthy mothers and the fetus with mild IUGR cases. Compared to a normal fetus, the fetus of

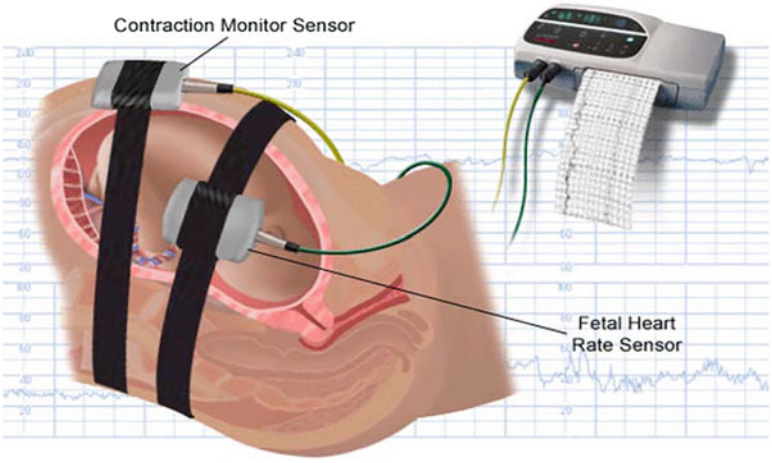

Fig. 9 CTG representation [50]

smokers' mothers exhibited a lower baseline heart rate. Simultaneously, parameters like skewness, bicorrelation, and kurtosis are higher in the smoker group than in normal ones. Other parameters like mutual information, Pearson autocorrelation coefficient, and algorithm complexity are reduced compared to the normal fetus. A reduction in the Hjorth complexity parameter is observed in the smoker group compared to the mild IUGR group. These all show that more major sympathetic development in the smoker group occurs than parasympathetic development. So even at the delivery time, this smoker group shows immature fetal development. It would be more interesting to study the difference in the frequency of fetal behavioral states between these groups [82].

Lobmaier et al. studied the effect of gestational diabetes mellitus (GDM) on ANS and cardiovascular function from the 32nd week onward using CTG. They compared the BPRSA method with the conventional CTG method. Average acceleration capacity (AAC) and average deceleration capacity (ADC), the indices calculated from BPRSA, showed significant differences between GDM fetuses and the control group. At the same time, traditional CTG results did not find any significant difference between these groups. A previous study done by this group found that AAC could differentiate between healthy and IUGR fetuses. They concluded that fetal ANS development could be analyzed using these parameters. Here, the difference in AAC and ADC between healthy and GDM fetuses shows a difference in fetal ANS activity for both groups. This effect of GDM on fetal ANS could not be analyzed using conventional CTG technology [13].

A recent study was done by Dirk Hoyer and a group in which they compared CTG with fMCG and fECG. They found that HRV parameters, except for pNN5, and acceleration capacity (ACst1) obtained from CTG were comparable with HRV parameters of fMCG and fECG. However, CTG did not represent vagally modulated

behavior. Still, fetal age prediction and SGR/FGR detection were possible using CTG with minor differences [26].

The major limitation of CTG is its low accuracy. Sometimes interpretation is challenging. Long-term variability can be observed clearly, but short-term variability interpretation is difficult.

3 Summary

All the noninvasive techniques discussed here are excellent techniques proven to provide information on fetal autonomic brain development at different gestational ages and during other fetal behavioral states. This chapter gives an insight into current best practices while using these techniques to study fetal brain development prenatally. Table 2 summarizes the noninvasive systems discussed so far.

4 Conclusion

Over the last 10 years, research advances in fetal imaging and usage of electrical/magnetic signals for neural/brain maturation noninvasively. Those are summarized in this chapter. Behavioral assessment of the fetus using 4D imaging gives a better understanding of fetal face expressions and emotion-like behaviors and their relation with brain maturation. Like newborns, the fetus also produces different facial expressions in response to various stimuli. These expressions indirectly help in the assessment of fetal neural/brain maturation. These reactions and expressions show the development and maturity of the central nervous system and different parts of the brain where these activities are controlled.

Additionally, individual stimuli responses reflected as facial expressions stipulate a high degree of brain function and development. Therefore, 4D ultrasound can analyze different stages of fetal development and brain functions through fetal facial expressions and movements. Fetal response to visual/auditory stimulus can be analyzed using fMRI/fMEG techniques. This response gives brain/neural maturation information. fMRI can do functional fetal imaging and detect stimulus-response based on the BOLD effect. fMRI could also detect the functional connectivity of neural networks. MEG system also detects fetal maturation based on visual/auditory stimuli. A decrease in latency for the response indicates the development of ANS. Fetal spontaneous patterns and their relationship with GA and behavioral state could be analyzed using the MEG system.

NI-fECG/fMCG gives a good signal source for monitoring fetal heart rate with fHRV quantification. CTG is also helpful in monitoring fetal heart rate, but it is less accurate than NI-fECG/fMCG. Increased variability cannot be observed in the fetal heart rate data obtained from the Doppler ultrasound during various stages of fetal breathing. Fetal behavior analysis is an inevitable part of fetal brain

Table 2 Comparison of noninvasive techniques

Method	Gestational age	Energy type	Advantages	Disadvantages	Inference on brain development
fMCG	16–41 weeks	Magnetic	Highly accurate unaffected by tissue resistance Comparatively easier to obtain fHR	Costly Need shielded rooms/low noise Need the practice to handle Affected by fetal/mother movements	Different fHRV parameters have studied for ANS development Developed a FABAS for fetal brain age prediction Few studies were done using maternal–fetal coupling Fetal behavioral states are considered in many studies
fECG	20–40 weeks	Electrical	Economical No need for expert help Can obtain beat to beat variability Comfortable long-term recording possible	Dependent on in utero fetal movement and orientation Difficulty in separating fHR from mHR	Different fHRV and maternal-fetal coupling parameters studied Some considered fetal behavioral states ANS maturation difference in males and females have studied
CTG	20–40 weeks	Ultrasonic	Can obtain continuous fHR data Obtain uterine contractions Economical No need for expert help	Less accurate Sometimes interpretationis difficult Difficult to observe short-term variability	Effect of smoking and diabetes studied Compared traditional CTG and BPRSA (AAC, ADC) method Vagally modulated behavior was not observed from CTG None of the studies considered fetal behavioral states
fMEG	28–40 weeks	Magnetic	Highly accurate unaffected by tissue resistance Good temporal and spatial resolution	Costly Need shielded rooms/low noise Need the practice to handle	Fetal spontaneous response and their relation with GA and fetal behavioral states The first technology to detect ASSR Effect of diabetes on brain activity
fMRI	24–40 weeks	Magnetic	Good resolution unaffected by tissue resistance Detection of subtle changes is possible	Costly Operator dependent High false-positive results	Studied the cerebral connectivity in the third trimester Learned the functional connectivity difference in males and females
4D ultra-sound	28–40 weeks	Ultrasonic	3D picture of a moving fetus in real time Real-time interpretation by the operator	Costly Operator dependent Good 4D image depends on maternal obesity, amniotic fluid, and the position of the fetus	Developed a KANET scoring system based on fetal facial expressions and movements Studied the effect of diabetes Frequency of facial expressions before and after 30 weeks Co-occurrence of mouthing and eye-blinking in the third trimester The difference in facial expressions in AGA, SGA, and FGR fetus

evaluation. Simultaneous fetal movement and fetal heart rate assessment throughout the pregnancy show that fMCG/NI-fECG is a valuable tool for neural and brain development analysis/research.

Autonomic nervous system maturation can be analyzed based on the relationship between fHRV and GA where increased fHRV can be observed as GA advances. Most studies included in this review used frequency domain and vagal maturation analysis based on HF parameters. Innovative HRV indices such as RQA, FABAS, entropy, PRSA, and binary symbolic dynamics remarkably improved the predictive value of the traditional HRV parameters like LTV and STV, frequency- and time-domain indices, and complexity measures on different time scales. Based on studies, it was concluded that the multivariate approach provides specific and sensitive scores as another aspect of autonomic control is reflected in other HRV parameters. As NI-fECG is a low-cost and easily accessible system than fMCG; further exploration of this technique could improve the obstetricians' judgment, especially during prematurity.

These methods will be highly helpful in controlling problems such as preeclampsia, utero asphyxia, prematurity, exposure to neurodevelopmental toxins, and fetal growth restriction. Prominently, information on fetal brain development might help the delivery timing in fetal stress by choosing the best place and method of delivery for those fetuses. Later on, this information might help start the perinatal neuroprotection medicines as early as possible. As of now, the cost is a confining segment for the usage of these techniques in clinics. Regardless, these strategies' benefit lies in assessing high-risk pregnancies since current antepartum fetal assessment tests experience a high false-positive rate (50–75%). It is anticipated that any of these techniques will eventually evolve as a further analysis after initial screening tests, thereby improving fetal health. Further investigation into the capability of these low-cost and readily available systems could guide obstetricians to assess fetal development, especially regarding prematurity, when clinical judgment is challenging.

Bibliography

1. B. Kolb, B.D. Fantie, *Development of the Child's Brain and Behavior*. *undefined* (2009), pp. 19–46. https://doi.org/10.1007/978-0-387-78867-8_2
2. B. Kolb, B. Fantie, *Development of the Child's Brain and Behavior* (1997), pp. 17–41. https://doi.org/10.1007/978-1-4757-5351-6_2
3. L. Vasung et al., Ex vivo fetal brain MRI: Recent advances, challenges, and future directions. NeuroImage **195**, 23 (2019)
4. L.E. May, A. Glaros, H.W. Yeh, J.F. Clapp, K.M. Gustafson, Aerobic exercise during pregnancy influences fetal cardiac autonomic control of heart rate and heart rate variability. Early Hum. Dev. **86**, 213–217 (2010)
5. N. Haddad et al., Correlation between fetal brain activity patterns and behavioral states: An exploratory fetal magnetoencephalography study. Exp. Neurol. **228**, 200 (2011)
6. D. Hoyer et al., Fetal autonomic brain age scores, segmented heart rate variability analysis, and traditional short term variability. Front. Hum. Neurosci. **8** (2014)

7. J. Brändle et al., Heart rate variability parameters and fetal movement complement fetal behavioral states detection via magnetography to monitor neurovegetative development. Front. Hum. Neurosci. **9**, 147 (2015)
8. F. Marzbanrad, Y. Kimura, M. Palaniswami, A.H. Khandoker, Quantifying the interactions between maternal and fetal heart rates by transfer entropy. PLoS One **10**, e0145672 (2015)
9. M.E. Thomason et al., Age-related increases in long-range connectivity in fetal functional neural connectivity networks in utero. Dev. Cogn. Neurosci. **11**, 96 (2015)
10. D.M. Garner, P. Van Leeuwen, D. Grönemeyer, S. Moosavi, Assessment of fetal development by HRV and chaotic global techniques. J. Hum. Growth Dev. **26**, 162–173 (2016)
11. F. Marzbanrad, A.H. Khandoker, Y. Kimura, M. Palaniswami, G.D. Clifford, Assessment of fetal development using cardiac valve intervals. Front. Physiol. **8**, 313 (2017)
12. P. Antsaklis, S. Porovic, G. Daskalakis, A. Kurjak, 4D assessment of fetal brain function in diabetic patients. J. Perinat. Med. **45**, 711–715 (2017)
13. S.M. Lobmaier et al., Influence of gestational diabetes on fetal autonomic nervous system: A study using phase-rectified signal-averaging analysis. Ultrasound Obstet. Gynecol. **52**, 347–351 (2018)
14. M.A.M. AboEllail, K. Kanenishi, N. Mori, O.A.K. Mohamed, T. Hata, 4D ultrasound study of fetal facial expressions in the third trimester of pregnancy. J. Matern. Fetal Neonatal Med. **31**, 1856–1864 (2018)
15. J. Zöllkau, E.M. Dölker, A. Schmidt, U. Schneider, D. Hoyer, Dependencies between maternal and fetal autonomic tone. J. Perinat. Med. **47**, 323–330 (2019)
16. K. Chen et al., Multiscale coupling of uterine electromyography and fetal heart rate as a novel indicator of fetal neural development. Front. Neurol. **10**, 760 (2019)
17. N. Mori et al., Fetal facial expressions in small-for-gestational-age and growth-restricted fetuses. J. Matern. Fetal Neonatal Med. **32**, 1426–1432 (2019)
18. M.D. Wheelock et al., Sex differences in functional connectivity during fetal brain development. Dev. Cogn. Neurosci. **36** (2019)
19. J.H. Zavala, L. Ecklund-Flores, M.M. Myers, W.P. Fifer, Assessment of autonomic function in the late term fetus: The effects of sex and state. Dev. Psychobiol. **62**, 224–231 (2020)
20. S.M. Lobmaier et al., Fetal heart rate variability responsiveness to maternal stress, non-invasively detected from maternal transabdominal ECG. Arch. Gynecol. Obstet. **301**, 405–414 (2020)
21. D. Niepel et al., A pilot study: Auditory steady-state responses (ASSR) can be measured in human fetuses using fetal magnetoencephalography (fMEG). PLoS One **15**, e0235310 (2020)
22. R. Avci et al., Studying the effect of maternal pregestational diabetes on fetal neurodevelopment using magnetoencephalography. Clin. EEG Neurosci. **51**, 331–338 (2020)
23. I.V. Lakhno, S.E. Malikova, Delayed neurological maturation is a cause for distress during fetal growth restriction. Reprod. Endocrinol., 82–85 (2020). https://doi.org/10.18370/2309-4117.2020.53.82-85
24. P. Mannella et al., A feasibility study on non-invasive fetal ECG to evaluate prenatal autonomic nervous system activity. Eur. J. Obstet. Gynecol. Reprod. Biol. **246**, 60–66 (2020)
25. X. Li, J. Hect, M. Thomason, D. Zhu, Interpreting Age Effects of Human Fetal Brain from Spontaneous fMRI using Deep 3D Convolutional Neural Networks. Proc. Int. Symp. Biomed. Imaging **2020**, 1424–1427 (2019)
26. D. Hoyer et al., Can fetal heart rate variability obtained from cardiotocography provide the same diagnostic value like from electrophysiological interbeat intervals? Physiol. Meas. **42**, 015006 (2021)
27. U. Schneider et al., The effect of antenatal steroid treatment on fetal autonomic heart rate regulation revealed by fetal magnetocardiography (fMCG). Early Hum. Dev. **86**, 319–325 (2010)
28. R.T. Wakai, Assessment of fetal neurodevelopment via fetal magnetocardiography. Exp. Neurol. **190**, 65–71 (2004)

29. U. Schneider et al., Fetal heart rate variability reveals differential dynamics in the intrauterine development of the sympathetic and parasympathetic branches of the autonomic nervous system. Physiol. Meas. **30**, 215–226 (2009)
30. A.L. Anderson, M.E. Thomason, Functional plasticity before the cradle: A review of neural functional imaging in the human fetus. Neurosci. Biobehav. Rev. **37**, 2220–2232 (2013)
31. M. Rutherford et al., MR imaging methods for assessing fetal brain development. Dev. Neurobiol. **68**, 700–711 (2008)
32. J. Fulford et al., Fetal brain activity and hemodynamic response to a vibroacoustic stimulus. Hum. Brain Mapp. **22**, 116 (2004)
33. J. Fulford et al., Fetal brain activity in response to a visual stimulus. Hum. Brain Mapp. **20**, 239–245 (2003)
34. V. Schöpf, G. Kasprian, P.C. Brugger, D. Prayer, Watching the fetal brain at 'rest'. Int. J. Dev. Neurosci. **30**, 11–17 (2012)
35. H. Eswaran, C.L. Lowery, J.D. Wilson, P. Murphy, H. Preissl, Functional development of the visual system in human fetus using magnetoencephalography. Exp. Neurol. **190**, 52–58 (2004)
36. C.L. Lowery, R.B. Govindan, H. Preissl, P. Murphy, H. Eswaran, Fetal neurological assessment using noninvasive magnetoencephalography. Clin. Perinatol. **36**, 701 (2009)
37. H. Eswaran et al., Short-term serial magnetoencephalography recordings of fetal auditory evoked responses. Neurosci. Lett. **331**, 128–132 (2002)
38. E. Schleussner, U. Schneider, Developmental changes of auditory-evoked fields in fetuses. Exp. Neurol. **190**, 59–64 (2004)
39. R. Draganova et al., Sound frequency change detection in fetuses and newborns, a magnetoencephalographic study. NeuroImage **28**, 354–361 (2005)
40. R. Draganova, H. Eswaran, P. Murphy, C. Lowery, H. Preissl, Serial magnetoencephalographic study of fetal and newborn auditory discriminative evoked responses. Early Hum. Dev. **83**, 199–207 (2007)
41. A.A. Benasich, P. Tallal, Infant discrimination of rapid auditory cues predicts later language impairment. Behav. Brain Res. **136**, 31–49 (2002)
42. C.J. Sheridan et al., Neonatal and fetal response decrement of evoked responses: A MEG study. Clin. Neurophysiol. **119**, 796–804 (2008)
43. D. Ayres-De-Campos, C.Y. Spong, E. Chandraharan, FIGO consensus guidelines on intrapartum fetal monitoring: Cardiotocography. Int. J. Gynaecol. Obstet. **131**, 13–24 (2015)
44. A. Agostinelli et al., Noninvasive fetal electrocardiography: An overview of the signal electrophysiological meaning, recording procedures, and processing techniques. Ann. Noninvasive Electrocardiol. **20**, 303–313 (2015)
45. R. Vullings, J.O.E.H. van Laar, Non-invasive fetal electrocardiography for intrapartum cardiotocography. Front. Pediatr. **8**, 854 (2020)
46. G.D. Clifford, I. Silva, J. Behar, G.B. Moody, Non-invasive fetal ECG analysis. Physiol. Meas. **35**, 1521–1536 (2014)
47. J. Reinhard, B.R. Hayes-Gill, Q. Yi, H. Hatzmann, S. Schiermeier, Comparison of non-invasive fetal electrocardiogram to Doppler cardiotocogram during the 1st stage of labor. J. Perinat. Med. **38**, 179–185 (2010)
48. J. Reinhard et al., Intrapartum signal quality with external fetal heart rate monitoring: A two way trial of external Doppler CTG ultrasound and the abdominal fetal electrocardiogram. Arch. Gynecol. Obstet. **286**, 1103–1107 (2012)
49. W.R. Cohen, B. Hayes-Gill, Influence of maternal body mass index on accuracy and reliability of external fetal monitoring techniques. Acta Obstet. Gynecol. Scand. **93**, 590–595 (2014)
50. E.W. Abdulhay et al., Review article: Non-invasive fetal heart rate monitoring techniques. Biomed. Sci. Eng. **2**, 53–67 (2014)
51. A. Matonia et al., Fetal electrocardiograms, direct and abdominal with reference heartbeat annotations. Sci. Data **71**(7), 1–14 (2020)
52. H.M. Yeh et al., A new method to derive fetal heart rate from maternal abdominal electrocardiogram: Monitoring fetal heart rate during cesarean section. PLoS One **10**, e0117509 (2015)

53. S. Campbell, A short history of sonography in obstetrics and gynaecology. Facts Views Vis. ObGyn **5**, 213 (2013)
54. T. Hata, Current status of fetal neurodevelopmental assessment: Four-dimensional ultrasound study. J. Obstet. Gynaecol. Res. **42**, 1211–1221 (2016)
55. T. Hata, S.Y. Dai, G. Marumo, Ultrasound for evaluation of fetal neurobehavioural development: From 2-D to 4-D ultrasound. Infant Child Dev. **19**, 99–118 (2010)
56. A. Kuno et al., Three-dimensional sonographic assessment of fetal behavior in the early second trimester of pregnancy. J. Ultrasound Med. **20**, 1271–1275 (2001)
57. A. Kurjak et al., New scoring system for fetal neurobehavior assessed by three- and four-dimensional sonography. J. Perinat. Med. **36**, 73–81 (2008)
58. M.A.M. Aboellail, T. Hata, Fetal face as important indicator of fetal brain function. J. Perinat. Med. **45**, 729–736 (2017)
59. T. Hata, K. Kanenishi, U. Hanaoka, G. Marumo, HDlive and 4D ultrasound in the assessment of fetal facial expressions. Fetal facial expressions. Donald Sch. J Ultrasound Obstet. Gynecol. **9**, 44–50 (2015)
60. M. Predojevic et al., An attempt to standardize Kurjak's antenatal neurodevelopmental test: Osaka consensus statement. Donald Sch. J. Ultrasound Obstet. Gynecol. **5**, 317–329 (2011)
61. M. Sato et al., 4D ultrasound study of fetal facial expressions at 20-24 weeks of gestation. Int. J. Gynaecol. Obstet. **126**, 275–279 (2014)
62. K. Kanenishi, U. Hanaoka, J. Noguchi, G. Marumo, T. Hata, 4D ultrasound evaluation of fetal facial expressions during the latter stages of the second trimester. Int. J. Gynaecol. Obstet. **121**, 257–260 (2013)
63. F. Yan et al., Four-dimensional sonographic assessment of fetal facial expression early in the third trimester. Int. J. Gynecol. Obstet. **94**, 108–113 (2006)
64. N. Reissland, B. Francis, J. Mason, K. Lincoln, Do facial expressions develop before birth? PLoS One **6**, e24081 (2011)
65. M. Kleven, W. Koek, Differential effects of direct and indirect dopamine agonists on eye blink rate in cynomolgus monkeys. *undefined* (1996)
66. G. Dreisbach et al., Dopamine and cognitive control: The influence of spontaneous eyeblink rate and dopamine gene polymorphisms on perseveration and distractibility. Behav. Neurosci. **119**, 483–490 (2005)
67. L.S. Colzato, W.P.M. Van Den Wildenberg, N.C. Van Wouwe, M.M. Pannebakker, B. Hommel, Dopamine and inhibitory action control: Evidence from spontaneous eye blink rates. Exp. Brain Res. **196**, 467 (2009)
68. N. Reissland, B. Francis, J. Mason, Development of fetal yawn compared with non-yawn mouth openings from 24–36 weeks gestation. PLoS One **7**, e50569 (2012)
69. N. Reissland, C. Mason, B. Schaal, K. Lincoln, Prenatal mouth movements: Can we identify co-ordinated fetal mouth and LIP actions necessary for feeding? Int. J. Pediatr. **2012**, 1–5 (2012)
70. N. Horimoto, T. Koyanagi, S. Nagata, H. Nakahara, H. Nakano, Concurrence of mouthing movement and rapid eye movement/non-rapid eye movement phases with advance in gestation of the human fetus. Am. J. Obstet. Gynecol. **161**, 344–351 (1989)
71. M. López-Teijón, Á. García-Faura, A. Prats-Galino, Fetal facial expression in response to intravaginal music emission. Ultrasound J. Br. Med. Ultrasound Soc. **23**, 216 (2015)
72. T. Hata et al., Three- and four-dimensional HDlive rendering images of normal and abnormal fetuses: Pictorial essay. Arch. Gynecol. Obstet. **286**, 1431–1435 (2012)
73. E. Chandraharan, Rational approach to electronic fetal monitoring during labour in 'all' resource settings. Sri Lanka J. Obstet. Gynaecol. **32**, 77 (2012)
74. Y. Sorokin et al., The association between fetal heart rate patterns and fetal movements in pregnancies between 20 and 30 weeks' gestation. Am. J. Obstet. Gynecol. **143**, 243–249 (1982)
75. T. Wheeler, A. Murrills, Patterns of fetal heart rate during normal pregnancy. BJOG Int. J. Obstet. Gynaecol. **85**, 18–27 (1978)

76. B. Zanini, R.H. Paul, J.R. Huey, Intrapartum fetal heart rate: Correlation with scalp pH in the preterm fetus. Am. J. Obstet. Gynecol. **136**, 43–47 (1980)
77. F. Goupil et al., Antepartum fetal heart rate monitoring: II. Deceleration patterns. Eur. J. Obstet. Gynecol. Reprod. Biol. **11**, 239–249 (1981)
78. D. Devane et al., Cardiotocography versus intermittent auscultation of fetal heart on admission to labour ward for assessment of fetal wellbeing. Cochrane Database Syst. Rev. **1** (2017)
79. L. Hruban et al., Agreement on intrapartum cardiotocogram recordings between expert obstetricians. J. Eval. Clin. Pract. **21**, 694–702 (2015)
80. A. Georgieva et al., Computer-based intrapartum fetal monitoring and beyond: A review of the 2nd Workshop on Signal Processing and Monitoring in Labor (October 2017, Oxford, UK). Acta Obstet. Gynecol. Scand. **98**, 1207–1217 (2019)
81. M.G. Signorini, N. Pini, A. Malovini, R. Bellazzi, G. Magenes, Integrating machine learning techniques and physiology based heart rate features for antepartum fetal monitoring. Comput. Methods Prog. Biomed. **185** (2020)
82. K.K. Spyridou, L.J. Hadjileontiadis, Analysis of fetal heart rate in healthy and pathological pregnancies using wavelet-based features. Annu. Int. Conf. IEEE Eng. Med. Biol. Soc. IEEE Eng. Med. Biol. Soc. Annu. Int. Conf. **2007**, 1908–1911 (2007)

Antepartum Noninvasive Evaluation of Fetal Myocardial Performance from Continuous Doppler Signals and Its Research Potential

Ahsan H. Khandoker and Amna Samjeed

1 Introduction

The prevalence of congenital heart defects (CHDs) is 3–8 per 1000 pregnancies at birth [1]. Early detection of fetuses with potential CHD and fetal distress (e.g., low oxygen levels in the fetus) results in an improvement in hemodynamic status, neonatal morbidity, and surgical outcome [2]. Fetal ECG (fECG) and Doppler ultrasound signals (DUS) provide clinically and physiologically significant information about the health status of a fetus. Therefore, improving techniques for evaluating fetal cardiac activity needs more attention. Given the challenges in processing highly nonstationary signal DUS, three major research questions require more investigation.

1. If it is possible to obtain beat-to-beat FHR reliably from fetal DUS signals compared to the same obtained by R–R intervals of fECG signals.
2. If timings of fetal cardiac events can be estimated based on electrical (fetal ECG extracted from abdominal ECG) and mechanical [Doppler ultrasound (DUS) signals] heart activity.
3. If fetal myocardial performance indices calculated from DUS-based systolic and diastolic intervals such as isovolumic contraction time (ICT), isovolumic relaxation time (IRT), ventricular ejection time (VET), and ventricular filling time (VFT) can have any clinical value (e.g., identifying sick fetuses).

The following is a summary of several research investigations answering the abovementioned research questions (RQ).

A. H. Khandoker (✉) · A. Samjeed
Department of Biomedical Engineering, Khalifa University, Abu Dhabi, United Arab Emirates
e-mail: ahsan.khandoker@ku.ac.ae

D. Pani (ed.), *Innovative Technologies and Signal Processing in Perinatal Medicine*, https://doi.org/10.1007/978-3-031-32625-7_6

2 Estimating Beat-to-Beat Fetal Heart Rate from Continuous DUS (RQ 1)

Continuous DUS, a method referred to as EMD-kurtosis, was applied to estimate fetal heart rate from beat-to-beat [3]. The oscillatory behavior of DUS was examined using EMD. It is a method that deals with nonstationary and nonlinear data sets. Based on the EMD method, signals are considered to be made up of different simple intrinsic oscillation modes. Before applying the method, the signal was cleaned by removing the background noise from the DUS signal by wavelet thresholding on the first 15 levels of Haar wavelets. The denoised signal was then decomposed into its intrinsic mode functions (IMFs) using the EMD method. After decomposing to IMF, kurtosis was calculated. Two conditions must be met for the IMFs to represent these oscillations: zero-crossings and extremes must either be equal or differ at most by one in the entire dataset, and a mean value should be zero in both the envelope defined by local maxima and minima.

Using the Chebyshev inequality, the kurtosis of each IMF was determined whether it was reliable for detecting the location of the DUS peak. For a fine selection of the best kurtosis vectors, two additional measures were also computed, which are a measure of mismatch error between the estimation of beat count based on the peaks of the selected kurtosis vectors and the actual R peak count (determined from fECG) and a standard deviation that measures the difference between the exact R peak location and the estimated beat location is used to estimate the variability of the estimated beat location. The selected vectors were then summed up, and a peak search was conducted with a minimum peak distance of 300 ms. Results obtained using EMD-kurtosis were compared with the conventional autocorrelation function (AF) method. Finally, the Kruskal–Wallis test was used to compare the estimated beat-to-beat with valid RR (using EMD-kurtosis methods and AF) in the mean, standard deviation (SDNN), and root mean square of successive difference (RMSSD).

Figure 1 illustrates an extracted fECG with its corresponding DUS and estimated beat location according to the EMD-kurtosis method. A quantified comparison between AF and EMD-kurtosis method shows that mean successive beat error and mismatch error are lower in all GA using the proposed EMD-kurtosis method (Fig. 2). In the early group, EMD-kurtosis significantly reduced the mismatch error (p 0.01); in the late group, EMD-kurtosis significantly reduced the mean successive beat error (p 0.05). A comparison of early and late groups using the same method showed no significant differences. The EMD-kurtosis method showed less than 10% error, while the AF showed some cases exceeding that error level. In the early group, there was a more significant percentage of mismatch error when using the AF method. Based on the EMD-kurtosis method, mean beat-to-beat was better estimated, while SNDD and RMSSD were significantly higher than true RRs using both EMD-kurtosis and AF methods (Fig. 3). The AF method performed better in estimating beat-to-beat intervals when true RR variability was negligible, whereas the EMD-kurtosis method performed better when true RR variability was high.

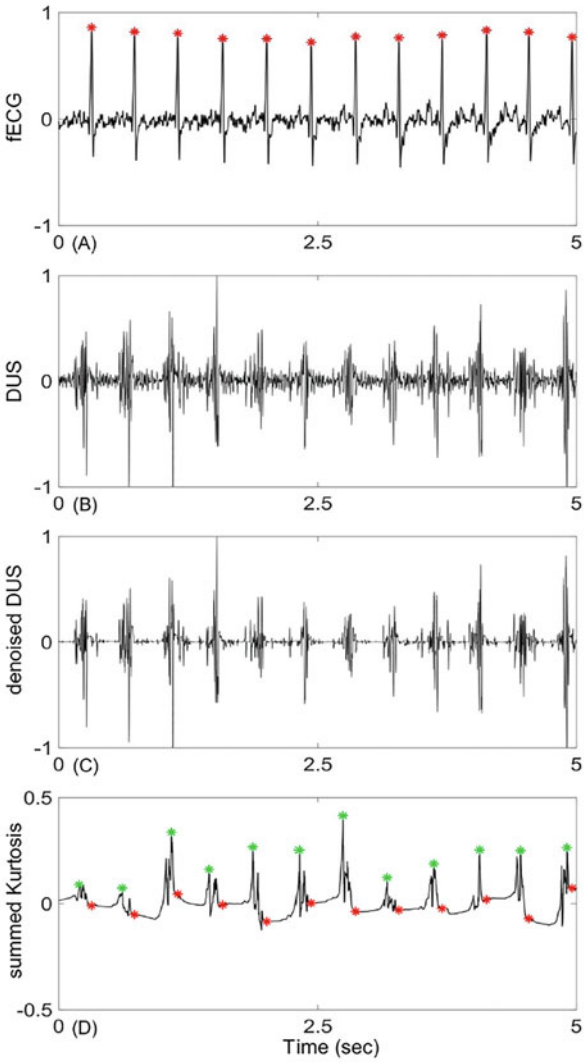

Fig. 1 (**a**) Fetal ECG signal; (**b**) Doppler ultrasound signal; (**c**) denoised DUS signal; (**d**) summed selected kurtosis signal (red starts are actual R peaks from fECG and green represents R peaks location using this method [3])

The Bland–Altman plots of the estimated mean beat-to-beat, SDNN, and RMSSD calculated using the two methods are shown in Fig. 4 compared to the true RR interval calculated from the fECG. By choosing the appropriate window size to compute the kurtosis, the number of beats and the variability between beats could be estimated more accurately. Optimal results were obtained by selecting a window size slightly smaller than the duration of the mean RR. Increasing or decreasing the window size increases the probability of missing true peaks in conditions of low SNR (the early group) and multiple peaks resulting from distinct wall and valve movements (the late group). There was a greater level of robustness

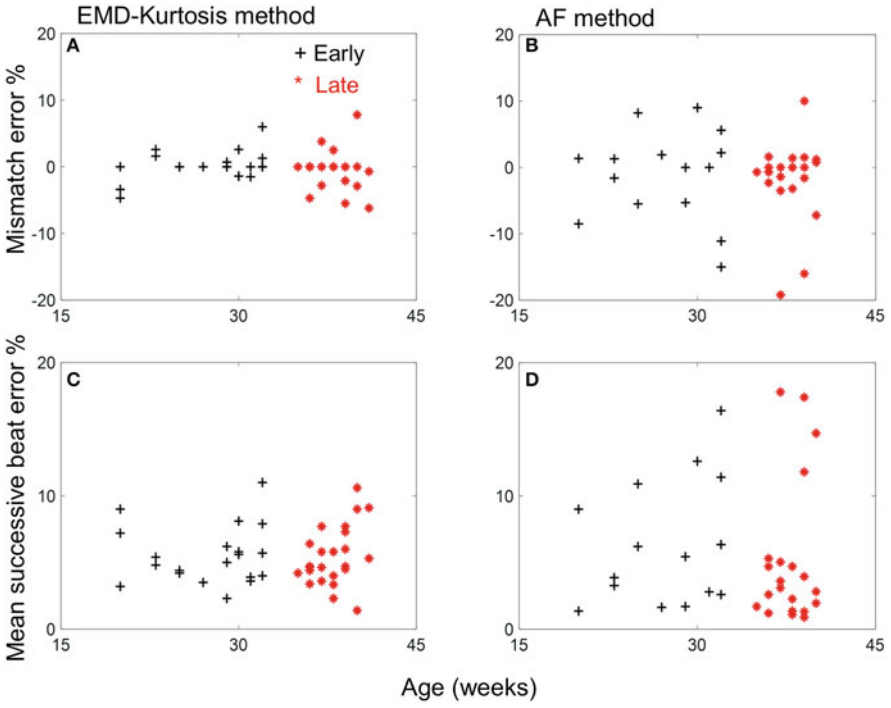

Fig. 2 Comparison of EMD-kurtosis method (**a**, **c**) and for the AF method (**b**, **d**), successive beat error, and mismatch error versus age in early and late gestational periods [3]

with the EMD-kurtosis method compared to the AF method when the SNR was low. Compared with the AF method, the mismatch error was reduced by four times for the early group and two times for the late group.

For an accurate estimation of HRV, even though the mean successive beat error for the EMD-kurtosis method was lower than for the AF method, the error was still deemed high. It is impossible to completely separate the movements of the heart valves, which are considered high frequency, from the activities of the wall, which are considered to be of a lower frequency, which results in increased variability when estimating HRV from DUS signals. It is also possible for HRV to be affected by other factors, such as the movement of the mother or baby and changes in the orientation of the Doppler probe to the fetal heart. In both early and late groups, the EMD-kurtosis method showed improved accuracy in estimating mean heart rate compared to the AF method. This research investigation proved that estimating beat-to-beat fetal heart rate from continuous Doppler signal is possible, and further exploration is needed before taking it into clinics.

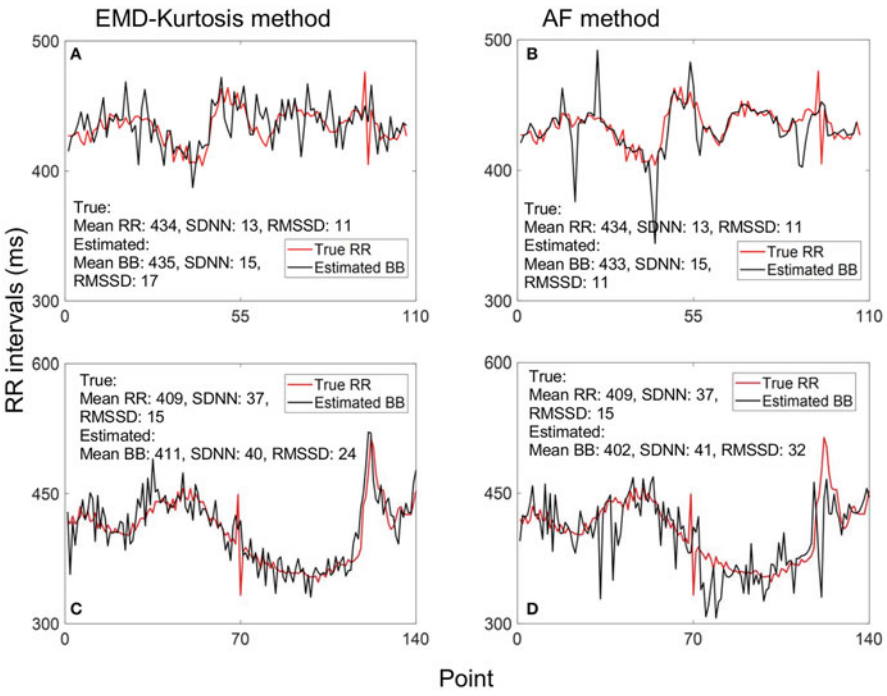

Fig. 3 (**a**, **c**) Illustrate how to estimate beat-to-beat intervals (BB) using the EMD-kurtosis method, respectively, and (**b**, **d**) using the AF method for the same signal. The red line indicates the actual RR interval as determined from the fECG signal. Signals with lower variability performed better when estimated using the AF method (**a**, **b**), while signals with higher RR variability performed better when estimated using the EMD-kurtosis method (**c**, **d**) [3]

3 Estimation of Fetal Cardiac Events from fECG and DUS (RQ2)

Two articles address this research question, one of which presents a novel non-invasive algorithm for identifying the timings of fetal cardiac events from fECG and DUS data [4]. The other article used an efficient model combining K-means clustering and hybrid SVM-HMM modeling techniques [5].

The P wave initiates atrial contraction in the ECG signal, whereas the R wave is responsible for ventricular contraction. Therefore, important content may be present in the ultrasound signal during these times. Aortic and mitral valve opening and closing timings are plotted in Fig. 5 based on the fECG. Cardiac activity is reflected as Doppler frequency shifts. The PEP refers to the entire time between the onset of electrical excitation and the opening of the aortic (semilunar) valve. The remaining systolic interval (VET) is the period between the opening of the aortic valve and its closure when blood flows from the ventricle to the aorta. There is a variation in the DUS signals over time primarily due to variations in the relative orientation of the

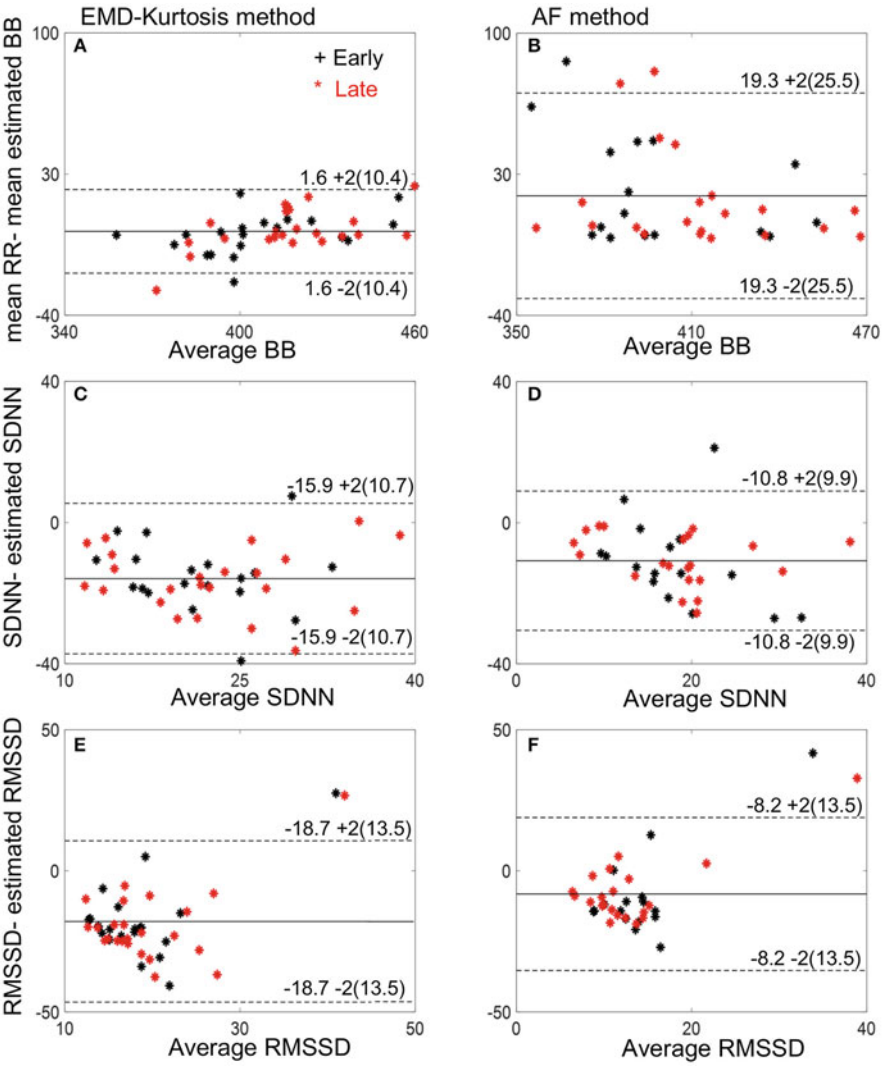

Fig. 4 Bland–Altman plots illustrate the estimated beat-to-beat (BB), SDNN, and RMSSD using the EMD-kurtosis method (**a**, **c**, **e**), and the AF (**b**, **d**, **f**), respectively. Early group cases are indicated by black stars, while late group cases are indicated by red stars [3]

ultrasound transducer and the fetal heart [6]. Therefore, it is unlikely to distinguish all timings of cardiac valve events throughout the cardiac cycle [7]. There is no doubt that fetal movement significantly impacts the received signal.

One study used time-frequency wavelet analysis to interpret DUS signals about cardiac valve movements. Wavelet analysis is becoming increasingly valuable as a tool for analyzing nonstationary signals with changing spectral characteristics

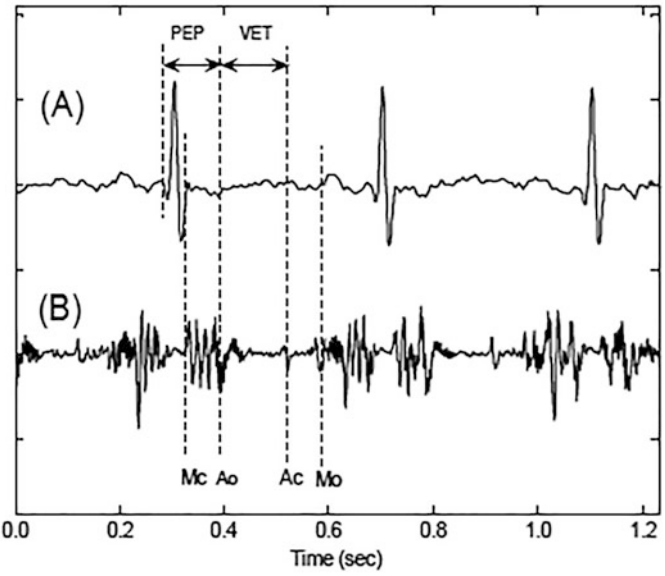

Fig. 5 (**a**) Fetal ECG signal; (**b**) DUS signal. Aortic opening (Ao), mitral opening (Mo), aortic closing (Ac), mitral closing (Mc), pre-ejection period (PEP), and ventricular ejection time (VET) [4]

over time. A wavelet transform (WT) decomposes a signal into its detailed and approximate components using a set of essential functions. We processed the detailed component at level 2 of the DUS signal (100–200 Hz) to extract the higher frequency content. An envelope of cubic splines was used to fit the maxima of the absolute values of the detailed signals.

Figure 6 shows an M-mode, B-mode, and pulsed DUS for examining the opening and closing timings of the aortic valve. This is used for the validation of the model. In the case of the fetal cardiovascular examination, the M-mode is a valuable adjunct because it enables the physician to measure the valve's structure accurately. The use of pulsed Doppler imaging allows a physician to determine the characteristics and direction of blood flow within the heart. This Doppler waveform of aortic blood flow was obtained from the five-chamber view of the heart using the long axis. During end-systole and end-diastole (closure of the atrioventricular valves), the M-mode cursor was placed perpendicular to the interventricular septum.

Figures 7 and 8 illustrate FECGs and DUS for several cardiac cycles, as well as detailed wavelet decompositions at level 2 for the DUS signal. Figure 7 represents the timings of the aortic valve motions concerning the ECG, while Fig. 8 illustrates mitral valve motions. These were highlighted in the DUS and confirmed by pulsed DUS in the bottom panel. The time durations from the R wave within each RR interval were chosen to detect the peak timings of the aortic valve and mitral valve motion events. For Ao, they ranged from 0.05 to 0.10 seconds, and for Ac, from 0.14

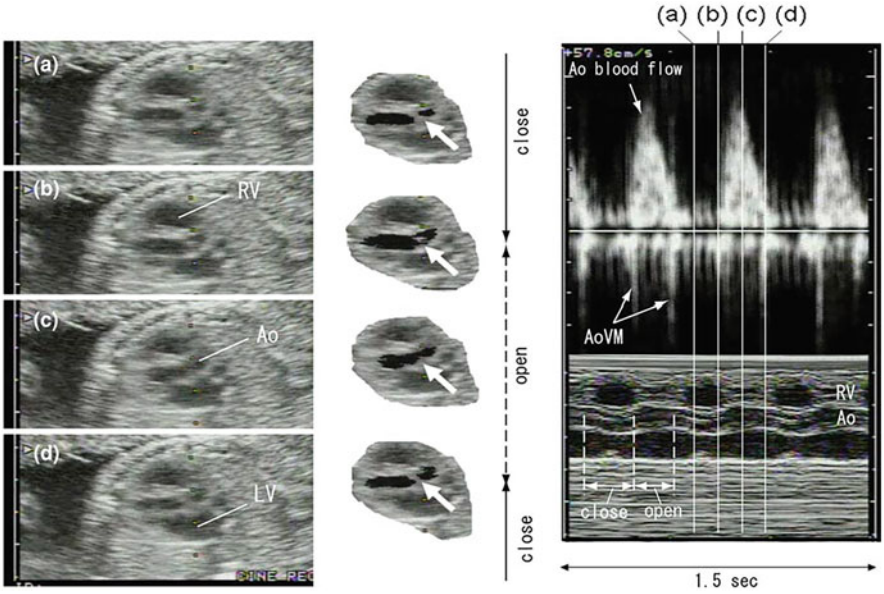

Fig. 6 Left panel shows B-mode views of the movements of a fetal aortic valve. Images derived from B-mode views are presented in the middle panels. (**a**) Ac, (**b**) onset of Ao, (**c**) Ao, and (**d**) Ac [4]. Aortic valve opening and closing are depicted in the right panels in pulsed-wave Doppler mode as well as their M-mode images during the same time phases. Ao aorta, RV right ventricle, AoVM aortic valve movement, LV left ventricle

to 0.26 seconds. However, concerning mitral valves' relative timings, we used 0.00–0.05 seconds for Mc and 0.26–0.33 seconds for Mo. Even though the QT interval can be measured using the ECG following delivery, it is impossible to do so in utero. An electromechanical Q-Ac interval is calculated from when the Q-wave begins to become visible until the aortic valve closes, thereby representing a QT interval that can be corrected for heart rate.

The mean duration of the aortic valve openings and closings within each RR interval from the onset of the Q-waves of FECG, respectively, Q-Ao and Q-Ac, were calculated. Results showed that there were cases in which all of the events were easily identifiable. In some cases, however, only certain events were observed. Abnormal fetuses' valve timing intervals did not differ significantly from those with normal fetuses' valve timing intervals.

Valve timings were significantly correlated in abnormal fetuses compared with those in normal fetuses. There was a strong correlation between Q-Ao, that is, PEP, and R-R intervals in abnormal fetuses ($r = 0.496$, $p = 0.0013$). In contrast, normal fetuses showed a weak correlation ($r = 0.0448$, $p = 0.459$). Normal fetuses showed a positive correlation between Q-Mc and RR, while abnormal fetuses showed a negative correlation. Additionally, Q-Mc and Q-Ac exhibited positive and negative correlations in abnormal and normal fetuses, respectively. R-R intervals and Ac-Ao

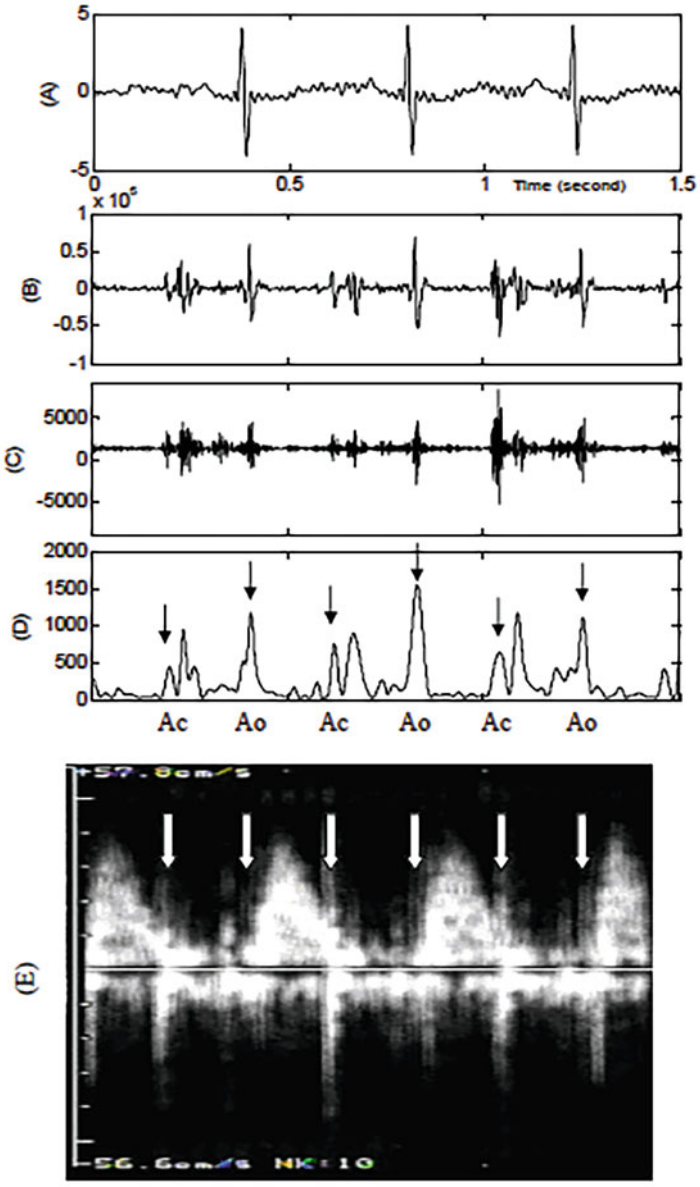

Fig. 7 (**a**) fECG signal. (**b**) DUS signal. (**c**) Wavelet decomposition of signal at level 2. (**d**) The cubic splines envelope of maxima of the detailed signal. (**e**) Pulsed-wave Doppler images. Aortic opening (Ao) and aortic closing (Ac) [4]

(i.e., VET) correlate more strongly in normal fetuses than in abnormal ones. As a result, we speculate that abnormal fetuses have different mechanisms for controlling

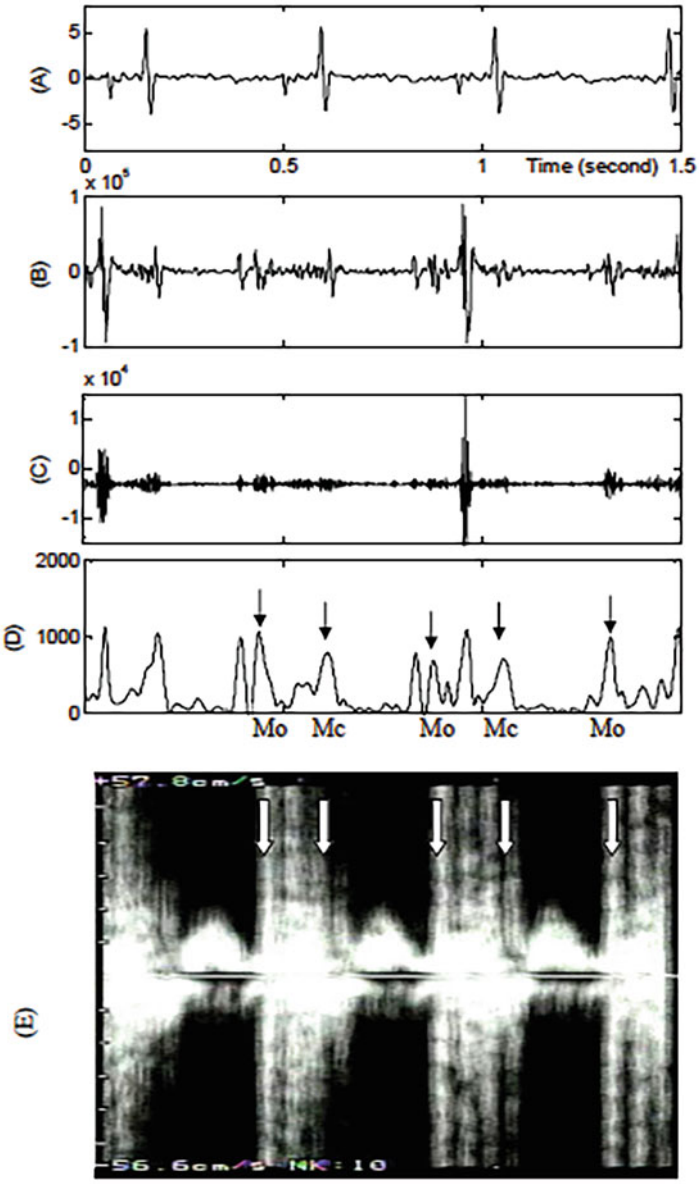

Fig. 8 (**a**) fECG signal. (**b**) DUS signal. (**c**) Wavelet decomposition of signal at level 2. (**d**) The cubic splines envelope of maxima of the detailed signal. (**e**) Pulsed-wave Doppler images. Mitral opening (Mo) and mitral closing (Mc) [4]

heart contractions than healthy fetuses, which may be related to abnormal fetuses' rigidity in controlling heart contractions. Due to a lack of flexibility in the opening

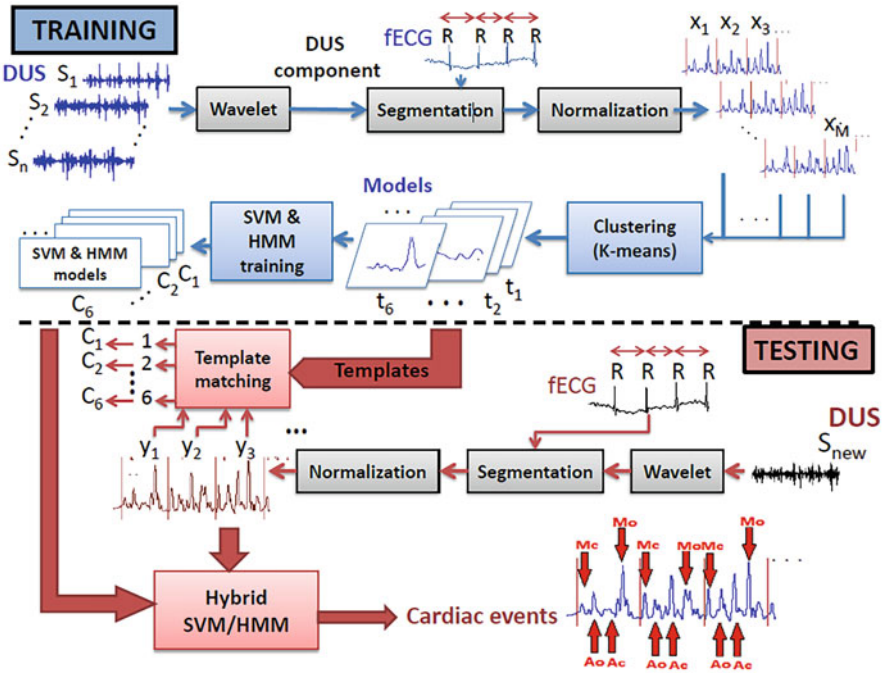

Fig. 9 Training and testing process block diagram [5]

and closing of the cardiac valves in abnormal fetuses, valve movement and timing intervals may be significantly correlated.

Using multiresolution wavelet analysis of Doppler signals, it was possible to identify the frequency contents associated with aortic and mitral valve opening and closing, as shown by M-mode and pulsed Doppler images. According to these findings, cardiac events contributing to the Doppler signal can be distinguished, and this could result in a more accurate clinical recognition of conditions such as fetal arrhythmia, anoxia, and heart failure. The results of this study could make it possible to record PEP and VET of the fetal heart continuously in real time.

Another article used an efficient model combining K-means clustering and hybrid SVM-HMM modeling techniques to identify the timings of fetal cardiac events from fECG and DUS data. In this work, the K-means clustering method is first used to find the patterns of the DUS components and match each beat-to-beat DUS component to one of the models. Then, the valve motion events are identified from the peaks of the DUS component using hybrid SVM-HMM explicitly trained for its corresponding cluster. In this study, six patterns were identified for DUS components. Each pattern's occurrence rate was also analyzed for early- and late-age fetuses to investigate its relationship with gestational age. The block diagram of the training and testing process is shown in Fig. 9.

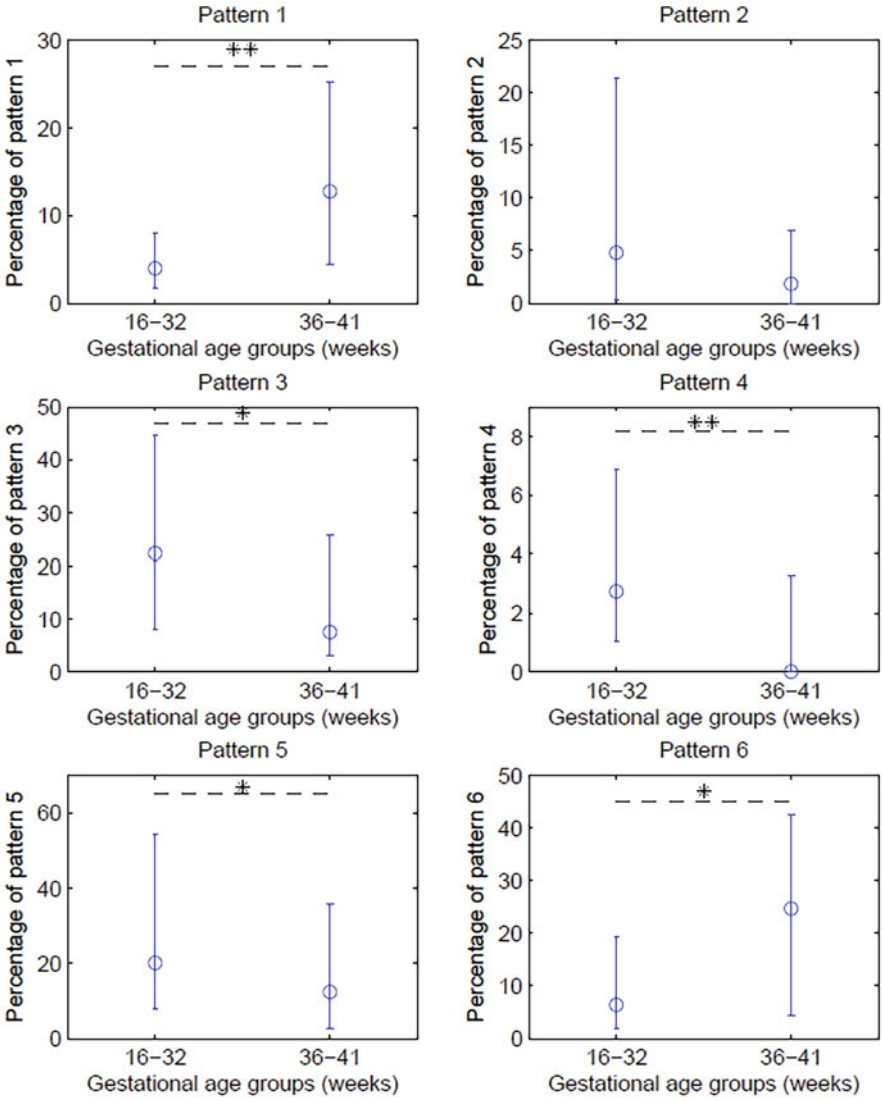

Fig. 10 A comparison of the occurrence rate of each pattern in early gestation (16–32 weeks) and late gestation (36–41 weeks) [5]

In the training phase, the segments of the DUS components were clustered by the K-means method. Six clusters with different patterns of the DUS component segments were obtained. The cluster centroids have peaks in the time range of the valve motion events but with different comparative amplitudes across six clusters. The percentage of occurrences of patterns in early and late gestation groups was compared (Fig. 10). The result shows that patterns 1 and 6 occurred at a significantly higher rate after 36 weeks compared to the cases before 32 weeks.

On the other hand, patterns 3–5 were observed with significantly higher rates for the early gestation group. The percentage difference between the two groups was not significant for pattern 2. This method showed average precision and recall of 83.4% and 84.2%, respectively.

The variability of the patterns is also attributed to fetal heart development and maturation. K-means was used to cluster the DUS component patterns into six groups. The DUS components showed peaks corresponding to valve motion in a standard range of timings and amplitudes within each group, which differed from other clusters. Using the training data specific to each set, we have determined the centroid of each cluster and the range of valve motion events. This shows the difference between the average amplitudes of peaks associated with each event. To decode the peaks of the DUS components based on trained SVM-HMM specific to the matched cluster, we used clustering to train the SVM-HMM for each group separately. This method achieved greater precision and recall than the method that did not utilize clustering. As a result of clustering the data before training, the peaks associated with each event were concentrated and more unified within a specific range of timing and amplitude, enabling better identification of valve openings and closings.

The systolic time interval (STI) is an essential indicator of myocardial function. As a sensitive indicator of the part of the fetal myocardium, PEP measures the time between the onset of the QRS complex and Ao. A prolonged PEP is an early sign of hypoxemia and acidosis [8]. An indicator of fetal cardiac contractility is the Mc-Ao interval [9]. This method could accurately identify the STIs that depend on the onset of QRS complex on fECG, Mc, Ao, and Ac with a 98.6% recognition rate and an 86.3% precision. Using DUS and fECG signals, beat-to-beat valve motion timings can be continuously evaluated with less time and skill set. To determine the cardiac intervals of the fetus, fetal echocardiography is currently used [10, 11]. Furthermore, due to pulsed-wave Doppler, only one valve (e.g., mitral or aorta) is recorded. In contrast, recorded DUS data and fECG signals are used to identify the opening and closing of the mitral and aorta in each beat. To verify the results of automated identification by this method, pulsed-wave Doppler images and M-mode were used. New ways effectively identified more than 98.6% of cardiac valve motion events. Both these studies answer the research question that fetal cardiac events estimation is possible from continuous DUS.

4 Clinical Perspective of Fetal Myocardial Performance Indices Calculated from DUS-Based Systolic and Diastolic Intervals (RQ 3)

We investigated how cardiac systolic, diastolic, and myocardial performance indicators were derived using DUS [12]. TI and modified TI (KI) could distinguish between normal cases and sick ones at various gestational stages. TI and the KI were

calculated using the formula (ICT + IRT)/VET and (ICT + IRT)/VFT, respectively. Tables 1 and 2 present demographic information about the normal and abnormal populations used in this study. Fetal HR variability may not necessarily indicate a distressed fetus in all cases [13, 14]. The myocardial performance index (TI) described by Tei was considered a combined measure of cardiac function at systole and diastole [15, 16].

Using fECG, the Tei index was used to assess the performance of the fetal myocardium in sick fetuses. Since fetal circulation is primarily controlled by the ventricles and is connected to the placenta, the VFT plays a significant role in monitoring fetal–maternal circulation. Another important myocardial blood flow assessment parameter is the diastolic time, which follows the STI interval. A diastolic period is characterized by IRT from Ac to Mo time, followed by VFT from Mo to Mc time [17, 18]. An assessment of the diastolic myocardial performance of human fetuses is carried out using the KI index [19]. Electromechanical valve timing intervals can be measured using the proposed method with greater accuracy. Compared to pulsed Doppler or traditional M-mode, this method is cost-effective and employs simple techniques. This study aimed to determine the impact of congenital structural defects and abnormal heartbeats associated with conduction problems on the heart. A structural defect may include a malfunctioning valve that allows blood to be pumped and squeezed or a defect in the heart's septum. There are a number of common heart defects, such as ventricular septal and atrial septal defects.

Additionally, there are complex conditions such as Tetralogy of Fallot and transposition of the great arteries, which result in inadequate blood flow to the body and lungs [20]. Typically, these defects are caused by underdeveloped chambers in the heart or blockages in blood vessels that prevent the appropriate amount of blood from reaching the body. As a result of these heart problems, the body does not receive enough oxygen. There may also be complications involving the heart's conduction system, which is responsible for maintaining a normal heart rate of 120–160 beats per minute. These complications include fetal tachycardia, PAC, AV block, WPW, and SSS. In general, fetal arrhythmias are defined as irregularities in the cardiac rhythm of the fetus [21]. Furthermore, this study included cases of non-CHDs, including hydrops fetalis, placental abruption, and IUGR.

4.1 Evaluation of the Myocardial Performance Indices of Normal Fetuses

PEP, ICT, VFT, and fRR calculated positively correlate with gestational age (Fig. 11) in normal fetuses. PEP was found to have the highest correlation with age ($r = 0.5, p < 0.01$). While an increase in PEP will result in the ejection time staying constant or decreasing during each cardiac cycle, this could indicate an increase in stroke volume as gestation progresses. In a study published by Mensah-Brown

Table 1 Demographic data for normal and abnormal fetuses

Cases	Gestational weeks	Maternal age (years)	Maternal BMI	EFBW	Para	Gravida	Status
Normal cases							
NE ($N = 13$)	24.2 ± 4.3	32.6 ± 4.8	21.8 ± 1.6	786.4 ± 563.5	1.7 ± 1.4	0.9 ± 1.2	Normal
NM ($N = 16$)	32.3 ± 2.0	27.2 ± 5.1	24.2 ± 0.9	1963 ± 572	0.7 ± 0.8	0.2 ± 0.4	Normal
NL ($N = 26$)	38 ± 1.5	29.8 ± 5.9	23.6 ± 2.7	2727 ± 108.4	0.8 ± 0.9	0.2 ± 0.4	Normal
Abnormal cases							Abnormality
1	37	40–45	22.7	–	–	–	Bradycardia for SSS
2	31	25–30	23	1623	0	0	IUGR
3	35	35–40	25.3	–	–	–	Acute crisis fetus (placental abruption)
4	36	30–35	19.7	–	–	–	CHD
5	30	30–35	21	665	3	1	CHD
6	34	30–35	23	2100	1	1	CHD
7	30	35–40	21.5	1157	–	–	Heart failure
8	22	30–35	21.7	–	–	–	CHD
9	22	45–40	21.5	–	–	–	CHD
10	37	25–30	23.6	–	0	0	PAC-IUGR
11	24	40–45	36.2	767	1	1	PA-CAVC-SA-AV block-Polysplenia syndrome
12	24	30–35		449	0	0	Placental dysfunction
13	23	20–25	22.1	–	–	–	VSD-ASD-CDH-chromosomal aberration
14	33	20–25	26	2600	0	0	Cardiac dilatation-CHD
15	35	25–40	24				AV block
16	31	30–35	21.8	–	–	–	Medical history of intrauterine fetal death
17	20	30–35	23	428	1	1	NIHF
18	33	35–40	25.5				Fetal tachycardia
19	35	20–25	25	2373	1	1	WPW
20	29	30–35	22.8	–	–	–	HF
21	35	30–35	21.1	2448	1	1	Fetal tachycardia
22	28	40–45	22.9	859	1	0	TOF-VSD-PA-MS-PAC
23	26	20–25	24	1332	0	0	Ebstain
24	27	–	–	–	–	–	AV block- CHD -SA-CAV
25	38	–	–	–	–	–	SSS

NE normal early group, *NM* normal middle group, *NL* normal late group, *EFBW* estimated fetal birth weight, *C-section* cesarean section. Abnormality abbreviations: (1) *SSS* sick sinus syndrome, (2) *IUGR* intrauterine growth restriction, (3) *CHD* congenital heart defect, (4) *TOF* tetralogy of Fallot, (5) *PAC* premature atrial contraction, (6) *PA* pulmonary atresia, (7) *CAVC* common atrioventricular canal, (8) *SA* single atrium, (9) *VSD* ventriculoseptal defect, (10) *ASD* atrial septal defect, (11) *CDH* congenital diaphragmatic hernia, (12) *NIHF* non-immune hydrops fetalis, (13) *HF* immune hydrops fetalis, (14) *WPW* Wolff–Parkinson–White syndrome, (15) *MS* mitral stenosis, (16) *CAV* cardiac allograft vasculopathy

Table 2 Mean ± SD of the cardiac intervals for the abnormal fetuses and groups of normal fetuses

Interval		fRR (ms)	PEP (ms)	ICT (ms)	IRT (ms)	VFT (ms)	VET (ms)
Group	**Values**	**Normal cases**					
NE	Mean	404 ± 20.1	65.3 ± 4.55	33.9 ± 1.61	86.2 ± 8.39	122 ± 23.6	161 ± 6.61
	SD	8.85 ± 4.95	14 ± 3.31[a]	10.6 ± 2.11	20.1 ± 3.85	22.1 ± 4.86	18.9 ± 4.3
NM	Mean	417 ± 30.8	71.0 ± 5.27[b]	35.7 ± 3.10	82.9 ± 9.45	136 ± 28.0	162 ± 7.29
	SD	14.9 ± 8.23	15.3 ± 3.85	11.7 ± 2.63	19.9 ± 4.01	26.0 ± 6.75	21.0 ± 4.21
NL	Mean	427 ± 27.0	73.4 ± 5.95[b]	36.6 ± 3.37[b]	83.8 ± 7.73	147 ± 27.8[b]	160 ± 6.35
	SD	15.0 ± 12.2[a]	13.6 ± 3.45	11.0 ± 2.44	17.0 ± 4.15	23.9 ± 9.94[a]	17.8 ± 4.69[a,c,d]
ID	**Number of cardiac cycles**	**Abnormal cases**					
1	103	572 ± 50.4	66.2 ± 19.5	35.5 ± 14.7	82.8 ± 104[c,d]	282 ± 57.3	160 ± 22.2[c,d]
2	155	386 ± 14.1	71.9 ± 13.1[c,d]	35.1 ± 10.6	68.8 ± 98.3[c,d]	117 ± 26.1[c,d]	149 ± 17.4[c,d]
3	156	395 ± 6.64	73.4 ± 14.9	39.4 ± 14.4	51.3 ± 63.8	147 ± 13.7	149 ± 15.9
4	96	414 ± 17.1	70.5 ± 19.6	34.9 ± 14.2	62 ± 80.8	135 ± 25[c,d]	170 ± 21.2[c,d]
5	134	445 ± 19.1	63.4 ± 14	35.3 ± 11.3	58 ± 79.5	174 ± 19.7	166 ± 20.1
6	150	395 ± 3.89	79.1 ± 18.3	36.3 ± 13.2	79 ± 104	103 ± 19.4	162 ± 20.1
7	120	404 ± 17.2	73.1 ± 13.8[c,d]	32.8 ± 10.5	53 ± 74.5[c,d]	142 ± 18.4[c,d]	164 ± 17.4[c,d]
8	132	450 ± 65.7[c,d]	71.8 ± 18.9[c,d]	36.3 ± 13.7	69.3 ± 101[c,d]	167 ± 65.2[c,d]	161 ± 25.2
9	122	491 ± 150	65.1 ± 13.1	33 ± 11.4	60 ± 93	217 ± 147	172 ± 25.4
10	116	514 ± 670	64 ± 13.7[c,d]	34 ± 9.83	76.5 ± 99	228 ± 673	162 ± 17.2
11	61	963 ± 167	61.2 ± 15	33.7 ± 9.7	75 ± 104[c,d]	669 ± 160	168 ± 22.4[c,d]
12	146	409 ± 5.23	65.3 ± 9.87	28.8 ± 6.46	56 ± 68	140 ± 19.4	174 ± 11
13	67	890 ± 8.74[c,d]	73.6 ± 13.2[c,d]	35.5 ± 11.3	76 ± 104[c,d]	608 ± 25.8[c,d]	162 ± 56.1
14	122	490 ± 171	72.7 ± 20.5	35.7 ± 14.9	76 ± 101	202 ± 176	166 ± 28.3
15	64	919 ± 337	67.3 ± 17.1[c,d]	34.1 ± 13.2	82 ± 102	634 ± 341	154 ± 21.8[c,d]
16	162	367 ± 12.7	62.5 ± 11.9	32.1 ± 8.5	83 ± 110[c,d]	88.3 ± 21.8[c,d]	150 ± 18.8[c,d]
17	77	770 ± 292	68.3 ± 14.7[c,d]	34.2 ± 12.5	73.5 ± 106[c,d]	499 ± 285	160 ± 22.5[c,d]
18	200	297 ± 71	82.1 ± 15.3[c,d]	35.3 ± 11.8	53 ± 74	71 ± 71.7	140 ± 23.9[c,d]
19	137	435 ± 15.4	83 ± 15[c,d]	34 ± 10.8	64.8 ± 84.3	158 ± 26.7[c,d]	168 ± 18.2[c,d]
20	143	417 ± 10.3	72 ± 18.7	35.5 ± 12.7	74 ± 108[c,d]	133 ± 29.9[c,d]	159 ± 26.7
21	175	342 ± 17.1	75.3 ± 14.7	36.6 ± 11.8	65.5 ± 96.5	76.8 ± 23.3[c,d]	148 ± 21.9
22	144	414 ± 96	66.2 ± 17.6[c,d]	35.3 ± 15	76 ± 101	122 ± 98.3	168 ± 20.4[c,d]
23	84	472 ± 16.1	66.8 ± 16.6[c,d]	37.8 ± 14.3	78 ± 96[c,d]	188 ± 21.9	162 ± 20.3[c,d]
24	67	885 ± 216	72.6 ± 13.2[c,d]	32.4 ± 10.9	70.3 ± 106[c,d]	607 ± 214	160 ± 24.1[c,d]
25	103	577 ± 285	64.5 ± 19.5	35.7 ± 13.2	85.3 ± 102	292 ± 287	162 ± 22.3[c,d]

PEP pre-ejection period, *ICT* isovolumetric contraction time, *IRT* isovolumetric relaxation time, *VET* ventricular ejection time, *VFT* ventricular filling time, *fRR* Fetal RR, *HR* heart rate in beat per minute (bpm), *SD* standard deviation, *w1,2* scale and shape coefficients of the Weibull fit, *NE* normal early gestational group, *NM* normal middle gestational group, *NL* normal late gestational group

[a]Not normally distributed data

[b]Significantly different from NE ($p < 0.05$)

[c]Normally distributed data

[d]Significantly different from NM ($p < 0.05$)

et al. [22], PEP was shown to increase with gestational age ($r = 0.57$, $p < 0.0001$). VET did not increase with gestational age and showed a statistically insignificant decrease with gestational age. The inverse relationship between KI values and fetal age (Fig. 12b) may indicate that the left ventricle takes longer to fill as the size of

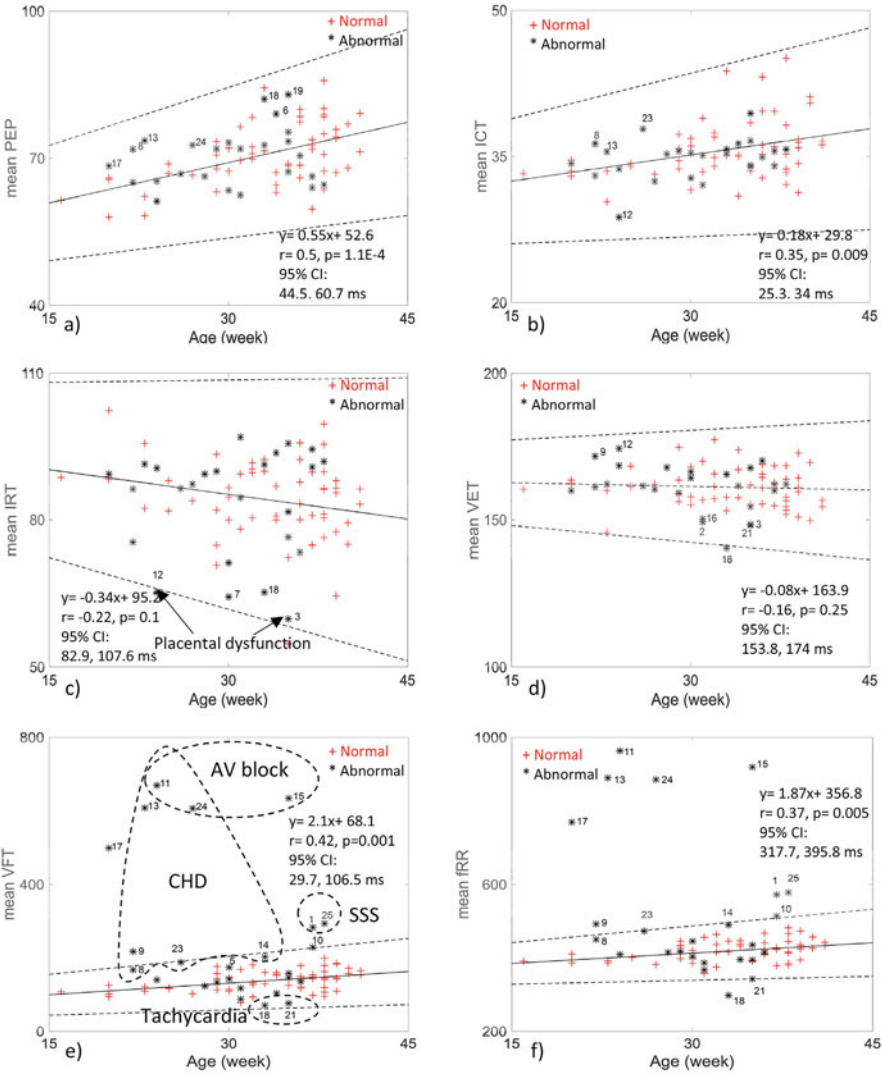

Fig. 11 Mean of myocardial performance indices vs. gestational age for normal and abnormal group. The dashed lines represent 95% confidence intervals. Number indicates an abnormal fetus' case ID. Equations representing the linear fit for normal fetuses are also given [12]

the heart increases. Because VET and IRT did not show any significant correlation with fetal age, TI did not also show a significant correlation with age, as illustrated in Fig. 12a. An explanation for the high correlation values with fRR could be that the ventricular blood flow is constrained through the continuous inward flow of oxygenated blood from the placenta. At mid and late gestational ages, VET correlated significantly with fRR intervals, which was also confirmed in previous

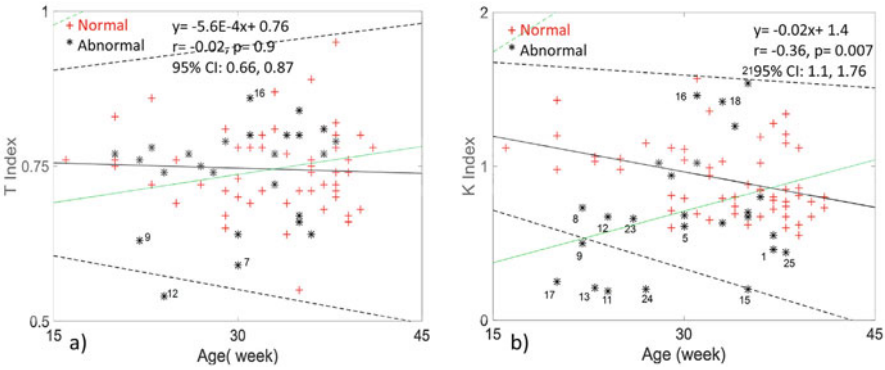

Fig. 12 (**a**) TI vs. GA for normal and abnormal group. (**b**) KI vs. GA for normal and abnormal group. The dashed lines represent the 95% confidence intervals [12]

studies of adult VET values [23]. IRT was negatively correlated with fRR intervals; however, when comparing mid-gestation ($r = -0.08$) cases, early and late groups ($r = -0.52$ and $r = -0.52$, respectively) have a high correlation. The heart rate determines the amount of time available for filling the ventricles. A decrease in heart rate during gestation increases the amount of time spent in diastole relative to systole, thereby increasing VFT. By the Frank–Starling mechanism, VFT follows RR intervals to match cardiac output with venous return. An inadequate filling of the ventricle is caused by decreased compliance of the ventricle wall, resulting in a decrease in the end-diastolic volume of the ventricle. As a result of the Frank–Starling mechanism, the reduced end-diastolic volume reduces the stroke volume. According to clinical studies conducted on adults, sympathetic and parasympathetic activity controls VFT [19, 24, 25].

4.2 CHD: Structural Defects

Figure 11e, f show that CHDs (ID 8,9,11,13,14,23,24) have higher mean RRs and VFTs than the normal ones. As illustrated in Figs. 11e and 13a, b, CHDs with AV block (ID 11, 13, 24) have higher VFT values, distinguishing them from the early normal fetal group. VFT and RR values also increased in other CHD cases (ID 8,9,14,23). In ID 23, the septal and posterior leaflets of the tricuspid valve were displaced toward the apex of the heart's right ventricle, resulting in Ebstein's anomaly [26]. There is a higher mean value and SD of VFT and RR in ID 22 (Tetralogy of Fallot). The differences in correlation parameters in heart anomalies are due to malfunctions in the control system. Further prospective studies are required to determine the precise explanation.

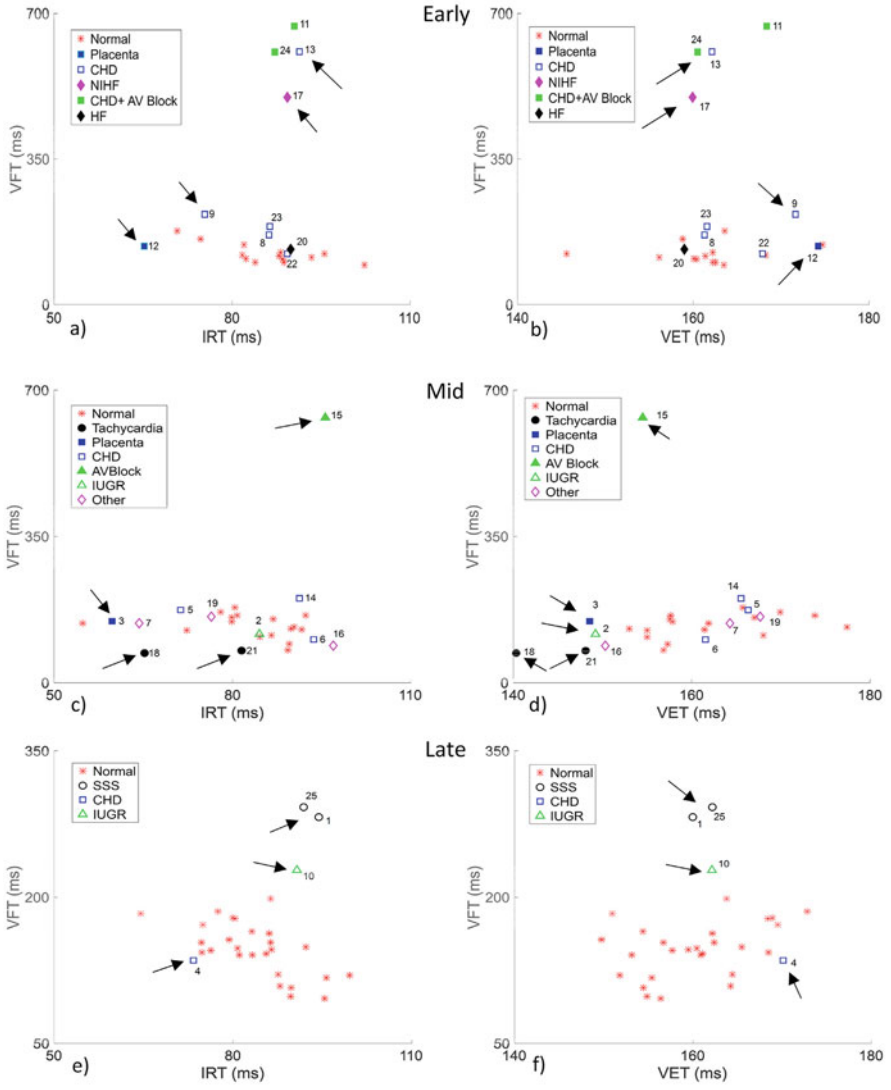

Fig. 13 Left panel shows plots of IRT vs. VFT (**a**, **c**, **e**). Right panel shows plots of VET vs. VFT (**b**, **d**, **f**). Number indicates an abnormal fetus' case ID [12]

4.3 CHD Defects: Conduction Pathways

4.3.1 Fetal Tachycardia

It is generally agreed that fetal tachycardia occurs when the heart rate exceeds 160–180 beats per minute (bpm) and usually falls within 170–220 bpm [27]. 0.4–1%

of pregnancies are estimated to be affected by this condition [28]. The abnormal electrical impulses are most often originating from the atria [27]. ID 18 and 21 are shown to have lower VFT, VET, IRT (Figs. 11c–e and 13c, d), and IRT (ID 18) along with lower RR (Fig. 11f). There is a direct relationship between heart rate and available time for ventricular filling and cardiac output. Shortening of the diastolic filling time is caused by increased heart rate (decrease in RR interval). A reduction in heart rate can improve impaired diastolic functioning under tachycardia by allowing a longer time for filling. As the heart rate increases above 180 bpm, the diastolic filling time is so short that cardiac output usually decreases.

4.3.2 Atrioventricular (AV) Block and Sick Sinus Syndrome (SSS)

It is possible to detect first-degree AV block in a fetus by using an ECG. AV block cases ID 11, 14, and 24 and SSS cases ID 1 and 25 had higher mean and SD VFT and RR values (Fig. 11e, f). This arrhythmia is an arrhythmia resulting from abnormalities in the sinus node. Electrocardiographic demonstrations of inappropriate sinus bradycardia, sinus arrest, or chronotropic incompetence are used to diagnose this arrhythmia type [29, 30].

4.3.3 Intrauterine Growth Restriction (IUGR)

It is estimated that 3–10% of pregnancies are affected by IUGR, and 20% of stillborn infants are affected by IUGR (IUGR statistics, 2018). It has been noted that ultrasound is the standard method for determining the pregnancy date and diagnosing IUGR [31]. Typically, ID 2 (IUGR) has a lower VET (Fig. 13d), and ID 10 (IUGR + PAC) has a higher mean VFT (Fig. 13f), which is reflected in longer mean RR intervals. There has also been a report that in a fetus with IUGR, afterload (placental vascular resistance) plays a significant role in ventricular ejection and preload (venous return) plays a substantial role in ventricular filling [32, 33]. We, therefore, speculate that lower preload and elevated afterload may be responsible for the decrease in VET and increase in VFT in growth-restricted fetuses. ID 10 has a comorbid condition called premature atrioventricular contraction (PAC), a fast electrical impulse that comes earlier than normal conduction, causing the heart to contract prematurely. A series of electrical impulses are generated in the atrium and are either transmitted to the ventricles or can be blocked. 1–2% of all congenital cardiac anomalies are diagnosed with PAC.

4.3.4 Hydrops Fetalis

In Fig. 13b, a nonimmune case with ID 17 has a significantly higher VFT and RR than an immune case with ID 20, which may result from an insufficient ventricular force (ID 17). Diastolic failure occurs due to the ventricle being unable to relax

or the wall being thick or rigid in the case of hydrops fetalis. Falkensammer et al. [34] report that fetuses with hydrops fetalis experience worse outcomes if their myocardial performance indices are higher. Compared to normal cases, ID 17 showed a very low KI index (Fig. 12b). However, TI was not able to distinguish it from a normal case. The development of fetal hydrops was also reported to be related to changes in ventricular filling that commonly impede venous return from the placenta [35].

4.3.5 Placental Abruption

IRT measures ventricular relaxation, which also correlates with invasive indices [36]. There were two cases of placental abruption (ID 3, 12), a severe complication of late pregnancy bleeding in which the placenta separates from the uterus before delivery. The IRT values in both cases were lower than those in normal cases (Figs. 11c and 13a, c). The cause of cardiovascular remodeling associated with diastolic function remains to be determined, whether placental abruption or placental damage occurs.

Modified TI (KI) may be an effective tool for monitoring fetal myocardial function and identifying fetuses with various CHDs and non-CHDs. Several possibilities could arise from this study results, including the development of simple Doppler-derived myocardial indices for clinical use that may be used in prenatal low-risk screenings as well as overall diagnostic algorithms for sick fetuses as preclinical or even clinical steps. This answers the research question that fetal myocardial performance indices estimation is possible from continuous DUS and was able to distinguish between normal and abnormal fetuses.

5 Conclusion

This chapter aims to summarize different noninvasive methods that can be used to estimate the timings of fetal cardiac events based on the analysis of the fECG and DUS. It is possible to evaluate systolic and diastolic function aspects in the developing fetal heart by utilizing fetal myocardial performance indices. As a first step, we presented a method for estimating beat-by-beat fetal heart rate and its variability from Doppler ultrasound using empirical mode decomposition (EMD) and kurtosis statistics. Additionally, a hybrid model based on multiresolution wavelet analysis enabled the frequency contents of the DUS to be correlated with the openings (o) and closings (c) of the heart's valves [aortic (A) and mitral (M)]. The timing of the opening and closing of these valves was verified using M-mode, B-mode, and pulsed Doppler ultrasound images. The systolic and diastolic intervals include the isovolumic contraction time (ICT), isovolumic relaxation time (IRT), ventricular ejection time (VET), and ventricular filling time (VFT). (ICT + IRT)/VET and (ICT + IRT)/VFT were used to calculate TI and KI. Finally,

we illustrated several examples of how fetal myocardial performance indices have been used to evaluate aspects of fetal cardiac systolic and diastolic function. This modified TI (KI) may be a useful tool for monitoring fetal myocardial function and identifying fetuses with various heart and nonheart defects. In addition to developing simple Doppler-derived myocardial indices that may be used for clinical purposes in low-risk prenatal screenings, this study results may also be used to develop general diagnostic algorithms for preclinical or clinical use for sick fetuses.

References

1. C. Ferencz et al., Congenital heart disease: Prevalence at livebirth. The Baltimore-Washington Infant Study. Am. J. Epidemiol. **121**, 31–36 (1985)
2. D. Bonnet et al., Detection of transposition of the great arteries in fetuses reduces neonatal morbidity and mortality. Circulation **99**, 916–918 (1999)
3. H.M. Al-Angari, Y. Kimura, L.J. Hadjileontiadis, A.H. Khandoker, A hybrid EMD-kurtosis method for estimating fetal heart rate from continuous doppler signals. Front. Physiol. **8**, 641 (2017)
4. A.H. Khandoker et al., Antepartum non-invasive evaluation of opening and closing timings of the cardiac valves in fetal cardiac cycle. Med. Biol. Eng. Comput. **47**, 1075–1082 (2009)
5. F. Marzbanrad et al., Model-based estimation of aortic and mitral valves opening and closing timings in developing human fetuses. IEEE J. Biomed. Health Inform. **20**, 240–248 (2016)
6. Y. Murata, C.B. Martin, Systolic time intervals of the fetal cardiac cycle. Postgraduate Med **61**, 127–134 (2016). https://doi.org/10.1080/00325481.1977.11714549
7. F. Marzbanrad et al., Automated estimation of fetal cardiac timing events from Doppler ultrasound signal using hybrid models. IEEE J. Biomed. Health Inform. **18**, 1169–1177 (2014)
8. L.W. Organ, A. Bernstein, P.A. Hawrylyshyn, The pre-ejection period as an antepartum indicator of fetal well-being. Am. J. Obstet. Gynecol. **137**, 810–819 (1980)
9. Y. Yumoto et al., Noninvasive measurement of isovolumetric contraction time during hypoxemia and acidemia: Fetal lamb validation as an index of cardiac contractility. Early Hum. Dev. **81**, 635–642 (2005)
10. M. Nii et al., Assessment of fetal atrioventricular time intervals by tissue Doppler and pulse Doppler echocardiography: Normal values and correlation with fetal electrocardiography. Heart **92**, 1831–1837 (2006)
11. R. Cruz-Martnez et al., Normal reference ranges from 11 to 41 weeks' gestation of fetal left modified myocardial performance index by conventional Doppler with the use of stringent criteria for delimitation of the time periods. Fetal Diagn. Ther. **32**, 79–86 (2012)
12. A.H. Khandoker, H.M. Al-Angari, F. Marzbanrad, Y. Kimura, Investigating myocardial performance in normal and sick fetuses by abdominal Doppler signal derived indices. Curr. Res. Physiol. **4**, 29–38 (2021)
13. K.W. Murphy et al., Birth asphyxia and the intrapartum cardiotocograph. Br. J. Obstet. Gynaecol. **97**, 470–479 (1990)
14. C.A. Vincent, T. Martin, M. Ennis, Obstetric accidents: The patient's perspective. Br. J. Obstet. Gynaecol. **98**, 390–395 (1991)
15. K. Ichizuka et al., The Tei index for evaluation of fetal myocardial performance in sick fetuses. Early Hum. Dev. **81**, 273–279 (2005)
16. G. Chao et al., Tei index: The earliest detectable cardiac structural and functional abnormality detectable in Hb Bart's foetal edema. Int. J. Cardiol. **134**(3), e150–e154 (2009)
17. H. Boudoulas, Systolic time intervals. Eur. Heart J. **11**, 93–104 (1990)

18. D. Friedman, J. Buyon, M. Kim, J.S. Glickstein, Fetal cardiac function assessed by Doppler myocardial performance index (Tei index). Ultrasound Obstet. Gynecol. **21**, 33–36 (2003)
19. A.H. Khandoker, F. Marzbanrad, Y. Kimura, S. Al Nuaimi, M. Palaniswami, Assessing the development of fetal myocardial function by a novel Doppler myocardial performance index. Annu. Int. Conf. IEEE Eng. Med. Biol. Soc. **2016**, 3753–3756 (2016)
20. Congenital Heart Disease. https://fetus.ucsf.edu/congenital-heart-disease/
21. E.A. Ibrahim, S. Al Awar, Z.H. Balayah, L.J. Hadjileontiadis, A.H. Khandoker, A comparative study on fetal heart rates estimated from fetal phonography and cardiotocography. Front. Physiol. **8**, 764 (2017)
22. N.A. Mensah-Brown, R.T. Wakai, B. Cheulkar, S. Srinivasan, J.F. Strasburger, Assessment of left ventricular pre-ejection period in the fetus using simultaneous magnetocardiography and echocardiography. Fetal Diagn. Ther. **28**, 167–174 (2010)
23. K. Mäkikallio, P. Jouppila, J. Räsänen, Human fetal cardiac function during the first trimester of pregnancy. Heart **91**, 334 (2005)
24. M.R. Pinsky, Cardiovascular issues in respiratory care. Chest **128**, 592S–597S (2005)
25. S.K. Frazier et al., Autonomic tone in medical intensive care patients receiving mechanical ventilation and during a CPAP weaning trial. Biol. Res. Nurs. **9**, 301–310 (2008)
26. T. Sharma, F. Habash, J. Mounsey, C. Baker, A.L. Candales, Ebstein's anomaly in disguise: Follow the cues and the diagnosis can be made. Cureus **12**, e10773 (2020)
27. M.A. Oudijk, G.H.A. Visser, E.J. Meijboom, Fetal tachyarrhythmia - part I: Diagnosis. Indian Pacing Electrophysiol. J. **4**, 104 (2004)
28. M.G.M. Bergmans, G.J. Jonker, H.C.L.V. Kock, Fetal supraventricular tachycardia. Review of the literature. Obstet. Gynecol. Surv. **40**, 61–68 (1985)
29. D.W. Benson et al., Congenital sick sinus syndrome caused by recessive mutations in the cardiac sodium channel gene (SCN5A). J. Clin. Invest. **112**, 1019–1028 (2003)
30. H.D. Allen, R.E. Shaddy, D.J. Penny, T.F. Feltes, F. Cetta, Moss and Adams' heart disease in infants, children, and adolescents, including the fetus and young adult, 6th Ed. Circulation **1–2**, 1–1900 (2001)
31. J.E.A.K. Bamfo, A.O. Odibo, Diagnosis and management of fetal growth restriction. J. Pregnancy **2011**, 640715 (2011)
32. W. Al-Ghazali, M.G. Chapman, L.D. Allan, Doppler assessment of the cardiac and uteroplacental circulations in normal and complicated pregnancies. Br. J. Obstet. Gynaecol. **95**, 575–580 (1988)
33. F. Tsyvian, K. Malkin, O. Artemieva, J.W. Wladimiroff, Assessment of left ventricular filling in normally grown fetuses, growth-restricted fetuses and fetuses of diabetic mothers. Ultrasound Obstet. Gynecol. **12**, 33–38 (1998)
34. C.B. Falkensammer, J. Paul, J.C. Huhta, Fetal congestive heart failure: Correlation of Tei-index and cardiovascular-score. J. Perinat. Med. **29**, 390–398 (2001)
35. C. Barrea et al., Prenatal cardiovascular manifestations in the twin-to-twin transfusion syndrome recipients and the impact of therapeutic amnioreduction. Am. J. Obstet. Gynecol. **192**, 892–902 (2005)
36. Y. Myreng, O.A. Smiseth, Assessment of left ventricular relaxation by Doppler echocardiography. Comparison of isovolumic relaxation time and transmitral flow velocities with time constant of isovolumic relaxation. Circulation **81**, 260–266 (1990)

Principles of Fetal Electrocardiography

Rik Vullings

1 Brief History of Fetal Electrocardiography and Its Relevance

Ever since Cremer [1] in 1906 recorded the first fetal electrocardiogram (ECG), researchers have shown interest in reproducing this feat and studying the clinical relevance of the fetal ECG [1–6]. In particular, at first interest was focused toward the extraction of the fetal heart rate from the ECG. It was already in 1821 that Jacques Alexandre le Jumeau de Kergaradec (1787–1877) stated "Would it not be possible to judge the state of health or illness of the fetus from the variations in the strength and frequency of the fetal heart beat?". With the discovery of electrocardiography, monitoring the fetal heart rate via the ECG became a real possibility and thus monitoring the health and illness of the fetus became as well.

In the search for fetal ECG measurements, we can distinguish two different trajectories: measuring the ECG in an invasive manner with electrodes making direct contact to the fetus and measuring the ECG non-invasively with electrodes on the maternal abdomen. Many attempts were made, but the quality of the ECG remained to low or the methods of measuring were unsuited for use in daily clinical routine. At last in 1963, Edward H. Hon (1917–2006) introduced the fetal scalp electrode, an invasive electrode connected to the fetal scalp, making it finally possible to monitor the fetal heart rate in clinical practice [7].

R. Vullings is cofounder and shareholder of Nemo Healthcare BV, The Netherlands.

R. Vullings (✉)
Eindhoven University of Technology, Department of Electrical Engineering, Signal Processing Systems Group, Biomedical Diagnostics Lab, Veldhoven, The Netherlands

Nemo Healthcare BV, Veldhoven, The Netherlands
e-mail: R.Vullings@tue.nl

D. Pani (ed.), *Innovative Technologies and Signal Processing in Perinatal Medicine*, https://doi.org/10.1007/978-3-031-32625-7_7

Besides the monitoring of the fetal heart rate—when compounded with monitoring of uterine activity referred to as the cardiotocogram (CTG)—the introduction of this fetal scalp electrode led to extensive new research regarding the diagnostic value of this fetal ECG [8–10]. Important markers for fetal compromise that were investigated include oxygenation, fetal growth, and congenital anomalies. Especially, research toward the fetal oxygenation, with studies focusing on the ST segment [11, 12] and PR interval [13, 14] of the ECG, led to promising results. Not surprisingly, part of this research finally converged to the introduction of the STAN® monitor [11, 12, 15–17]; a monitor that analyzes the ST segment of the fetal ECG and, in combination with CTG, can be used to assess fetal hypoxia [18]. In the early years of the twenty-first century, this STAN® monitor gained more momentum [19–21]. Later studies more and more debated the clinical value of the device [22–24], where it seems we now reached as status-quo where some obstetricians use the STAN® monitor to their satisfaction, while others have returned to the years before the STAN® monitor was introduced and use CTG as their dominant source of information.

Although the invasive fetal scalp electrode is superior to the non-invasive transabdominal electrodes when it comes to ECG measurements, they have a strong limitation. They can only be applied during parturition, with sufficient dilatation and after the fetal membranes have ruptured. In many situations, monitoring of the fetal condition is needed well before this stage is reached. While non-invasive fetal ECG could potentially fill this need, only in the last years the technological solutions have been developed to make this possible. Luckily, ultrasound-based technology has filled the void and provided the means to monitor the fetal heart rate and image the fetal anatomy and physiology in non-invasive ways, however with the drawbacks of having poor tolerance to high body mass index [25] and movements [26].

It is now almost 120 years after the discovery of fetal ECG by Cremer. Many technological innovations have come to make this discovery reproducible and applicable in clinical practice, some more successful than others. Now, in the era of artificial intelligence and big data, it might very well be that also the promise of Alexandre le Jumeau de Kergaradec might finally get fulfilled.

2 Relevant Electrophysiology

2.1 Physiology of the Heart

2.1.1 The Adult Heart

The adult heart is a muscular organ that consists of two separate pumps. The right part of the heart pumps blood through the lungs and the left part of the heart pumps the blood through the peripheral organs [27, 28]. Each of these parts is a pulsatile two-chamber pump composed of an atrium and a ventricle. The atrium functions in principle as a weak primer pump for the ventricle, helping the blood to move into

the ventricle. The ventricle, in turn, supplies the main force that thrusts the blood through either the pulmonary or peripheral circulation [27, 28].

The heart has a specialized system for generating rhythmical impulses—which cause rhythmical contractions of the heart muscle—and conducting these impulses rapidly throughout the heart [28]. When this system functions normally, the atria contract some time ahead of the ventricles, allowing additional filling of the ventricles before they thrust the blood through the lungs and peripheral circulation. Another special feature of this system is that it allows all parts of the ventricles to contract almost simultaneously, which is essential for effective pressure generation in the ventricular chambers.

The fibers of this specialized conducting system have the capability of self-excitation, a process that can cause automatic rhythmical discharge and subsequent contraction [27]. The fibers of the sinoatrial (SA) node exhibit this capability to the largest extent, and, therefore, the SA node ordinarily controls the rate of contractions of the complete heart [28]. Specifically, the fibers of the SA node self-excite at the highest rate and the impulses generated by the SA node subsequently propagate throughout the entire heart. After depolarization of a cell, the cell exhibits a refractory period in which no excitation can occur. This means that other cells, which also have the capability of self-excitation, are typically already excited because of the propagation of impulses that were generated by the SA node, essentially overruling their own excitation rate and forcing them to excite at the rate that is dictated by the SA node. At the end of the refractory period, the SA node is generally again the first to self-excite, and because of this, the SA node is responsible for the rate of contractions of the heart.

As said, the nodal fibers of the SA node discharge spontaneously. This causes an *action potential* (see Sect. 2.2.1) to propagate rapidly through both atria and from there through the atrioventricular (AV) bundle into the ventricles [27]. It is primarily this AV (or His) bundle that delays the transmission of action potentials from the atria into the ventricles, allowing time for the atria to empty their contents into the ventricles before ventricular contraction begins [27]. Figure 1 shows an illustration of the conduction path of action potentials throughout the heart.

After penetration of the fibrous tissue between the atrial and the ventricular muscles, the distal part of the AV bundle passes downward in the ventricular septum and splits into left and right bundle branches [27, 28]. Each branch spreads downward to the apex of the ventricle, progressively splitting into smaller branches that spread around each ventricular chamber and back toward the base of the heart. The terminal Purkinje fibers penetrate about one-third of the way into the muscular mass and then become continuous with the cardiac muscle fibers.

The Purkinje fibers lead from the AV node through the AV bundle branches into the ventricles and have characteristics quite opposite of those of the AV node. In order to allow all ventricular muscle fibers to contract almost simultaneously, the cardiac impulse has to appear at each muscle fiber at approximately the same time. For this reason, the Purkinje fibers are relatively large fibers that transmit the action potentials at velocities about six times larger than transmission velocities in cardiac muscle fibers [28].

2.1.2 The Fetal Heart: Differences with Respect to the Adult Heart

Relative to the adult heart, the physiology and anatomy of the fetal heart exhibit some significant differences. These differences originate from the fact that the fetal cardiovascular circulation is different from the adult circulation [29–31].

In the adult, gas exchange (i.e., the secretion of carbon dioxide from the blood and the intake of oxygen in the blood) takes place in the lungs [28]. From the lungs, oxygenized blood flows through the left part of the heart into the peripheral circulation. Since this peripheral circulation is larger than the pulmonary circulation, the left ventricle has to generate a substantially higher pressure than the right ventricle to ensure sufficient perfusion of the organs. Consequently, the muscular mass of the left ventricle is larger than the mass of the right ventricle.

In the fetus, gas exchange takes place in the placenta [32]. As a result, the fetal blood circulation needs to operate differently from the adult. This different circulation manifests itself, among other differences, by interconnections between the left and right parts of the heart. These interconnections consist of the foramen ovale, a gap in the septum dividing both sides of the heart, and the ductus arteriosus, a shunt between the pulmonary artery and the aorta [32]. Both the foramen ovale and ductus arteriosus are schematically illustrated in Fig. 1.

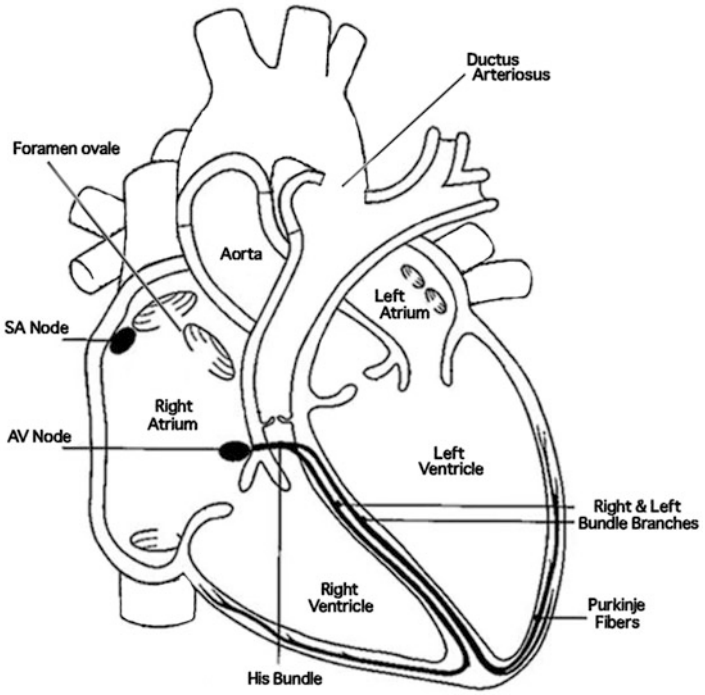

Fig. 1 Basic anatomy of the human fetal adult heart with the main components of the action potential conduction system indicated

Because of these interconnections, the left and right ventricle both generate the same pressure. However, in the fetal circulation, the right ventricle is responsible for about 60% of the total cardiac output, whereas the left ventricle accounts for the remaining 40% [30]. As a result of this higher output, the right ventricle of the fetal heart has a muscular mass exceeding that of the left ventricle. The effect of these different mass distributions between the fetal and adult heart on the ECG is discussed in Sect. 2.3.

2.2 Origin of the ECG

2.2.1 Cardiac Activity at Cellular Level

Cells in the human body can be considered as small containers that are filled with a fluid, i.e., intracellular fluid, which is encapsulated by a cell membrane. These cells float within the extracellular fluid. At rest, the electrical potential of the intracellular fluid is negative with respect to the potential of the extracellular fluid [27, 28]. This is caused by the different concentrations of Na^+, K^+, and Ca^{2+} across the cell membrane. When a cell is excited, for instance, because of an action potential that propagates along the cell, this action potential causes an increase in the Na^+ permeability of the membrane [27, 28]. Consequently, large numbers of Na^+ ions flow into the interior of the cell, reversing the potential of the intracellular fluid with respect to the potential of the extracellular fluid: the cell is depolarized [27].

Besides the increase in Na^+ permeability, the propagating action potential also causes an increase in the K^+ and Ca^{2+} permeability of the cell membrane, forcing K^+ ions to flow from the interior of the cell to the extracellular fluid and forcing Ca^{2+} ions to flow from the exterior to the intracellular fluid [27, 28]. However, the increase in K^+ and Ca^{2+} permeability arises more gradually than the increase in Na^+ permeability. In addition, the Ca^{2+} permeability decreases earlier than the K^+ permeability. As a result, the intracellular potential first rapidly increases to positive values due to the Na^+ inflow. Subsequently, the potential remains at a plateau for a short while due to the inflow of Ca^{2+} and outflow of K^+ ions. Finally, the potential returns to its rest value due to the persisting outflow of K^+ ions: the repolarization of the cell. In fact, toward the end of the plateau, the K^+ permeability even increases to ensure a rapid return to the rest potential [28]. It has to be noted that the description above only holds for cardiac cells and not for other excitable cells in the body, like nerve cells. Moreover, also the nodal cells in the heart that are responsible for the self-excitation of the heart behave differently [28].

Propagation of electrical impulses from cell to cell occurs in two manners, either passively or actively [27]. Passive propagation consists of the electrical conduction of stimuli that are too small to cause the depolarization of the cell. In this case, the cells act as a coaxial wire conducting the stimulus, but gradually reduce the stimulus amplitude due to leakage currents to the cell membrane. Active propagation occurs without degradation of the stimulus amplitude. The reason for this is that the

depolarization of a particular cell causes a supraliminal stimulus in the adjacent cell, initiating the depolarization of this cell. Active propagation can therefore also be described as the propagation of action potentials.

2.2.2 Cardiac Activity at Organ Level

Next to effects at the cellular level, the propagation of action potentials also has effect at the tissue and organ level. In fact, for the heart to contract, the propagating electrical stimulus needs to be converted to mechanical activity.

This conversion is accomplished in two steps: the electrical stimulus initiates a chemical process which in turn initiates the desired mechanical activity [27]. The propagating action potential causes the sarcoplasmic reticulum to release large quantities of Ca^{2+} ions into the myofibrils. These Ca^{2+} ions initiate attractive forces between the actin and myosin filaments in the fiber, causing them to slide together. This is the actual contraction of the muscle.

Besides this mechanical effect, the propagating action potentials also have an electrical effect on the tissue. As mentioned before, the depolarization of a particular cell causes a potential difference with respect to adjacent cells that are not yet depolarized. Consequently, the boundary between a depolarized cell and a cell at rest acts as a dipole. Moreover, as the action potentials propagate rather uniformly through the cardiac tissue, adjacent fibers depolarize virtually simultaneously: a dipole (or depolarization) wave travels through the heart [28].

2.2.3 Cardiac Activity at Cutaneous Level

The tissues surrounding the traveling dipole are, in general, conductive, and hence the dipole wave acts as a source for a circular current that is substantially larger than the circular current caused by the cellular potential difference itself. These currents spread all the way to the body surface where the skin impedance causes potential differences [33].

As the dipole wave travels through the cardiac tissues, the potential at a specific position on the skin is not constant but varies with the traveling dipole. The representation of the skin potential as a function of time is called the electrocardiogram (ECG) and can be measured by positioning electrodes on the skin [28].

2.3 Characteristics of the ECG

2.3.1 One-Dimensional ECG

The ECG is a representation of the skin potential as a function of time. In fact, the use of the word potential is not completely correct in this context: the ECG generally

constitutes a representation of the potential *difference* between two electrodes, referred to as a bipolar ECG recording [28]. Next to bipolar ECG recordings, the literature on electrocardiography typically also mentions unipolar or monopolar ECG recordings. These unipolar ECG recordings represent the difference between an electrode that measures the changes in electrical potential caused by the cardiac activity and an (virtual) electrode that does not measure this cardiac activity. In applications of fetal electrocardiography, this second electrode can be positioned relatively far away from the uterus; in adults, it is often a virtual electrode such as the Wilson Central Terminal [34]. In this chapter, we will focus on the bipolar ECG and simply refer to this as ECG. The ECG can be described by means of a few characteristic waves, which are associated with specific physiological events, and the segments and intervals between these waves. Figure 2 shows an example of a typical ECG signal.

The *P-wave* is associated with the depolarization of the atria [27, 28]. When the atria are completely depolarized, the net electrical field generated by the traveling dipole is zero and the ECG consequently has zero amplitude. This isoelectrical period lasts until the action potential has propagated through the AV bundle to the Purkinje fibers and is represented in the ECG by the PR (or better: PQ) interval. The *QRS complex* is associated with ventricular depolarization [27, 28]. The amplitude of the QRS complex exceeds the amplitude of the P-wave dramatically as the amount of muscle fibers in the ventricular walls is much larger than the amount of muscle fibers in the atrial walls. The reason for this is that the ventricles need to propel the blood into the peripheral circulation, whereas the atria only need to propel the blood into the ventricles. As a result of this and because the atrial repolarization coincides with the ventricular depolarization, the repolarization of the

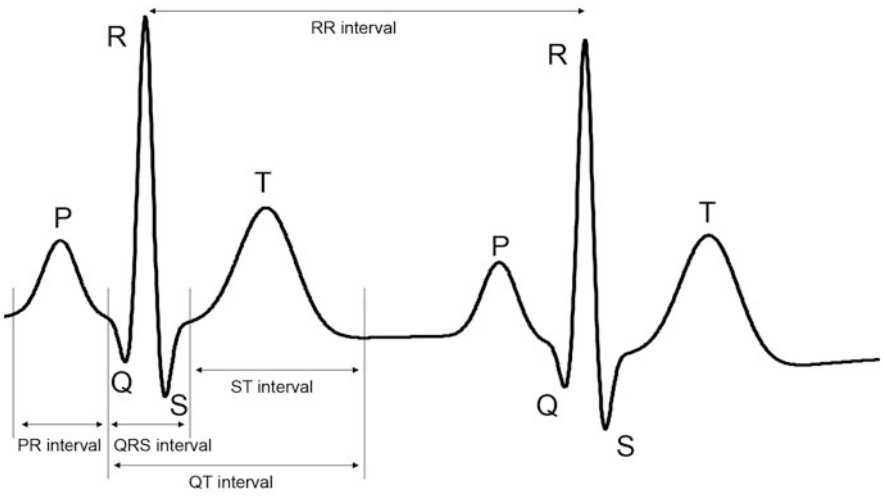

Fig. 2 Nomenclature of the ECG

atria cannot be distinguished in the ECG. After the ventricles have been completely depolarized, the net electrical field is again zero and the ECG has zero amplitude. The repolarization wave of the ventricles propagates in the opposite direction as the depolarization wave and is represented in the ECG by the *T-wave* [27, 28]. Because of the reversed propagation direction and the inversion of the signs in the resulting dipole wave, the T-wave has the same polarity as the QRS complex.

Besides being considered as the aforementioned potential difference between two electrodes, the ECG can also be regarded as the projection of the electrical field, which is generated by the traveling dipole, onto the lead vector that describes the positions of the involved electrodes with respect to one another [35]. This view on the ECG will be described in more detail in the following section but elucidates the title for this section: the ECG is a one-dimensional projection of the three-dimensional electrical field that is generated by the traveling dipole.

2.3.2 Three-Dimensional Vectorcardiogram

The traveling dipole produces a varying electrical field in the heart, which to a first-order approximation can be described by a single vector: the heart (or cardiac) vector [35, 36]. When the orientation of the heart vector on the cutaneous level is perpendicular to the lead vector between two electrodes, both these electrodes measure the same electrical field amplitude, and hence the bipolar ECG amplitude is zero. In other words, the projection of the heart vector onto the lead vector determines the instantaneous ECG amplitude. This is illustrated in Fig. 3, in which the three vectors composing the triangle—known as the Einthoven triangle, after the Dutch nobel laureate and inventor of electrocardiography: Willem Einthoven—are the lead vectors and the amplitude of the ECG is determined by the amplitude of the projection of the instantaneous heart vector onto these lead vectors [37]. In addition, this relation between the electrical field, the lead vector, and the ECG amplitude implies that the varying electrical field can be used to describe the ECG at the body surface. Consequently, one of the main interests in fetal ECG monitoring is the description of this electrical field vector over time: the fetal vectorcardiogram (VCG) [38].

Essentially, the VCG is the three-dimensional representation of the time-path of the heart vector during one cardiac cycle [34]. Figure 3 shows a two-dimensional illustration of the VCG. In fact, this depicted VCG represents a simplification of the actual physiology. As the heart vector originates from the propagating dipole wave, the origin of the vector travels with this wave through the heart. In the simplification that is used in the definition of the VCG, however, the origin of the heart vector remains stationary [39].

In general, the VCG consists of three closed loops associated with atrial depolarization, ventricular depolarization, and ventricular repolarization [38], the P-wave, QRS-complex, and T-wave, respectively, in the one-dimensional ECG. The largest of these loops, the ventricular depolarization loop, exhibits one particular

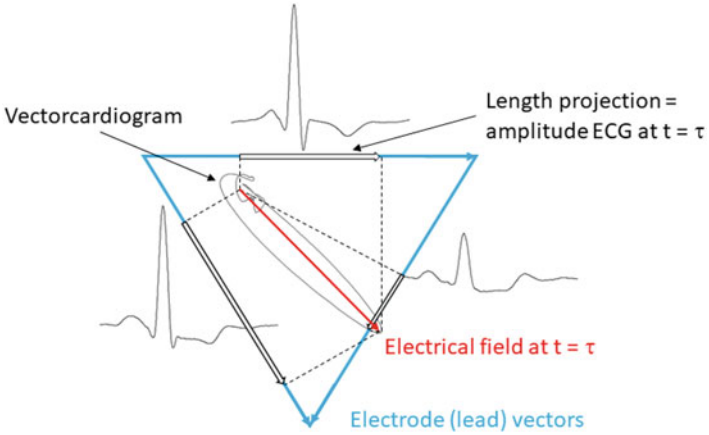

Fig. 3 Two-dimensional illustration of the VCG (in dark gray) and the instantaneous projection of the cardiac vector (in red) on the three leads of the Einthoven triangle (in light blue), resulting in three one-dimensional ECG leads [35]. The cardiac vector is determined at an arbitrary time $t = \tau$, about halfway in the QRS complex. The VCG is an elliptic shape where each point along the shape represents another time τ. For each cardiac vector (i.e., at each time point), the projections onto the electrode lead vectors are calculated and the length of these projections determines the amplitude of the ECG. The amplitude of the ECG is negative in case the projection points in the opposite direction of the corresponding lead vector

direction for which the cardiac vector has maximum amplitude. This direction is referred to as the electrical axis of the heart or the main heart axis [28].

For adults, the main heart axis is on average tilted 57° with respect to the transverse plane, i.e., approximately corresponding to the direction from the right shoulder to the left ankle (Einthoven lead II [37]), but deviations from −30° to 90° are considered normal [28].

2.3.3 Differences Between Fetal and Adult ECG

The direction of the electrical axis in the adult and fetal hearts is not the same. As mentioned, in the adult heart the electrical axis points toward the left ventricle, the ventricle with the largest mass. For the fetal heart, however, the mass of the right ventricle is larger than that of the left one [31]. Hence, the electrical axis of the fetal heart is expected to point toward the right ventricle [29]. This shift in the electrical axis between the fetal and adult implies that the fetal VCG is oriented differently as well with respect to the adult VCG. Hence, each ECG representation for the fetus—being the projection of the fetal VCG onto the appropriate lead vector—differs from the same ECG representation for the adult.

For clinical interpretation of the fetal ECG, therefore, standard guidelines used in the field of cardiology may no longer be valid, requiring the formulation of new guidelines for the fetal cardiology field.

3 Non-invasive Fetal ECG Recordings for Cardiotocography

3.1 Cardiotocography

Birth is among the biggest challenges a human being encounters in life. Not only does a newborn have to adjust to completely new surroundings, but also, moreover, the transition from life inside the uterus to life outside it is often associated with temporal hypoxia, a decrease of the oxygen level in peripheral tissues. In order to withstand the difficulties of labor well, the fetus is equipped with several protective mechanisms that enable it to cope with substantial oxygen deficiency. A healthy fetus that encounters hypoxia during labor but is able to handle this adequately is likely to develop normally after birth [40].

One of the main protective mechanisms of the fetus against hypoxia consists of blood flow regulation and distribution [41]. The driving force behind the control of variations in blood flow and blood pressure is the cardiovascular control system, which operates under the influence of the autonomic nervous system. This system consists of two parts, the sympathetic nervous system and the parasympathetic nervous system, between which an essential difference exists. The sympathetic system uses a network of neurons and ganglia for the transfer of action potentials, whereas innervation by the parasympathetic system takes place directly [42]. As a result, the sympathetic system is significantly slower than the parasympathetic system.

The assessment of blood pressure by the autonomic nervous system occurs by means of so-called baroreceptors [28]. These baroreceptors are located in the wall of blood vessels and are sensitive to strain. A decrease in blood pressure results in a decrease in the stimulation of baroreceptors, which in turn leads to increased sympathetic activity and lowered parasympathetic activity [43]. This change in sympathetic and parasympathetic activity causes an increase in heart rate and cardiac contraction power [2] and the occurrence of vasoconstriction (the narrowing of blood vessels), which results in an increase in blood pressure [43]. Thus, regulation of blood flow by the cardiovascular control system is achieved in two different ways: the primary way is regulation of the arterial blood pressure by altering the degree of vasoconstriction in blood vessels and the secondary way is the regulation of the heart rate.

Unfortunately, it is impossible to determine the fetal blood pressure inside the uterus. The fetal heart rate, on the other hand, can be determined during pregnancy [7, 44] and is currently the main source of information from which the physiological condition of the fetus is assessed.

The fetal heart rate can be determined in several ways, based on different physical principles. For instance, it can be determined with Doppler ultrasound measurements [45]. Ultrasonic waves experience a shift in frequency when they reflect at a moving interface. The magnitude and direction of this shift contains information

about the motion of that interface. This effect is known as the Doppler effect [46]. Since both the valves and the blood move in the fetal heart during contraction, Doppler ultrasound can be used as a non-invasive technique to determine the fetal heart rate. A second way to determine the fetal heart rate is based on assessment of the electrical activity of the fetal heart. This electrical activity can be measured by positioning electrodes either directly on the fetus or on the maternal abdomen. As mentioned in Sect. 1, positioning the electrodes directly on the fetus is an invasive technique and can only be performed during labor when the fetal membranes have ruptured. Positioning the electrodes on the maternal abdomen is preferable since it is a non-invasive technique that, therefore, can be applied in all stages of pregnancy. However, due to the low signal to noise ratio (SNR) of the recorded signals, determination of the fetal heart rate from abdominal electrophysiological recordings is challenging. Currently, of the presented ways for monitoring the fetal heart rate, the Doppler ultrasound way is most widely used in clinical practice [47].

Besides the fetal heart rate, clinicians are generally also interested in monitoring of the maternal uterine activity. As uterine contractions can impose stress on the fetus, the relationship between uterine activity and fetal heart rate provides more information on the fetal condition than the fetal heart rate alone does. For example, uterine contractions can lead to (partial) occlusion of the umbilical cord, reducing the blood flow from the mother to the fetus. The capability of the fetus to respond to this temporary oxygen deficiency by, among other reactions, adapting its heart rate is indicative for the fetal condition [48]. The relationship between uterine activity and fetal heart rate has, therefore, been investigated extensively through the years. Many guidelines and scoring systems have been proposed for the interpretation of these simultaneous recordings, referred to as cardiotocography (CTG; the simultaneous recording of fetal heart rate (cardio-) and uterine activity (toco-)) recordings, and several of these guidelines are used in clinical practice [49]. However, the information provided by CTG has turned out to be only sufficient when the condition of the fetus is clearly good or clearly bad [50, 51]. Very often, it is not possible to draw conclusions from CTG recordings and additional tests, such as fetal blood sampling (i.e., examination of a small droplet of blood, obtained invasively, from the fetus), are required to evaluate the condition of the fetus [52]. Besides this lack of information for accurately evaluating the fetal condition, the use of CTG, in case Doppler ultrasound is used to capture the fetal heart rate, is also associated with the drawback that CTG is very sensitive to motion and noise [53]. Not only does the ultrasound probe require frequent repositioning due to fetal movement, but also the dimensions of the ultrasound beam with respect to the dimensions of the fetal heart and vessels can cause other moving interfaces to contribute to the frequency shift of the reflected ultrasound beam. In addition, due to radiative loads, ultrasound cannot be applied 24/7.

3.2 Motivation for Pursuing Non-invasive Fetal ECG Recordings

From the above, it can be concluded that some of the main challenges in fetal monitoring lie in the safe and reliable determination of the fetal heart rate throughout pregnancy and in finding additional sources of information to assess the fetal condition. As discussed in Sect. 1, such an additional source of information might be provided by the fetal ECG [11, 54]. In addition to the analysis of the ST segment or PR interval for detecting fetal hypoxia, more information might be available from the fetal ECG. For example, changes in the orientation of the fetus with respect to the uterus can in principle be determined from fetal ECG signals that are recorded from the maternal cutaneous surface. These changes in orientation can be related to fetal movement, providing another parameter that can have clinical relevance in assessing the fetal condition. Furthermore, abnormalities in the morphology of the ECG might be associated with congenital heart disease.

Recent findings demonstrate that non-invasive recording of the fetal ECG with transabdominal electrodes might be the solution to providing the fetal heart rate in a safe and reliable manner and can provide extra information to assess the fetal condition [55–60]. First commercial applications of this technology for providing the CTG are currently also finding their way into clinical practice, e.g., Novii (GE Healthcare, USA) and Nemo Fetal Monitoring System (Nemo Healthcare, the Netherlands, of which the author of this chapter is co-founder and shareholder, Fig. 4).

The remainder of this chapter will therefore focus on *principles of non-invasive fetal electrocardiography*, as a promising enabler for safe and reliable monitoring of the fetal condition throughout pregnancy and labor and discuss the main limitations of this technology and discuss some of the possible solutions to overcome these limitations. It should be noted here that this chapter is not intended to provide a comprehensive overview of all related and relevant literature.

3.3 Signals Recorded from the Maternal Abdomen

3.3.1 Physiological Signals

As the maternal body acts as a conductor, several other electrophysiological signals that do not originate from the fetus are recorded by electrodes on the maternal abdomen [38]. These interferences include, but are not limited to, the maternal ECG, activity from the uterus (electrohysterogram (EHG)) [61, 62], and abdominal muscle activity (electromyogram, EMG).

The maternal ECG has about the same spectral properties as the fetal ECG, that is, a frequency content ranging from about 2 Hz to 80 Hz as shown in Abboud et al. [63], but has amplitudes that can exceed those of the fetal ECG by a factor of

Fig. 4 Illustration of the abdominal fetal ECG recordings with Nemo Fetal Monitoring System (Nemo Healthcare, The Netherlands). Electrodes are positioned on the maternal abdomen and the recorded electrophysiological signals are wirelessly transmitted to a data processing device where raw data is not only stored but also processed to calculate fetal heart rate, maternal heart rate, and uterine activity

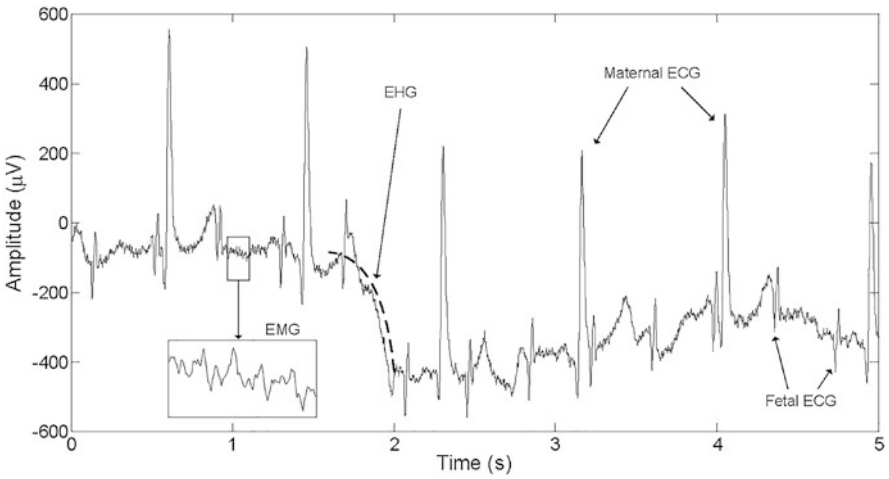

Fig. 5 Segment of composite abdominal fetal ECG recording. The contribution of the EHG is reflected by wandering of the baseline. This baseline wander is emphasized by the additionally drawn dashed arc

about 10 (Fig. 5). The EHG, in contrast, has a frequency content ranging from 0 Hz to approximately 3 Hz [64], whereas the EMG exhibits frequencies ranging from 0 Hz to 200 Hz [65]. These three interferences alone already illustrate the difficulty of fetal ECG extraction and hence explain the wide range of techniques proposed to achieve this extraction. To further exemplify this, in Fig. 5, a composite abdominal fetal ECG recording is shown with some of the contributing signals indicated.

3.3.2 Non-Physiological Signals

Although many non-physiological interferences exist, e.g., imperfections in the analog-digital converter of the recording equipment, the non-physiological interferences are dominated by the powerline grid [66].

The interference from the powerline grid is centered around 50 Hz (most of the world) or 60 Hz (predominantly in the USA) with harmonics at multiples of these frequencies and can be suppressed from the composite signal by either employing a series of notch filters with fixed cutoff frequencies or more adaptive filtering schedules [66, 67].

3.4 Complications in Fetal ECG Analysis Due to Changes in the Volume Conductor

In addition to the signals that corrupt the fetal ECG in the abdominal recordings, fetal ECG analysis is complicated for another reason as well. Changes in the volume conductor between the fetal heart on the one hand and the abdominal electrodes on the other hand can distort or attenuate/amplify the ECG [68–71]. In general, these changes originate from movement of the fetus, development of the vernix caseosa [68, 72], and movement of the mother.

Fetal movement is reflected in the transabdominal fetal ECG as spatially correlated changes in the morphology of the ECG waveform. In terms of the fetal VCG, movement of the fetus is reflected as a rotation of the VCG. However, fetal movement not only causes the fetal VCG to rotate with respect to the electrode configuration on the maternal abdomen but also causes the distance between the fetal heart and the various electrodes to change [73]. In case the conduction of the electrophysiological signals from the fetal heart to the maternal abdominal surface is not uniform, this change in distance causes both distortion and attenuation/amplification of the fetal ECG [68, 71]. In case of uniform conduction, typically assumed until gestational ages of about 28 weeks, only attenuation or amplification of the fetal ECG signals is expected. Specifically, in case fetal movement causes the distance between the heart and a particular electrode to decrease, amplification of the corresponding fetal ECG signal is expected. Conversely, an increase in the heart–electrode distance is expected to be accompanied by attenuation of the corresponding fetal ECG.

From about 28 weeks of gestation, the fetus develops a protective layer called the vernix caseosa [68, 72, 74, 75]. The vernix caseosa isolates the fetus electrically from its surroundings, making it more challenging to record a fetal ECG on the maternal abdomen. However, from about 32 weeks of gestation, this protective layer starts to break down, partly canceling the isolated environment of the fetus and thus restoring the possibility of transabdominal fetal ECG recording. As a consequence of the holes that are thus generated in the vernix caseosa, preferred conduction paths

for the electrical signals arise [72]. These conduction paths constitute a transition from uniform conduction before 28 weeks of gestation to non-uniform conduction after 32 weeks of gestation, significantly affecting the transabdominal fetal ECG [38]. After about 37 weeks of gestation, the vernix caseosa dissolves in the amniotic fluid restoring the uniform conduction characteristics of the volume conductor [68].

Another change in the volume conductor that causes fetal ECG distortions on the abdominal surface is caused by fetal breathing. By filling its lungs with amniotic fluid [76], the fetus changes the impedance of the conduction path from its heart to the abdominal electrodes, affecting the recorded fetal ECG.

A final reason for changes in the volume conductor mentioned here is movement of the electrodes, resulting from movement of the mother. At first glance, electrode movement might seem more appropriately placed among non-physiological interferences of the fetal ECG, rather than among changes in the volume conduction. However, movement of the electrodes causes the conductive layer between the skin and the electrodes to change and hence causes a change in the properties of the volume conductor. In case of conventional Ag/AgCl electrodes, this conductive layer is generated by the thermal excitation of metallic ions in the electrode [77]. These ions spread through the electrolyte, forming a layer balancing the electrode charge [77]. Although the ions can move freely through the electrolyte, the speed of movement is limited, and hence electrode movement is likely to disturb the balancing layer and hence the electrode-skin bias [77], resulting in artifacts in the recorded fetal ECG.

3.5 Signal Processing for Fetal Heart Rate Detection

As mentioned before, transabdominal fetal ECG recordings are predominantly used to determine the fetal heart rate for cardiotocographic analysis. The signal processing steps involved in the detection of the fetal heart rate from the ECG recordings can be divided into four categories:

1. Preprocessing
2. Maternal ECG suppression
3. Detection of fetal R-peaks
4. Postprocessing of fetal heart rate tracings

For each of these four categories, a short discussion is provided below. This discussion is not meant to give a comprehensive overview, but merely to provide some direction in possible strategies.

3.5.1 Preprocessing of Electrophysiological Recordings

One of the main aims of the preprocessing is to suppress out-of-band noiase and intereferences. This is typically done with relatively simple filtering steps,

such as (in)finite impulse response filters, or more complicated methods, such as wavelet transforms [78, 79]. These out-of-band interferences include the EHG signal, harmonics of powerline interferences, and part of electromyographic noise.

Another aim of most preprocessing strategies is to also suppress powerline interference. This typically involves the design of narrowband notch filters, adaptive cancellers such as proposed in [66, 67], or neural network approaches such as proposed in [80].

3.5.2 Maternal ECG Suppression

The development of effective methods for the suppression of the maternal ECG is probably the most widely studied domain within the field on non-invasive fetal electrocardiography. Most of the presented methods can be categorized as *template subtraction*, *source separation*, or *neural networks*.

Template Subtraction Methods In template subtraction methods, a parameterized or non-parameterized template of the maternal ECG is estimated based on information that is measured over a certain time window, thus exploiting *temporal* properties of the ECG. This time window can precede the ECG that needs to be estimated, yielding a causal method. The time window can also exploit future information to yield a non-causal method. One could argue that the non-causal method typically has a higher accuracy, but at the cost that online or real-time implementations are not possible.

Two key assumptions underlie the success of these template subtraction methods. The first assumption is that the ECG of one heartbeat looks like its predecessor, which in turn looks like the predecessor of that beat, and so on. This quasi-periodicity is exploited in the building of a template of the maternal ECG, which should look relatively close to the ECG of an individual heartbeat. The second assumption is that the heart rates of mother and fetus are uncorrelated. More specifically, it is assumed that the heartbeat of the fetus does not occur at the same point in time, relative to the heartbeat of the mother throughout the entire time window that was selected.

The simplest method to calculate the template is by averaging the ECG of all maternal heartbeats in the selected time window. Because of the uncorrelated fetal heart rate, the fetal ECG will occur at random places throughout this ensemble of maternal ECG complexes and will be effectively averaged out. More advanced methods exploit singular value decomposition [81, 82], Kalman filtering [83], or linear prediction [78] instead of ensemble averaging and derive separate templates for the individual waves within the ECG complex [78, 83].

An important property of most of the template subtraction methods is that they can operate on single-channel measurements. Basically, the only template-based method that cannot rely on adaptive filtering, where a referencematernal ECG

measurement is made, typically on the thorax or shoulders of the mother, and this ECG is adaptively filtered to generate an accurate estimate of the abdominal ECG [84].

Source Separation Methods Source separation methods aim to solve the problem:

$$\boldsymbol{Y} = \boldsymbol{A}\boldsymbol{X} + \boldsymbol{N}. \tag{1}$$

Here, $\boldsymbol{Y}$ is a matrix that contains the recorded signals within a multi-channel recordings. The dimensions of $\boldsymbol{Y}$ therefore describe the number of channels and the length of the recording. These recorded signals are considered the linear combination, described by mixing matrix $\boldsymbol{A}$, of a number of so-called source signals $\boldsymbol{X}$. The term $\boldsymbol{N}$ describes possible noise contributions. These noise contributions are often, for simplicity, modeled as one of the source signals, simplifying the expression to $\boldsymbol{Y} = \boldsymbol{A}\boldsymbol{X}$.

The problem statement in Eq. (1) is an underdetermined problem with an infinite amount of possible solutions. That is, to solve the source separation problem either $\boldsymbol{A}$ or $\boldsymbol{X}$ must be determined, starting from a recorded $\boldsymbol{Y}$. Once $\boldsymbol{A}$ or $\boldsymbol{X}$ has been determined, the other one is known from calculating the inverse and multiplying with $\boldsymbol{Y}$. It should be noted that this assumes that the inverse does exist. In most solutions, the unmixing matrix $\boldsymbol{W}$ is calculated, which can provide the source signals $\boldsymbol{X}$ through:

$$\boldsymbol{X} = \boldsymbol{W}\boldsymbol{Y}. \tag{2}$$

Because of the ambiguity of the problem statement, most source separation methods assume that the source signals $\boldsymbol{X}$ are uncorrelated or statistically independent, leading to principal component analysis and indepdendent component analysis (ICA) solutions, respectively [85–87].

Once the principal or independent components have been determined, the component that represents the fetal ECG can be determined, either via visual inspection or an automated selection algorithm and further processing can be done. This processing can not only be the detection of fetal R-peaks but also the *blanking* (i.e., multiplying by zero) of the components that represent unwanted interferences and inverting the *unmixing* of the recorded signals through Eq. (1).

Neural Networks Neural networks, or deep learning methods, are recently getting more and more attention for the suppression of maternal ECG [88–91]. Various neural network architectures have been proposed, differing mostly in either the performance in suppression the maternal ECG during various dynamic or noisy conditions or in computational complexity.

In most works, these neural networks are trained in a supervised manner. Simulated abdominal recordings are generated by adding clean ECG signals from a fetus, e.g., obtained from babies after birth or from manipulated adult ECG signals, to clean ECG signals or the mother, e.g., obtained from non-pregnant subjects. The

neural network then receives as input the combination of fetal ECG, maternal ECG, and generated noise and is trained to provide the clean fetal ECG.

These neural networks have proven to be very effective in extracting the fetal ECG, however often at the expense of relatively high computational loads. Yet, with innovations in deep learning methods and computational power almost appearing by the day, these methods are expected to become realistic possibilities for implementation in the clinic soon.

3.5.3 Fetal R-Peak Detection

The fetal heart rate is typically described as the reciprocal of the interval between consecutive fetal R-peaks:

$$FHR_i[\text{beats per minute, BPM}] = \frac{60[\text{seconds min}^{-1}]}{RR_i[\text{seconds}]}, \tag{3}$$

where FHR_i is the fetal heart rate, RR_i is the interval between successive fetal R-peaks, and i is the index of the heartbeat.

The key element to calculate the heart rate is therefore the detection of fetal R-peaks. It should be acknowledged here that other methods such as autocorrelation—which is the method employed in CTG devices based on Doppler ultrasound [92]—do not require the detection of R-peaks to calculate the heart rate; they essentially rely on the detection of the periodicity in a windowed representation of the recorded data.

Until now, the literature suggests that most attention has gone out to improve methods for suppression of the maternal ECG and far less attention has been paid to the detection of fetal R-peaks. Arguably, in case the maternal ECG is effectively suppressed and so are other interferences, the detection of fetal R-peaks should be relatively straightforward.

One could argue that the number of publications on maternal ECG suppression would either suggest that many satisfactory solutions exist, that each can suppress the maternal ECG to a sufficient amount given the particular experimental setup that was used by the authors, or that it could suggest that no one has solved the problem yet and researchers are iteratively converging to this solution with every new paper that appears. In my view, most presented maternal ECG suppression methods are up to par and the weakest link in the chain of signal processing steps that are needed to retrieve the fetal heart rate is the detection of fetal R-peaks.

Even though the suppression of maternal ECG has in my view been sufficiently resolved, the suppression of other interferences has not. That means that the detection of fetal R-peaks is not straightforward. Many researchers have resorted to the famous Pan–Tompkins algorithm for peak detection [93]. This algorithm performs very well under many circumstances, but its design does not necessarily make it the best algorithm for fetal R-peak detection. One of the main features of abdominal fetal ECG recordings that is not explicitly exploited in the Pan-

Tompkins algorithm is the fact that these measurements are often—yet admittedly not always—multi-channel. Considering the aforementioned relation between the VCG and ECG, one can see that fetal R-peaks in all channels must happen at approximately the same moment in time. Small time differences can occur because the maximum amplitude of the VCG is not seen in all projections (i.e., onto the lead vectors) at exactly the same moment in time.

To some extent, the multi-channel aspect of fetal ECG recordings can be exploited by using a blind source separation technique like ICA. This could capture all information related to the fetal ECG in one independent channel, yet leading to the additional challenge of selecting the component that contains the fetal component. Warmerdam et al. have therefore proposed a method that considers all channels (or in case ICA is used, all components) in the detection of the fetal R-peaks, combined with models of the fetal R-peak, models of the expected RR-intervals, and models of the noise [94]. This method was reported to outperform other methods in the detection of the fetal R-peaks.

The main conclusion from this finding could be that there is still ample room for improvement of the fetal R-peak detection. The work of Warmerdam et al. is arguably one of few attempts to develop a peak detection method for fetal ECG recordings truly based on the unique properties of these recordings, rather than making targeted adaptations to the Pan–Tompkins algorithm (e.g., tuning some parameters). Based on the findings of this work, having quite remarkably better performance in the detection of fetal R-peaks, it seems that indeed it would be worth the effort in shifting research focus from maternal ECG suppression to fetal R-peak detection methods. I have shown in a later publication, adding some artificial intelligence to the decision-making of the method by Warmerdam et al., that indeed improvement can be achieved with relative ease [56].

3.5.4 Postprocessing of Detected Fetal Heart Rate

In the postprocessing phase, the fetal heart rate is calculated from the detected fetal R-peaks using the interval between consecutive R-peaks, in combination with Eq. (3). To prevent misdetected R-peaks, i.e., either detected peaks that were in fact not R-peaks and R-peaks that were not detected, postprocessing aims to respectively omit or insert these misdetections.

The detection of these erroneous fetal R-peaks is typically based on physiology. The fetal heart rate can be assumed to range from 60 BPM to 220 BPM and consecutive heartrates (FHR_i vs FHR_{i-1}) should not deviate too much as the heart cannot accelerate or decelerate too strongly. Many studies use a cutoff of 20% difference between consecutive heartbeats to omit a possible wrong detection [95–97].

Other postprocessing methods can include the application of median or lowpass filters to suppress physiologically implausible heartrates.

4 Complimentary Information: Value of Fetal Electrocardiography Beyond the Cardiotocogram

4.1 Why Is Complimentary Information Needed?

Even if the technology regarding fetal ECG analysis would work perfectly for the determination of the CTG, the problems related to fetal monitoring will not have been resolved. Unfortunately, the CTG has been reported for having relatively low specificity [50]. About one-third of fetuses for which the CTG is not reassuring are in fact in distress and in need of clinical intervention such as instrumental delivery.

To prevent unnecessary interventions based on CTG alone, complimentary information is required to aid the specificity of the CTG in case of doubt. In present-day clinical practice, this complimentary information can, for example, come from fetal blood sampling [52, 98] or analysis of the fetal ECG. Specifically, the latter refers to analysis of the ST segment of the fetal ECG that is obtained with the invasive fetal scalp electrode.

In this section, some promising directions are briefly discussed in which the non-invasive abdominal fetal ECG can be used to compliment the CTG for clinical decision-making.

4.2 Signal Processing for Fetal ECG Quality Enhancement

As a first step toward the clinical use of the non-invasive fetal ECG, the quality of the fetal ECG must be enhanced. In Fig. 6, a typical example is shown of the fetal ECG that is obtained from the maternal abdomen, after having processed the signals with the preprocessing and maternal ECG suppression that were discussed in the previous section. This example illustrates the need for further enhancement of the signal quality: the characteristic waves in the fetal ECG are barely recognizable, if recognizable at all.

For enhancement of the fetal ECG, the same methods as discussed for the estimation and suppression of the maternal ECG can be used. Methods that have already been presented in literature include averaging over multiple heartbeats and denoising neural networks [100, 101]. The averaging methods aim to produce an average fetal ECG complex (an example is also shown in Fig. 6) and either use a fixed or variable number of averages, where this variable number depends on the quality of the recorded signals [99].

For detecting fetal compromise, it is worth to note here that most pathophysiologies do not require the possibility to analyze the *beat-to-beat* variations in the ECG morphology. For instance, ST analysis of the invasive fetal ECG is based on an average ECG that is obtained by averaging over 30 heartbeats [40] and has been reported to have high enough time resolution to detect emerging hypoxia. Alternatively, structural defects in the ECG that originate from congenital heart

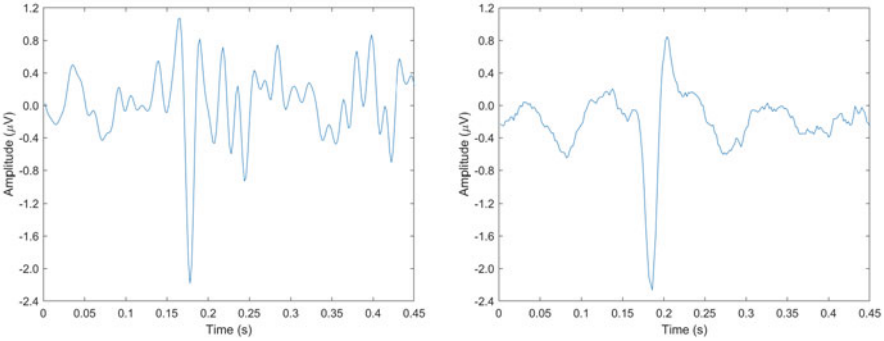

Fig. 6 Left: recorded fetal ECG complex after preprocessing and maternal ECG suppression. Right: for the same fetus the fetal ECG after averaging over multiple heartbeats. In this case, averaging was performed over all detected fetal R-peaks in the recordings, which were almost 2000 complexes

disease are expected to systematically alter the morphology of the ECG and hence remain visible after averaging, even over many more than 30 heartbeats [58]. Having said this, it should be mentioned that averaging the ECG over multiple heartbeats makes it impossible to study the original of fetal arrhythmia.

Although the previous paragraph discusses how averaging should not impede analysis of the fetal ECG too much, a problem for averaging over multiple heartbeats could occur if this is done during episodes of fetal movement. Because the electrodes in transabdominal fetal ECG recordings are placed on the maternal abdomen, the fetus can move with respect to these electrodes. Considering the aforementioned model where the VCG was projected onto electrode lead vectors to yield the ECG, the VCG could be regarded as the three-dimensional activity of the heart that moves along with the heart. If the fetus changed its orientation during movement, the heart and VCG would change their orientation with respect to the abdominal electrodes. Hence, the projections onto the lead vectors change as well and so will the ECG. When averaging over multiple heartbeats, the associated ECG complexes could have changed because of motion, and therefore the average ECG would be distorted. Luckily, some methods have been presented to compensate for such movement by calculating the fetal VCG and tracking its rotations over time [102, 103].

4.3 Possible Clinical Use of the Fetal ECG

Next to fetal movement, the ECG measured with non-invasive electrodes can also change between pregnancies because of variations in the fetal orientation, such as between cephalic and breech presentations. When aiming to use the non-invasive fetal ECG for monitoring hypoxia via ST analysis, it must be determined whether

cutoff values used for assessing whether the ST segment has changed significantly depend on the orientation of the fetus and to what extent significant changes in the ST segment could be caused by an emerging hypoxic state or by inadequate correction for fetal movements.

While it seems that non-invasive ST analysis is still far from ready for implementation in clinical practice, the use of the fetal ECG for diagnosing congenital heart disease seems more promising for the near future. As mentioned before, structural cardiac anomalies will systematically appear in the ECG, so averaging over multiple heartbeats is not a problem, provided that the ECGs are compensated for fetal movement. Specific congenital heart disease (CHD) will affect the fetal ECG, for instance, by changing the electrical heart axis [60] or distorting some ECG waves in a specific way. Given the fact that the detection rates of CHD during prenatal screening are relatively poor, with only about of severe CHD detected [104], ECG analysis could aid in the improvement of these detection rates. Especially, if ECG analysis were to be positioned next to ultrasound imaging—the current standard during prenatal screening—it could be envisioned that CHDs that affect the cardiac anatomy are detected by ultrasound but that CHDs that affect the (electrical) functionality of the heart are detected by ECG. The (near) future will probably tell and hopefully demonstrate that in this era of technological innovations, fetal monitoring will improve to enable safe childbirth for all.

References

1. H.P. van Geijn, F.J.A. Copray, *A Critical Appraisal of Fetal Surveillance* (Excerpta Medica, Amsterdam, New York, 1994)
2. I. Amer-Wåhlin, Fetal ECG waveform analysis for intrapartum monitoring. PhD Thesis, Lund University, Lund, Sweden, 2003
3. E. Symonds, D. Sahota, A. Chang, *Fetal Electrocardiography* (Imperial College Press, Londen, UK, 2001)
4. C. Smyth, Experimental electrocardiography of the foetus. Lancet **1**(6771), 1124–1126 (1953)
5. C. Sureau, Fetal electrocardiographic research during pregnancy and labor; first results of a new technic of registration by intrauterine electrodes. Gynecol. Obstet. (Paris) **55**(1), 21–33 (1956)
6. S. Kaplan, S. Toyama, Fetal electrocardiography; utilizing abdominal and intrauterine leads. Obstet. Gynecol. **11**(4), 391–397 (1958)
7. E. Hon, Instrumentation of fetal heart rate and fetal electrocardiography. II. A vaginal electrode. Am. J. Obstet. Gynecol. **86**, 772–784 (1963)
8. S. Larks, G. Larks, Components of the fetal electrocardiogram and intrauterine electrical axis: quantitative data. Biol. Neonat. **10**(3), 140–152 (1966)
9. S. Larks, G. Larks, Comparative aspects of the fetal and newborn electrocardiograms. evidence for the validity of the method for calculation of the electrical axis of the fetal heart. Am. J. Obstet. Gynecol. **96**(4), 553–555 (1966)
10. S. Larks, G. Larks, The electrical axis of the fetal heart: a new criterion for fetal well-being or distress. Am. J. Obstet. Gynecol. **93**(7), 975–983 (1966)
11. K. Rosén, I. Kjellmer, Changes in fetal heart rate and ECG during hypoxia. Acta Physiol. Scand. **93**, 59–66 (1975)
12. K. Rosén, K. Hökegård, I. Kjellmer, A study of the relationship between the electrocardiogram and hemodynamics in the fetal lamb during asphyxia. Acta Physiol. Scand. **98**(3), 275–284 (1976)

13. W. van Wijngaarden, D. Sahota, D. James, T. Farrell, G. Mires, M. Wilcox, A. Chang, Improved intrapartum surveillance with PR interval analysis of the fetal electrocardiogram: a randomized trial showing a reduction in fetal blood sampling. Am. J. Obstet. Gynecol. **174**(4), 1295–1299 (1996)
14. B. Strachan, W. van Wijngaarden, D. Sahota, A. Chang, D. James, Cardiotocography only versus cardiotocography plus PR-interval analysis in intrapartum surveillance: a randomised, multicentre trial. FECG study group. Lancet **355**(9202), 456–459 (2000)
15. K. Greene, G. Dawes, H. Lilja, K. Rosén, Changes in the ST waveform of the fetal lamb electrocardiogram with hypoxemia. Am. J. Obstet. Gynecol. **144**, 950–958 (1982)
16. H. Lilja, K. Karlsson, I. Kjellmer, K. Lindecrantz, T. Olsson, K. Rosén, Heart rate variability and electrocardiogram changes in the fetal lamb during hypoxia and beta-adrenoceptor stimulation. J. Perinat. Med. **12**(3), 115–125 (1984)
17. K. Rosén, A. Dagbjartsson, B. Henriksson, H. Lagercrantz, I. Kjellmer, The relationship between circulating catecholamines and ST waveform in the fetal lamb electrocardiogram during hypoxia. Am. J. Obstet. Gynecol. **149**(2), 190–195 (1984)
18. I. Amer-Wåhlin, C. Hellsten, H. Norén, H. Hagberg, A. Herbst, I. Kjellmer, H. Lilja, C. Lindoff, M. Månsson, L. Mårtensson, P. Olofsson, A. Sundström, K. Marsál, Cardiotocography only versus cardiotocography plus ST analysis of fetal electrocardiogram for intrapartum fetal monitoring: a swedish randomised controlled trial. Lancet **18**, 534–538 (2001)
19. A. Kwee, C. van der Hoorn-van den Beld, J. Veerman, A.H. Dekkers, G. Visser, STAN S21 fetal heart monitor for fetal surveillance during labor: an observational study in 637 patients. J. Matern. Fetal Neonatal. Med. **15**(6), 400–407 (2004)
20. K. Ojala, M. Vääräsmäki, K. Mäkikallio, M. Valkama, A. Tekay, A comparison of intrapartum automated fetal electrocardiography and conventional cardiotocography-a randomised controlled study. BJOG **113**(4), 419–423 (2006)
21. M. Westerhuis, G.H. Visser, K. Moons, E. van Beek, M. Benders, S. Bijvoet, H. van Dessel, A. Drogtrop, H. van Geijn, G. Graziosi, F. Groenendaal, J. van Lith, J. Nijhuis, S. Oei, H. Oosterbaan, M. Porath, R. Rijnders, N. Schuitemaker, L. Sopacua, I. van der Tweel, L. Wijnberger, C. Willekes, N. Zuithoff, B. Mol, A. Kwee, Cardiotocography plus ST analysis of fetal electrocardiogram compared with cardiotocography only for intrapartum monitoring: a randomized controlled trial. Obstet. Gynecol. **115**(6), 1173–1180 (2010)
22. P. Oian, E. Bix, Scarce scientific evidence for the use of cardiotocography plus fetal ECG ST interval analysis (STAN). Acta Obstet. Gynecol. Scand. **93**(6), 570 (2014)
23. P. Steer, L. Hvidman, Scientific and clinical evidence for the use of fetal ECG ST segment analysis (stan). Acta Obstet. Gynecol. Scand. **93**(6), 533–538 (2014)
24. M. Belfort, G. Saade, E. Thom, S. Blackwell, U. Reddy, J. Thorp Jr., A. Tita, R. Miller, A. Peaceman, D. McKenna, E. Chien, D. Rouse et al., A randomized trial of intrapartum fetal ECG ST-segment analysis. New Engl. J. Med. **373**, 632–641 (2015)
25. J. Dashe, D. McIntire, D. Twickler, Maternal obesity limits the ultrasound evaluation of fetal anatomy. J. Ultrasound Med. **28**(8), 1025–1030 (2009)
26. P. Hamelmann, R. Vullings, L. Schmitt, A. Kolen, M. Mischi, J. van Laar, J. Bergmans, Improved ultrasound transducer positioning by fetal heart location estimation during doppler based heart rate measurements. Physiol. Meas. **38**(10), 1821–1836 (2017)
27. J. Bernhards, L. Bouman, *Fysiologie van de mens*, 6th edn. (Bohn Stafleu Van Loghum, DL Houten, 1994)
28. A. Guyton, J. Hall, *Textbook of Medical Physiology*, 10th edn. (W.B. Saunders Company, Philadelphia, USA, 2000)
29. N. DePasquale, G. Burch, The electrocardiogram, ventricular gradient and spatial vectorcardiogram during the first week of life. Am. J. Cardiol. **12**, 482–493 (1963)
30. G. Mielke, N. Benda, Cardiac output and central distribution of blood flow in the human fetus. Circulation **103**(12), 1662–1668 (2001)
31. M. Artman, L. Mahony, D. Teitel, *Neonatal Cardiology* (McGraw-Hill Companies, USA, 2002)

32. S. Yagel, N. Silverman, U. Gembruch, *Fetal Cardiology? Embryology, Genetics, Physiology, Echocardiographic Evaluation, Diagnosis and Perinatal Management of Cardiac Diseases*, 2nd edn. (Informa Healthcare Inc., New York, USA, 2009)
33. D. Geselowitz, Dipole theory in electrocardiography. Am. J. Cardiol. **14**(9), 301–306 (1964)
34. J. Malmivuo, R. Plonsey, *Bioelectromagnetism - Principles and Applications of Bioelectric and Biomagnetic Fields* (Oxford University Press, New York, 1995)
35. E. Frank, General theory of heart-vector projection. Circ. Res. **2**, 258–270 (1954)
36. H. Burger, J. Van Milaan, Heart-vector and leads. Br. Heart J. **8**(3), 157–161 (1946)
37. W. Einthoven, Weiteres über das elektrokardiogram. Pflüger Arch. ges Physiol. **122**, 517–548 (1908)
38. T. Oostendorp, Modelling the foetal ECG. PhD Thesis, K.U.Nijmegen, The Netherlands, 1989
39. E. Frank, An accurate, clinically practical system for spatial vectorcardiography. Circulation **13**, 737–749 (1956)
40. A. Sundström, D. Rosén, K. Rosén, *Fetal surveillance* (Tech. Rep, Neoventa Medical AB, 2002)
41. H. Cohn, E. Sacks, M. Heymann, A. Rudolph, Cardiovascular responses to hypoxemia and acidemia in fetal lambs. Am. J. Obstet. Gynecol. **120**, 817–824 (1974)
42. R. Eckert, D. Randall, *Animal Physiology* (WH Freeman and Company, New York, 1983)
43. W. de Jong, Blood pressure variability in neonates. PhD Thesis, Technische Universiteit Eindhoven, Eindhoven, the Netherlands, 2000
44. W. Johnson, H. Stegall, J. Lein, R. Rushmer, Detection of fetal life in early pregnancy with an ultrasonic doppler flowmeter. Obstet. Gynecol. **26**, 305–307 (1965)
45. G. Lawson, R. Belcher, G. Dawes, C. Redman, A comparison of ultrasound (with autocorrelation) and direct electrocardiogram fetal heart rate detector systems. Am. J. Obstet. Gynecol. **147**(6), 721–722 (1983)
46. C. Kittel, W. Knight, M. Ruderman, *Mechanics (Berkeley Physics Course)* (McGraw-Hill, USA, 1965)
47. M. Peters, J. Crowe, J. Piéri, H. Quartero, B.H. Gill, D. James, J. Stinstra, S. Shakespeare, Monitoring the fetal heart non-invasively: a review of methods. J. Perinat. Med. **29**, 408–416 (2001)
48. R. Freeman, T. Garite, M. Nageotte, *Fetal Heart Rate Monitoring* (Lippincott Williams & Wilkins, Philadelphia, PA, USA, 2003)
49. F. subcommittee on Standards in Perinatal Medicine, Guidelines for the use of fetal monitoring. Int. J. Gynecol. Obstet. **25**(3), 159–167 (1987)
50. Z. Alfirevic, D. Devane, G. Gyte, Continuous cardiotocography (CTG) as a form of electronic fetal monitoring (EFM) for fetal assessment during labor. Cochrane Database System. Rev. **2017**(2), CD006066 (2017)
51. K. Nelson, J. Dambrosia, T. Ting, J. Grether, Uncertain value of electronix fetal monitoring in predicting cerebral palsy. New Eng. J. Med. **334**(10), 613–618 (1996)
52. P. van den Berg, S. Schmidt, J. Gesche, E. Saling, Fetal distress and the condition of the newborn using cardiotocography and fetal blood analysis during labour. Br. J. Obstet. Gynaecol. **94**(1), 72–75 (1987)
53. C. Peters, E. ten Broeke, P. Andriessen, B. Vermeulen, R. Berendsen, P. Wijn, S. Oei, Beat-to-beat detection of fetal heart rate: Doppler ultrasound cardiotocography compared to direct ECG cardiotocography in time and frequency domain. Physiol. Meas. **25**(2), 585–593 (2004)
54. R. Myers, Two patterns of perinatal brain damage and their conditions of occurrence. Am. J. Obstet. Gynecol. **116**(2), 246–276 (1972)
55. C. Lempersz, L. Noben, G. van Osta, M. Wassen, B. Meershoek, P. Bakker, Y. Jacquemyn, M. Cuerva, R. Vullings, M. Westerhuis, S. Oei, Intrapartum non-invasive electrophysiological monitoring: a prospective observational study. Acta Obstet. Gynecol. Scand. **99**(10), 1387–1395 (2020)
56. R. Vullings, J. van Laar, Non-invasive fetal electrocardiography for intrapartum cardiotocography. Front Pediatr. **8**(599049), (2020). https://doi.org/10.3389/fped.2020.599049

57. L. Noben, S. Clur, J. van Laar, R. Vullings, Prenatal diagnosis of a bundle branch block based on the fetal ECG. BMJ Case Rep. **12**(7), e229998 (2019)
58. C. Lempersz, L. Noben, S. Clur, K. Verdurmen, G. Warmerdam, J. van der Post, N. Blom, T. Delhaas, S. Oei, R. Vullings, The standardized 12-lead fetal electrocardiogram of the healthy fetus in mid-pregnancy: a cross-sectional study. PLoS One **15**(4), e0232606 (2020)
59. C. Lempersz, L. Noben, S. Clur, E. van den Heuvel, Z. Zhan, M. Haak, S. Oei, R. Vullings, J. van Laar, The electrical heart axis of the fetus between 18 and 24 weeks of gestation: a cohort study. PLoS One **16**(12), e0256115 (2021)
60. L. Noben, C. Lempersz, E. van den Heuvel, Z. Zhan, F. Vandenbussche, A. Coumans, M. Haak, R. Vullings, S. Oei, S. Clur, J. van Laar, The electrical heart axis in fetuses with congenital heart disease, measured with non-invasive fetal electrocardiography. PLoS One **17**(10), e0275802 (2022)
61. C. Marque, J. Duchêne, S. Leclercq, G. Panczer, J. Chaumont, Uterine ehg processing for obstetrical monitoring. IEEE Trans. Biomed. Eng. **BME-33**(12), 1182–1187 (1986)
62. C. Rabotti, Characterization of uterine activity by electrohysterography. PhD Thesis, Technische Universiteit Eindhoven, Eindhoven, the Netherlands, 2010
63. S. Abboud, D. Sadeh, Spectral analysis of the fetal electrocardiogram. Comput. Biol. Med. **19**(6), 409–415 (1989)
64. C. Rabotti, M. Mischi, J. Van Laar, S. Oei, J. Bergmans, Estimation of internal uterine pressure by joint amplitude and frequency analysis of electrohysterographic signals. Physiol. Meas. **29**, 829–841 (2008)
65. C. Buhimschi, M. Boyle, R. Garfield, Electrical activity of the human uterus during pregnancy as recorded from the abdominal surface. Obstet. Gynecol. **90**(1), 102–111 (1997)
66. S. Martens, M. Mischi, S. Oei, J. Bergmans, An improved adaptive powerline interference canceller for electrocardiography. IEEE Trans. Biomed. Eng. **53**, 2220–2231 (2006)
67. G. Warmerdam, R. Vullings, L. Schmitt, J. van Laar, J. Bergmans, A fixed-lad Kalman smoother to filter power line interference in electrocardiogram recordings. IEEE Trans. Biomed. Eng. **64**(8), 1852–1861 (2017)
68. T. Oostendorp, A. van Oosterom, Electrical properties of tissues involved in the conduction of foetal ECG. Med. Biol. Eng. Comput. **27**, 322–324 (1989)
69. T. Oostendorp, A. van Oosterom, H. Jongsma, The effect of changes in the conductive medium on the fetal ECG throughout gestation. Clin. Phys. Physiol. Meas. **10**(Suppl B), 11–20 (1989)
70. T. Oostendorp, A. van Oosterom, H. Jongsma, The fetal ECG throughout the second half of gestation. Clin. Phys. Physiol. Meas. **10**(2), 147–160 (1989)
71. J. Stinstra, Reliability of the fetal magnetocardiogram. PhD Thesis, Universiteit Twente, Enschede, the Netherlands, 2001
72. J. Oldenburg, M. Macklin, Changes in the conduction of the fetal electrocardiogram to the maternal abdominal surface during gestation. Am. J. Obstet. Gynecol. **129**(4), 425–433 (1977)
73. The University of Nottingham, J. Crowe, D. James, B. Hayes-Gill, C. Barratt, J.-F. Pieri, Fetal surveillance, International patent WO/2005/039410, 2004–10-13
74. A. Kahn, Transmission characteristics in fetal electrocardiography, in *Proceedings of the Sixteenth ANN Conference on Engineering* (Medicine and Biology, Baltimore, USA, 1963), p.134
75. J. Roche, E. Hon, The fetal electrocardiogram v. comparison of lead systems. Am. J. Obstet. Gynecol. **92**, 1149–1159 (1965)
76. R. Brace, Physiology of amniotic fluid regulation. Clin. Obstet. Gynecol. **40**(2), 180–189 (1997)
77. O. Stern, Sur Theorie der Elektrolytischen Doppelschit. Electrochem **30**, 508 (1924)
78. R. Vullings, C. Peters, R. Sluijter, M. Mischi, S. Oei, J. Bergmans, Dynamic segmentation and linear prediction for maternal ECG removal in antenatal abdominal recordings. Physiol. Meas. **30**, 291–307 (2009)

79. G. Lenis, N. Pilia, A. Loewe, W. Schulze, O. Dössel, Comparison of baseline wander removal techniques considering the preservation of ST changes in the ischemic ECG: a simulation study. Comput. Math. Methods Med. **2017**, 9295029 (2017)
80. J. Mateo, J. Rieta, Application of artificial neural networks for versatile preprocessing of electrocardiogram recordings. J. Med. Eng. Technol. **36**(2), 90–101 (2012)
81. P. Kanjilal, S. Palit, G. Saha, Fetal ECG extraction from single-channel maternal ECG using singular value decomposition. IEEE Trans. Biomed. Eng. **44**(1), 51–59 (1997)
82. M. Varanini, G. Tartarisco, L. Billeci, A. Macerata, G. Pioggia, R. Balocchi, An efficient unsupervised fetal QRS complex detection from abdominal maternal ECG. Physiol. Meas. **35**(8), 1607–1619 (2014)
83. R. Sameni, M. Shamsollahi, C. Jutten, G. Clifford, A nonlinear bayesian filtering framework for ECG denoising. IEEE Trans. Biomed. Eng. **54**(12), 2172–2185 (2007)
84. B. Widrow, J.R. Glover, J. McCool, J. Kaunitz, C.S. Williams, R.H. Hearn, J.R. Zeidler, E. Dong, R. Goodlin, Adaptive noise cancelling: principles and applications. Proc. IEEE **62**, 1692–1716 (1975)
85. V. Zarzoso, A. Nandi, Noninvasive fetal electrocardiogram extraction: blind separation versus adaptive noise cancellation. IEEE Trans. Biomed. Eng. **48**(1), 12–18 (2001)
86. J. Behar, J. Oster, G.D. Clifford, Non-invasive FECG extraction from a set of abdominal sensors. Comput. Cardiol. **2013**, 297–300 (2013)
87. K. Knuth, Bayesian source separation and localization, in *SPIE'98 Proceedings: Bayesian Inference for Inverse Problems*, vol. 3459, pp. 147–158, San Diego, July 1998
88. W. Zhong, L. Liao, X. Guo, G. Wang, A deep learning approach for fetal QRS complex detection. Physiol. Meas. **39**(4), 045004 (2018)
89. K. Vo, T. Le, A. Rahmani, N. Dutt, H. Cao, An efficient and robust deep learning method with 1-D octave convolution to extract fetal electrocardiogram. Sensors (Basel) **20**(13), 3757 (2020)
90. A. Rasti-Meymandi, A. Ghaffari, AECG-DecompNet: abdominal ECG signal decomposition through deep-learning model. Physiol. Meas. **42**(4), (2021). https://doi.org/10.1088/1361-6579/abedc1
91. A. Shokouhmand, N. Tavassolian, Fetal electrocardiogram extraction using dual-path source separation of single-channel non-invasive abdominal recordings. IEEE Trans. Biomed. Eng. (2022)
92. H. van Geijn, Developments in CTG analysis. Baillieres Clin. Obstet. Gynaecol. **10**(2), 185–209 (1996)
93. J. Pan, W. Tompkins, A real-time QRS detection algorithm. IEEE Trans. Biomed. Eng. **32**(3), 320–326 (1985)
94. G. Warmerdam, R. Vullings, L. Schmitt, J. van Laar, J. Bergmans, Hierarchical probabilistic framework for fetal R-peak detection, using ECG waveform and heart rate information. IEEE Trans. Sig. Proc. **66**(16), 4388–4397 (2018)
95. C. Peters, R. Vullings, J. Bergmans, G. Oei, P. Wijn, The effect of artifact correction on spectral estimates of heart rate variability, in *Proceedings of the IEEE EMBC*, pp. 2669–72, Vancouver, Canada, 2008
96. C. Peters, R. Vullings, M. Rooijakkers, J. Bergmans, S. Oei, P. Wijn, A continuous wavelet transform-based method for time-frequency analysis of artefact-corrected heart rate variability data. Physiol. Meas. **32**(10), 1517–1527 (2011)
97. L. Campana, R. Owens, G. Clifford, S. Pittman, A. Malhotra, Phase-rectified signal averaging as a sensitive index of autonomic changes with aging. J. Appl. Physiol. **108**(6), 1668–1673 (2010)
98. E. Saling, Amnioscopy and foetal blood sampling: observations on foetal acidosis. Arch. Dis. Child **41**(219), 472–476 (1966)
99. R. Vullings, B. de Vries, J. Bergmans, An adaptive Kalman filter for ECG signal enhancement. IEEE Trans. Biomed. Eng. **58**(4), 1094–1103 (2011)
100. E. Fotiadou, T. Konopczynski, J. Hesser, R. Vullings, End-to-end trained encoder-decoder convolutional neural network for fetal electrocardiogram signal denoising. Physiol. Meas. **41**(1), 015005 (2020)

101. E. Fotiadou, R. Vullings, Multi-channel fetal ECG denoising with deep convolutional neural networks. Front Pediatr. **8**(508), (2020). https://doi.org/10.3389/fped.2020.00508
102. L. Sörnmo, Vectorcardiographic loop alignment and morphologic beat-to-beat variability. IEEE Trans. Biomed. Eng. **45**(12), 1401–1413 (1998)
103. R. Vullings, M. Mischi, S. Oei, J. Bergmans, Novel Bayesian vectorcardiographic loop alignment for improved monitoring of ECG and fetal movement. IEEE Trans. Biomed. Eng. **60**(6), 1580–1588 (2013)
104. C. van Velzen, S. Clur, M. Rijlaarsdam, C. Bax, E. Pajkrt, M. Heymans, M. Bekker, J. Hruda, C. de Groot, N. Blom, M. Haak, Prenatal detection of congenital heart disease - results of a national screening programme. BJOG **123**(3), 400–407 (2016)

Modern Signal Processing Tools for Fetal Electrocardiogram Extraction from Single-Channel Transabdominal Maternal Electrocardiogram

Pei-Chun Su and Hau-Tieng Wu

1 Introduction

Extracting fetal electrocardiogram (ECG) from a single-channel transabdominal maternal ECG (ta-mECG) is a challenging signal processing mission. The mission could be understood as the single-channel blind source separation (scBSS); that is, we could simply model the ta-mECG as a summation of one maternal ECG (mECG) and one (or more if multiple birth) fetal ECG (fECG), which is contaminated by various noises and artifacts, and ask how to decompose mECG and fECG from the ta-mECG. The challenge we face when we deal with this fECG extraction problem could be categorized into the following points:

(C1) Both maternal and fetal ECGs are oscillatory and spike-like, so the traditional filtering technique cannot be applied directly.
(C2) Since there is only one channel, the widely applied adaptive filter, principal component analysis (PCA), or independent component analysis (ICA) [3] cannot be applied directly.
(C3) Both maternal and fetal ECGs have time-varying frequency due to the heart rate variability and time-varying amplitude due to respiration. Moreover, the oscillatory pattern changes from one cycle to the next, and the change is nonlinearly related to the time-varying frequency and amplitude. This fact imposes more challenges.

P.-C. Su
Department of Mathematics, Duke University, Durham, NC, USA
e-mail: peichun.su@duke.edu

H.-T. Wu (✉)
Department of Mathematics and Department of Statistical Science, Duke University, Durham, NC, USA
e-mail: hauwu@math.duke.edu

D. Pani (ed.), *Innovative Technologies and Signal Processing in Perinatal Medicine*, https://doi.org/10.1007/978-3-031-32625-7_8

(C4) The noise and artifact like uterine contraction are inevitable, and both are non-stationary in nature.

To handle these challenges, the traditional and standard approach is the *template subtraction* (TS) [5, 8, 9, 17, 33, 47–49], among other approaches like time–frequency analysis [2, 4, 19, 21, 24], sequential total variation [25], or state space reconstruction via lag map [18, 22, 38]. Inspired by these previous works and the need for a better fECG extraction algorithm when only single-channel ta-mECG is available, we developed a new fECG extraction algorithm [27, 43, 44], which is based on two modern signal processing tools. The first one is a nonlinear-type time–frequency analysis tool, the de-shape algorithm, and the second one is a random matrix theory tool, the optimal shrinkage (OS). These two tools, with a proper combination, could be viewed as nonlinear variations of existing TS tools that are designed to handle the fECG extraction problem that leads to a high-quality fECG. To be more specific, the main function of the de-shape algorithm is detecting the maternal R peaks, particularly when the heights of fetal R peaks are compatible with the heights of maternal R peaks and the signal-to-noise ratio is low. The main function of OS is recovering the mECG by removing the fECG under a proper setting, so that the mECG and fECG are decomposed from the ta-mECG. Below, we detail each algorithm step by step with example, in the order that leads to the desired fECG extraction algorithm, and refer the readers with interest to [27, 43, 44] for its practical performance and [13, 29, 34, 46] for theoretical justifications. The step-by-step Matlab implementation of the proposed algorithm is provided for the reproduction purpose in https://github.com/PeiChunSu/fECG-decomposition.

From a time–frequency analysis perspective, the de-shape algorithm is inspired by the analysis of non-sinusoidal oscillatory signals, such as ECG. When the goal of signal processing is to obtain the instantaneous frequency of a signal, the non-sinusoidal nature of an oscillatory signal can result in a complex time–frequency representation that includes undesired harmonics. This complexity is further exacerbated when multiple oscillatory components are present, like the ta-mECG we discuss in this note. In fact, even when the instantaneous frequencies of different oscillatory components do not intersect and well separated, the instantaneous frequencies of their harmonics can intersect, leading to spectral leakage and blurring in the time–frequency representation. This challenge cannot be overcome by techniques like the synchrosqueezing transform (SST) [10], which is designed to enhance the contrast of the time–frequency representation but treats all harmonics equally. The de-shape algorithm leverages the periodic pattern in the time–frequency representation to cancel out these harmonics. While SST and de-shape are designed for different purposes, they can be combined to further improve the contrast of the resulting time–frequency representation. We will not further elaborate this to keep things simple and refer the readers with interest to [28] for details.

Before detailing the algorithm, we shall mention that each developed tool could be separately or jointly applied to other biomedical time series, particularly when the single-channel time series is composed of multiple oscillatory components with

complicated statistical features. For example, de-shape could be applied to analyze photoplethysmogram [26] and its motion artifacts [32], estimate gait cadence from accelerometer signal [50], estimate heart rate and respiratory rate from pressure sensitive mat [15], etc.; OS could be applied to evaluate the ECG T wave quality [45], denoise the noisy otoacoustic emission signal [31], remove stimulation artifact from the intracranial electroencephalogram (EEG) [1], remove cardiogenic artifact from the EEG [7], etc.

2 Proposed Algorithm

The proposed algorithm falls in the category of scBSS algorithm for the general purpose. Specifically, the algorithm separates the fECG and mECG out of the recorded ta-mECG. There are four main steps in addition to the standard preprocessing step.

(Step 1) Estimate the maternal heart rate based on the de-shape algorithm called de-shape short-time Fourier transform (dsSTFT) [27, 43]. De-shape algorithm removes the undesired information in the spectrogram so that the maternal heart rate could be accurately estimated.

(Step 2) With the maternal heart rate information, apply the peak tracking algorithm to determine the maternal R peaks.

(Step 3) Divide the ta-mECG into pieces according to the maternal R peaks so that each piece contains one maternal cardiac cycle. By aligning maternal cardiac cycles by their R peaks and viewing fECG as noise, we could utilize OS to remove fetal cardiac activities and noise from each maternal cardiac cycle [44, 46] and obtain the recovered mECG by attaching each denoised maternal cardiac cycle.

(Step 4) The fECG is then obtained by subtracting the recovered mECG from the ta-mECG. The fECG is still contaminated by the noise and possible residue of the mECG, so we call it the *rough fECG*. By repeating Step 1 to Step 3 on rough fECG, the fECG is recovered.

See Fig. 1 for a summary of the proposed algorithm. Below we detail the algorithm step by step for the reproducibility purpose.

2.1 Input Data

Fix a subject and a ta-mECG recording. If the sampling rate of the recording is less than 1000 Hz, the signal is upsampled to 1000 Hz [23] for the sake of enhancing the R peak alignment needed in the following steps. Thus, we assume below that all signals are sampled at $f_s = 1000$ Hz. Note that a higher sampling rate can be

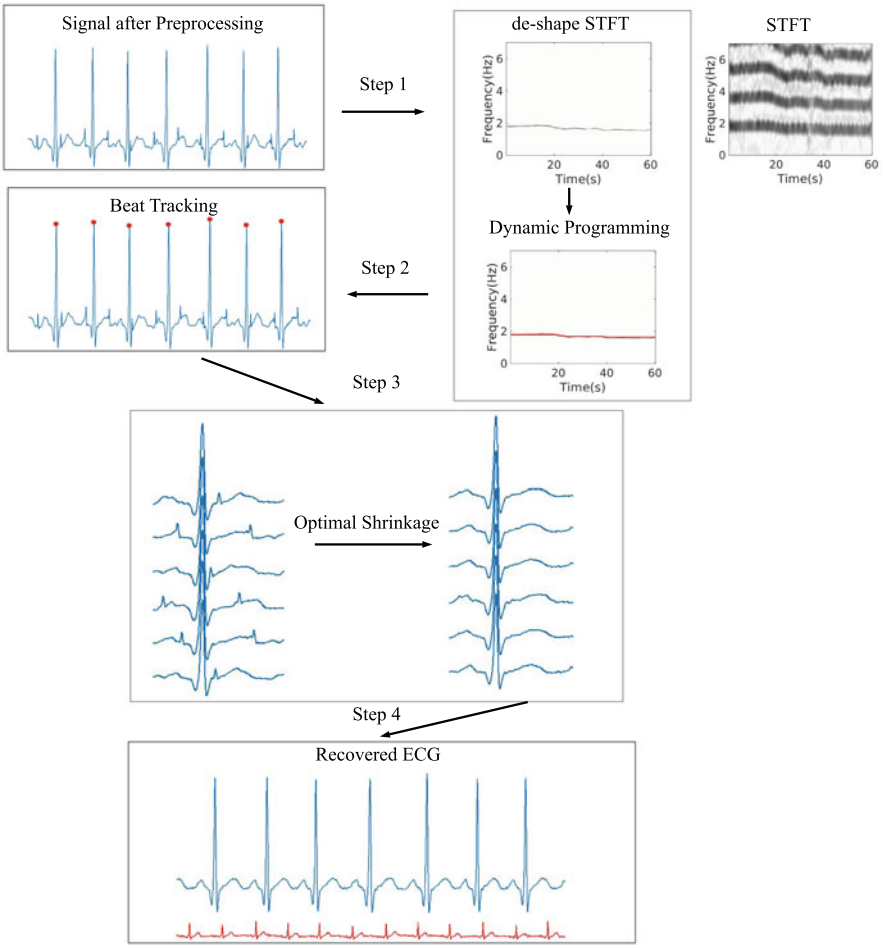

Fig. 1 An illustration of the fECG extraction algorithm. The signal is from the first channel of the first subject in CinC2013 [40] database. In Step 0, we preprocess the ta-mECG. In Step 1, we obtain the time–frequency representation of the ta-mECG by applying the de-shape STFT. The maternal instantaneous heart rate could be acquired by the dynamic programming algorithm, which is superimposed as the red line in the time–frequency representation. In Step 2, with the estimated maternal instantaneous heart rate, the maternal R peaks are estimated by the beat tracking algorithm and showed as the red circles. In Step 3, for each maternal R peak, the associated ta-mECG cycles are stacked together with the associated maternal R peaks aligned. Only six beats are shown to enhance the visualization. By applying the optimal shrinkage on the stacked segments, the noise and fECG are suppressed, and hence the mECG signal is reconstructed. In Step 4, the rough fECG is obtained by subtracting the reconstructed mECG (blue line) from the ta-mECG, and the final fECG could be obtained by applying Steps 1–4 on the rough fECG. Note that in this example, the fECG is relatively weak compared with the mECG

considered, but in practice we found its benefit marginal but the computational time is increased. Denote the ta-mECG signal as $\mathbf{x}^0 \in \mathbb{R}^N$, where $N \in \mathbb{N}$ is the number of samples; that is, the recording is over an interval of $T = N/f_s = N/1000$ seconds. For a long signal with large T, we can simply divide the signal into smaller segments, like 300 seconds long, and apply the following steps on each segment. See Sect. 3.2 for a discussion of the signal length issue.

2.2 Step 0: Preprocessing and Linear Combination

The Butterworth low-pass filter of order 5 with the cut-off frequency of 100 Hz and a notch filter with the notch centered at 60 Hz or 50 Hz, depending on the region, are applied on the ta-mECG to remove high-frequency noises and the power line interference. In addition to high-frequency noise and power line interference, baseline wandering is inevitable in ta-mECG, which corresponds to low-frequency noise caused by a variety of sources including respiration, body movements, and poor electrode contact. To remove baseline wandering, we apply the following two-stage moving window median filter with window sizes 200 and 600 ms, where we denote the operators of median filters with short and long window sizes as $\mathbf{D}_S$ and $\mathbf{D}_L$, respectively. The baseline wandering of $\mathbf{x}^0$ is thus estimated by $\mathbf{D}_L\mathbf{D}_S\mathbf{x}^0_j$, and hence the detrended signal is obtained by

$$\mathbf{x} = \mathbf{x}^0 - \mathbf{D}_L\mathbf{D}_S\mathbf{x}^0 .$$

This two-stage moving window median filter not only can preserve a higher signal-to-noise ratio (SNR) [39] but also can preserve fECG morphology [36], which is the desired feature for our problem. The Matlab implementation of this step is `step0_preprocess.m`. To call this function, in Matlab, run the following code:

```
x = step0_preprocess(x0, fs);
```

where the input `x0` is the raw signal $\mathbf{x}^0$ and `fs` is the sampling rate f_s, and the output `x` is the preprocessed signal $\mathbf{x}$.

2.3 Step 1: Estimate the Maternal Instantaneous Heart Rate by De-shape STFT

We apply the de-shape STFT to extract the instantaneous heart rate (IHR), or the instantaneous frequency (IF), information of the maternal and fetal cardiac activities from the signal $\mathbf{x}$. The theoretical explanation of de-shape STFT will be further explained in a later section.

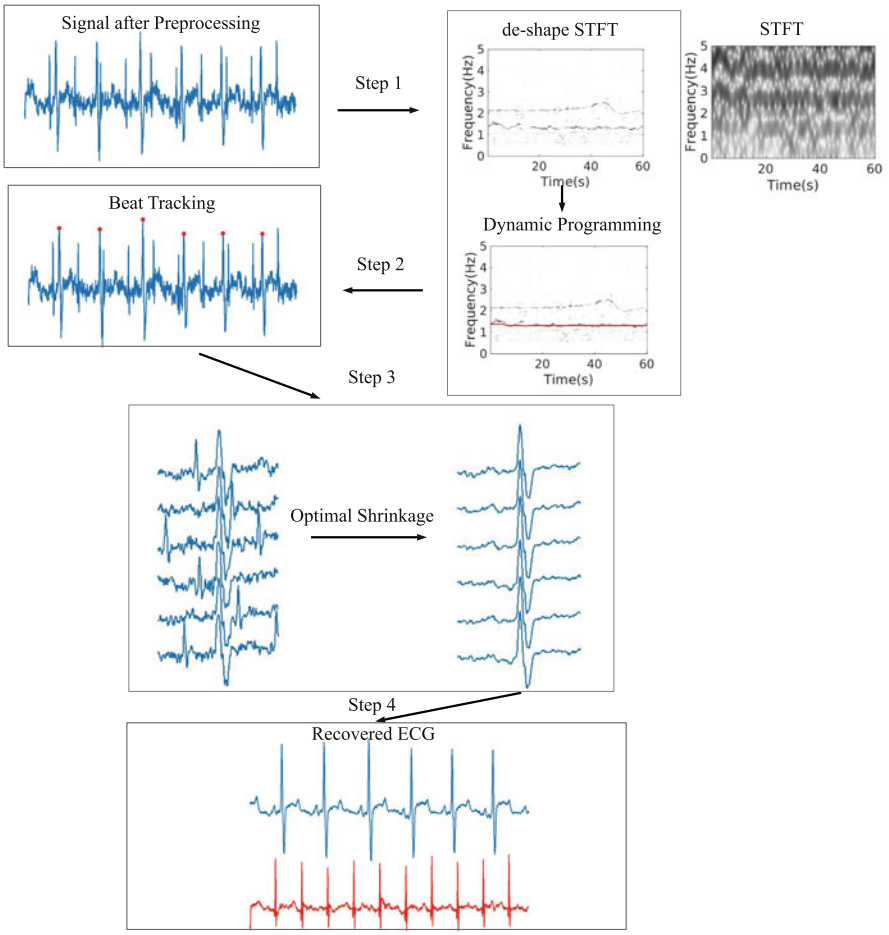

Fig. 2 An illustration of the fECG extraction algorithm. The signal is from the third channel of the fourth subject in CinC2013 [40] database. The explanation of the figure is the same as that of Fig. 1, with the difference that the fECG is stronger so that the fetal R peak heights are comparable with the maternal R peak heights

Before introducing the algorithm, we shall briefly mention the challenge. First, note that it is not always possible to directly apply the traditional peak detection algorithm to determine the maternal R peaks from the ta-mECG, since it is possible that the fetal R peaks have similar heights as those of maternal R peaks (see an example in Fig. 2). On the other hand, in the spectrogram shown in Figs. 1 and 2, we can see a complicated pattern that is caused by the nontrivial nonlinear interaction of mECG and fECG, particularly in Fig. 2, due to the non-sinusoidal nature of the ECG. De-shape STFT is an algorithm that is designed to remove the impact of non-

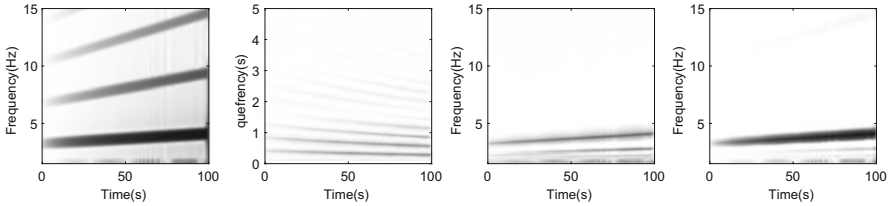

Fig. 3 An illustration of the de-shape STFT algorithm. The input signal is $f(t) = (1 + t^{1.5}/50)y(3.5(t + (t/20)^2))$, where the input t is time in second (s) and the function $y(\cdot)$ is a periodic function such that $y(2k + 1) = 0.5$ and $y(2k) = -0.5$ for $k \in \mathbb{N}$, and for $x \in (k, k + 1)$, $y(x)$ is the linear interpolation between $y(k)$ and $y(k + 1)$. From left to right, the spectrogram, the STCT, the iSTCT and the de-shape STFT

sinusoidal oscillatory patterns in the spectrogram so that we could accurately obtain the IHR.

Fix the frequency resolution of the STFT by $\frac{f_s}{2M}$, where $M \in \mathbb{N}$ is the desired number of discretization points in the frequency axis. The numerical implementation of the de-shape STFT is summarized as the following steps, and please see Fig. 3 for a step-by-step illustration of the algorithm in a simulated signal.

- Take the input data, including the signal $\mathbf{x} \in \mathbb{R}^N$, a discretized window function $\mathbf{h} \in \mathbb{R}^{2k+1}$, where $k \in \mathbb{N}$ is associated with the bandwidth of the window, a sufficiently small $\gamma > 0$, and an upsample factor $\alpha \in \mathbb{N}$.
- Evaluate the STFT of $|\mathbf{x}|$, denoted as $\mathbf{V}_\mathbf{x} \in \mathbb{C}^{N,2M}$, by

$$\mathbf{V}_\mathbf{x}(n, m) = \frac{1}{f_s} \sum_{l=-k}^{k} \mathbf{x}(n + l)\mathbf{h}(l + k + 1)e^{-i\pi n(m-M)/M},$$

  where $m = 1, \ldots, 2M$, and we pad $\mathbf{x}$ by 0 so that $\mathbf{x}(l) = 0$ when $l < 1$ and $l > N$ in the summation.
- Evaluate the short-time cepstrum transform (STCT) of $\mathbf{x}$, denoted as $\mathbf{C}_\mathbf{x} \in \mathbb{C}^{N,2M}$, by

$$\mathbf{C}_\mathbf{x}(n, m') := \frac{f_s}{2M} \sum_{m=1}^{2M} |\mathbf{V}_\mathbf{x}(n, m)|^\gamma e^{-i\pi m'(m-M)/M},$$

  where $m' = 1, \ldots, 2M$. In other words, at each time n, run the Fourier transform of the weighted spectrum $|\mathbf{V}_\mathbf{x}(n, m)|^\gamma$.
- Upsample the positive quefency axis of $\mathbf{C}_\mathbf{x}$ to be α-time finer by the linear interpolation; that is, construct a new matrix $\tilde{\mathbf{C}}_\mathbf{x} \in \mathbb{C}^{N,\alpha M}$, where

$$\tilde{\mathbf{C}}_{\mathbf{x}}(n, m'') := \mathbf{C}_{\mathbf{x}}\left(n, M + \left\lfloor \frac{m''}{\alpha} \right\rfloor - 1\right) + \left(\frac{m''}{\alpha} - \left\lfloor \frac{m''}{\alpha} \right\rfloor\right)\left(\mathbf{C}_{\mathbf{x}}\left(n, M + \left\lfloor \frac{m''}{\alpha} \right\rfloor\right) - \mathbf{C}_{\mathbf{x}}\left(n, M + \left\lfloor \frac{m''}{\alpha} \right\rfloor - 1\right)\right)$$

for all $n = 1, \ldots, N$ and $m'' = 1, \ldots, \alpha M$.

– Evaluate the iSTCT of $\mathbf{x}$, denoted as $\mathbf{U}_{\mathbf{x}} \in \mathbb{C}^{N,M}$, where

$$\mathbf{U}_{\mathbf{x}}(n, m) := \sum_{m'': 1/m'' \in [\lceil m - \frac{1}{2} \rceil, \lceil m + \frac{1}{2} \rceil]} \tilde{\mathbf{C}}_{\mathbf{x}}\left(n, m''\right),$$

where $n = 1, \ldots, N$ and $m = 1, \ldots, M$.

– Evaluate the de-shape STFT of $\mathbf{x}$, denoted as $\mathbf{W}_{\mathbf{x}} \in \mathbb{C}^{N,M}$, by

$$\mathbf{W}_{\mathbf{x}}(n, m) := \mathbf{V}_{\mathbf{x}}(n, m)\mathbf{U}_{\mathbf{x}}(n, m),$$

where $m = 1, \ldots, N$ and $n = 1, \ldots, M$.

– The output is the de-shape STFT of $\mathbf{x}$, $\mathbf{W}_{\mathbf{x}}$.

The Matlab implementation of the above algorithm can be found in `step1_deshape.m`. To call this function, in Matlab, run the following code:

```
W = step1_deshape(x, fs, fr, gamma, alpha, win_len, win_type);
```

where `fs` is the sampling rate f_s, `fr` is the frequency resolution in STFT (in Hz), `gamma` and `alpha` are γ and α, respectively, `win_len` and `win_type` are the window length and the window type of $\mathbf{h}$, respectively, and the output `W` is the discretized time–frequency representation as a matrix $\mathbf{W}_{\mathbf{x}}$. We suggest taking the flattop window with the window length of 5 seconds for $\mathbf{h}$, and frequency resolution as 0.02 Hz such that $M = \lfloor \frac{f_s}{2f_r} \rceil$, $\gamma = 0.3$, and $\alpha = 10$ in the numerical implementation. The above parameter suggestion deserves a discussion. M is chosen to balance in between computational complexity and time–frequency resolution. Note that theoretically it might be beneficial to take $M = N^{3/2}$ [14], but in our application the benefit of taking such a high resolution is marginal. The selection of bandwidth k is under the empirical rule of thumb that the non-negligible part of the window should cover roughly 6–10 cycles, so that the IHR information could be well captured. We shall mention that an automatic selection of the optimal window bandwidth with a theoretical guarantee is so far an open problem.

We shall discuss some details of the algorithm. First of all, note that it is the *full rectification* of $\mathbf{x}$, that is, $|\mathbf{x}|$, that is used to evaluate the STFT but not $\mathbf{x}$. The rectification is useful for the purpose of enhancing the fundamental component of mECG, while its theoretical guarantee, to our knowledge, is still open [42]. To be more specific, note that the QRS complex of the mECG, particularly when R and S have equal weight, could be approximated by the differentiation of a

narrow Gaussian function. Thus, when this approximation holds true, the power spectrum of the mECG would be weak in the low-frequency region, particularly around the fundamental frequency. In the worst case, the fundamental component may not even exist. It is easy to see that the weaker the fundamental component is, the more difficult we could estimate the fundamental frequency of the mECG. We shall mention that other rectification or nonlinear activation functions could be applied to $\mathbf{x}$ before running STFT. The $|\mathbf{V}_{\mathbf{x}}(n,m)|^{\gamma}$ in the STCT is nothing but an approximation of $\log|\mathbf{V}_{\mathbf{x}}(n,m)|$ when γ is small since $\log(x) = \lim_{\gamma\to 0}\frac{x^{\gamma}-1}{\gamma}$ when $x > 0$. Note that taking log is an essential step in the cepstrum analysis. In short, due to the uneven strength of harmonics of a maternal cardiac cycle, we could view the spectrum of a maternal cardiac cycle as a delta chain with a slowly varying envelope. log is used here to convert the slowly varying envelop associated with the amplitude variation of harmonics that comes from the non-sinusoidal oscillation into a low-frequency "trend," so that the Fourier transform of $|\mathbf{V}_{\mathbf{x}}(n,m)|^{\gamma}$ could further emphasize the information of the oscillatory period. See [35] for more information on cepstrum. The upsample factor α is introduced to avoid the low sampling issue when we invert the STCT in iSTCT; that is, when m is small (or large) in $\mathbf{U}_{\mathbf{x}}(n,m)$, the associated tick $1/m$ in $\mathbf{C}_{\mathbf{x}}(n,\cdot)$ would be coarser (finer) than the original frequency tick of $\mathbf{C}_{\mathbf{x}}(n,\cdot)$. Increasing the resolution in the quefrency domain could help this numerical issue. Note that we can implement this step in various alternative ways, like evaluate the STCT with a finer quefrency axis directly, or implement some interpolation during upsampling. We use the current simple minded approach to keep the algorithm easy to process.

It has been reported in [29] that the IHR of the mECG and fECG is represented as dominant curves in the time–frequency representation (TFR) determined by the de-shape STFT. This allows us to extract the salient IHR information of each oscillatory component [29], where we could apply dynamic programming (DP), dynamic Bayesian networks, adaptive filters, and others. To balance between the accuracy and computational time, we apply the DP curve extraction algorithm [6] to track the most dominant curve in the TFR $\mathbf{W}_{\mathbf{x}}$. The extracted curve, when adjusted with the frequency resolution, denoted as $\eta_1 \in \mathbb{R}^N$, represents the IHR of either mECG or fECG. To be more precise, suppose the most dominant component at time n is located at $\mathbf{W}_{\mathbf{x}}(n, j_n)$, then $\eta_1(n) = \frac{j_n f_s}{2M}$. We could repeat this process after masking out a band from $0.94\eta_1$ to $1.06\eta_1$ around η_1 inside $\mathbf{W}_{\mathbf{x}}$ and carry out the same DP algorithm to extract another curve, denoted as η_2. Note that 0.94 and 1.06 are chosen for the band to guarantee that the impact of the most dominant curve is eliminated. This simple algorithm guarantees that η_1 is the maternal IHR (mIHR), denoted as η_m under the assumption that the mECG is strong than the fECG, but when the fECG is stronger, η_1 is the fetal IHR (fIHR). To avoid the case that fECG is stronger than mECG, we compare the mean of η_1 and η_2 and assign the slower IHR to be the mIHR. See Figs. 1 and 2 for an illustration of the extracted mIHR. The Matlab implementation can be found in `step1_IHR.m`. To call this function, in Matlab, run the following code:

```
eta = step1_IHR(W, fr);
```

where the inputs are the time–frequency representation `W` and the frequency resolution `fr` and the output `eta` is the estimated mIHR η_m.

2.3.1 Step 2: Obtain the Maternal R Peaks by the Beat Tracking Algorithm

Note that the IHR is directly related to the R peak to R peak interval (RRI) time series, but they are different. To obtain the exact R peak location, we leverage the extracted mIHR η_m and apply the beat tracking technique from the music signal analysis proposed in [43].

Denote the maternal instantaneous heart beat period as $\delta_m(n) := 1/\eta_m(n)$, which is the inverse of the mIHR. Our goal is to find a strictly increasing sequence $\mathbf{R}^{(m)} = \{R^{(m)}(i)\}_{i=1}^{n^{(m)}}$, where $n^{(m)} \in \mathbb{N}$ is the number of heart beats, $1 \leq R^{(m)}(i) \leq N$ so that $R^{(m)}(i)$ is the index of i-th maternal R peak position and $(R^{(m)}(i) - R^{(m)}(i-1))/f_s$ is close to the maternal instantaneous heart beat period at time $R^{(m)}(i)/f_s$, $\delta_m(R^{(m)}(i))$. We call $R^{(m)}$ the *maternal beat sequence*. This problem can be formulated as the following optimization problem [12]:

$$\widetilde{\mathbf{R}}^{(m)} = \underset{\mathbf{R}^{(m)}}{\operatorname{argmax}} \Big[\sum_{i=1}^{n^{(m)}} \mathbf{x}(R^{(m)}(i)) + \lambda_{\mathtt{BT}} \sum_{i=2}^{n^{(m)}} P(R^{(m)}(i), R^{(m)}(i-1)) \Big], \tag{1}$$

where $P(R^{(m)}(i), R^{(m)}(i-1)) := -\left(\log_2\left(\frac{(R^{(m)}(i)-R^{(m)}(i-1))/f_s}{\delta_m(R^{(m)}(i))}\right)\right)^2$ and $\lambda_{\mathtt{BT}} \geq 0$ is the penalty term determined by the user. Here, $P(R^{(m)}(i), R^{(m)}(i-1))$ measures how different the maternal heart period determined by the detected maternal R peak and the maternal instantaneous heart beat period, $\delta_m(n)$ are, with the maximal value zero. Clearly, if they are close, then $\frac{(R^{(m)}(i)-R^{(m)}(i-1))/f_s}{\delta_m(R^{(m)}(i))} \approx 1$, and $P(R^{(m)}(i), R^{(m)}(i-1))$ is small. Thus, $\lambda_{\mathtt{BT}}$ is chosen to balance the amplitude of the detected maternal R peaks quantified in the first term and the estimated maternal RRI. Note that the first term in the objective function in (1) reaches its maximal value when $R^{(m)}(i)$ matches the true maternal R peak location.

The optimization problem (1) can be efficiently solved effectively by the DP. The main idea is that the objective function (1) is an accumulation in time. We could thus divide the problem into a set of subproblems, each of which optimizes the objective function up to a prescribed time step, and the solution is the combination of these optima at every time step. This idea is implemented by introducing two additional vectors, $\mathbf{C} \in \mathbb{R}^N$ and $\mathbf{D} \in \mathbb{R}^N$, where $\mathbf{C}(n)$ records the maximum of the objective function accumulated from 1 to n, where $n = 1, \ldots, N$, and $\mathbf{D}(n)$ records the estimated beat position yielding this maximum at the time step of $n-1$. Here, $\mathbf{D}$ allows us to trace previous beat positions, and this step is called the *backtracking*. The whole procedure is sketched in Algorithm 1.

Algorithm 1 Beat tracking by dynamic programming

[INPUT] the ECG signal $\mathbf{x} \in \mathbb{R}^N$; the instant heart rate η_m; an weighted parameter ; $\lambda_{\mathtt{BT}}$; the penalty function $P : \mathbb{N} \times \mathbb{N} \to \mathbb{R}$
[STEP 2-1] Initialize $\mathbf{C}(0) = 0, \mathbf{D}(0) = 0$
[STEP 2-2] Accumulate the objective function and store the result
for $i = 1$ **to** N **do**
  $\mathbf{C}(n) = \mathbf{x}(n) + \max_{m=1,\ldots,n-1}[\mathbf{C}(m) + \lambda_{\mathtt{BT}} P(n, m)]$;
  $\mathbf{D}(n) = \operatorname{argmax}_{m=1,\ldots,n-1}[\mathbf{C}(m) + \lambda_{\mathtt{BT}} P(n, m)]$;
end for
[STEP 2-3] Backtracking
$a_1 = \operatorname{argmax}_n \mathbf{C}(n)$;
while $\mathbf{D}(a_l) > 0$ **do**
  $l \leftarrow l + 1$; $a_l = \mathbf{D}(a_{l-1})$;
end while
[OUTPUT] the optimal beat sequence $\widetilde{\mathbf{R}}^{(m)} = \{\widetilde{R}^{(m)}(j)\}_{j=1}^{n^{(m)}}$, where $\mathbf{R}^{(m)}(j) = a_{n^{(m)}-j+1}$.

The resulting beat sequence $\widetilde{\mathbf{R}}^{(m)} = \{\widetilde{R}^{(m)}(i)\}_{i=1}^{n^{(m)}}$ provides an estimate of R peaks location; that is, $\widetilde{R}^{(m)}(i)$ is an estimate of the i-th R peak location. See Fig. 1 for an illustration of the result. In our experiments, setting $\lambda_{\mathtt{BT}}$ between 20 and 50 turns out to yield a suitable tradeoff, and the result is not sensitive to $\lambda_{\mathtt{BT}}$. See the Matlab implementation of this algorithm for the fECG extraction application in `step2_Rpeaks.m`. To call this function, in Matlab, run the following code:

```
Rm = step2_Rpeaks(x, eta, fs, fr, lambdaBT);
```

where `lambdaBT` in the input is the penalization $\lambda_{\mathtt{BT}}$ in (1), and the output `Rm` is the maternal R peak locations $\widetilde{R}^{(m)}$ of $\mathbf{x}$. More information of this beat tracking algorithm can be found in http://labrosa.ee.columbia.edu/projects/beattrack/.

2.4 Step 3: Estimate Maternal Cardiac Cycles by Optimal Shrinkage

Once we get maternal R peaks, we are ready to decompose mECG and fECG from the ta-mECG. Recall the challenges (C1) and (C2). Due to these limitations, we need the TS-based approach. However, due to the challenge (C3), we found that the traditional template subtraction (TS) approach might be limited. We thus consider the following optimal shrinkage (OS) algorithm, which is a nonlinear version of the common singular value decomposition (SVD)-based denoising algorithm. The algorithm is composed of two steps—truncate the ta-mECG into pieces and run the singular value decomposition to recover the mECG.

First, we truncate the ta-mECG into maternal cardiac cycles according to the maternal R peaks, align these truncated pieces by the maternal R peaks, and put these pieces into columns of a data matrix $\tilde{S} \in \mathbb{R}^{p \times n}$, where p is the number of

samples of each truncated maternal cardiac cycle, and n is the number of truncated maternal cardiac cycles. Under the mild assumption that the fetal heart beat does not synchronize with maternal heartbeat, the fetal cardiac cycles would happen irregularly in the truncated maternal cardiac cycle. See Fig. 1 for an illustration. This step also happens in the traditional TS algorithm. We could then model the truncated maternal cardiac cycles as a signal-plus-noise data matrix, where the signal part, denoted as S, is the maternal cardiac cycles, and the noise part, denoted as Z, is the fetal cardiac cycles and other inevitable noise; that is, we have $\tilde{S} = S + Z$. The goal is "denoising" this noisy data matrix $\tilde{S}$ and recovering S. If we could successfully denoise the noisy data matrix, we recover the maternal cardiac cycles and hence the mECG. To achieve this goal, we apply the SVD denoise but respect the fact that singular vectors and singular values of $\tilde{S}$ are both biased estimators of singular vectors and singular values of S when p and n are of the same order. When p and n are of the same order, we say that the data is contaminated by a *high-dimensional noise* (or we face a *large p and large n* problem). This denoise scheme is called OS. This step is usually not considered in the traditional TS approach. Below, we detail these steps under a relatively simple assumption and discuss possible variations later. We refer the readers to the Matlab code `step3_OS.m` for an implementation. To call this function, in Matlab, run the following code:

$$\texttt{Sphi} = \texttt{step3\_OS}(\texttt{x}, \texttt{Rm}, \texttt{loss});$$

where the input `loss` is the type of norm used in the loss function for OS, including the Frobenius, operator, and nuclear norm, and the output `Sphi` is the matrix of denoised maternal cardiac activities $\widehat{S}_{\widehat{\varphi}}$ shown below in (14). We recommend using the Frobenius norm as the loss. The detailed steps are in the following.

- **Construct a data matrix of mECG templates.** Fix the i-th maternal cardiac cycle determined by the i-th R peak. Denote $w \in \mathbb{N}$ to be the rounding number of the 95% quantile of R to R intervals of $\mathbf{x}$. Denote the corresponding ECG segment over the cardiac cycle as

$$\widetilde{\mathbf{s}}_i^{(m)} := \left[\mathbf{x}\left(R^{(m)}(i) - \lceil c_1 w \rceil\right), \ldots, \mathbf{x}\left(R^{(m)}(i) + \lceil c_2 w \rceil\right)\right]^\top \in \mathbb{R}^{p^{(m)}}, \tag{2}$$

  where $c_1, c_2 > 0$ are parameters chosen by the user, $\lceil x \rceil$ is the smallest integer larger than $x > 0$, and $p^{(m)} := \lceil c_1 w \rceil + \lceil c_2 w \rceil + 1$. Based on the physiological knowledge of PR and QT durations, we suggest setting $c_1 = 3/8$ and $c_2 = 5/8$ so that the whole maternal cardiac cycle, including P, QRS, and T waveforms, is covered. Collect all truncated templates in a set $\mathscr{L}^{(m)} := \{\widetilde{\mathbf{s}}_i^{(m)}\}_{i=1}^{n^{(m)}}$, where $n^{(m)}$ is the number of truncated templates. Construct a data matrix $\widetilde{S}$ of size $p^{(m)} \times n^{(m)}$ consisting of all segments of $\mathscr{L}^{(m)}$ in the columns; that is,

$$\widetilde{S} = \left[\widetilde{\mathbf{s}}_1^{(m)} \ \ldots \ \widetilde{\mathbf{s}}_{n^{(m)}}^{(m)}\right] \in \mathbb{R}^{p^{(m)} \times n^{(m)}}. \tag{3}$$

- **Remove nuisance variables by optimal shrinkage**. To obtain maternal cardiac cycles, we need to reduce the influence of the fECG and noises from $\widetilde{S}$. Based on the low-rank assumption of the clean data matrix associated with mECG, we apply the optimal shrinkage (OS) method. Below, to simplify the notation, we remove the superscript $^{(m)}$ from $p^{(m)}$ and $n^{(m)}$. Suppose $\beta = \frac{p}{n} \leq 1$. If not, transpose $\tilde{S}$ and run the following algorithm. The OS is applied as follows:
  - Denote the SVD of the data matrix $\widetilde{S}$ as

$$\widetilde{S} = \sum_{i=1}^{p} \sqrt{\widetilde{\lambda}_i}\widetilde{\boldsymbol{\xi}}_i\widetilde{\boldsymbol{\zeta}}_i^{\top}, \tag{4}$$

    where $\widetilde{\lambda}_1 \geq \widetilde{\lambda}_2 \geq \cdots \geq \widetilde{\lambda}_{\min\{p,n\}} \geq 0$ are common eigenvalues of $\widetilde{S}\widetilde{S}^{\top}$, and $\widetilde{\boldsymbol{\xi}}_i$ and $\widetilde{\boldsymbol{\zeta}}_i$ are the i-th left and right singular vectors corresponding to the singular value $\tilde{\lambda}_i$.
  - (estimate the rank associated with the maternal cardiac cycle as signal) Compute

$$\widehat{\lambda}_+ := \widetilde{\lambda}_{n^c+1} + \frac{1}{2^{2/3}-1}\left(\widetilde{\lambda}_{n^c+1} - \widetilde{\lambda}_{2n^c+1}\right), \tag{5}$$

    where $c > 0$ is a fixed small constant. In our application, we recommend choosing $c = 1/2$. Then, compute

$$\widehat{r}^{+} = \left|\{\widetilde{\lambda}_i | \widetilde{\lambda}_i > \widehat{\lambda}_+ + n^{-1/3}\}\right|. \tag{6}$$

  - (Impute the missing singular values associated with fECG as noise) Fix $k = 2\widehat{r}^{+}$. Compute

$$\widehat{\lambda}_j := \widetilde{\lambda}_{k+r^+ +1} + \frac{1-\left(\frac{j-1}{k}\right)^{2/3}}{2^{2/3}-1}\left(\widetilde{\lambda}_{k+r^+ +1} - \widetilde{\lambda}_{2k+r^+ +1}\right), \quad \text{for } j = 1, \ldots, k. \tag{7}$$

  - (Reconstruct the singular value spectrum associated with fECG as noise) Compute

$$F_{imp}(x) := \frac{1}{p}\sum_{j=k+1}^{p} \mathbf{1}(\widetilde{\lambda}_j \leq x) + \frac{1}{p}\sum_{j=1}^{k} \mathbf{1}(\widehat{\lambda}_j \leq x), \tag{8}$$

  - (Prepare for the OS) For $1 \leq i \leq \widehat{r}^{+}$, compute

$$\widehat{m}_{1,i} :== \int \frac{dF_{imp}(x)}{x - \widetilde{\lambda}_i} = \frac{1}{p}\left(\sum_{j=1}^{k} \frac{1}{\widehat{\lambda}_j - \widetilde{\lambda}_i} + \sum_{j=k+1}^{p} \frac{1}{\widetilde{\lambda}_j - \widetilde{\lambda}_i}\right),$$

$$\widehat{m}_{2,i} := \frac{1-\beta}{\widetilde{\lambda}_i} + \beta \widehat{m}_1(\widetilde{\lambda}_i). \tag{9}$$

$$\widehat{m}'_{1,i} = \frac{1}{p}\left(\sum_{j=1}^{k} \frac{1}{(\widehat{\lambda}_j - \widetilde{\lambda}_i)^2} + \sum_{j=k+1}^{p} \frac{1}{(\widetilde{\lambda}_j - \widetilde{\lambda}_i)^2}\right), \ \widehat{m}'_{2,i} = \frac{1-\beta}{\widetilde{\lambda}_i^2} + \beta \widehat{m}'_{1,i}. \tag{10}$$

$$\widehat{\mathscr{T}}_i = \widetilde{\lambda}_i \widehat{m}_{1,i} \widehat{m}_{2,i}, \quad \widehat{\mathscr{T}}'_i = \widehat{m}_{1,i} \widehat{m}_{2,i} + \widetilde{\lambda}_i \widehat{m}'_{1,i} \widehat{m}_{2,i} + \widetilde{\lambda}_i \widehat{m}'_{2,i} \widehat{m}_{1,i}, \tag{11}$$

$$\widehat{d}_i = \sqrt{\frac{1}{\widehat{\mathscr{T}}_i}}, \quad \widehat{a}_{1,i} = \frac{\widehat{m}_{1,i}}{\widehat{d}_i^2 \widehat{\mathscr{T}}'_i}, \text{ and } \widehat{a}_{2,i} = \frac{\widehat{m}_{2,i}}{\widehat{d}_i^2 \widehat{\mathscr{T}}'_i}. \tag{12}$$

– (Reconstruct singular values associated with maternal cardiac cycles as signal) For $1 \le i \le \widehat{r}^+$, the estimator of the optimal shrinkers is

$$\widetilde{\varphi}_i = \widehat{d}_i \sqrt{\widehat{a}_{1,i} \widehat{a}_{2,i}}, \tag{13}$$

and $\widetilde{\varphi}_i = 0$ otherwise.

– The OS estimator of the clean data matrix, S, is denoted as

$$\widehat{S}_{\widehat{\varphi}} = \sum_{i=1}^{\widehat{r}^+} \widetilde{\varphi}_i \widetilde{\boldsymbol{\xi}}_i \widetilde{\boldsymbol{\zeta}}_i^\top. \tag{14}$$

We shall discuss this seemingly complicated OS algorithm. First, since the maternal cardiac cycles are in general similar, once they are aligned according to the maternal R peaks, we could assume that the *inaccessible* clean data matrix S is of low rank to simplify the discussion in the following algorithm; that is, we have

$$\widetilde{S} = S + Z = \sum_{i=1}^{r} \varphi_i \boldsymbol{\xi}_i \boldsymbol{\zeta}_i^\top + Z \in \mathbb{R}^{p \times n}, \tag{15}$$

where $\sum_{i=1}^{r} \varphi_i \boldsymbol{\xi}_i \boldsymbol{\zeta}_i^\top$ is the singular value decomposition (SVD) of S, $r \ge 1$ is assumed to be small compared with p and n, $\boldsymbol{\xi}_i \in \mathbb{R}^p$ and $\boldsymbol{\zeta}_i \in \mathbb{R}^n$ are left and right singular vectors, and $\varphi_i > 0$ are the associated singular values. Note that the noise matrix Z, as described above, comes from the fECG and the assumption that fetal heart beats do not synchronize with maternal heart beats. It is clear that Z as noise is structured. In [46], we model such noise by

$$Z = A^{1/2} X B^{1/2}, \tag{16}$$

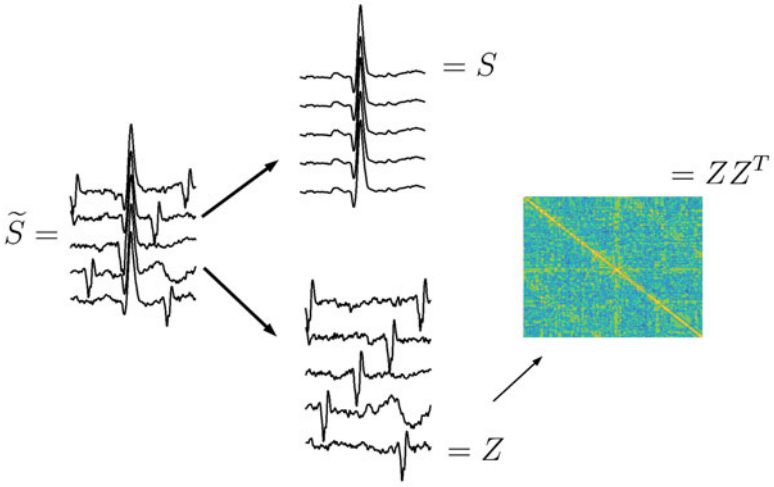

Fig. 4 An illustration of the model (16) by decomposing ta-mECG into mECG and fECG and the covariance structure of the fECG as noise

where the entries of X are i.i.d. with zero mean and mild moment conditions, and A and B are, respectively, $p \times p$ and $n \times n$ deterministic positive-definite matrices that describe the colorness and dependence of noise, respectively. Z is said to satisfy the *separable covariance* structure [37]. See Fig. 4 for an illustration of this model, where the nontrivial covariance structure of Z is shown.

Under the low-rank model (16), the main challenge of directly applying the SVD denoise algorithm to our problem could be summarized into two parts. First, the rank r is in general unknown. Second, when p and n are proportional, it has been well known from the random matrix theory that $\widetilde{\varphi}_i$, $\widetilde{\boldsymbol{\xi}}_i$, and $\widetilde{\boldsymbol{\zeta}}_i$ are biased estimators of φ_i, $\boldsymbol{\xi}_i$, and $\boldsymbol{\zeta}_i$, respectively. OS is a generalization of the well-known Stein—James shrinkage aiming to handle such biases. The basic idea is by fixing a loss function, and we find a proper nonlinear shrinkage function to trim the biased singular values so that the matrix S is optimally recovered. In (13), the Frobenieus norm is considered in the loss function. The idea of OS under very general noise model was first established in [34] under strong assumptions, including the knowledge of r and a technical "delocalization" property of singular vectors, and only the Frobenieus norm was considered. The algorithm is called *OptShrink*. The above OS algorithm was first proposed in [46], where the rank estimator, $\widehat{r}^{+}$ in (6), was designed based on a theoretical study of the spectral behavior of $\widetilde{S}$, and the OptShrink was generalized to various norms. We refer the readers with interest in technical details to [46].

We shall mention that in the previous published work [44], A and B are assumed to be the identity matrices. In that case, the OS has a precise closed form that was derived in [11, 41].

2.5 Step 4: Maternal ECG Recovery

The columns of $\widehat{S}_{\widehat{\varphi}}$ are the estimated maternal cardiac cycles, denoted as $\widehat{\mathbf{s}}_i^{(m)}$, where $i = 1, \ldots, n^{(m)}$. After obtaining all estimated maternal cardiac cycles, we reconstruct the estimated mECG signal from $\left\{\widehat{\mathbf{s}}_i^{(m)}\right\}_{i=1}^{n^{(m)}}$ by the standard stitching approach [43]. Denote the estimated mECG from $\mathbf{x}$ as $\widehat{\mathbf{x}}^m$. This step is implemented in the code `step4_stitch`.m. In Matlab, run the following code:

```
xm = step4_stitch(Sphi, x, Rm);
```

where the output `xm` is the estimated mECG $\widehat{\mathbf{x}}^m$.

2.6 Step 5: Obtain the fECG

For $\mathbf{x}$ with the estimated mECG $\widehat{\mathbf{x}}^m$, we obtain the *rough fECG* by a simple subtraction:

$$\mathbf{x}^{rf} = \mathbf{x} - \widehat{\mathbf{x}}^m. \tag{17}$$

We repeat Step 1 on $\mathbf{x}^{rf}$ to acquire the fetal heart beat locations. Denote the total number of detected fetal R peaks in $\mathbf{x}^{rf}$ by $n^{(f)}$. Then, repeat Step 3 to obtain a set of denoised fetal cardiac cycles, denoted as $\widetilde{\mathscr{L}}^{(f)} := \{\widetilde{\mathbf{s}}_i^{(f)}\}_{i=1}^{n^{(f)}}$, where $\widetilde{\mathbf{s}}_i^{(f)}$ is the i-th denoised fetal cardiac cycle. Reconstruct the fECG signal $\widetilde{\mathbf{x}}^f$ from $\widetilde{\mathscr{L}}^{(f)}$ by the standard stitching approach [43]. This step is implemented in the code `step5_fECG`.m. In Matlab, run the following code:

```
xf = step5_fECG(x, xm, fs, fr, gamma, alpha, ...
        win_len, win_type, lambdaBT, loss, eta);
```

where the output `xf` is the extracted fECG $\widetilde{\mathbf{x}}^f$.

2.7 Step 6: Enhance the mECG and rfECG by Iteration

We could enhance the whole process by iterating Steps 1–5. First, improve the mECG estimation by repeating Steps 1–4 on $\widetilde{\mathbf{x}}^{rm} := \mathbf{x} - \widetilde{\mathbf{x}}^f$. Note that the fECG component is now suppressed in $\widetilde{\mathbf{x}}^{rm}$. We could then recover the mECG, denoted as, by abusing the notation, $\widehat{\mathbf{x}}^m$, and hence the rough fECG, denoted as, by again

abusing the notation, $\mathbf{x}^{rf}$. Finally, we repeat Step 5 on $\mathbf{x}^{rf}$ to acquire the fetal heart beat locations and repeat Step 3 on $\mathbf{x}^{rf}$ to obtain our proposed estimator of the fECG, denoted as $\widehat{\mathbf{x}}^{f}$. In practice, we found that applying this iteration once helps the overall performance, but the benefit quickly becomes marginal after that. See `step6_fECG.m` for an implementation of this iteration step. In Matlab, run the following code:

```
[xm, xf, Rm, Rf] = step6_fECG(x, xf, fs, fr, gamma, ...
                    alpha, win_len, win_type, lambdaBT, loss);
```

where `Rm` and `Rf` are the final estimated maternal and fetal R peak locations after the iteration.

2.8 (Optional) Step 7: Enhance the fECG Signal by the Nonlocal Median

When the fetus is normal sinus rhythmic, we may further improve the fECG morphology by applying the nonlocal median. Denote $\widehat{\mathscr{L}}^{(f)} := \{\widehat{\mathbf{s}}_i^{(f)}\}_{i=1}^{n^{(f)}}$ to be the set of fetal cardiac cycles in $\widehat{\mathbf{x}}^{f}$. Take $k_m \in \mathbb{N}$, and denote $\mathscr{N}_i = \{\widehat{\mathbf{s}}_{i_\ell}^{(f)}\}_{\ell=1}^{k_m}$ to be those $\widehat{\mathbf{s}}_{i_\ell}^{(f)} \in \widehat{\mathscr{L}}^{(f)}$ that have the most similar R–R intervals compared with that of $\widehat{\mathbf{s}}_i^{(f)}$. With $\mathscr{N}_i$, we take the entry-wise median of these segments as the estimation of corresponding fetal P-QRS-T waveform; that is, the i-th fetal P-QRS-T waveform in $\mathbf{z}$ is estimated by

$$\widehat{\mathbf{s}}_i^{(cf)} := \text{median}\{\widehat{\mathbf{s}}_i^{(f)}, \widehat{\mathbf{s}}_{i_1}^{(f)}, \ldots, \widehat{\mathbf{s}}_{i_{k_m}}^{(f)}\}. \tag{18}$$

Since the median filter is not applied to consecutive cycles, it is called the nonlocal median filter. The nonlocal median filtered fECG is determined by stitching $\{\widehat{\mathbf{s}}_i^{(cf)}\}_{i=1}^{n^{(f)}}$. See `step7_nonlocalmedian.m` for an implementation of this nonlocal median filter. In Matlab, run the following code:

```
xcf = step7_nonlocalmedian(xf, Rf, km);
```

where `km` in the input is the number of nearest neighbors the user choose and the output `xcf` is the enhanced fECG $\widehat{\mathbf{x}}^{cf}$. We suggest setting `km` $= 10$ when applying the code.

3 Extensions and Other Considerations

Among many possible extensions and considerations of the proposed algorithm and fECG extraction problem, we discuss three of them below.

3.1 Signal Quality

Signal quality is a big concern in any biomedical signal processing tasks, and fECG extraction is not an exception. We could, for example, when we run the algorithm, apply the bSQI [16] to determine the signal quality index (SQI) of the input ta-mECG or the obtained rough fECG. Those segments with low SQI could be abandoned in the following analysis or handled separately.

3.2 Manifold Model

In the OS step, we made an assumption that the clean data matrix associated with the maternal cardiac cycles is low rank. This assumption might not hold if the signal gets longer. See Fig. 5 for a visualization of 5000 maternal cardiac cycles by PCA. We could see a clear nonlinear structure inside. From the mathematical perspective, we could model these cycles by parametrizing them by a low-dimensional manifold M embedded in a high-dimensional Euclidean space [30]; that is, S is sampled from M. The noisy data matrix $\widetilde{S}$ is thus a noisy set of sampled from M. Suppose we assume that the maternal cardiac cycles do not vary too much over a short time, we could safely assume the low-rank structure, but we need to handle the high-dimensional noise issue mentioned in Sect. 2.4. Mathematically, it means that over a short time, the maternal cardiac cycles live in a small geodesic ball so that the low-rank assumption holds. On the other hand, when the signal length increases, the variability of maternal cardiac cycles increases and the rank increases, which breaks the low-rank structure, but the high-dimensional noise issue is relieved. When the low-rank structure is broken, we need a different denoise strategy. That is the one reason we suggest considering ta-mECG signal of length around 300 second or shorter in Sect. 2.1. From the perspective of manifold model, the proposed algorithm could be viewed as a manifold denoise algorithm. A systematic treatment of this problem with theoretical supports will be reported in our future work.

3.3 Multiple Channels

In general, if we have many ta-mECG channels, we could apply ICA-based algorithms. But when we have only 2 or 3 channels, it is a bit embarrassing to decide what to apply. A solution is provided in [27, 44] based on the dipole current

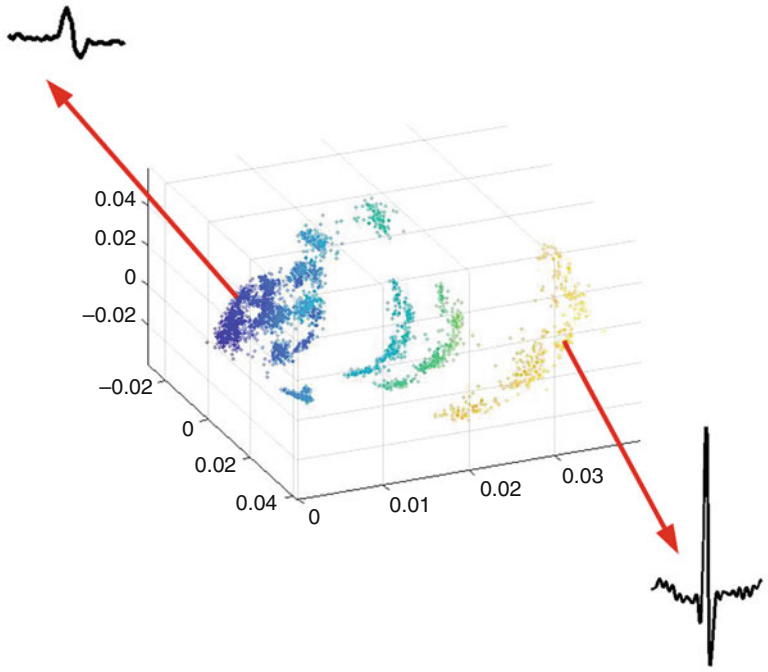

Fig. 5 An illustration of the manifold of cardiac activities from 5000 maternal cardiac activities from CinC2013 database [40]. From blue to yellow, the data points have smaller to larger R peak amplitude. Locally, cardiac activities with similar R peak amplitude form a low-dimensional manifold

model for ECG [20]. The idea is simple. Among all possible linear combinations of available channels, we choose the combination that has the strongest fECG so that we could successfully apply the proposed single-channel algorithm. We refer the readers with interest and need to [27, 44] for details.

References

1. S. Alagapan, H.W. Shin, F. Fröhlich, H.-T. Wu, Diffusion geometry approach to efficiently remove electrical stimulation artifacts in intracranial electroencephalography. J. Neural Eng. **16**(3), 036010 (2019)
2. R. Almeida, H. Gonçalves, J. Bernardes, A.P. Rocha, Fetal QRS detection and heart rate estimation: a wavelet-based approach. Physiol. Meas. **35**(8), 1723–1735 (2014)
3. F. Andreotti, J. Behar, S. Zaunseder, J. Oster, G.D. Clifford, An open-source framework for stress-testing non-invasive foetal ECG extraction algorithms. Physiol. Measur. **37**(5), 627 (2016)
4. E. Castillo, D.P. Morales, G. Botella, A. Garcia, L. Parrilla, A.J. Palma, Efficient wavelet-based ECG processing for single-lead FHR extraction. Digital Signal Process. **23**(6), 1897–1909 (2013)

5. S. Cerutti, G.B. Baselli, S. Civardi, E. Ferrazzi, A.M. Marconi, M. Pagani, G. Pardi, Variability analysis of fetal heart rate signals as obtained from abdominal electrocardiographic recordings. J. Perinat. Med. **14**(6), 445–452 (1986)
6. Y.-C. Chen, M.-Y. Cheng, H.-T. Wu, Non-parametric and adaptive modelling of dynamic periodicity and trend with heteroscedastic and dependent errors. J. R. Stat. Soc. B (Stat. Methodol.) **76**(3), 651–682 (2014)
7. N.-T. Chiu, S. Huwiler, M.L. Ferster, W. Karlen, H.-T. Wu, C. Lustenberger, Get rid of the beat in mobile eeg applications: a framework towards automated cardiogenic artifact detection and removal in single-channel eeg. Biomed. Signal Process Control **72**, 103220 (2022)
8. I. Christov, I. Simova, R. Abächerli, Extraction of the fetal ECG in noninvasive recordings by signal decompositions. Physiol. Meas. **35**, 1713–1721 (2014)
9. A.A. Damen, J. Van Der Kam, The use of the singular value decomposition in electrocardiography. Med. Biol. Eng. Comput. **20**(4), 473–482 (1982)
10. I. Daubechies, J. Lu, H.-T. Wu, Synchrosqueezed wavelet transforms: an empirical mode decomposition-like tool. Appl. Comput. Harmonic Anal. **30**, 243–261 (2011)
11. D.L. Donoho, M. Gavish, I.M. Johnstone, Optimal shrinkage of eigenvalues in the spiked covariance model. Ann. Stat. **46**(4), 1742 (2018)
12. D.P.W. Ellis, Beat tracking by dynamic programming. J. New Music Res. **36**(1), 51–60 (2007)
13. M. Gavish, D.L. Donoho, Optimal shrinkage of singular values. IEEE Trans. Inf. Theory **63**(4), 2137–2152 (2017)
14. M.G. Genton, P. Hall, Statistical inference for evolving periodic functions. J. R. Stat. Soc. B (Stat. Methodol.) **69**(4), 643–657 (2007)
15. W. Huang, M. Bulut, R. van Lieshout, K. Dellimore, Exploration of using a pressure sensitive mat for respiration rate and heart rate estimation, in *2021 43rd Annual International Conference of the IEEE Engineering in Medicine & Biology Society (EMBC)* (IEEE, 2021), pp. 298–301
16. A.E.W. Johnson, J. Behar, F. Andreotti, G.D. Clifford, J. Oster, Multimodal heart beat detection using signal quality indices. Physiol. Measur. **36**(8), 1665 (2015)
17. P.P. Kanjilal, S. Palit, G. Saha, Fetal ECG extraction from single-channel maternal ECG using singular value decomposition. **44**(1), 51–59 (1997)
18. E.C. Karvounis, M.G. Tsipouras, Detection of fetal heart rate through 3-d phase recordings. IEEE Trans. Biomed. Eng. **56**(5), 1394–1406 (2009)
19. E.C. Karvounis, M.G. Tsipouras, D.I. Fotiadis, K.K. Naka, An automated methodology for fetal heart rate extraction from the abdominal electrocardiogram. IEEE Trans. Inf. Technol. Biomed. **11**(6), 628–638 (2007)
20. J. Keener, *Mathematical Physiology* (Springer, New York, 1998)
21. A.H. Khamene, S. Negahdaripoure, A new method for the extraction of fetal ECG from the composite abdominal signal. IEEE Trans. Biomed. Eng. **47**(4), 507–516 (2000)
22. M. Kotas, J. Jezewski, A. Matonia, T. Kupka, Towards noise immune detection of fetal QRS complexes. Comput. Methods Programs Biomed. **97**(3), 241–256 (2010)
23. P. Laguna, L. Sörnmo, Sampling rate and the estimation of ensemble variability for repetitive signals. Med. Biol. Eng. Comput. **38**(5), 540–546 (2000)
24. G. Lamesgin, Y. Kassaw, D. Assefa, Extraction of fetal ECG from abdominal ECG and heart rate variability analysis. Adv. Intell. Syst. Comput. **334**, 147–161 (2015)
25. K. Lee, B. Lee, Sequential total variation denoising for the extraction of fetal ECG from single-channel maternal abdominal ECG. Sensors **16**(7), 1020 (2016)
26. F. Li, W. Song, C. Li, A. Yang, Non-harmonic analysis based instantaneous heart rate estimation from photoplethysmography, in *ICASSP 2019–2019 IEEE International Conference on Acoustics, Speech and Signal Processing (ICASSP)* (IEEE, 2019), pp. 1279–1283
27. R. Li, M.G. Frasch, H.-T. Wu, Efficient fetal-maternal ECG signal separation from two channel maternal abdominal ECG via diffusion-based channel selection. Front. Physiol. **8**, 277 (2017)
28. C.-Y. Lin, L. Su, H.-T. Wu, Wave-shape function analysis – when cepstrum meets time–frequency analysis. J. Fourier Anal. Appl. **24**(2), 451–505 (2018)

29. C.-Y. Lin, L. Su, H.-T. Wu, Wave-shape function analysis. J. Fourier Anal. Appl. **24**(2), 451–505 (2018)
30. Y.-T. Lin, J. Malik, H.-T. Wu, Wave-shape oscillatory model for biomedical time series with applications. Preprint (2019). arXiv:1907.00502
31. T.-C. Liu, Y.-W. Liu, H.-T. Wu, Denoising click-evoked otoacoustic emission signals by optimal shrinkage. J. Acoust. Soc. Am. **149**(4), 2659–2670 (2021)
32. A.K. Maity, A. Veeraraghavan, A. Sabharwal, Ppgmotion: model-based detection of motion artifacts in photoplethysmography signals. Biomed. Signal Process. Control **75**, 103632 (2022)
33. S.M.M. Martens, C. Rabotti, M. Mischi, R.J. Sluijter, A robust fetal ECG detection method for abdominal recordings. Physiol. Meas. **28**, 373–388 (2007)
34. R.R. Nadakuditi, Optshrink: an algorithm for improved low-rank signal matrix denoising by optimal, data-driven singular value shrinkage. IEEE Trans. Inform. Theory **60**(5), 3002–3018 (2014)
35. A.V. Oppenheim, R.W. Schafer, From frequency to quefrency: a history of the cepstrum. IEEE Signal Process. Mag. **21**(5), 95–106 (2004)
36. D. Panigrahy, P.K. Sahu, Extraction of fetal ECG signal by an improved method using extended Kalman smoother framework from single channel abdominal ECG signal. Aust. Phys. Eng. Sci. Med. **40**(1), 191–207 (2017)
37. D. Paul, J.W. Silverstein, No eigenvalues outside the support of the limiting empirical spectral distribution of a separable covariance matrix. J. Multivar. Anal. **100**(1), 37–57 (2009)
38. M. Richter, T. Schreiber, D.T. Kaplan, Fetal ECG extraction with nonlinear state-space projections. IEEE Trans. Biomed. Eng. **45**(1), 133–137 (1998)
39. R. Sameni, Extraction of fetal cardiac signals from an array of maternal abdominal recordings. Ph.D. thesis, Institut National Polytechnique de Grenoble-INPG; Sharif University of . . ., 2008
40. I. Silva, J. Behar, R. Sameni, T. Zhu, J. Oster, G.D. Clifford, G.B. Moody, Noninvasive fetal ECG: the physionet/computing in cardiology challenge 2013, in *Computing in Cardiology 2013* (IEEE, 2013), pp. 149–152
41. A. Singer, H.-T. Wu, Two-dimensional tomography from noisy projections taken at unknown random directions. SIAM J. Imaging Sci. **6**(1), 136–175 (2013)
42. S. Steinerberger, H.-T. Wu, Fundamental component enhancement via adaptive nonlinear activation functions. Appl. Comput. Harmonic Anal. **63**, 135–143 (2023)
43. L. Su, H.-T. Wu, Extract fetal ECG from single-lead abdominal ECG by de-shape short time fourier transform and nonlocal median. Front. Appl. Math. Stat. **3**, 2 (2017)
44. P.-C. Su, S. Miller, S. Idriss, P. Barker, H.-T. Wu, Recovery of the fetal electrocardiogram for morphological analysis from two trans-abdominal channels via optimal shrinkage. Physiol. Meas. **40**(11), 11,5005 (2019)
45. P.-C. Su, E.Z. Soliman, H.-T. Wu, Robust t-end detection via t-end signal quality index and optimal shrinkage. Sensors **20**(24), 7052 (2020)
46. P.-C. Su, H.-T. Wu, Adaptive optimal shrinkage of singular values under colored and dependent noise. Preprint (2022). arXiv:2207.03466
47. M. Ungureanu, J.W.M. Bergmans, S.G. Oei, R. Strungaru, Fetal ECG extraction during labor using an adaptive maternal beat subtraction technique. Biomed. Technik **52**(1), 56–60 (2007)
48. A. van Oosterom, Spatial filtering of the fetal electrocardiogram. J. Perinatal Med. **14**(6), 411–419 (1986)
49. J. Vanderschoot, D. Callaerts, W. Sansen, J. Vandewalle, G. Vantrappen, J. Janssens, Two methods for optimal MECG elimination and FECG detection from skin electrode signals. IEEE Trans. Biomed. Eng. **34**(3), 233–243 (1987)
50. H.-T. Wu, J. Harezlak, Application of de-shape synchrosqueezing to estimate gait cadence from a single-sensor accelerometer placed in different body locations. Preprint (2022). arXiv:2203.10563

Information Theory and Fetal Heart Rate Variability Analysis

Massimo W. Rivolta

1 Introduction

Information Theory has found a wide room of application in the context of the characterization of physiological signals and time series. A large body of evidence is indeed available and reports differences between healthy and pathological conditions under different perspectives, such as signal/series' power, mean value, frequency content, entropy, *etc.*

A major research topic that makes use of Information Theory widely is Heart Rate Variability (HRV) analysis. HRV studies the time fluctuations of the heart rate (HR) to infer information about the regulation performed by the autonomic nervous system (ANS), known to continuously modulate body activities, including the HR. Typically, the characterization of such fluctuations is performed after extracting the inter-beat time interval series (RR), defined as the time interval between two consecutive beats. More formally, given the positions R[k] of the R peaks in the electrocardiogram (ECG), the RR series is defined as

$$\mathrm{RR}[k] = \mathrm{R}[k+1] - \mathrm{R}[k]. \tag{1}$$

In the context of pregnancy monitoring and labor, the characterization of the fetal well-being is achieved by quantifying the fetal HR (FHR) and its variability (FHRV). The available technology is able to extract either the ECG of the fetus at the skin of the mother and then compute the fetal RR (FRR) series or directly the FHR (in beats per minute, bpm) leveraging the Doppler effect via Cardiotocography (CTG). The CTG output is formed by two signals sampled at 4 Hz (or sometimes at 2

M. W. Rivolta (✉)
Dipartimento di Informatica, Università degli Studi di Milano, Milan, Italy
e-mail: massimo.rivolta@unimi.it

D. Pani (ed.), *Innovative Technologies and Signal Processing in Perinatal Medicine*, https://doi.org/10.1007/978-3-031-32625-7_9

Hz) representing the sequence of FHR samples and the uterine contraction. Despite which sensing modality is used, FHRV analysis represents the only available proxy to assess the well-being of the fetus through the evaluation of the fetal ANS condition.

In this chapter, we discuss the application of Information Theory to extract relevant information to characterize the health status of a fetus during pregnancy monitoring and labor. In particular, the application of entropy-based measures and Phase-Rectified Signal Averaging (PRSA) parameters is reviewed in this context.

2 Entropy and Entropy Rate

In the mid-50s, in the rising field of telecommunication, Claude E. Shannon was investigating on the optimization of a source transmitting messages in the form of symbols on a communication channel. Each symbol was supposed to be encoded with a variable length code composed of a sequence of bits (e.g., $a = 0$, $b = 10$, and $c = 110$), and the code was uniquely decodable. In this very general scenario, he was able to prove that the average number of bits per symbol necessary to encode the message has a lower limit completely defined by the statistical property of the source and by the number of symbols [1, 2]. The quantity characterizing the source was called Shannon Entropy (ShEn), defined as follows:

$$\mathrm{H}(X) = -\sum_{i=1}^{S} p(x_i) \log_2 p(x_i), \tag{2}$$

where X is the random process generating the symbols x_i by the source, $p(x_i)$ is the probability of generating the symbol x_i, and S is the total number of possible symbols. In order words, ShEn is defined as the negative expected value of $\log p(x_i)$ with respect to $p(x_i)$.

The main intuition behind such a result is the following. In order to minimize the overall message length (e.g., *abaacaa* ...), one may think to encode the most likely symbols with a lower number of bits. Conversely, rare symbols would require longer sequences of bits. This intuition can be formally represented by constructing the Information Content (IC) as follows: $I(e) = -\log p(e)$ for each symbol e. In this way, the IC takes large values for unlikely events and values close to 0 when the event is almost sure. The ShEn can therefore be seen as the expected value of the IC and gets its maximum value when each symbol is equiprobable (i.e., $p(x_i) = 1/S$), reaching $\mathrm{H}(X) = \log(S)$. Consequently, ShEn can therefore be interpreted as degree of "complexity," "randomness," or "unpredictability."

The ShEn is very often used to characterize signals and time series (e.g., RR series) and has been extensively used on data with biological origins. In fact, pathological conditions might often be detected by changes in the probability

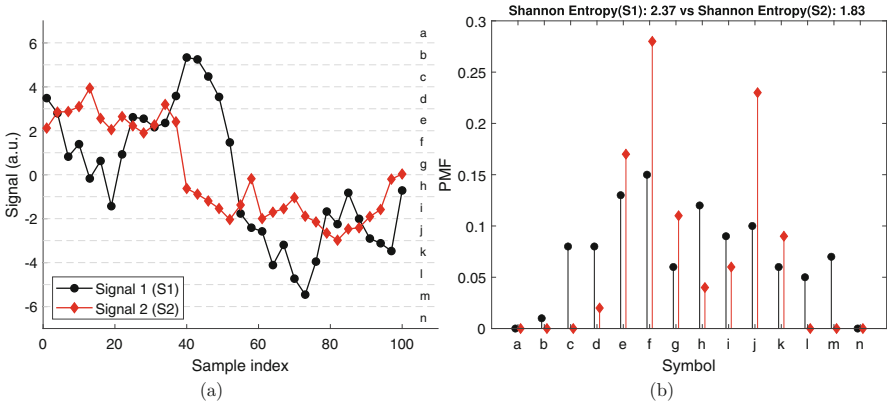

Fig. 1 Example of computation of ShEn for two different signals. (**a**) Two signals with different power are transformed into a sequence of symbols (i.e., *a*, *b*, *c*, *etc.*) using equal-size binning. (**b**) PMF of the two sequences of symbols, along with their correspondent ShEn (natural logarithm has been used)

distribution of the signal/series of interest, which is likely to be reflected in the ShEn as well. In order to compute the quantity, the numerical sequence of data is firstly converted into a sequence of symbols using a binning technique. Then, the ShEn can be computed using (2). For example, the FRR variability measured during labor is well known to be reduced for compromised fetuses [3]. This change in variability is also reflected in the ShEn. Indeed, given a fixed bin size, the sequence of symbols associated with the series with the lower variance shows a lower number of symbols as well. In this case, the number of symbols required to describe the FRR series of a compromised fetus is lower than that of a healthy fetus (when considering equal bin sizes), thus showing a reduced ShEn. The FHRV is also known to increase with the gestational age, and this is reflected in the ShEn as well [4]. Figure 1 reports an example on how two signals with different power are characterized by a different ShEn.

One of the main limitations in applying the ShEn on signal/time series is the lack of the temporal dimension. In fact, completely different series (e.g., a pure sinusoidal function and a uniform noise) but with the same probability mass function (PMF) display the exact same ShEn, despite the two sequences of symbols are very different from each other. This result comes from the fact that the ShEn only uses the PMF of the amplitude of the signal/time series, while it totally discards temporal relationships. In order to characterize multiple random variables, such as those forming a random process $\mathcal{X} = \{X_t\}$, the Joint Entropy of two discrete random variables X_i and X_j of the random process is defined as follows:

$$\mathrm{H}(X_i, X_j) = -\sum_{x \in X_i} \sum_{y \in X_j} p(x, y) \log p(x, y). \tag{3}$$

The formula can be easily extended to deal with a sequence of N random variables, i.e., $\mathrm{H}(X_1, \cdots, X_N)$. Similarly, the Conditional Entropy is defined as

$$\mathrm{H}(X_j|X_i) = \mathrm{H}(X_i, X_j) - \mathrm{H}(X_i) \tag{4}$$

and represents the average IC of X_j when X_i is known.

Another important quantity used to characterize the signal/time series is the entropy rate, defined as follows:

$$\mathcal{H}(\mathcal{X}) = \lim_{n \to +\infty} \frac{1}{n} \mathrm{H}(X_1, X_2, \ldots, X_n). \tag{5}$$

In many situations, biological signals and time series can be assumed to be stationary, i.e., their probability distributions do not change when shifted in time. For this class of random process, the entropy rate in (5) can be simplified with

$$\mathcal{H}(\mathcal{X}) = \lim_{n \to +\infty} \mathrm{H}(X_n|X_{n-1}, X_{n-2}, \ldots, X_1), \tag{6}$$

or, alternatively, using the Conditional Entropy in (4), it becomes

$$\mathcal{H}(\mathcal{X}) = \lim_{n \to +\infty} \mathrm{H}(X_n, X_{n-1}, X_{n-2}, \ldots, X_1) - \mathrm{H}(X_{n-1}, X_{n-2}, \ldots, X_1). \tag{7}$$

The latter equation reports an operative formula that can be applied on signals/time series. However, there are two problems for its practical application. First, signals and time series have a finite number of samples, so the limit cannot be computed. Second, the computation suffers of the so-called curse of dimensionality. Indeed, estimating the PMF in a high-dimensional space requires a huge amount of samples. For example, if binning with B levels is applied to the amplitude of the signal/time series of N samples, the PMF has B^N possible probabilities that need to be estimated from only N samples. These two problems have led researchers to accept a simplification of (7) by discarding the limit operator and considering small values of n (typically in the range of 1–3).

2.1 Approximate Entropy and Sample Entropy

Trajectories of dynamical systems show different behaviors including equilibrium points, cycles, and chaotic attractors. Kolmogorov and Sinai proposed to characterize the predictability of the trajectory by dividing the space into boxes of a given dimension and counting the time spent by the trajectory within each box, in the

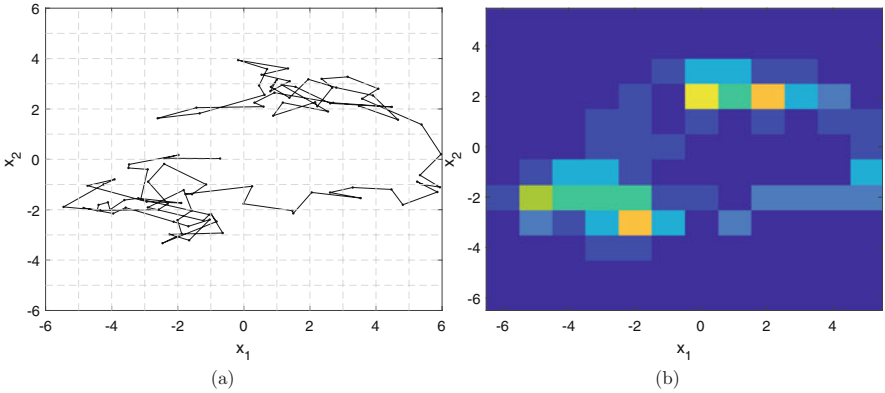

Fig. 2 (**a**) Example of trajectory formed by the variables x_1 and x_2. (**b**) PMF of the trajectory

limit of time going to infinity. This allows to estimate a PMF,[1] and then a sort of entropy rate can be computed to characterize the dynamical system. Figure 2 shows an example of trajectory in a two-dimensional space of a discrete dynamical system and the estimate of its PMF.

The impossibility to estimate the Kolmogorov and Sinai's entropy on real signals and time series led Steven M. Pincus to create a family of statistics called Approximate Entropy (ApEn) [5]. The main idea was to consider the signal/time series as a trajectory generated by a dynamical system and to assess how much repetitive it is. The ApEn of a signal/time series of N samples is computed in three steps. First, the series is embedded into an m-dimensional embedding space. This means that all sequences of m samples in the original series are stored as vectors $\mathbf{x}_i \in \mathbb{R}^m$ with i from 1 to $N-m+1$, and each vector is a point in this m-dimensional space.

The box counting procedure is equivalent to determine the proportion of times the embedded vectors $\mathbf{x}_i$ are close to a given vector $\mathbf{x}_j$ within a tolerance threshold r. The distance defines the way to quantify the repetitiveness of patterns. Formally, the second step requires the computation of the following quantity:

$$C_j^m(r) = \frac{\sum_{i=1}^{N-m+1} 1_{d(\mathbf{x}_j,\mathbf{x}_i)<r}}{N-m+1}, \tag{8}$$

where 1_c is the indicator function with condition c, $C_j^m(r)$ is an estimate of the probability of observing patterns similar to $\mathbf{x}_j$ and $d(\mathbf{x}_j, \mathbf{x}_i)$ is a distance measure between the two vectors $\mathbf{x}_j$, and $\mathbf{x}_i$. In the original manuscript, $d(\mathbf{x}_j, \mathbf{x}_i)$ was defined as the maximum norm of $\mathbf{x}_j - \mathbf{x}_i$.

[1] Kolmogorov and Sinai's definition of entropy is more sophisticated than what described here and involves limits on the size of the boxes and dimension of the embedded space as well.

Third, the entropy rate resembling the one reported in (7) is computed. In order to do so, one has to determine the expected value of $\log p(\mathbf{x})$ with respect to $p(\mathbf{x})$. In this case, such expectation can be determined using the sample mean of $\log C_j^m$ over all j vectors, as follows:

$$\Phi^m(r) = \frac{1}{N-m+1} \sum_{j=1}^{N-m+1} \log C_j^m(r), \tag{9}$$

and ApEn is defined as

$$\mathrm{ApEn}(m, r, N) = \Phi^m(r) - \Phi^{m+1}(r). \tag{10}$$

What ApEn quantifies can be easily understood when N goes to $+\infty$. In fact,

$$\begin{aligned}
\lim_{N\to+\infty} \mathrm{ApEn}(m, r, N) &= \lim_{N\to+\infty} \Phi^m(r) - \Phi^{m+1}(r) \\
&= -\frac{1}{N} \sum_{j=1}^{N} \log \left(\frac{C_j^{m+1}(r)}{C_j^m(r)} \right) \\
&\approx -\frac{1}{N} \sum_{j=1}^{N} \log \left(\frac{p(d(\mathbf{X}^{m+1}, \mathbf{x}_j^{m+1}) < r)}{p(d(\mathbf{X}^m, \mathbf{x}_j^m) < r)} \right) \\
&= -\frac{1}{N} \sum_{j=1}^{N} \log p \left(d(\mathbf{X}^{m+1}, \mathbf{x}_j^{m+1}) < r | d(\mathbf{X}^m, \mathbf{x}_j^m) < r \right),
\end{aligned} \tag{11}$$

where $\mathbf{X}^m$ and $\mathbf{X}^{m+1}$ are the multivariate random variables containing m and $m+1$ variables, respectively. ApEn approximates the negative average of the natural logarithm of the conditional probability that two sequences similar for m points remain similar at the next point too. The approximation sign in (11), rather than equality, is due to the fact that (8) counts the self-matches too. On the one hand, this prevents $\log 0$ to occur in short series, but on the other hand, it creates a biased estimate of the probability (for example, in presence of only one occurrence of $\mathbf{x}_j^m$, the probability $C_j^m(r) = 1/(N-m+1)$, but no similar patterns are found).

A few years later, Richman and Moorman proposed an improved family of statistics called Sample Entropy (SampEn). The SampEn is defined exactly as the negative natural logarithm of the conditional probability that two sequences similar for m points remain similar at the next point, where self-matches are not included in the calculation of the probability [6]. Formally, the algorithm requires to compute

$$\mathrm{SampEn}(m, r, N) = -\log \frac{A^{m+1}}{A^m}, \tag{12}$$

where

$$C_j^m(r) = \frac{\sum_{i=1, i\neq j}^{N-m-1} 1_{d(\mathbf{x}_i, \mathbf{x}_j)<r}}{N-m},$$
$$A^m = \frac{\sum_{j=1}^{N-m} C_j^m(r)}{N-m}. \tag{13}$$

The main practical problems related to the application of ApEn and SampEn are the length N of the series, which might be too short for a reliable estimate of the probabilities, and the selection of the parameters m and r. The former is dictated by the data acquisition protocol and little can be done in many circumstances. An attempt to deal with short series has been carried out by Aktaruzzaman and Sassi [7] who investigated on the theoretical values of ApEn and SampEn for stationary Gaussian processes. They modeled the short series with an autoregressive model and used its coefficients to compute the analytical value of both entropies. The second problem concerns the optimal selection of m and r which depends on the specific application.

In the context of HRV, typical values of m and r are 1 and $0.2 \times$ std(RR), respectively. The reasons are due to the fact that when m increases also the number of samples N needed for ensuring reliable estimates increases as well, but with an exponential growth. Also, r defines a sort of bin size for comparing embedded vectors $\mathbf{x}_i$ and $\mathbf{x}_j$. Making r proportional to the standard deviation of the series is a strategy which has pros and cons. On the one hand, it makes SampEn computed on series with different amplitudes comparable with each other, thus focusing only on the temporal regularity of the series. On the other hand, the dependency of the entropy to the standard deviation is lost. This problem becomes clear when analyzing FRR series during labor. In fact, during the initial and late phases of labor, profound changes are induced by the presence of the maternal contractions, which produce decelerations of the FHR. The decelerations increase the overall standard deviation of the FRR series, and thus the value of r becomes large, implying a lower SampEn value. When the value of r is instead kept constant across different phases of the time series, the value of SampEn is seen to increase as expected. This behavior has been observed on data coming from an animal model of labor [8]. In addition, the standard deviation is highly dependent on the amount of noise present in the FRR, typically in the form of spikes, that might alter the value of SampEn.

Many are the scientific contributions investigating the characterization of FHRV using entropy measures. In a recent review about the use of nonlinear methods [9], it was found that half of the manuscripts focused on entropy for a wide range of applications, such as detection of hypoxia/acidemia, assessment of fetal maturation, identification of intrauterine growth restriction, and evaluation of fetal well-being/distress. According to the review, the entropy measures mostly used are ApEn, SampEn, and ShEn, with the former two covering more than 30% of the total publications.

2.2 Bubble Entropy

The problem of selecting the values of m and r described in the previous section has motivated the investigation of an entropy measure "free" of parameters or at least with a minimal dependency. Recently, Manis, Aktaruzzaman, and Sassi proposed an entropy measure, called Bubble Entropy (bEn), in which the concept of regularity of a signal/time series is associated with the effort required for sorting its values using the Bubble Sort algorithm [10]. The Bubble Sort algorithm sorts the values stored into an array by comparing pairs of adjacent numbers. In case the number coming first in the array is higher than the next one, the algorithm swaps the two numbers. These swaps resemble an air bubble going up in glass of sparkling water: that is the reason for this particular name. bEn removed completely the dependency on the parameter r and was found minimally dependent on the embedding dimension m, so that the authors described bEn as an entropy almost free of parameters.

The effort for sorting the embedded sequences is defined by counting the number of swaps that Bubble Sort needs to perform on each embedded m-dimensional vector. The probability distribution over the number of swaps is then estimated from all embedded vectors. Then, bEn is computed as follows [11]:

$$\mathrm{bEn}(m) = \frac{H^{m+1}_{\mathrm{swaps}} - H^{m}_{\mathrm{swaps}}}{W^{m+1}_{\mathrm{swaps}} - W^{m}_{\mathrm{swaps}}}, \tag{14}$$

where H^{m}_{swaps} is the Rényi Entropy (a generalization of ShEn) of the PMF of the number of swaps, that is,

$$H^{m}_{\mathrm{swaps}} = -\log \sum_{i=0}^{\binom{m}{2}} p_i^2 \tag{15}$$

with p_i being the probability of having i swaps.

The denominator in (14) is a normalization factor to enforce $\mathrm{bEn} = 1$ in the presence of a White Gaussian Noise (WGN). Its value can be found analytically [11] (in addition, it can be found for any autoregressive model when $m \leq 3$ [12]). A quick demonstration can be reported for $m = 2$ and $m = 3$. For the former, only sequences of two values are considered. In this case, the swap of the two values may or may not occur with probability $p_0 = p_1 = 1/2$, thus obtaining $W^{2}_{\mathrm{swaps}} = \log 2$. For sequences of 3 values, the maximum number of swaps is 3 and four are the quadrant probabilities of a bivariate Gaussian variable to compute, i.e., $p_0 = P(x_1 < x_2 < x_3)$, $p_1 = P(x_1 < x_3 < x_2) + P(x_2 < x_1 < x_3)$, $p_2 = P(x_2 < x_3 < x_1) + P(x_3 < x_1 < x_2)$, and $p_3 = P(x_3 < x_2 < x_1)$, which are $1/6$, $1/3$, $1/3$, and $1/6$, respectively. Hence, $W^{3}_{\mathrm{swaps}} = \log 18/5$, and $W^{3}_{\mathrm{swaps}} - W^{2}_{\mathrm{swaps}} = \log 9/5$.

It is worth noting that bEn has, at least, two major differences with respect to ApEn and SampEn. Indeed, when computed on a stationary Gaussian process, these latter two display the highest value when the process is white and are invariant to

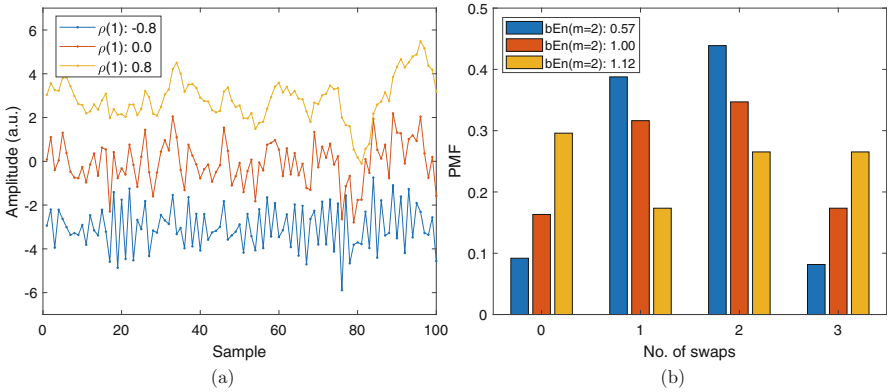

Fig. 3 (**a**) Example of three simulated time series with different 1-step autocorrelation coefficient. Time series were generated using an autoregressive model of order 1 with WGN as input. The three time series were normalized to have unit variance. (**b**) PMF of the number of swaps, for each simulated time series, with an embedding dimension $m = 3$. Values in the legend represent bEn with $m = 2$

time-reversal of the series. On the contrary, bEn is neither maximum for a WGN nor displays such time invariance (see the figure in [12]). It was indeed recently observed that the PMF of the number of swaps tends to flatten when the one-step autocorrelation grows toward 1 [13], thus resulting in a higher bEn with respect to that of a WGN. Figure 3a shows an example of three simulated Gaussian processes with different 1-step autocorrelation coefficient, while Fig. 3b reports the PMF of the number of swaps for $m = 3$, along with bEn computed for $m = 2$. The figure depicts the dependency described.

Recently, bEn was tested for the identification of acidemia at birth together with ShEn, ApEn, and SampEn [14]. It was found to perform similarly to ApEn and SampEn, but without the need of selecting the r parameter and allowing the computation with embedding dimensions $m > 20$.

3 Phase-Rectified Signal Averaging

Synchronous averaging is a fundamental tool for the analysis of physiological signals. It is based on the fact that when averaging M time windows, all anchored to a specific time event, the signal components not correlated with the event itself reduce their contribution progressively with increasing M. In other words, the signal-to-noise ratio improves of a factor M. An example of its use is in the design of brain–computer interfaces based on visual stimuli. After each stimulus, the event-related potentials collected using electrodes positioned on the scalp are then averaged to reduce the effect of non-correlated noise and make the so-called P300 wave appear [15].

In the context of HRV analysis, many are the use of synchronous averaging, or, more in general, analysis synchronized on events, to extract meaningful information from the time series. For example, the well-known tilt-test is an experiment aiming to evaluate the change in HR and blood pressure (BP) before and after a quick postural change of the subject from supine to standing. One of the outcome of this test is the baroreflex sensitivity that quantifies the rate of change between RR and BP series. Among the many ways to quantify such sensitivity [16], one of the most common is called the Sequence Method and it quantifies the slope between the RR (or HR) and BP, usually computed via least squares, only after having selected increasing ramps concurrently occurring in both time series (i.e., the event). Another example of the application of synchronous averaging in HRV analysis is represented by the well-known Heart Rate Turbulence (HRT) [17]. This technique has been inspired by the observation of Schmidt and colleagues which noted that the HR of low-risk patients immediately after a ventricular ectopic beat (VPB) followed a different pattern with respect to that of high-risk patients (they investigated the risk of death in patients after acute myocardial infarction). They formalized the technique by means of four steps. First, all VPBs have to be detected on a 24-h Holter ECG. Second, a temporal alignment of all windows comprising of 20 consecutive RR values after each VPB is performed (i.e., synchronization on the VPB). Third, all temporally aligned windows are then averaged to form the average pattern. Finally, the maximum RR slope of 5 consecutive samples within the average pattern is then retained to characterize the patient.

More recently, Bauer et al. [18] proposed a technique similar to HRT in which the RR windows are anchored on increasing or decreasing trends in the series itself (somehow similar to the ramps to identify for the BRS computation). The main rationale behind this anchoring strategy was the following. Being the RR series continuously modulated by internal and external factors, the RR series contains sequences of periodic windows that are interrupted by the change of these factors. This produces phase de-synchronizations of the periodic windows, and anchoring on the increasing/decreasing trends should maximize the probability of detecting patterns with similar periodicities [18]. The technique was called Phase-Rectified Signal Averaging.

The PRSA algorithm is divided into two steps. First, anchor points are identified on the time series RR[k]. Each time index k that satisfies the condition

$$\frac{1}{T}\sum_{i=0}^{T-1}\mathrm{RR}[k+i] > \frac{1}{T}\sum_{i=1}^{T}\mathrm{RR}[k-i] \tag{16}$$

is inserted in the anchors' point list $\mathcal{A}$. The condition in (16) determines all those anchor points associated with a deceleration of the HR. If one is interested in anchor points related to HR accelerations, then the sign of the inequality in (16) has to be flipped. Consequently, there might be two different lists of anchor points, formally

$$\begin{aligned}\mathcal{A}_{\text{DEC}} &= \left\{k : \frac{1}{T}\sum_{i=0}^{T-1}\text{RR}[k+i] > \frac{1}{T}\sum_{i=1}^{T}\text{RR}[k-i]\right\} \\ \mathcal{A}_{\text{ACC}} &= \left\{k : \frac{1}{T}\sum_{i=0}^{T-1}\text{RR}[k+i] < \frac{1}{T}\sum_{i=1}^{T}\text{RR}[k-i]\right\},\end{aligned} \tag{17}$$

where DEC and ACC stand for deceleration and acceleration, respectively. The parameter T refers to the number of RR intervals involved in the identification of anchor points, and it plays a role of frequency selector (see Sect. 3.1).

The second step involves synchronous averaging. All windows of $2L$ elements centered on each anchor point are aligned (anchor points are located at the $L+1$ sample with the first sample indexed as 1), and then synchronous averaging is performed. The parameter L defines the slowest RR oscillation detectable by the algorithm [18]. Such series of $2L$ averaged elements is the PRSA series. Formally,

$$\text{PRSA}[i] = \frac{1}{|\mathcal{A}|}\sum_{k\in\mathcal{A}}\text{RR}[k-L+i-1] \tag{18}$$

with i from 1 to $2L$, and $\mathcal{A}$ being one of those associated with DEC or ACC, and $|\mathcal{A}|$ is the cardinality of the set $\mathcal{A}$. The PRSA series compacts the RR series into one of a much shorter dimension, i.e., $2L \ll N$. Figure 4 reports an example of identification of the anchor points and the corresponding PRSA series.

The PRSA series has been leveraged to determine two features named Average Acceleration Capacity and Average Deceleration Capacity (AC and DC, respectively). These two quantities are computed using the same following formula:

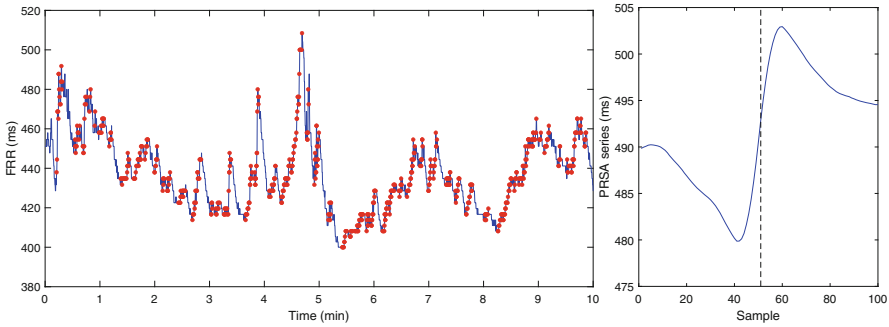

Fig. 4 (**a**) Example of FRR series with anchor points (red dots) determining decelerations with $T = 10$. (**b**) PRSA series associated with the FRR series for $T = 10$ and $L = 50$. The black dashed line represents the position of the anchor point at $L + 1$

$$\text{DC (or AC)} = \frac{\sum_{i=1}^{s} \text{PRSA}[L+i] - \text{PRSA}[L-i+1]}{2s}. \tag{19}$$

where s is the third and last parameter of this algorithm. The main difference between the two quantities is on how the anchor points are selected, i.e., using $\mathcal{A}_{\text{DEC}}$ or $\mathcal{A}_{\text{ACC}}$. A complete description of the PRSA algorithm can be found in [18, 19].

These two quantities have been extensively evaluated for the characterization of fetal well-being during pregnancy monitoring and labor. For example, evaluation of AC/DC for surveillance of growth-restricted fetuses [20, 21] at different gestational age [22] or to detect brain sparing [23] has been carried out. During labor, DC was found a better predictor of acidemia at birth than other traditional measures in large cohorts of babies [24, 25], and it was found able to detect the risk of hypoxic-ischemic encephalopathy as early as 120 minutes before birth [26].

Giving a meaning to what AC and DC actually measure is not straightforward. For example, at the very beginning of their introduction, AC and DC were supposed to be sensitive to sympathetic and parasympathetic activations of the ANS, given the fact that they are responsible for increasing and decreasing the HR. This interpretation was shown to be mathematically unsupported. In fact, when the RR series is stationary and Gaussian distributed (situation often occurring during monitoring at rest), AC and DC turn to be the exact same number [19].

3.1 Understanding the PRSA Series

Following its definition loosely, the PRSA series is the average increasing (or decreasing) trend in the RR series (computed with (18)) after identifying all trends using a moving average filter (computed with (17)). Furthermore, the computation of AC and DC involves a moving average filter too (computed with (19)). Therefore, one may expect that the parameters T and s would play a role of frequency selector. In order to investigate on such observation, the PRSA algorithm has been studied using computerized simulations [27]. In particular, sinusoidal functions were synthetically generated at varying frequencies, and the value of AC and DC was computed for a specific range of parameters T and s. Here, we repeated the analysis by generating the random sinusoidal function with power of 1 using an autoregressive model whose coefficients were $[1, -2A\cos(\omega), A^2]$ with $A = 0.999$ and ω being the angular velocity ranging from 0 to π. For this class of signals, AC and DC are equal (see below). Therefore, we computed only the value of DC.

The results of the simulations are reported in Fig. 5 and can be summarized into four major outcomes. First, both T and s play a role of frequency selector (Fig. 5a vs Fig. 5c). In particular, the higher the values, the lower and narrower is the frequency band mostly affecting the DC value. Second, the value of DC does not change significantly while varying T when s is kept fixed (Fig. 5a vs Fig. 5b). Third, with respect to T, the parameter s plays a stronger role in the selection of which frequencies to retain (Fig. 5a/5b vs Fig. 5c). Finally, the frequencies mostly

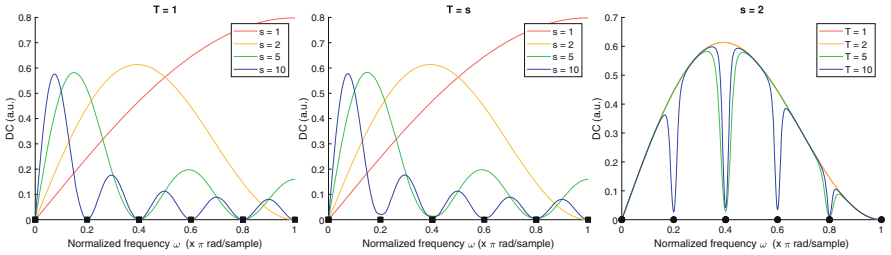

Fig. 5 Value of DC while varying the frequency of the sinusoidal wave injected into the PRSA algorithm for three different simulation settings. (**a**) $T = 1$ and s varying. (**b**) $T = s$. (**c**) T varying and $s = 2$. The input wave had a power of 1 a.u. The frequency is reported in normalized units (1 equal to π)

attenuated are those identified by the zeros of the moving average filters used for the anchor point identification (circles in Fig. 5c) or capacity computation (squares in Fig. 5a and 5b).

Another important step toward a clearer understanding of the information contained in the PRSA series has been recently achieved by demonstrating that AC and DC are the exact same quantity in certain circumstances. Specifically, it was investigated on the expected value of the PRSA series when computed on a stationary Gaussian process [19]. In this scenario, a stationary Gaussian process is fully characterized by the autocovariance function $\rho(\tau)$ and any sequence of $2L$ consecutive random variables forming the process is distributed as a multivariate normal distribution with mean vector $\boldsymbol{\mu}$ with entries equal to 0 and covariance matrix Σ, as follows:

$$\mathbf{x} \sim N(\mathbf{0}, \Sigma). \tag{20}$$

The PRSA series at i-th position is defined as the expected value of this sequence of random variables only in the portion of the space containing anchor points, that is,

$$\mathrm{PRSA}[i] = 2 \int\limits_{\mathbf{g}^\intercal \mathbf{x} > 0} \mathbf{e}_i^\intercal \mathbf{x} \frac{1}{(2\pi)^L \sqrt{\det \Sigma}} e^{-\frac{1}{2}\mathbf{x}^\intercal \Sigma^{-1} \mathbf{x}} d\mathbf{x}, \tag{21}$$

where the factor 2 normalizes the probability density function (pdf) to 1 (half of the space is excluded by the anchor point definition), $\mathbf{e}_i$ is the unit vector with 1 at position i, and $\mathbf{g}^\intercal \mathbf{x} > 0$ defines the space containing anchor points (as in (17)).

In order to solve the integral, two changes of variable are instrumental. The first one involves a whitening procedure of the Gaussian variable by converting the multivariate normal distribution into one with unitary diagonal covariance matrix. The second change of variables is represented by a rotation in such a way that the

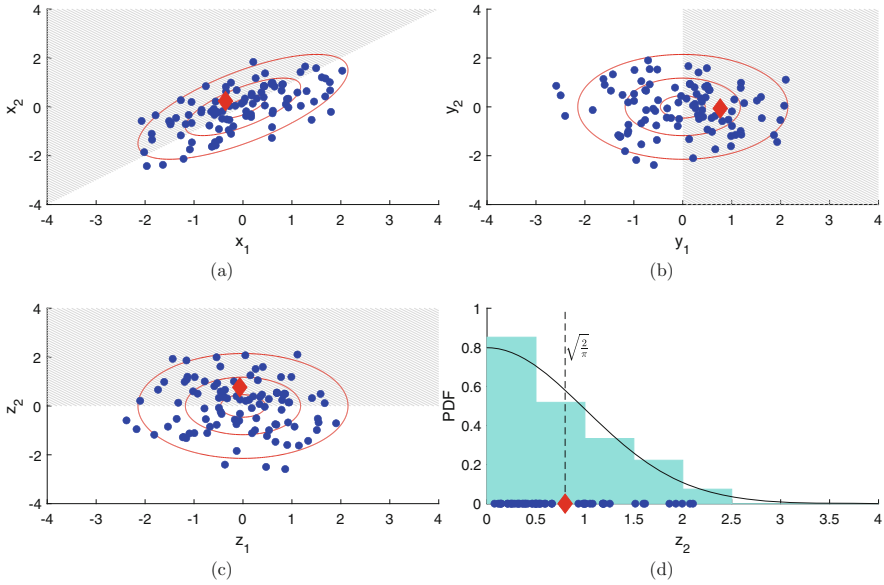

Fig. 6 Visual example describing the mathematical transformations to compute the expected value of the PRSA series with $L = T = 1$. (**a**) Scatter plot of 100 random samples taken from a bivariate normal distribution with a variance of 1 and covariance of 0.7. (**b**) Output of the whitening procedure on the original samples. (**c**) Rotation of the space to have the hyperplane orthogonal to $\mathbf{e}_2$. (**d**) Histogram of z_2 when $z_2 \geq 0$ and half normal distribution. Red lines in (**a**), (**b**), and (**c**) depict the contour plot of the bivariate normal distribution (for visualization purpose). The gray area represents the portion of space containing anchor points, i.e., $x_2 > x_1$. The red diamond points to the estimate of the PRSA series on the original space and after the two transformations. In (**d**), the red diamond shows its equivalence to the expected value of a half normal distribution, i.e., $\sqrt{\frac{2}{\pi}}$

hyperplane defining the region containing the anchor points becomes orthogonal to one of the canonical axes. This second operation allows a direct computation of the expected value because the integral becomes a summation of expected values along all independent axes (such summation involves only one term different from 0, that is, the expected value of a half normal distribution, i.e., $\sqrt{\frac{2}{\pi}}$). Figure 6 depicts an example describing the mathematical transformations to obtain the expected value. It is possible to show that the PRSA series stored into a $2L$-dimensional vector is

$$\mathbf{PRSA} = \sqrt{\frac{2}{\pi}}\mathbf{U}\mathbf{D}^{\frac{1}{2}}\mathbf{H}^{\intercal}\mathbf{e}_{L+1}, \tag{22}$$

where $\mathbf{U}$ contains the eigenvector of Σ, $\mathbf{D}$ is a diagonal matrix containing the eigenvalues of Σ, and $\mathbf{H}$ is a rotation matrix (specifically, the Householder transformation). Mathematical details are reported in the original manuscript [19].

Another important result from (21) is the fact that the PRSA series associated with HR accelerations is equal to that one computed for decelerations (except a sign). In fact, considering the variable $\mathbf{y} = -\mathbf{x}$, it is possible to show that

$$\begin{aligned} \mathrm{PRSA}_{\mathrm{DEC}}^{y=-x}[i] &= 2 \int\limits_{\mathbf{g}^{\intercal}\mathbf{y}>0} \mathbf{e}_i^{\intercal}\mathbf{y} \frac{1}{(2\pi)^L \sqrt{\det \Sigma}} e^{-\frac{1}{2}\mathbf{y}^{\intercal}\Sigma^{-1}\mathbf{y}} d\mathbf{y} \\ &= -2 \int\limits_{\mathbf{g}^{\intercal}\mathbf{x}<0} \mathbf{e}_i^{\intercal}\mathbf{x} \frac{1}{(2\pi)^L \sqrt{\det \Sigma}} e^{-\frac{1}{2}\mathbf{x}^{\intercal}\Sigma^{-1}\mathbf{x}} d\mathbf{x} \\ &= -\mathrm{PRSA}_{\mathrm{ACC}}^{x}[i]. \end{aligned} \tag{23}$$

The equivalence reported in the previous equation has a major consequence for the association between AC/DC and the sympathovagal regulation. Indeed, it is clear that a stationary Gaussian process has AC and DC identical in magnitude (i.e., AC $= -$DC) being their PRSA series identical too and, therefore, they cannot carry different information about the two ANS branches.

The result has motivated the introduction of a new PRSA-based metric, potentially relevant for characterizing FHR series. Dissimilarities in AC and DC values arise when asymmetric increasing or decreasing trends appear in the signal [27], a situation that is common in FHR during labor. Also, capacities might differ from each other in presence of non-stationarities and non-Gaussianities. In order to capture such dissimilarities, a new metric called "Deceleration Reserve" was recently introduced [19], defined as follows:

$$\mathrm{DR} = \mathrm{DC} + \mathrm{AC}. \tag{24}$$

Note that AC is a negative quantity for RR series and DR inherits the dependency to the PRSA parameters L, T, and s. DR was introduced very recently and, up to date, only few works investigated for its potential use in the clinical setting. Specifically, DR was found among the most powerful predictors of acidemia at birth [19], and it was found lower on FRR series associated with labor occurring at the preterm condition with respect to at term [28].

In order to shed further light for the potential use of PRSA-based parameters in the context of labor monitoring, investigations on FRR series collected from animal models were carried out too. The values of AC and DC were found correlated with the worsening of the biomarkers (pH, base deficit, and level of lactates) caused by prolonged and severe umbilical cord occlusions (UCOs) applied to fetal sheep [29]. In addition, DC was found associated with the development of fetal hypotension in a different animal model of labor and predicted it about 120 minutes (median value) earlier than the end of the stimulation protocol [30]. Furthermore, AC and DC were found capable to detect fetal sheep in chronically hypoxic condition (fetal sheep in this condition are a model of IUGR) [19]. In the same setting, DR was found a better predictor of chronic hypoxia during the severe phase of UCOs, with respect to other

PRSA-based parameters [19]. This result suggested the investigation of what DR may capture during labor. Recently, it was found that DR highly correlated with the asymmetric growing and decaying trend induced by the uterine contraction [31]. In this recent study, the deceleration morphology induced by the UCO was modeled as a trapezoid. The time intervals required to adapt the FHR from the onset of the UCO to nadir of the deceleration and from the nadir to the baseline were extracted on this model. Fetal sheep under chronic hypoxia were found to adapt their FHR slower than healthy fetuses when stimulated with complete umbilical cord occlusions and DR highly correlated with the difference of these time intervals. Another interesting relationship is between the well-known deceleration area (DA) and PRSA-based parameters. In fact, DA was found as good as DC in detecting fetal hypotension [30], and DA and DR were found highly correlated, with the latter mostly influenced by DC [31]. All these findings suggested that the deceleration morphology may presents asymmetric trends, and hence it motivates the use of different strategies for detecting the anchor points, perhaps by means of asymmetric weights in (17). Preliminary results in this regard showed slightly better performance in detecting acidemia at birth with respect to traditional PRSA [32].

Acknowledgments The author thanks Prof. Roberto Sassi (Dipartimento di Informatica, Università degli Studi di Milano) for the valuable discussion and revision of the content of this chapter.

References

1. C.E. Shannon, A mathematical theory of communication. Bell Syst. Tech. J. **27**(3), 379–423 (1948)
2. C.E. Shannon, A mathematical theory of communication. Bell Syst. Tech. J. **27**(4), 623–656 (1948)
3. D. Ayres-de Campos, C.Y. Spong, E. Chandraharan, et al., FIGO consensus guidelines on intrapartum fetal monitoring: cardiotocography. Int. J. Gynaecol. Obstet. **131**(1), 13–24 (2015)
4. A.H. Khandoker, F. Marzbanrad, A. Voss, S. Schulz, Y. Kimura, M. Endo, M. Palaniswami, Analysis of maternal-fetal heart rate coupling directions with partial directed coherence. Biomed. Signal Process Control **30**, 25–30 (2016)
5. S.M. Pincus, Approximate entropy as a measure of system complexity. Proc. Natl. Acad. Sci. USA **88**(6), 2297–2301 (1991)
6. J.S. Richman, J.R. Moorman, Physiological time-series analysis using approximate entropy and sample entropy. Am. J. Physiol. Heart Circ. Physiol. **278**(6), H2039–H2049 (2000)
7. Md. Aktaruzzaman, R. Sassi, Parametric estimation of sample entropy in heart rate variability analysis. Biomed. Signal Process Control **14**, 141–147 (2014)
8. M.W. Rivolta, Md. Aktaruzzaman, T. Stampalija, D. Casati, M.G. Frasch, E. Ferrazzi, R. Sassi, Regularity of fetal HRV changes in an in-vivo sheep model of labor. Comput. Cardiol. **43**, 901–904 (2016)
9. M. Ribeiro, J. Monteiro-Santos, L. Castro, L. Antunes, C. Costa-Santos, A. Teixeira, T.S. Henriques, Non-linear methods predominant in fetal heart rate analysis: a systematic review. Front Med. **8**, (2021). https://doi.org/10.3389/fmed.2021.661226
10. G. Manis, Md. Aktaruzzaman, R. Sassi, Bubble entropy: an entropy almost free of parameters. IEEE Trans. Biomed. Eng. **64**(11), 2711–2718 (2017)

11. G. Manis, M. Bodini, M.W. Rivolta, R. Sassi, A two-steps-ahead estimator for bubble entropy. Entropy **23**(761), 1–13 (2021)
12. M. Bodini, M. W. Rivolta, G. Manis, R. Sassi, Analytical formulation of Bubble Entropy for autoregressive processes, in *2020 11th Conference of the European Study Group on Cardiovascular Oscillations (ESGCO)* (IEEE, July 2020)
13. G. Manis, M. Bodini, M.W. Rivolta, R. Sassi, Bubble entropy of fractional gaussian noise and fractional brownian motion. Comput. Cardiol. **48**, 1–4 (2021)
14. G. Manis, R. Sassi, Relation between fetal HRV and value of umbilical cord artery pH in labor, a study with entropy measures, in *2017 IEEE 30th International Symposium on Computer-Based Medical Systems (CBMS)* (IEEE, 2017)
15. L.A. Farwell, E. Donchin, Talking of the top of your head: toward a mental prosthesis utilizing event-related brain potentials. Electroencephalogr. Clin. Neurophysiol. **70**, 510–523 (1988)
16. C.A. Swenne, Baroreflex sensitivity: mechanisms and measurement. Neth. Heart J. **21**(2), 58–60 (2013)
17. G. Schmidt, M. Malik, P. Barthel, R. Schneider, K. Ulm, L. Rolnitzky, A.J. Camm, J.T. Bigger Jr, A. Schömig, Heart-rate turbulence after ventricular premature beats as a predictor of mortality after acute myocardial infarction. Lancet **353**(9162), 1390–1396 (1999)
18. A. Bauer, J.W. Kantelhardt, A. Bunde, P. Barthel, R. Schneider, M. Malik, G. Schmidt, Phase-rectified signal averaging detects quasi-periodicities in non-stationary data. Phys. A **364**, 423–434 (2006)
19. M.W. Rivolta, T. Stampalija, M.G. Frasch, R. Sassi, Theoretical value of deceleration capacity points to deceleration reserve of fetal heart rate. IEEE Trans. Biomed. Eng. **67**(4), 1176–1185 (2020)
20. S.M. Lobmaier, E.A. Huhn, S. Pildner von Steinburg, A. Müller, T. Schuster, J.U. Ortiz, G. Schmidt, K.T. Schneider, Phase-rectified signal averaging as a new method for surveillance of growth restricted fetuses. J. Matern. Fetal Neonatal. Med. **25**, 2523–2528 (2012)
21. S. Tagliaferri, A. Fanelli, G. Esposito, F.G. Esposito, G. Magenes, M.G. Signorini, M. Campanile, P. Martinelli, Evaluation of the acceleration and deceleration phase-rectified slope to detect and improve IUGR clinical management. Comput. Math. Methods Med. **2015**, 236,896 (2015)
22. T. Stampalija, D. Casati, M. Montico, R. Sassi, M.W. Rivolta, V. Maggi, A. Bauer, E. Ferrazzi, Parameters influence on acceleration and deceleration capacity based on trans-abdominal ECG in early fetal growth restriction at different gestational age epochs. Eur. J. Obstet. Gynecol. Reprod. Biol. **188**, 104–112 (2015)
23. T. Stampalija, D. Casati, L. Monasta, R. Sassi, M.W. Rivolta, M.L. Muggiasca, A. Bauer, E. Ferrazzi, Brain sparing effect in growth-restricted fetuses is associated with decreased cardiac acceleration and deceleration capacities: a case-control study. BJOG **123**(12), 1947–1954 (2016)
24. A. Georgieva, A.T. Papageorghiou, S.J. Payne, M. Moulden, C.W. Redman, Phase-rectified signal averaging for intrapartum electronic fetal heart rate monitoring is related to acidaemia at birth. BJOG **121**, 889–894 (2014)
25. J. Weyrich, J.U. Ortiz, A. Müller, G. Schmidt, C.E. Brambs, O. Graupner, B. Kuschel, S.M. Lobmaier, Intrapartum prsa: a new method to predict fetal acidosis? A case-control study. Arch. Gynecol. Obstet. **301**, 137–142 (2020)
26. J. Vargas-Calixto, Y. Wu, M. Kuzniewicz, M.-C. Cornet, H. Forquer, L. Gerstley, E. Hamilton, P. Warrick, R. Kearney, Temporal evolution of intrapartum fetal heart rate features. Comput. Cardiol. **48**, 1–4 (2021)
27. R. Sassi, T. Stampalija, D. Casati, E. Ferrazzi, A. Bauer, M.W. Rivolta, A methodological assessment of phase-rectified signal averaging through simulated beat-to-beat interval time series. Comput. Cardiol. **41**, 601–604 (2014)
28. C. López-Justo, A.C. Pliego-Carrillo, C.I. Ledesma-Ramírez, H. Mendieta-Zerón, M.Á. Peña Castillo, J.C. Echeverría, J. Rodríguez-Arce, J.J. Reyes-Lagos, Differences in the asymmetry of beat-to-beat fetal heart rate accelerations and decelerations at preterm and term active labor. Sensors **21**(24), 8249 (2021)

29. M.W. Rivolta, T. Stampalija, D. Casati, B.S. Richardson, M.G. Ross, M.G. Frasch, A. Bauer, E. Ferrazzi, R. Sassi, Acceleration and deceleration capacity of fetal heart rate in an in-vivo sheep model. PLoS ONE **9**(8), e104193 (2014)
30. A. Georgieva, C.A. Lear, J.A. Westgate, M. Kasai, E. Miyagi, T. Ikeda, A.J. Gunn, L. Bennet, Deceleration area and capacity during labour-like umbilical cord occlusions identify evolving hypotension: a controlled study in fetal sheep. BJOG **128**, 1433–1442 (2021)
31. M.W. Rivolta, M. Barbieri, T. Stampalija, R. Sassi, M.G. Frasch, Relationship between deceleration morphology and phase rectified signal averaging-based parameters during labor. Front. Med. **25**(8), 626,450 (2021)
32. M.W. Rivolta, M. Biraghi, M. Barbieri, T. Stampalija, R. Sassi, Ranking of different wavelets in the computation of phase-rectified signal averaging for fetal acidemia identification. Comput. Cardiol. **48**, 1–4 (2021)

Fetal Heart Rate Analysis with Gaussian Processes

Guanchao Feng, J. Gerald Quirk, Cassandra Heiselman, and Petar M. Djurić

1 Introduction to Gaussian Processes

Gaussian processes (GPs) provide a flexible and data-efficient Bayesian nonparametric approach to modeling unknown functions and mappings [1]. They were first introduced in geostatistics where they are known as kriging [2]. GPs have shown good performance in many challenging tasks, for example, in human motion modeling [3], or in artifact removal from electroencephalogram (EEG) recordings [4], or for detection of neonatal seizures from EEG signals [5].

Learning latent functions or mappings lies at the core of solving many machine learning tasks. Within the GP framework, we can directly specify a prior distribution for the latent function using a GP, and with a Gaussian likelihood, the posterior of the latent function is also Gaussian, which can be derived conveniently after incorporating the observed data in Bayes' rule. The prior distribution is specified by the mean and covariance function of the GP, which are usually parameterized by hyperparameters. We note that the latent function itself remains nonparametric. This offers great flexibility since it liberates us from assuming a specific analytical form of the latent function, and our prior knowledge is then encoded in the prior distribution.

G. Feng · P. M. Djurić (✉)
Department of Electrical and Computer Engineering, Stony Brook University, Stony Brook, NY, USA
e-mail: Guanchao.Feng@stonybrook.edu; Petar.Djuric@stonybrook.edu

J. Gerald Quirk · C. Heiselman
Department of Obstetrics/Gynecology, Renaissance School of Medicine, Stony Brook University, Stony Brook, NY, USA
e-mail: J.Gerald.Quirk@stonybrookmedicine.edu; Cassandra.Heiselman@stonybrookmedicine.edu

D. Pani (ed.), *Innovative Technologies and Signal Processing in Perinatal Medicine*, https://doi.org/10.1007/978-3-031-32625-7_10

Before we proceed, we briefly describe the notation. Regular small letters refer to scalars, small bold letters denote vectors, and capital bold letters are matrices. The symbol for a Gaussian distribution is $\mathcal{N}(\cdot, \cdot)$, and we write a function f of a vector $\mathbf{x}$ as $f(\mathbf{x})$. The expectation operator is written as $\mathbb{E}$.

1.1 A Brief Review of GP Regression

A GP is a stochastic process with every finite set of its random variables having a multivariate normal distribution [1]. A GP extends a multivariate Gaussian distribution to infinite dimensionality. Therefore, a GP can be seen as a distribution of a real-valued function $f(\mathbf{x})$, where $\mathbf{x}$ denotes the input and is usually a vector. The infinite dimensionality is actually easy to work with, given the marginalization property of multivariate Gaussian distributions. Furthermore, latent functions can be conveniently marginalized out when computing model evidence.

A GP is characterized by its mean function $m(\mathbf{x})$ and a covariance function $k_f(\mathbf{x}_i, \mathbf{x}_i)$, which are defined by $m(\mathbf{x}) = \mathbb{E}[f(\mathbf{x})]$, and $k_f(\mathbf{x}_i, \mathbf{x}_j) = \mathbb{E}[(f(\mathbf{x}_i) - m(\mathbf{x}_i))(f(\mathbf{x}_j) - m(\mathbf{x}_j))]$. To reduce the number of hyperparameters, in practice, a GP is assumed to be zero mean, that is, $m(\mathbf{x}) = 0$ for every $\mathbf{x}$. Furthermore, to preserve the tractability of the marginal likelihood, additive white Gaussian noise is usually adopted for modeling the observation noise, or we write

$$y = y(\mathbf{x}) = f(\mathbf{x}) + \epsilon, \tag{1}$$

where $\epsilon \sim \mathcal{N}(0, \sigma_\epsilon^2)$ is additive white Gaussian noise. The covariance matrix $\mathbf{K}_{ff}$ for training data can be obtained by evaluating the covariance function on $\mathbf{X}$, i.e., $\mathbf{K}_{ff} = \mathbf{k}_f(\mathbf{X}, \mathbf{X})$, where $\mathbf{X} = \{\mathbf{x}_i\}_{i=1}^N$ denotes the collection of all the training inputs. Then, the likelihood of $\mathbf{f}(\mathbf{X})$ is given by

$$p(\mathbf{y}|\mathbf{f}) = \mathcal{N}(\mathbf{y}; \mathbf{f}, \sigma_\epsilon^2 \mathbf{I}), \tag{2}$$

and the prior probability density function of $\mathbf{f}(\mathbf{X})$, which is specified by a GP, can be written as

$$p(\mathbf{f}|\mathbf{X}, \boldsymbol{\theta}) = \mathcal{N}(\mathbf{f}; \mathbf{0}, \mathbf{K}_{ff}), \tag{3}$$

where $\boldsymbol{\theta}$ denotes the set of hyperparameters used for modeling the covariance function.

Training refers to learning model parameters, which include the hyperparameters $\boldsymbol{\theta}$ and the variance of the observation noise σ_ϵ^2 from the training data. The training is carried out by maximizing the marginal likelihood. In practice, we use the logarithm of the marginal likelihood, $\log p(\mathbf{y}|\mathbf{X}, \boldsymbol{\theta})$, as our objective function, where

$$\begin{aligned}\log p(\mathbf{y}|\mathbf{X},\boldsymbol{\theta}) &= \log \mathcal{N}(\mathbf{y};\,\mathbf{0},\;\mathbf{K}_{ff}+\sigma_\epsilon^2\mathbf{I}) \\ &= \log \mathcal{N}(\mathbf{y};\,\mathbf{0},\;\mathbf{K}) \\ &= -\frac{1}{2}\mathbf{y}^T\mathbf{K}^{-1}\mathbf{y}-\frac{1}{2}\log|\mathbf{K}|-\frac{n}{2}\log 2\pi.\end{aligned} \tag{4}$$

In this equation, the last three terms have interpretations. The first one, $-\frac{1}{2}\mathbf{y}^T\mathbf{K}^{-1}\mathbf{y}$, is known as data-fit, which is the only term that involves the observations $\mathbf{y}$. This term measures how well the model explains the data. The second term, $\frac{1}{2}\log|\mathbf{K}|$, is known as penalty for the model complexity, and it depends on both the covariance function and the inputs. The third term, $-\frac{n}{2}\log 2\pi$, is just a normalization constant. The trade-off between data-fit and model complexity is automatic, which means that the tendency of the log marginal likelihood to favor more complex models is counterbalanced by the penalty for additional complexity (i.e., we have Occam's razor principle at play here). It can be shown that the partial derivatives of the log marginal likelihood w.r.t. a hyper-parameter θ_j have the following form [1]:

$$\frac{\partial \log p(\mathbf{y}|\mathbf{X},\boldsymbol{\theta})}{\partial\theta_j}=\frac{\mathbf{y}^\top\mathbf{K}^{-1}\frac{\partial\mathbf{K}}{\partial\theta_j}\mathbf{K}^{-1}\mathbf{y}-\mathrm{tr}\left(\mathbf{K}^{-1}\frac{\partial\mathbf{K}}{\partial\theta_j}\right)}{2}, \tag{5}$$

where $\mathrm{tr}(\cdot)$ stands for the trace of the matrix in the argument of the operator. The model parameters can be tuned by using a gradient-based optimizer.

For the test input $\mathbf{X}_*$, the predictive distribution of the test output, $p(\mathbf{f}_*|\mathbf{X}_*,\mathbf{X},\boldsymbol{\theta})$, will be a Gaussian distribution with a mean and a covariance given by [1]

$$\mathbb{E}(\mathbf{f}_*)=[\mathbf{K}_f(\mathbf{X}_*,\mathbf{X})]\mathbf{K}^{-1}\mathbf{y}, \tag{6}$$

$$cov(\mathbf{f}_*)=\mathbf{K}_f(\mathbf{X}_*,\mathbf{X}_*)-[\mathbf{K}_f(\mathbf{X}_*,\mathbf{X})]\mathbf{K}^{-1}[\mathbf{K}_f(\mathbf{X}_*,\mathbf{X})]^\top. \tag{7}$$

We should note that the prediction is provided by way of a predictive distribution instead of a simple point estimate, which is preferable in many situations, particularly, in decision-making. Since the mode of a Gaussian distribution is the same as its expectation, the mean of a predictive distribution, i.e., $\mathbb{E}(\mathbf{f}_*)$, is also the maximum a posteriori (MAP) estimate.

1.2 The Covariance Function

The covariance function transforms distance or similarity between inputs to covariance between outputs, and therefore, the design of the covariance function is critical in modeling. Perhaps the most widely adopted covariance function is the squared exponential or radial basis function (RBF). Its one-dimensional form is given by

$$k_{RBF}(x_i, x_j) = \sigma_f^2 \exp\left(-\frac{1}{l}(x_i - x_j)^2 \right), \tag{8}$$

where the characteristic length scale $l > 0$ and the signal variance σ_f^2 are its hyperparameters, which are interpretable. In particular, σ_f^2 measures the strength or variability of the corresponding function, whereas l controls the model complexity in that dimension since the input distance is scaled by l. Therefore, if l is small, a small change in the input distance will cause a large change in the covariance of the outputs and vice versa. Equivalently, one can define a relevance weight by $r = \frac{1}{l}$ to measure the importance or relevance of that variable in the modeling. When $\mathbf{x}$ is a vector, we can compute the r values for each variable where, e.g., each variable could be a different feature, and then use the computed weights for feature selection. This is known as automatic relevance determination (ARD) [1] and is used in supervised learning and automatic dimensionality reduction in unsupervised learning [6–8].

Another popular family of covariance functions is the Matérn class of functions. The parameter that defines them is a positive number and is denoted by ν. When ν is half integer, it can be shown that the Matérn covariance functions become simply a product of an exponential and a polynomial. Its one-dimensional form corresponding to $\nu = 3/2$ is as follows:

$$k_{\nu=3/2}(d) = \sigma_f^2 \left(1 + \sqrt{3}d/l\right) \exp\left(-\sqrt{3}d/l\right), \tag{9}$$

where d is the distance between x_i and x_j. The Matérn covariance functions are used to model rough processes.

In general, not every function can be utilized as a valid covariance function. The reason is that the entries of the covariance matrix are obtained from the covariance function, and a valid covariance matrix must be positive semidefinite (PSD). We point out that new covariance functions can be obtained by summation and multiplication of valid covariance functions. More information on the designing of covariance functions can be found in [1].

2 Introduction to Deep Gaussian Processes

The general GP framework has two stiff limitations, high computational cost and the assumption of joint Gaussianity of the output and the function. The high computational cost, which is $O(N^3)$, comes from the need of finding the inverse of $\mathbf{K} \in \mathbb{R}^{N \times N}$, as shown in (6). This renders applying the plain version of GP on any dataset with a few thousand training examples impractical. A common approach to alleviate the high computational complexity is by way of using sparse GPs. The approach is based on reducing the rank of the covariance matrix. Popular methods include the Deterministic Training Conditional (DTC) approximation [9]

and the Fully Independent Training Conditional (FITC) approximation [10]. The underlying idea is to introduce a small set of inducing points whose locations need to be optimized. Another approach is to approximate the covariance function with a finite Fourier series [11, 12]. Although the joint Gaussianity in the definition of a GP allows us to conveniently marginalize out $\mathbf{f}$, as shown in (4), it limits the expressiveness of the model. When the ground truth does not fit the joint Gaussianity assumption, the variance of the data will be mainly explained by the variance of the noise.

It turns out that the two limitations of the GPs mentioned above can readily be addressed. As pointed out, the computational cost can be reduced by using a small set of pseudo-input and output pairs, which are known as inducing points. On the other hand, the joint Gaussianity limitation can be overcome by using multiple GPs in hierarchical settings known as deep Gaussian processes (DGPs). The settings introduce nonlinear mappings that will not preserve Gaussianity. However, the challenge in DGPs is that, without joint Gaussianity, the latent function cannot easily be marginalized out, and thus, the log marginal likelihood is intractable.

The DGPs were first introduced in [13], and the intractability was addressed by utilizing inducing points within a variational framework for deriving tractable evidence lower bound, which could be used as an objective function for learning. Since the number of inducing points is usually less than the available training data points and their locations are optimized to be more informative about the training data, the computational cost after training is effectively reduced. The inducing points can also be further optionally marginalized out so that the model can be more robust to over-fitting. In our work, we also adopt this inference framework of DGPs. Many efforts have been made for improving the inference of DGPs, e.g., in [14], the posterior is learned using stochastic gradient Hamiltonian Monte Carlo to better accommodate the possible multi-modal distributions. In [15], the relationship between rates of convergence and the selection of inducing points were discussed.

Essentially, DGPs can be seen as function compositions, similar to deep neural networks. In [16], the equivalence between infinitely wide deep networks and GPs was derived. Therefore, DGPs can be regarded as a generalization of deep neural networks [17], but with more attractive features compared to deep neural networks. For instance, the nonlinearity in deep neural networks is implemented using activation functions with assumed analytical form, whereas in DGPs the nonlinearity is governed by GPs which are more principled. The dimensionality reduction across layers in DGPs is automatically controlled by ARD weights instead of relying on pooling layers. More importantly, the DGPs are capable of propagating and quantifying uncertainties through each layer. Finally, unlike deep neural networks that are often "data hungry," the DGPs are robust to data scarcity [18].

The general form of DGPs is shown in Fig. 1, where $\mathbf{Y} \in \mathbb{R}^{N \times d_y}$ represents observations that are the output of the network. The symbol N is the number of observation vectors and d_y is the dimension of the vectors $\mathbf{y}_n$. The matrices $\{\mathbf{X}_h\}_{h=1}^{H-1} \in \mathbb{R}^{N \times d_x}$ are intermediate latent variables whose dimensions $\{d_h\}_{h=1}^{H-1}$

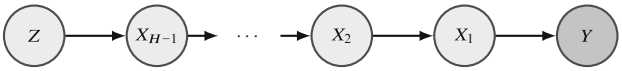

Fig. 1 The general form of DGPs. The arrows represent GPs

are potentially different. Finally, the variable $\mathbf{Z} \in \mathbb{R}^{N \times d_z}$ is the input to the network that may be observed or not observed. For unsupervised learning, $\mathbf{Z}$ is not observed, and the prior distribution of $\mathbf{Z}$ is assumed to be $p(\mathbf{Z}) = \mathcal{N}(\mathbf{Z}|\mathbf{0}, \mathbf{I})$. Conversely, for supervised learning, $\mathbf{Z}$ is known and used to constrain the latent spaces of the DGP. In our work, we rely on the RBF covariance function for all the GPs of the DGPs. A detailed description of the inference process is provided in [13].

3 Open Access Intrapartum CTG Database

Before we introduce applications of GPs in solving tasks in FHR analysis, we briefly describe the open access intrapartum CTG database, which we used for all our experiments. Unlike communities such as computer vision and natural language processing where large databases with labels are available for research purposes, in computerized FHR analysis, the largest and most frequently adopted open access intrapartum CTG database is the CTU-UHB database. The data were collected and anonymized at the University Hospital in Brno (UHB) and de-identified at the Czech Technical University (CTU). The CTU-UHB database contains 552 CTG recordings, which were selected from 9164 intrapartum recordings with clinical as well as technical considerations in mind. Both FHR and UA signals were sampled at 4Hz. Birth outcomes such as Apgar score and umbilical artery pH at birth are also available for each fetus. Full description of the database and selection criteria are available in [19].

4 Application I: Estimation of Missing Samples in Fetal Heart Rate Recordings

Electronic Fetal Monitoring (EFM) is predominantly utilized for assessing fetal status immediately preceding or during labor through the use of CTG for monitoring FHR and UA simultaneously. Changes in FHR are recorded via Doppler ultrasound (external) or direct fetal ECG measurements (internal) with a fetal scalp electrode, whereas UA is usually monitored externally with a tocodynamometer. External FHR monitoring is more popular since it is non-invasive and is very suitable for continuous or intermittent monitoring. However, it is more prone to signal loss, for instance, due to fetal or maternal movements and misplaced electrodes [20, 21]. Empirically, the percentage of missing samples in FHR recordings varies from

0–40% for external ultrasound measurements and 0–10% for internal direct fetal ECG measurements [22]. Clinicians may tolerate such high percentages of missing samples in FHR as their assessments are mainly focused on morphological features and their visual perception is robust to loss of samples. However, the distortion introduced by missing FHR samples can cause serious problems in computerized analysis if not properly handled since such distortion affects the features extracted from FHR. For example, in [22], the authors investigated the stability of several popular short-term variability (STV) and long-term variability (LTV) features when 0–50% missing samples were randomly selected in a 5-minute FHR segment. These missing samples were then linearly interpolated before computing the features. Their results indicated that the values of many features have changed considerably.

In feature-based computerized FHR analysis, the original FHR tracing is completely described by the extracted features. This means the missing samples introduce some additional uncertainties into the model. We notice that there are still no guidelines or standards on what percentage of missing samples will disqualify an FHR recording from visual inspection or from computerized analysis.

In the suppression of distortions in computerized FHR analysis, the first step is usually pre-processing. Its aim is improving the quality of FHR recordings. This often involves artifacts removal (a popular algorithm is described in [23]), interpolation, and gap treatments. More specifically, in practice, small segments of missing samples are interpolated using linear or cubic spline interpolation, while bigger segments, for example, segments of a duration of 15 seconds or more, are often entirely removed [24]. In the literature, the estimation of missing FHR samples is addressed using methods based on sparse representation and dictionary learning, where the sparse coding step and dictionary update step are applied in an alternating fashion until convergence [20, 25]. However, such methods usually exploit linear transformations, while the underlying relationship may be better modeled by nonlinear transformations. More importantly, they are not able to provide estimation results within a probabilistic framework. Instead, they produce only point estimates of the missing samples, i.e., the uncertainty of the estimates is not captured and quantified. Furthermore, these methods only focus on FHR tracings although their corresponding UA tracings are often available as an additional source of information.

4.1 GP-Based Recovery of Missing FHR Samples

In this section, we describe a GP-based approach for estimating missing samples in FHR recordings. Our approach is capable of (i) capturing and quantifying uncertainty in modeling and (ii) incorporating information from other intrapartum signals such as uterine activity and maternal heart rate when they are available. Particularly, let y_i denote the ith sample of the FHR recording y, and suppose we model the value of y_i as a function of time and its synchronized UA sample (i.e., u_i), with additive Gaussian white noise, i.e.,

$$y_i = f(\mathbf{x}_i) = f\left([i, u_i]^\top\right) + \epsilon_i, \tag{10}$$

where $\mathbf{x}_i = [i, u_i]^\top$ is a two-dimensional vector and $\epsilon_i \sim \mathcal{N}(0, \sigma_\epsilon^2)$ is Gaussian white noise. The intuition is that if a missing FHR sample is located far away (in time) from the observed FHR samples in a recording, such observed samples contain very limited information about that missing sample, whereas its nearby UA and MHR samples may contain important information about its true value.

Our goal is to learn the latent function f in (10), and we assign a GP with zero mean and covariance function $k_f\left(\mathbf{x}_i, \mathbf{x}_j\right)$ to govern the latent function f, i.e., $f \sim \mathrm{GP}\left(0, k_f\left(\mathbf{x}_i, \mathbf{x}_j\right)\right)$. We design the covariance function $k_f\left(\mathbf{x}_i, \mathbf{x}_j\right)$ as a sum of an RBF covariance function, a Matérn covariance function (with $\nu = 3/2$), and a linear covariance function:

$$\begin{aligned} k_f(\mathbf{x}_i, \mathbf{x}_j) = {\alpha_1}^2 & \left[1 + \sqrt{3}\left[(\mathbf{x}_i - \mathbf{x}_j)^\top \Lambda_1 (\mathbf{x}_i - \mathbf{x}_j)\right]^{\frac{1}{2}}\right] \\ & \times \exp\left[-\sqrt{3}\left[(\mathbf{x}_i - \mathbf{x}_j)^\top \Lambda_1 (\mathbf{x}_i - \mathbf{x}_j)\right]^{\frac{1}{2}}\right] \\ & + {\alpha_2}^2 \exp\left[-\frac{1}{2}\left[(\mathbf{x}_i - \mathbf{x}_j)^\top \Lambda_2 (\mathbf{x}_i - \mathbf{x}_j)\right]^{\frac{1}{2}}\right] \\ & + \left[(\mathbf{x}_i)^\top \Lambda_3 (\mathbf{x}_j)\right], \end{aligned} \tag{11}$$

where $\Lambda_1 = \begin{pmatrix} \beta_1 & 0 \\ 0 & \beta_2 \end{pmatrix}$, $\Lambda_2 = \begin{pmatrix} \beta_3 & 0 \\ 0 & \beta_4 \end{pmatrix}$, and $\Lambda_3 = \begin{pmatrix} \beta_5 & 0 \\ 0 & \beta_6 \end{pmatrix}$ are diagonal matrices. The assumption behind this design is that FHR signals can be decomposed into three components: a slow varying (low frequency) component that can be modeled by the RBF covariance function, a rapid varying (high frequency) component that can be modeled by the Matérn covariance function, and finally, a linear component that can be expressed by a linear covariance function. We observe that this model is flexible. When u_i is not available, we can simply remove it from $\mathbf{x}_i$. When a synchronized MHR sample is also available, it can be added to $\mathbf{x}_i$. This will not affect the general form of the covariance function in (11); we only need to adjust the number of hyperparameters accordingly.

For inference, the hyperparameters can be learned from (4) and (5). For a new test input, we use the mean of the predictive distribution in (6) (i.e., the MAP estimate) as the recovered value. The variance of the predictive distribution given by (7) quantifies the uncertainty of that value.

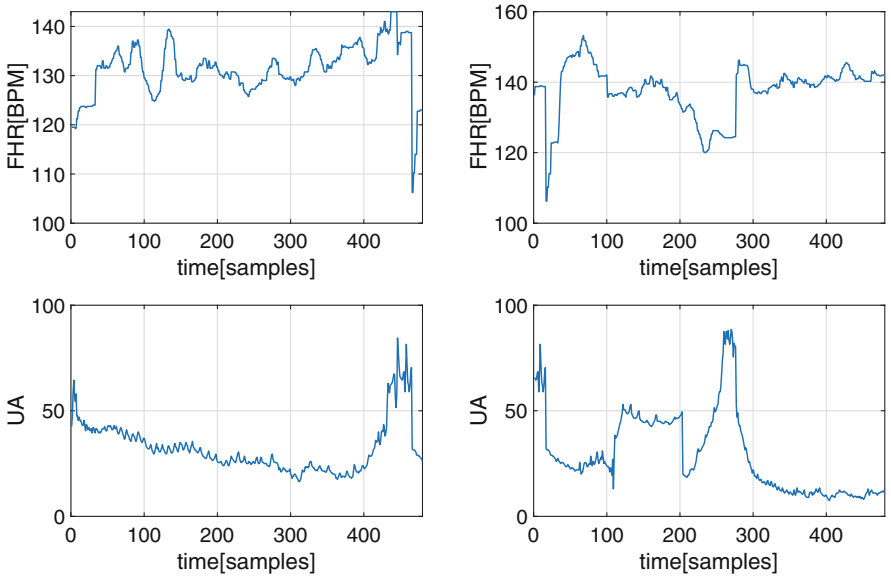

Fig. 2 The CTG segments used in the experiments of estimating missing samples in FHR. Both segments have 480 samples (2 min) of FHR and UA signals

4.2 Experiments and Results

We tested the GP-based approach on two short segments of a CTG recording from the aforementioned CTU-UHB database. The segments had 480 samples (2 min, since the sampling rate for both FHR and UA is 4Hz), as shown in Fig. 2. In these CTG segments, both FHR and UA signals are intact, i.e., they do not have missing samples, which allows us to evaluate the performance accurately. For comparison purposes, we additionally included cubic spline interpolation as a benchmark method as it is widely applied in practice. The recovery performance was measured by the mean squared error (MSE) in logarithmic scale and the signal-to-noise ratio (SNR), which are defined by

$$\text{Log MSE} = \log_e \left(\frac{\left\| \mathbf{s} - \hat{\mathbf{s}} \right\|^2}{N} \right), \tag{12}$$

and

$$\text{SNR} = 10 \log_{10} \left(\frac{\|\mathbf{s}\|^2}{\left\| \mathbf{s} - \hat{\mathbf{s}} \right\|^2} \right), \tag{13}$$

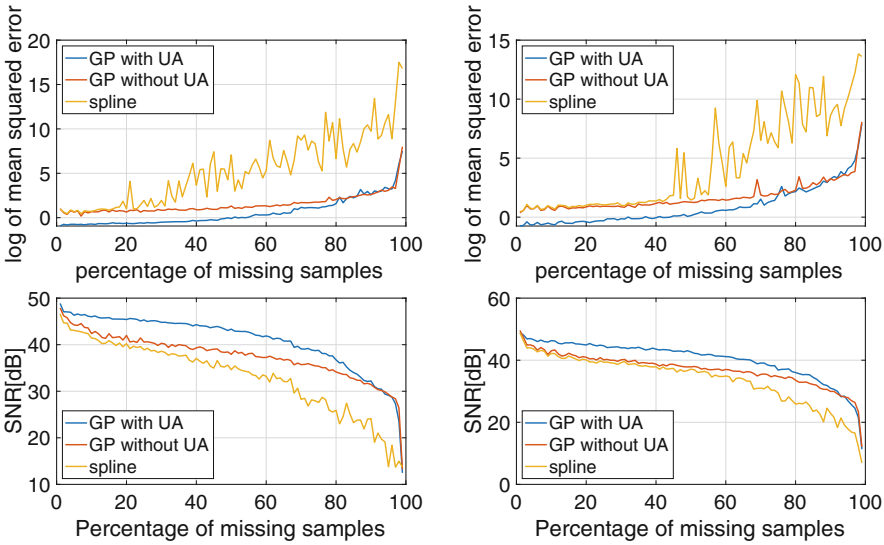

Fig. 3 The experimental results for the first CTG segment (left-hand side of Fig. 2), and the experiment results for the second CTG segment (right-hand side of Fig. 2). The MSE (upper plot, in logarithmic scale) and SNR (bottom plot) of each method under different percentages of missing samples are presented. The results were obtained by averaging over 100 experiments

where N is the number of missing samples, $\mathbf{s}$ is the ground truth, and $\hat{\mathbf{s}}$ is the reconstructed signal.

In this experiment, we evaluated the performance of our method by investigating the recovery performance with respect to different percentages of missing samples, which ranged from 1% to 99% with a step size of 1% on both CTG segments. To model the missing samples of the FHR signal, for each percentage, the missing samples were randomly selected and then set to zero. Finally, the experiment was repeated 100 times and the performance metrics were averaged over 100 results. The recovery results for both CTG segments are shown in Fig. 3 from which we can see that (1) incorporating UA signals can improve the accuracy of the estimates of the missing samples of the FHR signals because the UA signals also contain information on the fetal well-being and (2) the GP-based method consistently outperformed the cubic spline interpolation. Because MHR signals are not available in the CTU-UHB database, we were not able to incorporate MHR in our experiments. It is reasonable to believe that incorporating MHR signals will further improve the recovery performance.

Finally, we point out that the time instants of the missing samples were assumed to have a uniform distribution. However, in reality, the missing samples are more likely to occur in a consecutive manner, i.e., in the form of bursts. In the CTU-UHB database, we observe that the most frequently occurring gap length or burst length (i.e., the number of consecutive missing samples) is 5 samples (1.25 s). Estimating consecutive missing samples in long bursts is challenging and the results are often unreliable.

5 Application II: Classification of Fetal Heart Rate Recordings

During labor, a fetus can be deprived of adequate levels of oxygen and can become hypoxic and acidotic. If the oxygen supply drops below a certain threshold, asphyxia occurs, and this can lead to permanent brain damage or even death of the fetus/newborn. The current gold standard for labeling the FHR recordings in computerized analysis is using pH value of umbilical cord blood at birth, since umbilical cord blood acid-base alterations may be associated with subsequent adverse outcome events for neonates [26–28]. Therefore, many efforts have been made in developing machine learning methods for pH-based FHR recording classification [28]. In this section, we describe a DGP-based FHR classification method.

5.1 CTG Features

Although in the literature many FHR classification methods only focus on FHR signals, we additionally adopted features extracted from the corresponding UA signals instead of only using features from FHR signals. Particularly, we extracted 14 FHR features and 6 UA features from the last 30 minutes of the CTG signals. Our FHR features are summarized in Table 1. They can be categorized into three groups: time domain, nonlinear, and frequency domain features [29].

The 14 FHR features are from different domains, and they are summarized in Table 1. In addition to classical heart rate variability measurements comprised of short-term irregularity (STI), long-term irregularity (LTI), short-term variability (STV), and long-term variability (LTV) [30], we also used nonlinear features, the Poincaré plot (SD1 and SD2) [31], and the complex correlation measurement (CCM) [32]. To extract frequency domain FHR features, we chose the definitions of frequency bands from [33], particularly, very low frequency (VLF: 0–0.06 Hz), low frequency (LF: 0.06–0.3 Hz), medium frequency (MF: 0.3–1 Hz), and high frequency (LF: 1–2 Hz). The frequency domain features are energy in each band and the ratio of energies defined by LF/(MF+HF).

The information in the UA signals is characterized by 6 binary UA features (i.e., having values of either 0 or 1) proposed in [34]. They are summarized in Table 2.

Table 1 Features for FHR

Category	Feature
Time domain	Mean, standard deviation, STV, STI, LTV, LTI
Nonlinear	Poincaré SD1, Poincaré SD2, CCM
Frequency domain	VLF, LF, MF, HF, $\frac{\text{LF}}{\text{MF+HF}}$

Table 2 Features for UA

	Normal (0)	Abnormal (1)
Frequency	≤8 contractions	> 8 uterine contractions (tachysystole)
Duration	< 90s	> 90s
Increased tonus	With toco	Prolonged > 120s
Interval A	Interval—peak to peak	< 2min
Interval B	Interval—offset of UC to onset of next UC	< 1min
Rest time	> 50%	< 50%

The pH value of umbilical cord blood can change over time and is only measured at birth. From this point of view, the FHR and UA signals near birth time are more informative. However, the signal quality also deteriorates noticeably near birth time, e.g., there is a large amount of missing samples in both FHR and UA signals.

5.2 Labeling of CTG Recordings

There is no consensus on the cut-off value or threshold of pH value to define normal and abnormal groups in pH-based FHR analysis. For instance, in [35, 36], the cut-off value of pH was fixed at 7.2, in [37] a cut-off pH value of 7.05 was used, and in [38], the cut-off pH value was set to 7.15. In [39], the authors studied 51,519 deliveries within the Oxford Radcliffe Hospital NHS Trust between 1991 and 2009 and reported that the median arterial pH was 7.22 and that the absolute risk of an adverse neurological outcome was significantly increased when pH was below 7.1. In our work, the criteria of umbilical blood pH for the negative (normal) class and positive (abnormal) class are pH $\geq$ 7.2 and pH $\leq$ 7.1, respectively. In the CTU-UHB database, this labeling scheme provides us with 358 negative cases and 62 positive cases.

5.3 DGP Structure Description

Our DGP network had two layers, and in each layer, we set the initial latent dimension to five. This is because principal component analysis (PCA) reveals that the dimensionality of our feature set can be reduced to five and the fact that the GPs are capable of automatic nonlinear dimensionality reduction. The number of inducing points, in each layer for variational inference, was set to 50, and their locations were learned during the training. The number of inducing points was chosen to be the same as the number of training pairs.

Table 3 pH-based classification results

Classifier	Feature	Specificity	Sensitivity	Geometric mean
SVM	FHR	0.82	0.73	0.77
	FHR+UA	0.82	0.82	0.82
Deep GP	FHR	0.91	0.73	0.82
	FHR+UA	0.82	0.91	0.86

5.4 Experiments and Results

For training, we randomly selected 50 positive and 50 negative recordings, and for testing we used the remaining 12 positive recordings and 12 negative recordings randomly selected from the remaining negative recordings. To measure the performance, in addition to sensitivity and specificity, we also computed their geometric mean to account for the imbalanced performance measured by them. Instead of implementing cross-validation, due to the limited number of positive recordings in the highly imbalanced database (below 15%), we repeated our experiment five times and all performance metrics were averaged over the experiments. For benchmarking purposes, we additionally include the performance of a support vector machine (SVM) for comparison. In order to prevent over-fitting, the feature space was reduced using PCA before applying the SVM. The parameters in the SVM as well as the number of principal components were set using grid search to achieve the best performance. The results are summarized in Table 3. It can be seen that the performance of the DGP was consistently better than that of the SVM and was further improved by additionally incorporating the features extracted from UA recordings.

6 Application III: Clustering of Fetal Heart Rate Recordings

We have pointed out the wide use of the umbilical cord blood pH value at birth for labeling FHR recordings. Indeed, most of the studies of FHR define abnormality by pH value solely, while some do combine other fetal outcome measures with the pH value. However, there has been a controversy regarding the validity of this labeling approach due to its weak correlation with FHR patterns. Besides, no consensus has yet been reached regarding the threshold between healthy and pathological fetuses. To address these challenges, unsupervised learning is a promising direction as it is able to help discover patterns and characteristics that can be used to categorize FHR recordings.

In this section, we present DGP-based unsupervised learning for FHR recordings, particularly, DGP-based clustering of FHR recordings with manifold learning. Instead of using features, we directly work with raw FHR recordings and simply treat each time instant as a dimension in the feature vector. We assume that the

FHR recordings are generated by their low-dimensional manifolds, and our goal is to learn their manifolds using DGP. The intuition is that the resulting low-dimensional manifold is more informative and easy to work with, because distance measures, e.g., Euclidean distance, in low dimensions are usually better for machine learning purposes than those in high dimensions. Because of the FHR signal quality deterioration when approaching the time of delivery, in the experiments we processed the first 30 minutes (7200 samples) of the recordings.

6.1 Labeling

Although labels are not needed in unsupervised learning, they are required for proper evaluation and interpretation of the learning results. Since, the pH-based labeling is controversial and the assessment provided by obstetricians suffers from high variability, for improved reliability of labeling, we took both labeling approaches into consideration. To be more specific, we only used the FHR recordings with agreement between the pH value-based labeling and that of the obstetricians. Finally, we worked with only 10 FHR recordings for this experiment, where three recordings were labeled as positive (with pH values of 6.97, 6.98, and 7.02), and seven were labeled as negative.

6.2 Implementation Details

The number of layers in the DGP networks for manifold learning was guided by the log-likelihood. Specifically, an extra layer was added if the log-likelihood was improved by incorporating an extra layer. To gradually reduce the dimensions of the latent spaces, we initialized the dimensions of the latent space in the layers as $d_{x_{1:5}} = [6, 5, 5, 4, 3]^T$, i.e., the dimensions of the latent spaces decreased or stayed the same with every additional layer. If more layers were needed, which was guided by the log-likelihood, the initial dimension for the layers after the fifth layer was going to be set to three. The reason was that further reduction of the initial dimension below three could cause severe information loss. The observations were represented by a matrix $\mathbf{Y}$ of size 10×7200, i.e., $\mathbf{Y} \in \mathbb{R}^{10\times 7200}$, where each row of $\mathbf{Y}$ was an observed FHR recording. Compared to DGP networks for classification where the inputs are features, here more layers were added for manifold learning as the information in the raw recordings should be richer than that in the features.

6.3 Experiments and Results

We validated the usefulness of the resulting manifolds by the clustering performance in the latent spaces. As a performance metric for evaluation of the unsupervised learning or clustering, we adopted the number of errors in the latent space for one

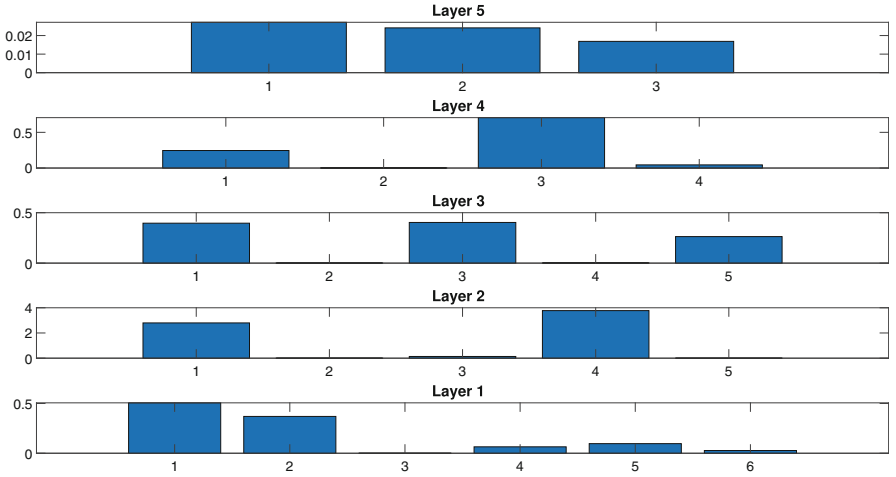

Fig. 4 The relevance weights of each dimension in the various layers. The marks on the abscissa are the indexes of the dimensions and the ordinate shows the relevance weights. The irrelevant dimensions are "switched off" by having very small weights

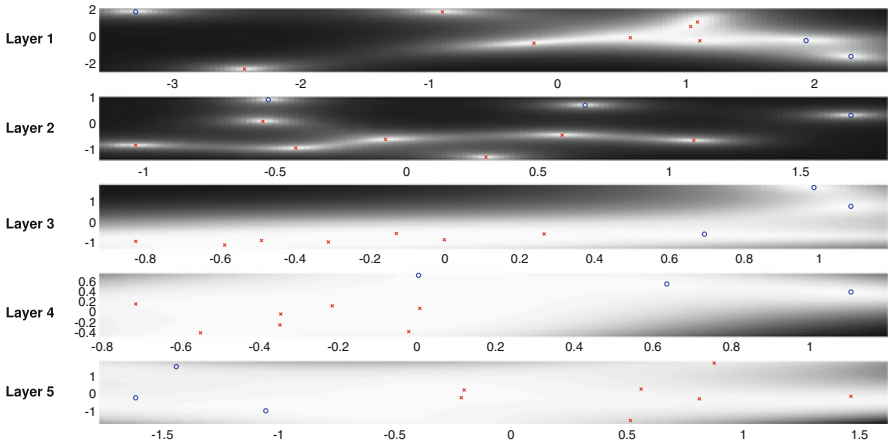

Fig. 5 A 2D projection of the recordings in the latent space from layer 1 (top) to layer 5 (bottom). The normal recordings are shown in red and the abnormal recordings in blue. The total errors for nearest neighbor in layers 1 to 5 were 2, 2, 1, 1, and 0, respectively

nearest neighbor. Ideally, given an FHR recording, its nearest neighbor in the latent space should have the same label. The DGP was capable of learning the importance or relevance of the latent dimensions automatically with the ARD technique, as shown in Fig. 4. The higher the weight assigned to a dimension, the more important that dimension was in the modeling. From Fig. 4, we observe that the number of dominant dimensions in each latent space was two. Therefore, in Fig. 5, we further simplified the model by removing the dimensions except the two most important

dimensions in each layer. The pixel intensity in the background represents the precision as it is inversely proportional to uncertainty. The positive FHR recordings are plotted in blue and the negative FHR recordings are plotted in red. Then, the total number of errors for one nearest neighbor in each layer was computed. Specifically, an error occurred when the closest neighbor of a positive (abnormal) recording was a negative (normal) one and vice versa. The total errors for one nearest neighbor in layers 1 to 5 were 2, 2, 1, 1, and 0, respectively. This indicates that the DGP was capable of separating the positive FHR recordings from the negative ones gradually, also, while the DGP reduced the error from two in the first layer to 0 in the last layer and the uncertainty was also gradually reduced across each layer.

Acknowledgment The authors thank the support of NIH under Award 1RO1HD097188-01.

References

1. C.E. Rasmussen, C.K.I. Williams, *Gaussian Processes for Machine Learning*, vol. 2(3) (The MIT Press, Cambridge, 2006),
2. M.S. Handcock, M.L. Stein, A Bayesian analysis of kriging. Technometrics **35**(4), 403–410 (1993)
3. J.M. Wang, D.J. Fleet, A. Hertzmann, Gaussian process dynamical models for human motion. IEEE Trans. Pattern Anal. Mach. Intell. **30**(2), 283–298 (2008)
4. S. Noorzadeh, B. Rivet, P.-Y. Guméry, An application of Gaussian processes on ocular artifact removal from EEG, in *2015 37th Annual International Conference of the IEEE Engineering in Medicine and Biology Society (EMBC)* (IEEE, 2015), pp. 554–557
5. S. Faul, G. Gregorcic, G. Boylan, W. Marnane, G. Lightbody, S. Connolly, Gaussian process modeling of EEG for the detection of neonatal seizures. IEEE Trans. Biomed. Eng. **54**(12), 2151–2162 (2007)
6. N.D. Lawrence, Gaussian process latent variable models for visualisation of high dimensional data, in *Advances in Neural Information Processing Systems* (2004), pp. 329–336
7. A. Damianou, C. Ek, M. Titsias, N. Lawrence, Manifold relevance determination. Preprint (2012). arXiv:1206.4610
8. A.C. Damianou, M.K. Titsias, N.D. Lawrence, Variational inference for latent variables and uncertain inputs in Gaussian processes. J. Mach. Learn. Res. **17**(1), 1425–1486 (2016)
9. M. Seeger, C. Williams, N. Lawrence, Fast forward selection to speed up sparse Gaussian process regression, in *Artificial Intelligence and Statistics 9*, no. EPFL-CONF-161318, 2003
10. E. Snelson, Z. Ghahramani, Sparse Gaussian processes using pseudo-inputs, in *Advances in Neural Nnformation Processing Systems* (2006), pp. 1257–1264
11. Y. Gal, R. Turner, Improving the Gaussian process sparse spectrum approximation by representing uncertainty in frequency inputs, in *International Conference on Machine Learning* (2015), pp. 655–664
12. T.N. Hoang, Q.M. Hoang, B.K.H. Low, A unifying framework of anytime sparse Gaussian process regression models with stochastic variational inference for big data, in *ICML* (2015), pp. 569–578
13. A. Damianou, N. Lawrence, Deep Gaussian processes, in *Artificial Intelligence and Statistics* (2013), pp. 207–215
14. M. Havasi, J.M. Hernández-Lobato, J.J. Murillo-Fuentes, Inference in deep Gaussian processes using stochastic gradient hamiltonian monte carlo, in *Advances in Neural Information Processing Systems* (2018), pp. 7506–7516

15. D.R. Burt, C.E. Rasmussen, M. Van Der Wilk, Rates of convergence for sparse variational Gaussian process regression. Preprint (2019). arXiv:1903.03571
16. J. Lee, Y. Bahri, R. Novak, S.S. Schoenholz, J. Pennington, J. Sohl-Dickstein, Deep neural networks as Gaussian processes. Preprint (2017). arXiv:1711.00165
17. T. Bui, D. Hernández-Lobato, J. Hernandez-Lobato, Y. Li, R. Turner, Deep Gaussian processes for regression using approximate expectation propagation, in *International Conference on Machine Learning* (2016), pp. 1472–1481
18. A. Damianou, Deep Gaussian processes and variational propagation of uncertainty, PhD dissertation, University of Sheffield, 2015
19. V. Chudáček, J. Spilka, M. Burša, P. Janků, L. Hruban, M. Huptych, L. Lhotská, Open access intrapartum CTG database. BMC Pregnancy Childbirth **14**(1), 16 (2014)
20. V.P. Oikonomou, J. Spilka, C.D. Stylios, L. Lhotská, An adaptive method for the recovery of missing samples from FHR time series, in *CBMS* (2013), pp. 337–342
21. E.W. Abdulhay, R.J. Oweis, A.M. Alhaddad, F.N. Sublaban, M.A. Radwan, H.M. Almasaeed, Review article: non-invasive fetal heart rate monitoring techniques. Biomed. Sci. Eng. **2**(3), 53–67 (2014)
22. J. Spilka, V. Chudáček, M. Burša, L. Zach, M. Huptych, L. Lhotská, P. Janků, L. Hruban, Stability of variability features computed from fetal heart rate with artificially infused missing data, in *Computing in Cardiology (CinC), 2012* (IEEE, 2012), pp. 917–920
23. J. Bernardes, C. Moura, M. de Sa, P. Joaquim, L. Pereira Leite, The Porto system for automated cardiotocographic signal analysis. J. Perinatal Medicine-Official J. WAPM **19**(1–3), 61–65 (1991)
24. J.C. Sprott, J.C. Sprott, *Chaos and Time-Series Analysis*, vol. 69 (Citeseer, 2003)
25. F. Barzideh, J. Urdal, K. Hussein, K. Engan, K. Skretting, P. Mdoe, B. Kamala, S. Brunner, Estimation of missing data in fetal heart rate signals using shift-invariant dictionary, in *2018 26th European Signal Processing Conference (EUSIPCO)* (IEEE, 2018), pp. 762–766
26. N. Wiberg, K. Källén, A. Herbst, P. Olofsson, Relation between umbilical cord blood pH, base deficit, lactate, 5-minute Apgar score and development of hypoxic ischemic encephalopathy. Acta Obstetricia et Gynecologica Scandinavica **89**(10), 1263–1269 (2010)
27. L. Armstrong, B. Stenson, Use of umbilical cord blood gas analysis in the assessment of the newborn. Arch. Dis. Child. Fetal Neonatal Ed. **92**(6), F430–F434 (2007)
28. A. Georgieva, P. Abry, V. Chudáček, P.M. Djurić, M.G. Frasch, R. Kok, C.A. Lear, S.N. Lemmens, I. Nunes, A.T. Papageorghiou et al., Computer-based intrapartum fetal monitoring and beyond: a review of the 2nd workshop on signal processing and monitoring in labor (October 2017, Oxford, UK). Acta Obstetricia et Gynecologica Scandinavica **98**(9), 1207–1217 (2019)
29. J. Spilka, Complex approach to fetal heart rate analysis: a hierarchical classification model, in *Czech Technical University, Faculty of Electrical Engineering, Prague*, pp. 35–47 (2013)
30. J. De Haan, J. Van Bemmel, B. Versteeg, A. Veth, L. Stolte, J. Janssens, T. Eskes, Quantitative evaluation of fetal heart rate patterns: I. Processing methods. Eur. J. Obstet. Gynecol. **1**(3), 95–102 (1971)
31. M.B. Tayel, E.I. AlSaba, Poincaré plot for heart rate variability, in *World Academy of Science, Engineering and Technology, International Journal of Medical, Health, Biomedical, Bioengineering and Pharmaceutical Engineering*, vol. 9(9), pp. 708–711 (2015)
32. C.K. Karmakar, A.H. Khandoker, J. Gubbi, M. Palaniswami, Complex correlation measure: a novel descriptor for poincaré plot. Biomed. Eng. Online **8**(1), 17 (2009)
33. M.G. Signorini, G. Magenes, S. Cerutti, D. Arduini, Linear and nonlinear parameters for the analysisof fetal heart rate signal from cardiotocographic recordings. IEEE Trans. Biomed. Eng. **50**(3), 365–374 (2003)
34. R.D. Eden, M.I. Evans, S.M. Evans, B.S. Schifrin, The "fetal reserve index": re-engineering the interpretation and responses to fetal heart rate patterns. Fetal Diagn. Ther. **43**(2), 90–104 (2018)

35. C. Rotariu, A. Pasarica, H. Costin, D. Nemescu, Spectral analysis of fetal heart rate variability associated with fetal acidosis and base deficit values, in *2014 International Conference on Development and Application Systems (DAS)* (IEEE, 2014), pp. 210–213
36. V. Chudáček, J. Spilka, B. Rubackova, M. Koucky, G. Georgoulas, L. Lhotska, C. Stylios, Evaluation of feature subsets for classification of cardiotocographic recordings, in *2008 Computers in Cardiology* (IEEE, 2008), pp. 845–848
37. A. Illanes, M. Haritopoulos, Fetal heart rate feature extraction from cardiotocographic recordings through autoregressive model's power spectral-and pole-based analysis, in *2015 37th Annual International Conference of the IEEE Engineering in Medicine and Biology Society (EMBC)* (IEEE, 2015), pp. 5842–5845
38. J. Spilka, V. Chudáček, M. Koucký, L. Lhotská, Assessment of non-linear features for intrapartal fetal heart rate classification, in *2009 9th International Conference on Information Technology and Applications in Biomedicine* (IEEE, 2009), pp. 1–4
39. P. Yeh, K. Emary, L. Impey, The relationship between umbilical cord arterial pH and serious adverse neonatal outcome: analysis of 51 519 consecutive validated samples. BJOG Int. J. Obstet. Gynaecol. **119**(7), 824–831 (2012)

Intrapartum Cardiotocography Feature Detection and Fetal State Estimation Using Signal Processing and Machine Learning

Philip A. Warrick

1 Introduction

Although childbirth is a natural process with good outcomes in the vast majority of (developed world) cases, approximately 1–7 in 1000 babies experience sufficient oxygen deprivation in labor to cause death or brain injury in the form of Hypoxic Ischemic Encephalopathy (HIE) [1, 2]. It is estimated that 50% of such injuries are related to preventable medical error and most of these errors are due to incorrect analysis of the fetal heart rate (FHR) [4].

Since its introduction into obstetrical care in the 1960s, the primary objective of intrapartum fetal monitoring using cardiotocography (CTG), also known as Electronic Fetal Monitoring (EFM), has been the prevention of birth-related brain injury. Although it is an indirect measure of fetal O_2 deprivation of tissue (hypoxia), it is a non-invasive modality that has been widely adopted as a clinical standard of care.

However, the subjective interpretation of the clinical guidelines on the use of CTG has led to significant inter- and intra-observer variability [5] and low specificity rates associated with its use. This, coupled with the fear of medico-legal ramifications—Obstetrics and Gynecology is the most litigated specialty—has resulted in significant uncertainty for decision-making among clinicians. This has led to a sharp rise in Cesarean section rates in many countries (see Table 1). The clinical and economic costs of higher section rates are significant in terms of longer recovery times, short- and long-term maternal and fetal complications, and the

P. A. Warrick (✉)
PeriGen Inc., Westmount, QC, Canada

McGill University, Montreal, QC, Canada
e-mail: philip.warrick@perigen.com

D. Pani (ed.), *Innovative Technologies and Signal Processing in Perinatal Medicine*, https://doi.org/10.1007/978-3-031-32625-7_11

Table 1 Cesarean section rates for various regions in 2018

Region	#Countries	CS rate	Source
Latin America/Caribbean	$n = 38$	42.8%	[WHO2021]
USA	$n = 1$	31.9%	[CDC2020]
Canada	$n = 1$	29.1%	[CIHI2020]
EU	$n = 38$	25.7%	[WHO2021]
Asia	$n = 40$	23.1%	[WHO2021]
Africa	$n = 44$	9.2%	[WHO2021]

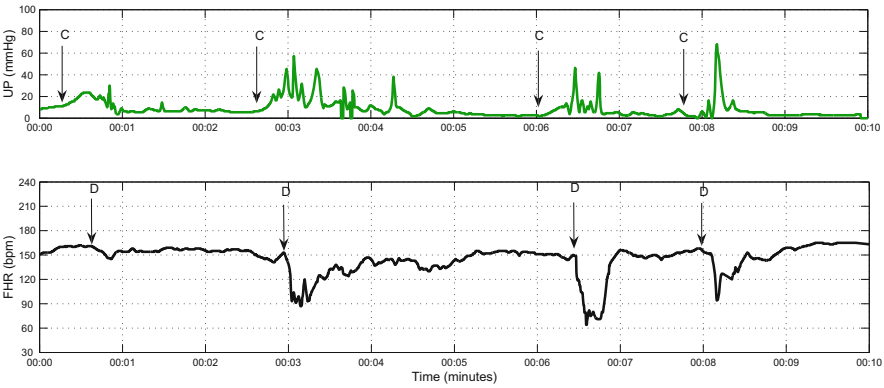

Fig. 1 Uterine pressure (UP, top) and fetal heart rate (FHR, bottom) are routinely monitored (90%) during labor and delivery. Clinicians observe FHR deceleration (indicated by the "D" arrows) intensity, frequency, and timing with respect to UP contractions (indicated by the "C" arrows)

impact on the high-volume medical expenses associated with obstetrical care (80% of women have at least one child).

2 Clinical Cardiotocography

Uterine pressure (UP) and fetal heart rate (FHR) are routinely monitored (approximately 90% of the time) during labor and delivery. As indications of fetal state, clinicians observe FHR deceleration intensity, frequency, and timing with respect to UP contractions (see Fig. 1) as well as FHR accelerations, baseline, and variability (HRV). There are significant signal processing challenges associated with CTG because the signals can be very noisy due to loss of sensor contact and the superposition of maternal heart rate interference.

3 Automated CTG Decision-Making

To provide clinicians with more objective and consistent CTG interpretation, there have been research efforts to automate this analysis. The two main objectives here are (1) the detection of the key CTG patterns that correspond to clinical guidelines and (2) the assessment of the fetal state from the CTG patterns.

The first goal intends to relieve clinical staff from tedious monitoring and highlight truly important features. An example of this analysis for some selected CTG segments is shown in Fig. 2. These approaches combine time-domain signal processing with either conventional machine learning [9, 12–14] or deep learning [11] techniques.

The second goal of assessing the fetal state is more ambitious: could automated CTG interpretation help clinicians intervene at the right time, for the right reasons? Small improvements in sensitivity and specificity could have significant impact on the quality and cost of obstetrical care. The following describes one such approach that combines system identification, auto-regressive, and linear models to model FHR components with a conventional machine learning classifier [15, 16].

4 Fetal State Classification via System Identification (SI)

The first goal of this approach is to model FHR with a desired characterization that encompasses fidelity, parsimony, and dynamics. A good model will accurately describe the underlying physical phenomenon over time with a small number of parameters. In the case of the dual-signal CTG, it will capture the dynamics of the UP and FHR. Figure 3 shows one model, which captures these elements (from

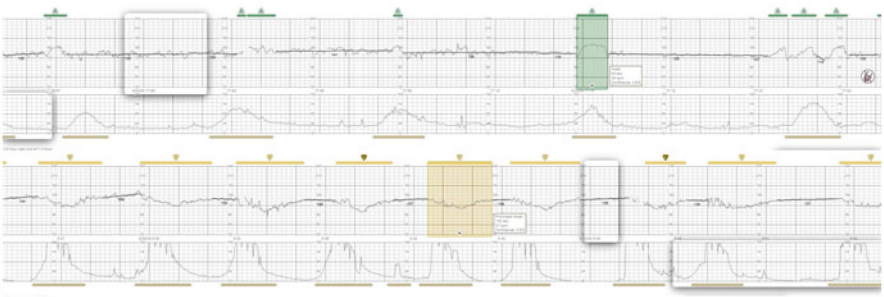

Fig. 2 Results of automated detection of CTG Patterns with PeriGen Patterns software © for two 30-min recording segments, one with accelerations prominent (highlighted in green, top) and the other with decelerations (highlighted in yellow, below). In each case, the UP is below the FHR

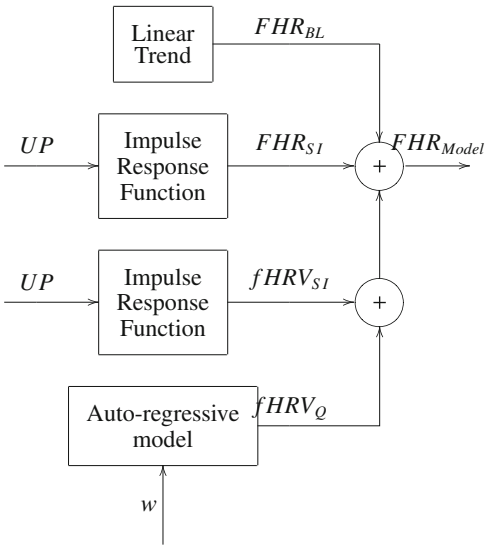

Fig. 3 Model of FHR components. FHR_{BL} models the baseline (cardiac output). FHR_{SI} models the deceleration response to contraction (linear CNS response to cord compression). $fHRV_{SI}$ models heart rate variability response to contraction (nonlinear CNS response to cord compression) and $fHRV_Q$ models the quiescent heart rate variability (background CNS activity)

[10, 16]). This model will be described in more detail below, with emphasis on the system identification model generating the output FHR_{SI}. The linear trend output describing the baseline, FHR_{BL} and the fetal heart rate variability characterization from $fHRV_Q$, will be briefly described. Finally, these features will be used as inputs for an SVM classifier of fetal state.

The data for this modeling effort included CTG intrapartum recordings with the following characteristics:

- Intrapartum recordings, >3 hours
- Birth gestational age > 36 weeks, no known genetic malformations
- Clinical CTG monitor provides:
  - FHR: RR intervals interpolated, regularly sampled at 4Hz
  - UP: sampled at 1Hz
  - Much artifact (sensor dropouts, maternal HR interference)

Each recording was *labelled by outcome* according to arterial umbilical-cord base deficit at birth (BD) and neonatal indications of neurological impairment. This included fetuses in three classes:

- 5429 normal (BD < 8 mmol/L)
- 85 severely pathological (BD ≥ 12 mmol/L with neurological evidence of Hypoxic Ischemic Encephalopathy: HIE)
- 216 metabolic acidosis (BD ≥ 12 mmol/L, Apgar5 < 8, no neurological impairment): “near misses”

4.1 Models

Marmarelis [6] makes a useful distinction between hypothesis-driven modeling, where a priori knowledge or physical equations are explicitly part of the model, and exploratory data-driven modeling. The data-driven system identification model of UP and FHR can be contrasted with a more conventional hypothesis-driven feature extraction modeling approach in the following ways:

– Feature Extraction (hypothesis)
  * Detect UP contractions and FHR decelerations from noisy signals
  * Strength and timing of response measured explicitly as amplitude ratios and time delays
– System Identification (exploration)
  * Models dynamic relationship of UP (input) and FHR (output)
  * Implicitly captures the strength and timing of the FHR response to UP
  * Methodologies incorporate noise reduction (e.g., SVD)
  * Summarizes persistent patterns rather than capturing isolated events

4.2 System Identification: Predicting FHR from UP

The system identification model of Fig. 4 predicts FHR samples from previous UP samples according the following convolution equation:

$$\begin{aligned} f_n &= h * u_n \\ &= h_0 u_n + h_1 u_{n-1} + \ldots + h_{M-1} u_{n-M+1} \end{aligned}$$

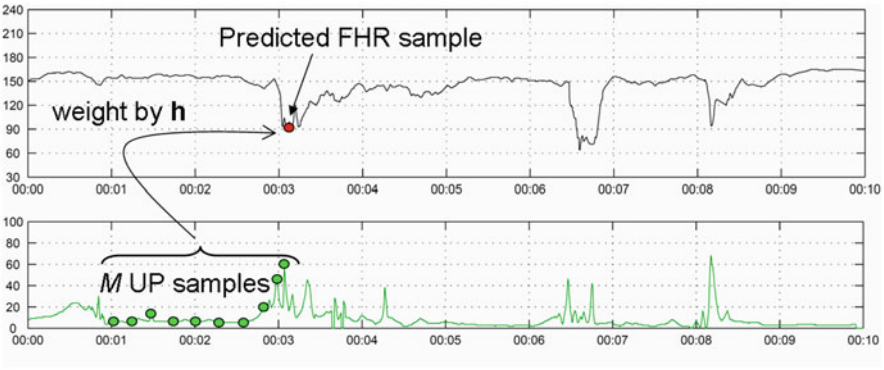

Fig. 4 The system identification model finds coefficients h_i for $i = 0, 1, \ldots, M-1$ that express FHR as a function of last M samples of UP (e.g., $M = 240$ 1s samples)

where u is the input UP signal and f_n is the predicted FHR. The best fit of h_i over a defined epoch (e.g., 20 min) can be obtained by multivariate linear regression, as described in the following section.

System identification is challenging because of several problem hurdles that need to be overcome:

- Clinical data: measurement disturbances are prevalent
- Non-stationarity, so we limit data length (20 min sliding window)
- Ill-posed problem: (uncontrolled) UP input has narrow bandwidth, is not calibrated and is subject to unknown measurement delay

To address these issues, data cleaning, regularization, and validation are required. h is estimated by least-squares and noise reduced using a pseudoinverse.

4.3 UP–FHR Dynamics

To be more precise, the model output FHR f_{SI} is a convolution of impulse response function (IRF) $\mathbf{h}$ and input UP $\mathbf{u}_n$ according to

$$f_{SI}(n) \approx \sum_{i=0}^{M-1} (h_i \Delta t) u_{n-d-i} = \mathbf{h} * \mathbf{u}_n$$

where

- N is the number of samples and $n = \{1, \ldots, N\}$, $N \sim 20$ min
- Δt is the sampling period
- $\mathbf{h}$ is IRF beginning at sample d (*delay*) and of length M (*memory*)
- For causal systems, $d \geq 0$, but in presence of *input measurement delay* (our case), d may be negative

One of many challenges here is that the delay d is a combination of measurement ($-$ve) from the UP sensor and the more physiological (+ve) delays and these two delays are indistinguishable. We are more interested in the more informative physiological delay which can range from 0 to 60s; the measurement delay is a source of noise and can range from 0 to 20s.

4.4 Estimating the IRF $\hat{\mathbf{h}}$

To obtain the multivariate linear regression IRF estimate, we use a least-squares approach. Let the covariance matrix $\mathbf{U}$ of the input be an $N \times M$ Toeplitz matrix formed from M-length lagged versions of the input $\mathbf{u}_n$. The least-squares solution to determine the IRF estimate $\hat{\mathbf{h}}$ is given by

$$\begin{aligned}\hat{\mathbf{h}} &= (\mathbf{U}^T\mathbf{U})^{-1}\mathbf{U}^T\mathbf{f} \\ &\approx \boldsymbol{\Phi_{uu}}^{-1}\boldsymbol{\phi_{uf}},\ (N \sim 20\ \mathsf{min} \gg M)\end{aligned}$$

A pseudoinverse to replace $(\mathbf{U}^T\mathbf{U})^{-1}$ is required for noise suppression because the input UP is narrowband, making the problem ill-posed numerically. We compute this pseudoinverse $\mathbf{V}\mathbf{S}^{-1}\mathbf{V}^T$ by the singular value decomposition (SVD) of $(\mathbf{U}^T\mathbf{U})^{-1}$:

$$\begin{aligned}\hat{\mathbf{h}} &= \underbrace{(\mathbf{U}^T\mathbf{U})^{-1}}_{\mathbf{V}\mathbf{S}^{-1}\mathbf{V}^T}\mathbf{U}^T\mathbf{f} \\ &\cdots \\ &\approx \sum_{i=1}^{k}\hat{\mathbf{h}}_i\end{aligned} \tag{1}$$

where $k < M$ retained eigenvectors from SVD are chosen by minimum description length (MDL). The MDL criterion for model selection favors both fidelity and parsimony, two of our design objectives.

4.5 State-Space IRF Estimate

An alternative formulation for the impulse response function that is more amenable to signal gaps, which are common in CTG signals, can be derived from the state-space equations:

$$\begin{aligned}x(k+1) &= Ax(k) + Bu(k) + Ke(k) \\ f(k) &= Cx(k) + Du(k) + e(k)\end{aligned}$$

where

- $u(k)$ and $y(k)$ are the UP input and FHR output
- $x(k)$ is the inferred state
- $e(k)$ is a white noise sequence (the innovation)
- A, B, C, D, and K are estimated by Past Outputs Multivariable Output Error State-Space (PO-MOESP) subspace identification [8].

The PO-MOESP estimation of system matrices and state vectors is obtained as follows:

- For each continuous segment:
  - QR factorization of input–output Hankel matrices

$$[R'_{23}\, U_f\, U_p\, Y_p\, Y_f] = [Q_1\, Q_2\, Q_3] \begin{bmatrix} R_{11} & R_{12} & R_{13} \\ 0 & R_{22} & R_{23} \\ 0 & 0 & R_{33} \end{bmatrix} \tag{2}$$

  - After SVD, keep only state-dimension $p = 2$ "significant" eigenvectors

$$R_{23} = U_{SVD}\, \Sigma\, V_{SVD}^T$$

- Using U_{SVD}, we can obtain matrices A and C. Then, by linear regression, B, D, and initial condition $x(0)$ can be calculated. Finally, by iterating the state-space equations, we obtain the state vectors $x(1), x(2), \ldots, x(n)$.

Given these state-space matrices and state-space vector we can calculate an indirect IRF estimation as follows:

$$\hat{h}(k) = \begin{cases} 0 & k < d \\ D & k = d \\ CA^{k-1}B & k = d+1, d+2, \ldots, d+M-1 \end{cases}$$

Notice that there is no need for length M continuity as before. Rather, the required continuity is controlled by the subspace scale parameter s ($<< M$). We can choose s from 2^j, $j = 3, 4, \ldots 7$, to obtain multiresolution responses. We choose delay d as in the least-squares case by shifting input/output and selecting the best model.

4.6 Model Significance Through Surrogate Data

This modeling elicits the question as to whether the model has captured system dynamics or is only fitting noise. To address this, we apply the following assumption: a model is trustworthy if its fidelity with original FHR $\gg$ that with generated surrogate FHR. Surrogates can be generated by several approaches, but the simplest is that of amplitude adjusted Fourier Transform (AAFT) [7]. The significance is determined as follows: compute the variance accounted for (VAF) of original and 99 surrogate outputs. VAF is defined as

$$\%\text{VAF} = 100 \times \left(1 - \frac{\sigma_e^2}{\sigma_f^2}\right) \tag{3}$$

where σ_e^2 and σ_f^2 are the variances of the residual error and observed signals, respectively; lower residual energy corresponds to higher VAFs and better models. The model is accepted if the original measured FHR has a model with VAF in the top 5th percentile. Therefore, the probability that, by chance, the original has K-th largest VAF is $\alpha = \frac{K}{M+1}$. Then, one can assign the model significance level $\gamma = 1 - \alpha$ (e.g., choose $M = 99$ for a significance level of $\gamma = 95\%$).

4.7 Baseline and HRV Estimates

FHR was detrended by high-pass filter with cutoff frequency 30 mHz, corresponding to the lower limit of the LF band of fetal HRV. FHR baseline was determined by a linear fit. Fetal HRV f_{HRV} was modeled as the output of an auto-regressive (AR) model given some unknown Gaussian white input noise v [3].

4.8 Resulting Models

4.8.1 Models

Figures 5 and 6 show sample IRF models for a normal and pathological fetus for a single 20-min epoch. Figure 7 shows these models again over time, that is, in the last two hours of labor and delivery. Figure 8 shows an estimated FHR baseline. Figure 9 shows the fetal HRV in terms of the power spectral density across the LF, MF, and HF bands.

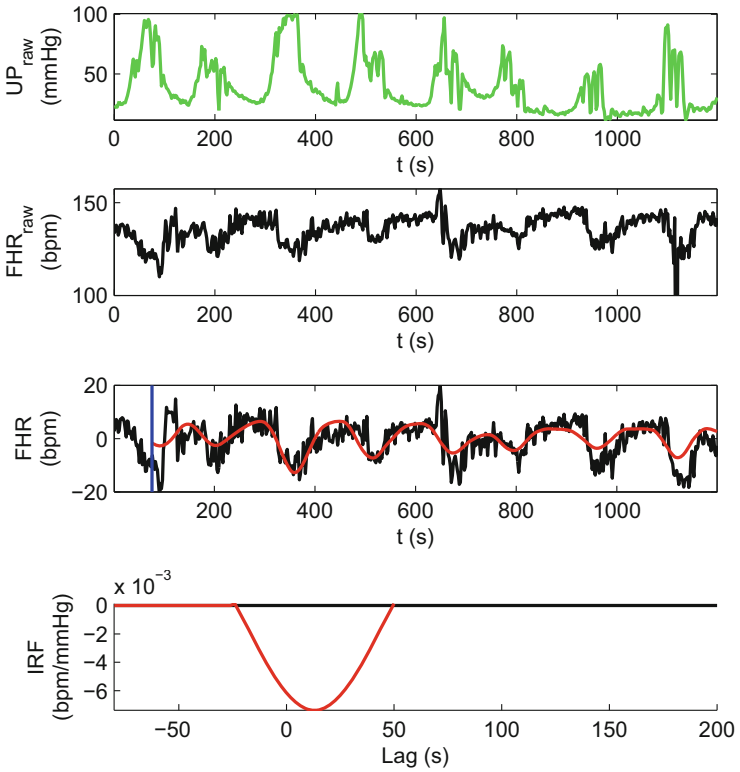

Fig. 5 Example IRF: Normal case. From [15]

4.8.2 Classification

Figure 10 shows the predictions of an SVM classifier using the model parameters IRF gain (the sum of the IRF coefficients) and d, the delay, to discriminate normal from pathological fetuses from the CTG during labor. Training data are labeled by green (normal) and red (pathological) circles. The classifier decision function $\mathcal{H}$ is indicated by turquoise ($\mathcal{H} < 0$, normal) and gold ($\mathcal{H} > 0$, pathological) regions separated by solid white lines ($\mathcal{H} = 0$). Most of the support vectors (684 of 1499 training samples, outlined in black) lie the two regions between the contours $\mathcal{H} = \pm 1$ (dotted white lines), where classification is less certain. The trajectory highlighted by a solid red line is a non-training pathological case whose classification transitions from normal to pathological. The arrows indicate increasing time.

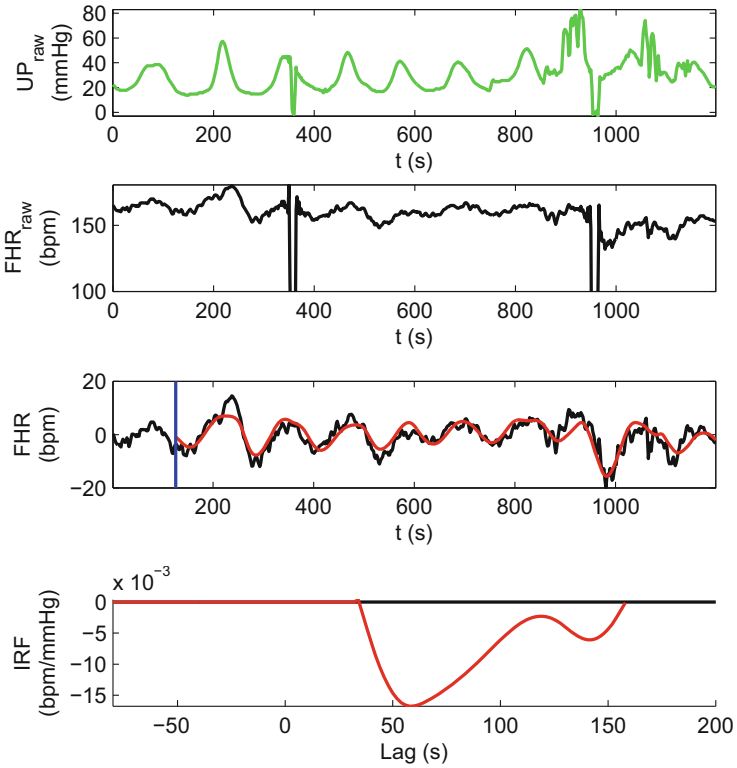

Fig. 6 Example IRF: Pathological case. From [15]

5 Conclusions

This chapter describes the motivation for clinical CTG and selected automated methods of interpretation that are being developed to overcome the known limitations of visual interpretation of clinical CTG. A data-driven approach that decomposes the fetal heart rate into key constitutive components is explained. Derived features from this decomposition are used in a classifier of fetal state using clinical outcome data.

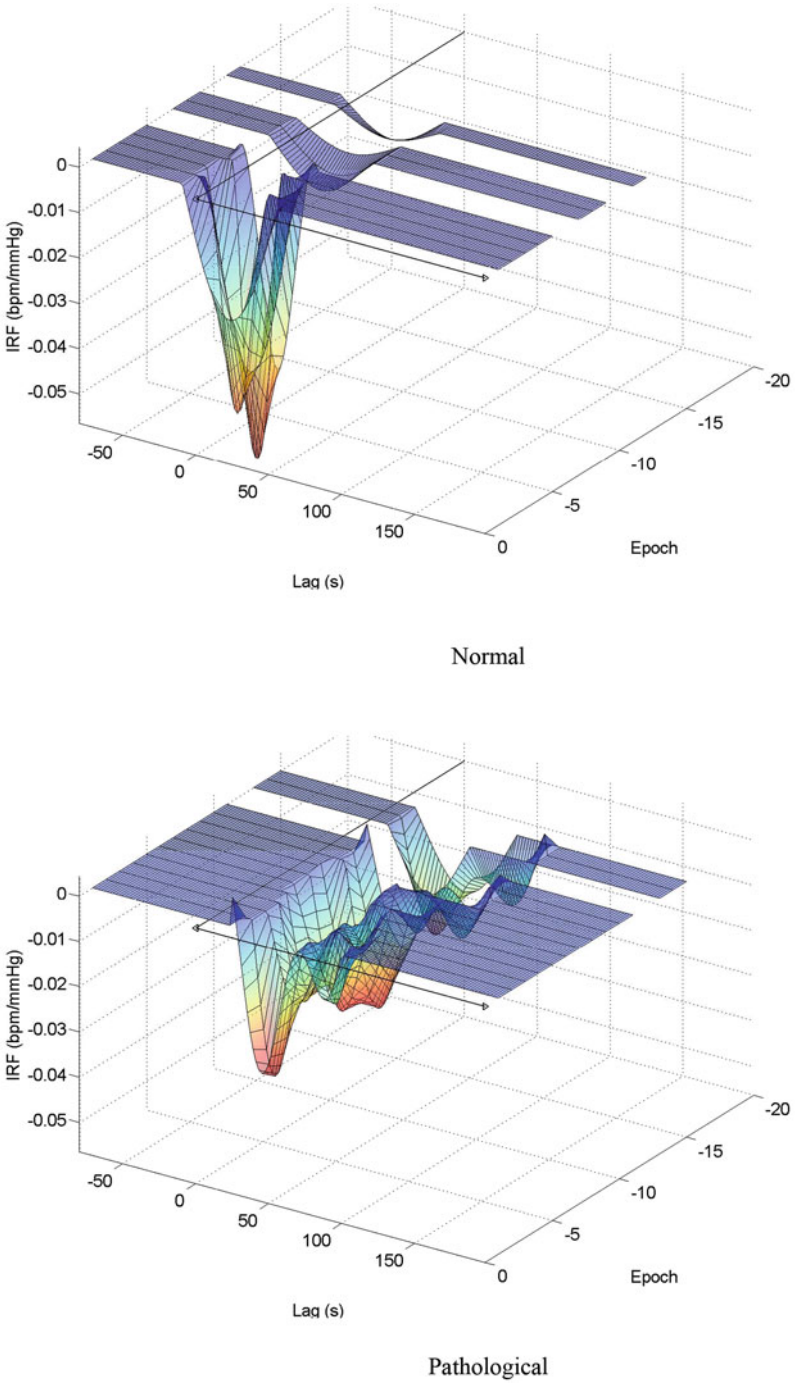

Fig. 7 Example IRFs over time. From [15]

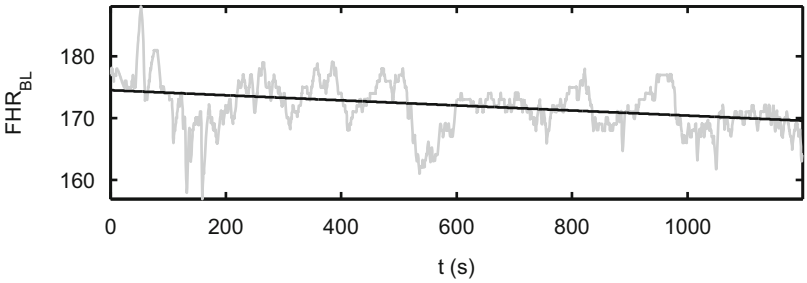

Fig. 8 Estimated baseline f_{BL} by performing linear fit of the filtered FHR, characterized by offset and slope. From [16]

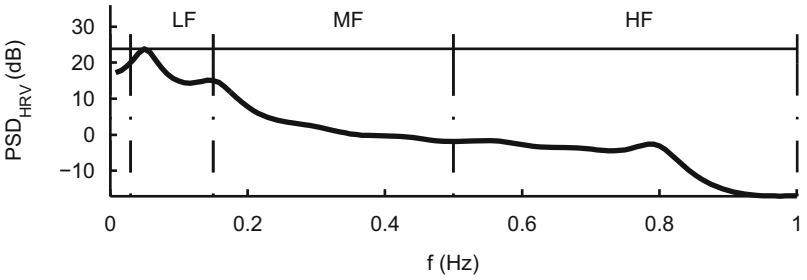

Fig. 9 Power spectral densities (PSD) of HRV auto-regressive models computed for bands LF (30–150 mHz, neural sympathetic and parasympathetic fetal activity), MF (150–500 mHz, fetal movement) and HF (0.5–1.0 Hz, fetal breathing). From [16]

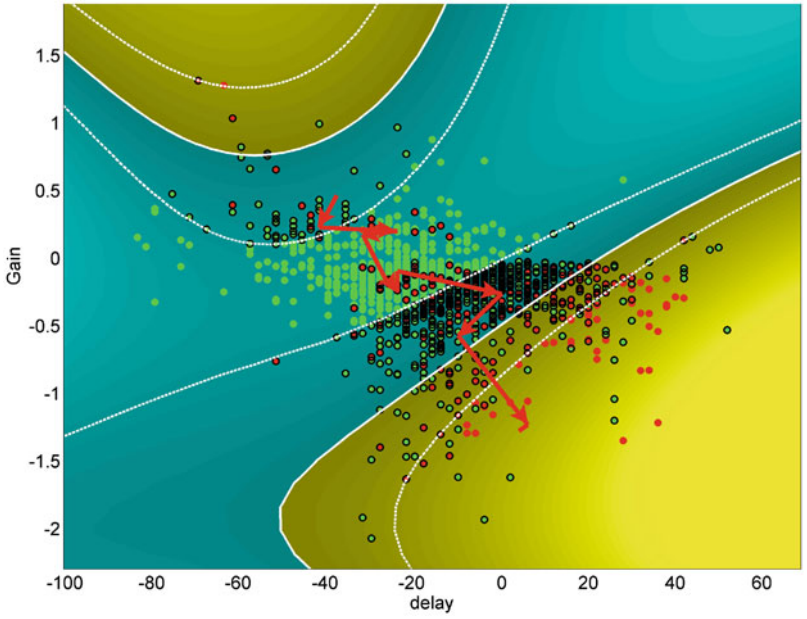

Fig. 10 Feature and decision space for one fold of a system identification support-vector machine classifier. From [16]

References

1. ACOG, *Neonatal Encephalopathy and Cerebral Palsy: Defining the Pathogenesis and Pathophysiology*. ACOG Task force on Neonatal Encephalopathy and Cerebral Palsy (2003)
2. N. Badawi, J. Kurinczuk, J. Keogh, L.M. Alessandri, F. O'Sullivan, P.R. Burton, P.J. Pemberton, F.J. Stanley, Antepartum risk factors for newborn encephalopathy: the Western Australian case-control study. BMJ **317**, 1549–1553 (1998)
3. S. Cerutti, S. Civardi, A. Bianchi, M.G. Signorini, E. Ferrazzi, G. Pardi, Spectral analysis of antepartum heart rate variability. Clin. Phys. Physiol. Meas. **10**, 27–31 (1989)
4. E.S. Draper, J.J. Kurinczuk, C.R. Lamming, M. Clarke, D. James, D. Field, A confidential enquiry into cases of neonatal encephalopathy. Arch. Dis. Child Fetal Neonatal. Ed. **87**, F176–F180 (2002)
5. C.M. Farquhar, S. Armstrong, V. Masson, J.M.D. Thompson, L. Sadler, Clinician identification of birth asphyxia using intrapartum cardiotocography among neonates with and without encephalopathy in New Zealand. JAMA Network Open **3**(2), e1921363–e1921363 (2020)
6. V.Z. Marmarelis, *Nonlinear Dynamic Modeling of Physiological Systems* (Wiley Interscience, Hoboken, NJ, 2004)
7. T. Schreiber, A. Schmitz, Surrogate time series. Phys. D Nonlinear Phenom. **142**(3–4), 346–382 (2000)
8. M. Verhaegen, V. Verdult, *Filtering and System Identification: A Least Squares Approach* (CUP, Cambridge, UK, 2007)
9. P. Warrick, E. Hamilton, M. Macieszczak, Neural network based detection of fetal heart rate patterns. *Proceedings of the 2005 IEEE International Joint Conference on Neural Networks, 2005*, vol. 4, (2005a), pp. 2400–2405
10. P.A. Warrick, E.F. Hamilton, Subspace detection of the impulse response function from intrapartum uterine pressure and fetal heart rate variability, in *Computing in Cardiology* (2013), pp. 417–420
11. P.A. Warrick, E.F. Hamilton, Antenatal fetal heart rate acceleration detection, in *Computing in Cardiology*, vol. 43 (2016)
12. P.A. Warrick, D. Precup, E.F. Hamilton, R.E. Kearney, Fetal heart rate deceleration detection from the discrete cosine transform spectrum, in *Proceedings of the 2005 IEEE Engineering in Medicine and Biology 27th Annual Conference* (2005b), pp. 5555–5558
13. P.A. Warrick, D. Precup, E.F. Hamilton, R.E. Kearney, Fetal heart rate deceleration detection using a discrete cosine transform implementation of singular spectrum analysis, in *Proceedings of the 5th International Workshop On Biosignal Interpretation* (3rd-prize in student competition) (2005c), pp. 151–154
14. P.A. Warrick, D. Precup, E.F. Hamilton, R.E. Kearney, Fetal heart rate deceleration detection using a discrete cosine transform implementation of singular spectrum analysis. Methods Inf. Med. **46**(2), 196–201 (2007)
15. P.A. Warrick, E.F. Hamilton, D. Precup, R.E. Kearney, Classification of normal and hypoxic fetuses from systems modeling of intrapartum cardiotocography. IEEE Trans. Biomed. Eng. **57**(4), 771–779 (2010a)
16. P.A. Warrick, E.F. Hamilton, D. Precup, R.E. Kearney, A machine learning approach to the detection of fetal hypoxia during labor and delivery, in *The Twenty-Second Innovative Applications of Artificial Intelligence Conference (IAAI)* (2010b)

Open Data: Valuable Resources and Opportunities for the Researchers in Fetal Cardiac Monitoring

Giulia Baldazzi and Danilo Pani

1 Introduction

According to the Open Knowledge Foundation, in its Open Definition,[1] "Open data are data that can be freely used, re-used and redistributed by anyone—subject only, at most, to the requirement to attribute and sharealike." Open data represent a philosophy and practice that can provide invaluable benefits to the researchers. In fact, by providing open data, it is possible to reduce the costs associated to the research and, along with them, the barriers that hinder the entry into the research arena for several researchers with limited funding, who could provide a valuable contribution. Moreover, open data make it possible to assess the reliability of new research findings on large populations, perform rigorous benchmarking and validation of signal processing algorithms and, in general, promote and produce new knowledge and innovation in the scientific community. Its paramount importance is evidenced by the fact that open data are progressively more frequently required by governmental and funding agencies, beyond journal publishing policies. In this perspective, in order to guarantee a good scientific data management and stewardship, the FAIR (Findable, Accessible, Interoperable, and Reusable) guiding principles have been introduced [1]. Due to the importance of promoting good practices to ensure reproducibility and reusability of health research data, the

[1] https://opendefinition.org/

G. Baldazzi (✉) · D. Pani
MeDSP, Medical Devices and Signal Processing Lab, DIEE, Department of Electrical and Electronic Engineering, University of Cagliari, Cagliari, Italy
e-mail: giulia.baldazzi@unica.it; danilo.pani@unica.it

D. Pani (ed.), *Innovative Technologies and Signal Processing in Perinatal Medicine*, https://doi.org/10.1007/978-3-031-32625-7_12

FAIR4Health project was funded,[2] with the aim of introducing new tools for the FAIRification of health data [2].

Open data play a key role in biomedical research and, specifically, in the antenatal assessment of the fetal cardiac well-being by facilitating the development and benchmarking of new strategies for antenatal diagnosis and monitoring. Accordingly, this chapter focuses on open data released for fetal cardiac monitoring. In this context, several datasets have been released so far, in particular concerning noninvasive fetal electrocardiography (fECG), fetal phonocardiography (fPCG), and cardiotocography (CTG). This chapter is mainly dedicated to freely available datasets targeting noninvasive fECG, whereas those related to fPCG and CTG will be briefly introduced in the last section. As the available datasets differ in several aspects, our aim is to help the readers in finding the right dataset for their specific needs, along with inspiring new studies by discovering some peculiarities of famous and less known data collections.

2 Open Data for Researchers: PhysioNet as a Research Resource for Complex Physiological Signals

PhysioNet[3] [3] provides free access to both biomedical research data and open-source software for processing and analysis of biomedical signals, with the aim of enabling more reliable analysis of health data and benchmarking of new algorithms. This resource, conceived in 1999 for research on complex physiological signals, includes data (PhysioBank) and software tools (PhysioToolkit) carefully characterized and reviewed by expert investigators. It also supports clinically relevant challenges for bioengineers, as the annual G. B. Moody PhysioNet Challenge, in collaboration with Computing in Cardiology, and provides tutorials for exploration and analysis of data and software tools. *PhysioBank* is a comprehensive archive of physiological signals and time series, which can be accessed by all users (open access) or by registered ones (credentialed/restricted access). It spans from electrophysiological recordings performed in different conditions, either from healthy and unhealthy subjects, as electrocardiography (ECG), electromyography (EMG), electroencephalography (EEG), and polysomnographic signal acquisitions, to clinical and imaging data, but also other biomedical measurements as heart rate, electrodermal and cardiorespiratory activity, blood pressure, glucose, and biomechanical assessments as gait analysis, balance evaluation, and motion tracking. While *PhysioBank* is aimed at distributing datasets provided with accurate information by authors, *PhysioToolkit* represents an extensive software library including facilities for signal processing and analysis of biomedical signals and time series, their simulation and modeling, as also for the detection of clinically relevant events. Specifically, it also encloses the Waveform Database Software Package

[2] https://www.fair4health.eu/

[3] https://PhysioNet.org/

(WFDB) [4–7], a specialized collection of functions for reading, processing, and analyzing PhysioBank data, which is currently available for different programming languages.

3 Generation of Synthetic Data by Open-Source Tools: The Open-Source Electrophysiological Toolbox (OSET) and the FECGSYN Toolbox

OSET [8] is a powerful collection of codes for generating and modeling ECGs from adults and fetuses, but also for processing and filtering electrophysiological signals. It has been released for the first time in 2006, and from 2018 a GitHub repository has been made publicly available.[4] As regards fECG, besides providing examples of fECG traces, OSET provides a collection of tools for the generation of physiologically plausible noninvasive fECG recordings and some related extraction algorithms (exploiting different approaches, e.g., template subtraction, or blind source separation), along with some signal quality indexes on fetal contributions, fetal QRS detectors, and codes for the estimation of fetal monitoring parameters (i.e., uterine contractions and heart rate parameters) and algorithm testing.

FECGSYN [9, 10] is an open-source toolbox expressly designed for noninvasive fECG research, with the aim of fostering and easing the collaboration among researchers by sharing data and processing methods. It can be freely accessed on GitHub[5] or downloaded from the dedicated website.[6] FECGSYN is primarily an open-source simulator of multichannel fetal–maternal mixtures, featuring several parameters and physiological events. Specifically, simulations of singleton or multiple pregnancies can be performed by considering the single heart dipole model, and choosing among several cardiac models and different parameterizable realistic noise sources (i.e., muscular artifact, baseline wander, and electrode motion). Furthermore, any user-defined number of electrodes on the maternal torso can be simulated to sense the fECG and the maternal ECG (mECG). Time-varying conditions of noisy sources, cardiac dipole movements, respiratory and heart rates, can be also simulated, thus allowing to experiment physiologically plausible scenarios where signal processing algorithms can be tested and validated. Among the most recent capabilities that have been introduced in FECGSYN, it is worth mentioning the possibility to adopt an asymmetric volume conductor for the torso, thus allowing to model abdominal ECG signals in presence of inhomogeneous distributions of vernix caseosa [11]. Despite it being mainly used as simulator of cardiac signals, especially for fECGs but also for adult ECGs, FECGSYN also makes available open-source algorithms for noninvasive fECG extraction, and several benchmarking tools in terms of fetal QRS detection and morphological analyses. The toolbox is

[4] https://github.com/alphanumericslab/OSET.git

[5] https://github.com/fernandoandreotti/fecgsyn

[6] https://github.com/fernandoandreotti/fecgsyn/archive/master.zip

also provided with several examples, not only for the generation of ECG signal but also for fECG extraction, signal quality assessment, and the benchmarking of algorithms in terms of fetal QRS detection and morphological analysis.

4 Freely Available Datasets for Noninvasive fECG Research

Noninvasive fECG is currently the frontier of continuous fetal monitoring and antenatal diagnostics [12–14]. Noninvasive fECG refers to the study of the electrical activity of fetal heart by applying surface electrodes on maternal abdomen, thus allowing for the assessment of the fetal well-being without any risks for both the mother and the fetus. Since fECG can be recorded starting from the 18th week of gestation [15], it could enable antenatal, affordable, long-term, and risk-free monitoring, thanks to its noninvasiveness and to the nature of the signal [16, 17]. Moreover, noninvasive fECG could potentially enable the detection and diagnosis of arrhythmias and other cardiac diseases inducing changes in ECG rhythm and waveform morphology [13]. As such, it could be a powerful tool enabling prompt treatment in utero or immediately after birth, as also planning the most appropriate delivery strategies and labor assistance.

However, noninvasive fECG is not adopted in the clinical practice in such a broad sense because of the variable quality of the extracted fECG traces. For several years, the advancements in the bioengineering research on noninvasive fECG has been hampered by the lack of adequate public datasets including a gold standard reference for the fECG and clinical information [15]. To solve this problem, in recent years some datasets for noninvasive fECG research have been released. They exhibit different features in terms of number of recordings, number of channels, signals duration, presence of a reference gold standard, study population, gestational ages, and clinical information. In order to provide a synthetic bird's eye view of the available resources, Table 1 summarizes the principal characteristics of the noninvasive fECG datasets that will be presented in this chapter. Remarkably, to be adopted for morphological analysis, noninvasive fECG datasets should be recorded by acquisition systems with broad dynamic range, to avoid saturations, and a number of channels between 8 and 32, with reference thoracic mECG. Moreover, a bandwidth between 0.05 Hz and 250 Hz or 1 kHz, at least 16-bit resolution, and sampling frequency above 1 kHz are recommended [15, 18]. However, these requirements could be relaxed for specific purposes.

The first freely available fECG dataset is represented by the *Database for the Identification of Systems*, also known as *DaISy* [19], which has been released in 1997 and still currently attainable [20]. It consists of an 8-lead signal (i.e., five abdominal and three thoracic channels), lasting for 10 s, which was recorded from a single pregnant woman at a sampling frequency of 250 Hz. Similarly, the *OB-1* [21] *fetal ECG database* is based on a single recording, which was collected as a part of a larger dataset aimed at studying fetal distress and heart rate variability. The OB-1 recording lasts less than 6 minutes, and it is composed of a fECG invasively acquired

Table 1 Comparison table of freely available datasets for noninvasive fECG research in terms of number of recordings, number and type of recorded channels, duration of signals, homogeneity of electrode positioning, acquisition settings, presence of a gold reference, and eventual demographic and clinical information

	DaISy	OB-1	NIFECG	CinC2013	FECGSYNDB	ADFECG	B1	B2	NIFEA	ARS (real)	ARS (simul.)	NInFEA
N. of recordings	1	1	55	175	1750	5	10	12	26 (12 arrhythmic)	21	40	60
N. of abdominal channels (+ # thoracic channels)	5 (+3)	1 invasive fECG + uterine EMG	4 or 3 (+2)	4	32 (+2) + 32 noiseless fECG	4 + 1 invasive fECG	4 + 4 extracted fECG	4 + 1 invasive fECG	4 or 5 (+1)	3 (+3) + 3 extracted fECG	1 fECG + white and pink noises	24 (+3) + PWD + maternal respiration
Signal duration	10 s	<6 min	~2÷47 min	1 min	5 min	5 min	20 min	5 min	~7÷32 min	15 s	10 s	~7 s÷2 min
Homogeneous electrode positioning	NA	NA	No	No	Yes	Yes	Yes	Yes	Yes	Yes	Yes	Yes
Sampling frequency and resolution	250 Hz, ND bits	ND	1 kHz, 16 bits	1 kHz, ND bits	250 Hz, 16 bits	1 kHz, 16bits	500 Hz, 16 bits	500 Hz for abdominal signal, 1 kHz for invasive fECG, 16 bits	500 Hz or 1 kHz, 16 bits	2.048 kHz, 22 bits	2.048 kHz (double-precision floating-point format)	2.048 kHz, 22 bits

(continued)

Table 1 (continued)

	DaISy	OB-1	NIFECG	CinC2013	FECGSYNDB	ADFECG	B1	B2	NIFEA	ARS (real)	ARS (simul.)	NInFEA
Data bandwidth and processing	ND	ND	0.01÷100 Hz + 50-Hz notch filter	ND	None	1÷150 Hz + digital filtering for powerline (50 Hz) and baseline drift removal	0.05/1÷150 Hz + powerline and low-frequency noise removal	0.05/1÷150 Hz + powerline and low-frequency noise removal	ND	0÷550 Hz (raw), baseline wander removal and adaptive filtering for fECG extraction	None	0÷550 Hz, no processing
Presence of a gold reference	No	Yes	No	Yes (for 75 out of 175 signals)	Yes	Yes	Yes	Yes	No	Yes	Yes	Yes
Population and gestational age	1 volunteer, ND w.o.g.	1 volunteer, ND w.o.g.	1 volunteer, 21st–40th w.o.g.	ND	10 simulations of pregnancies	5 volunteers, 38th–41st w.o.g.	ND volunteers, 32nd–42nd w.o.g.	ND volunteers, 38th–42nd w.o.g.	24 volunteers, 20th–41st w.o.g.	17 volunteers, 21st–27th w.o.g. (real)	40 simulations of pregnancies	39 volunteers, 21st–27th w.o.g.
Clinical information available	No	Yes	No	No	NA	No	No	No	No	No	NA	Yes

NA not applicable, *ND* not defined, *w.o.g.* week of gestation

from the fetal scalp, with annotations corresponding to the fetal R peaks, along with the simultaneous uterine EMG activity. Although the authors of the dataset claimed they collected more than 100 signals during in-hospital labor and delivery, the original aim of enlarging the dataset was not accomplished, to the best of our knowledge. Also, the *Non-Invasive Fetal Electrocardiogram Database (NIFECG)* has been acquired on a single participant, but a larger number of acquisitions is provided. This dataset was released in 2007, and it is also available on PhysioNet [22]. Specifically, it is a collection of 55 multichannel noninvasive recordings acquired weekly between the 21st and 40th week of gestation, even though in some cases more records were collected in the same week. Signal recording was performed by Ag/AgCl electrodes and a g.BSamp Biosignal Amplifier, with an unspecified analog-to-digital converter with 16-bit resolution and a sampling rate of 1 kHz. In the acquisition stage, an analog 50-Hz notch filter was applied by the amplifier. EDF/EDF+ format was chosen for data storage, in which the recording information and the gestational age (week + day) are included. Each recording consists of two thoracic signals and, typically, four abdominal signals, despite in some cases only three abdominal channels are made available. According to the characteristics of the adopted bioamplifier, the recorded channels are supposed to be differential. However, the different electrode placements exploited by the authors to reduce noise and the low number of available channels hampers testing independent component analysis or source localization algorithms, which are commonly exploited for fECG extraction and analysis. Nonetheless, other methods can be applied, also exploiting the maternal QRS annotations that are provided.

Undoubtedly, the *PhysioNet/Computing in Cardiology Challenge 2013* (*CinC2013*) *dataset* [23–25] stands out among the most frequently adopted datasets for noninvasive fECG research. It has been made available in order to give a boost to the community in conceiving effective algorithms to be applied on noninvasive fECG for the estimation of fetal heart rate (fHR), fetal interbeat intervals, and QT intervals. The CinC2013 dataset includes three subsets of data (A, B, and C) with different characteristics, for a total of 447 abdominal recordings from five collections overall, either real and synthetic (but labels for this aspect are not provided in the dataset). Indeed, each recording is composed of four abdominal channels sampled at 1 kHz, lasting one minute. However, expressly for the purpose of the challenge, signal acquisition was not performed homogeneously, involving different instrumentation and configurations, and using unknown electrodes positioning. Furthermore, only some recordings (i.e., 175 out of 447) were publicly released to the participants, and specifically those concerning sets A and B. Moreover, despite fetal R-peak locations were annotated for all subsets by crowdsourcing, sometimes exploiting the simultaneous invasive fECG, only signals from set A (i.e., 75 out of 175) have been supplied with such annotations. An example of abdominal recording belonging to this dataset is shown in Fig. 1.

The *Fetal ECG Synthetic Database (FECGSYNDB)* [9, 26] was released some years later by including only simulated abdominal mixtures by the FECGSYN simulator. FECGSYNDB involves 1750 5 min-long, multichannel synthetic signals differing for the adopted vectorcardiogram models (for both the mother and fetuses),

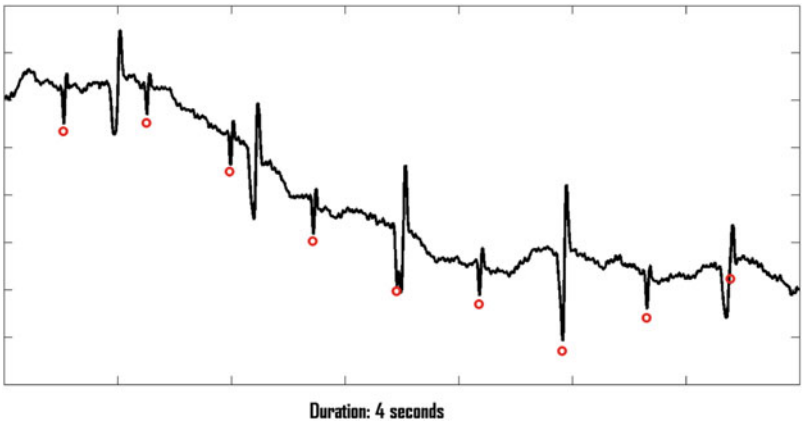

Fig. 1 An example of abdominal recording with marked fetal R-peaks (red circles) included in the PhysioNet/Computing in Cardiology Challenge 2013 (CinC2013) dataset [23]

additive noise level, and physiological events eventually included (i.e., baseline wander, fetal movements, heart and respiratory rate variations either for mother and fetus, maternal and fetal heart spatial positions, uterine contractions, etc.). Each mixture was simulated by considering two mECG and 32 abdominal channels with a sampling frequency of 250 Hz, thus allowing to benchmark multiple extraction algorithms. Simulated datasets are provided with both maternal and fetal R-peak annotations, thus enabling also the test of QRS detectors on adult ECGs and fECGs. However, the principal limitation of this dataset is the synthetic nature of signals that, although physiologically plausible, lack the unpredictable behavior of real signals.

Conversely, a freely available dataset of real signals for fECG research is the *Abdominal and Direct Foetal Electrocardiogram Database (ADFECG)* [27], which can be found in EDF/EDF+ format on PhysioNet [28]. This dataset contains simultaneous abdominal ECG and invasive fECG signals that have been recorded between the 38th and the 41st weeks of gestation from five women in labor. All signals last five minutes and have been acquired by the KOMPOREL system (ITAM Institute, Zabrze, Poland) with a sampling rate of 1 kHz and 16-bit resolution. Specifically, four abdominal ECGs have been acquired in each session as bipolar signals by placing four Ag/AgCl electrodes on the maternal abdomen around the navel. Furthermore, a reference electrode and an active-ground electrode were also exploited, the former above the pubic symphysis while the latter on the left leg, as shown in Fig. 2. Conversely, the direct fECG was acquired by a spiral electrode invasively from the fetus' scalp, providing a reference for the fECG waveform analysis. In addition, the authors provided clinically validated fetal R-peak locations. These signals (r01, r04, r07, r08, r10) have been also included in another dataset recently released by the same authors [29] and publicly available online by Scientific Data [30], including two sets of data, that is, an antenatal (B1)

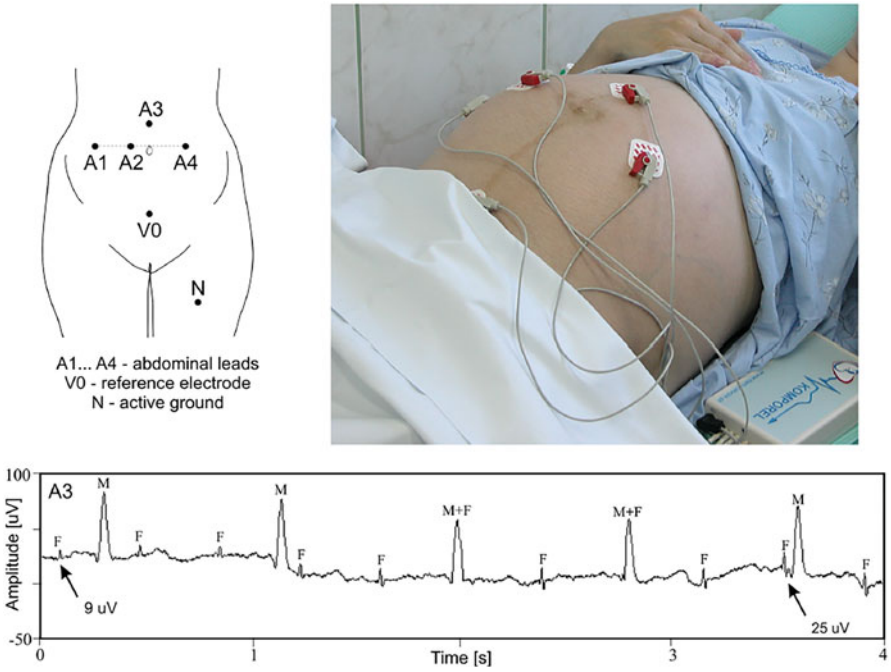

Fig. 2 Electrode positioning adopted for noninvasive fECG acquisition in B1 and B2 datasets, along with an example of abdominal recording. (Adapted with permission from [29])

dataset, and an intrapartum (B2) dataset. In particular, *B1* dataset consists of ten 20 min-long, four-channel abdominal signals acquired between the 32nd and the 42nd week of gestation. All abdominal signals have been recorded according to the same electrode positioning presented in ADFECG (see Fig. 2) and sampled at 500 Hz with 16-bit resolution by the KOMPOREL System. Furthermore, both fetal R-peaks locations and reference fHR signals were provided to the readers, representing a useful ground truth. Fetal R peaks have been preliminarily identified by an automatic fetal QRS detection algorithm, and then manually corrected by clinical experts. In this regard, fetal R-peak annotations were accompanied by reliability flags, thus identifying trustworthy and less reliable annotations. fHR signals have been automatically annotated by the MONAKO System, providing the reader with graphical and quantitative information about instantaneous and overall fHR variability (see Fig. 3 for an example). Moreover, the maternal R-peak locations and the fECG signals recovered after maternal ECG suppression were provided for all the channels. Several indexes quantifying the mECG and fECG relative levels, their energies and their amplitudes with respect to noise, are also provided.

B2 dataset is composed of twelve 5 min-long, multichannel signals that were acquired in labor between the 38th and the 42nd gestational week. In addition to the four abdominal channels, recorded in the same way as in the B1 dataset, a direct

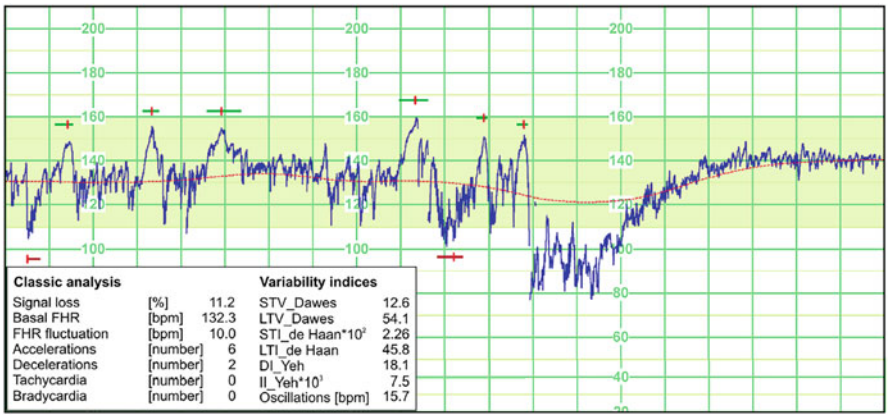

Fig. 3 Example of fHR signal included in B1 dataset, with features. (Adapted with permission from [29])

fECG was acquired using a spiral scalp electrode by the KOMPOREL System, at 1 kHz. Also in this case, the annotations of maternal and fetal R peaks, and the relative fHR signals with related indexes, were made available, but in this case fetal beats were detected on the direct fECG, and then clinically validated.

Remarkably, both invasive and abdominal recordings (for B1 and B2 datasets) have been preprocessed in order to remove low-frequency and powerline noises. In the same years of B1 and B2 datasets, three other real datasets have been made available.

The *Non-Invasive Fetal ECG Arrhythmia Database (NIFEA)* [31, 32] has been released in 2019, and it is the only dataset that includes noninvasive fECG recordings from healthy ($n = 14$) and arrhythmic ($n = 12$) fetuses. Specifically, each recording contains multichannel abdominal ECG signals (with four or five leads) and a thoracic mECG signal, following the electrode placement depicted in Fig. 4. Noninvasive fECG recordings have been performed by the portable Cardiolab ECG monitoring device (KhAI Medica, Ukraine) after echocardiography, with 16-bit resolution in a range of ± 8 mV. All cases have been acquired at 1 kHz, whereas acquisitions from four arrhythmic fetuses have been performed at 500 Hz. In this dataset, signals from 24 pregnant women were included, in the gestational period between the 22nd and the 41st week for the arrhythmic fetuses, and between 20th and 36th week for the healthy ones. Remarkably, in the latter case, also recordings from two pregnant women with twins have been included.

In 2020, the *Annotated Real and Synthetic Datasets for Non-Invasive Fetal Electrocardiography Post-Processing Benchmarking (ARS)* has been released [33, 34]. As suggested by the name, it includes both real and synthetic signals, along with fetal R-peak annotations, in .csv files. In the real set, 21 15s-long recordings from 17 voluntary pregnant women between the 21st and the 27th week of gestation are included. Real signals have been acquired by the Porti7 portable physiological

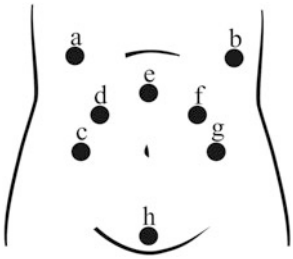

Fig. 4 Schematic representation of electrode positioning adopted in NIFEA dataset. Specifically, six abdominal leads were acquired by electrodes (c), (d), (e), (f), (g) referenced to electrode (h), whereas electrode (b) records the mECG with respect to the same common reference. In this configuration, electrode (a) represents the active ground. (Adapted from [31])

measurement system (TMSi, The Netherlands). Signals have been sampled at 2048 Hz with 22-bit resolution, with a bandwidth of 0–550 Hz. Each real recording consists of three thoracic non-coplanar mECG leads, three raw bipolar abdominal leads, the corresponding fECGs extracted by adaptive filtering, and the manual location of fetal R peaks provided by clinical experts. For signal recording, six electrodes were placed on the maternal thorax for the acquisition of the three bipolar mECG leads, as reported in Fig. 5. Then, three raw bipolar abdominal channels were digitally computed for examining the fetal cardiac projections in horizontal, vertical, and oblique directions, by considering 3 out of 24 unipolar channels, as shown in Fig. 5, each one analogically referenced to their common average. After baseline removal, the fECG signal was extracted from each abdominal channel by QRD-RLS multi-reference adaptive filtering [35] and made available along with the identification of the best two out of three extracted leads for each recording, which have been previously adopted for postprocessing benchmarking [36].

Being conceived for fECG postprocessing methods benchmarking, also a synthetic set of data was included in ARS. It encloses 40 10 s-long fECG signals simulated by means of the FECGSYN toolbox, including additive white and pink noises, with different intensity (see Fig. 6 for the noisiest case). A differential, horizontal fECG lead free of any maternal interference has been digitally obtained from two unipolar channels, at 2048 Hz, in order to reproduce the same real acquisition setup as closely as possible. Remarkably, despite being synthetic data, as for the FECGSYNDB, this part of ARS allows researchers to assess the performance of their fECG extraction and postprocessing algorithms in terms of morphology preservation by providing the true noiseless fECGs beyond the fetal R-peak annotations.

More recently, the *Non-Invasive Multimodal Foetal ECG-Doppler Dataset for Antenatal Cardiology Research (NInFEA)* [37–39] has been published, along with the MATLAB functions allowing for data access, visualization, and processing. NInFEA represents the only public dataset that encompasses both electrical and mechanical fetal cardiac activity. It is composed of 60 noninvasive recordings, performed on 39 pregnant women with healthy fetuses between the 21st and

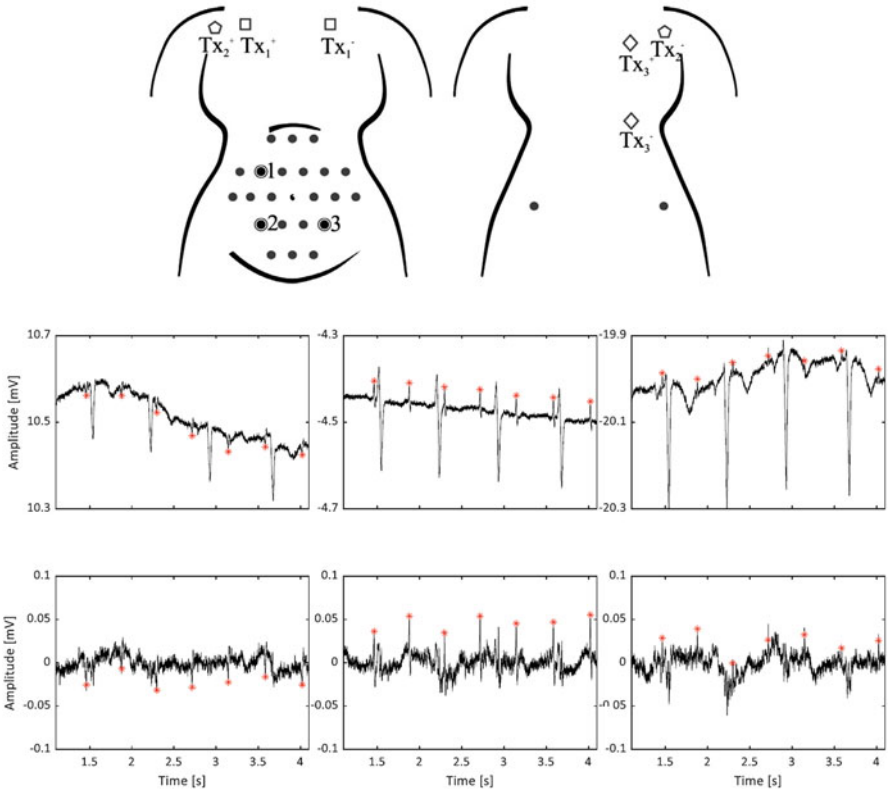

Fig. 5 Electrode positioning (top) adopted for the acquisition of real signals belonging to the ARS dataset, with examples of abdominal traces (middle) and corresponding recovered fECGs (bottom). Circles represent the electrodes adopted for unipolar abdominal recordings, whereas encircled ones those used for differential recordings. Thoracic mECG was acquired by pairs of electrodes indicated by Tx_1, Tx_2, Tx_3. (Adapted with permission from [33])

27th week of gestation at the Pediatric Cardiology and Congenital Heart Disease Unit of the San Michele Hospital (Brotzu) in Cagliari, Italy. In each session, the electrophysiological signals and the fetal cardiac pulsed-wave Doppler (PWD) were recorded simultaneously. For the PWD acquisition, an apical five-chamber view was adopted to assess blood flow in the four cardiac chambers and in the first part of the aorta. In this regard, the Philips iE33 Ultrasound Machine (Philips Healthcare, The Netherlands) has been used for PWD acquisition at a frame rate of 60 Hz and with 1680 $\times$ 1050 pixels resolution. Frame grabbing was performed with a USB3HDCAP USB3.0 Video Capture Device (StarTech, UK) with post hoc synchronization. Starting from the PWD videos, single-wide PWD images have been composed by the authors and released in .bmp format, along with the PWD envelopes (see red and blue curves in Fig. 7). Remarkably, after all processing stages, a sampling rate of 284 Hz can be assumed for PWD envelopes.

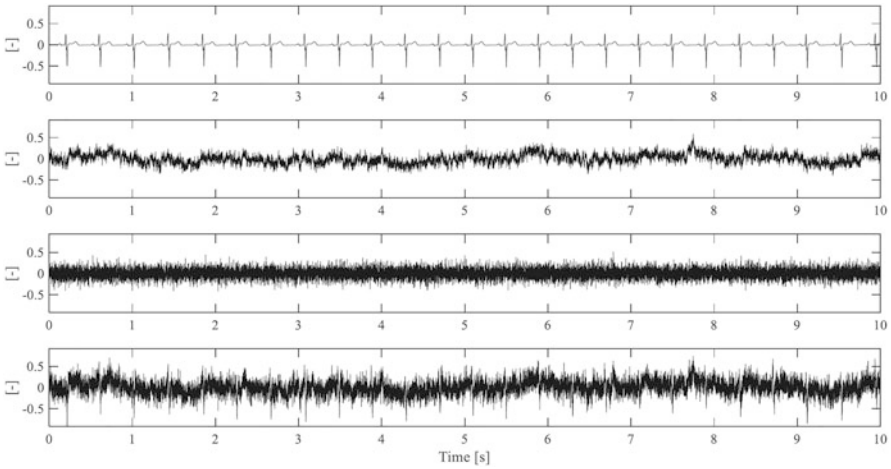

Fig. 6 Noisiest fECG signal included in the synthetic set of ARS. The noiseless fECG is reported on top, along with the pink (second row) and white (third row) noises, and the result of their mixing, that is, the noisy fECG trace (bottom). (Adapted with permission from [33])

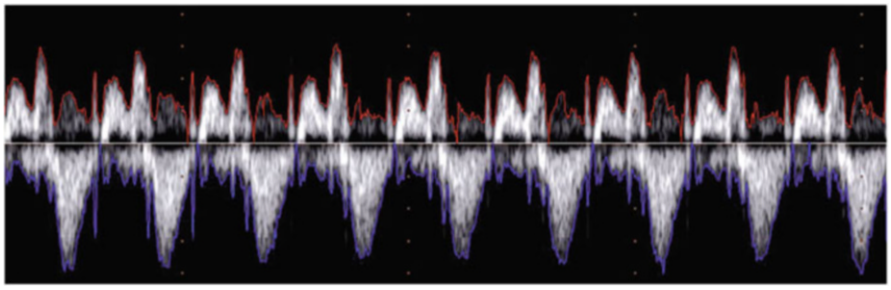

Fig. 7 An example of PWD recording from the NInFEA dataset, with the upper (in red) and lower (in blue) envelopes. (Adapted with permission from [37])

As regards the electrophysiological signals, recordings were performed by using the DC-coupled Porti7 portable physiological measurement system (TMSi, The Netherlands), with a sampling rate of 2048 Hz, 22-bit resolution (i.e., 71.5 nV amplitude resolution), and bandwidth up to 550 Hz. Electrophysiological and respiration traces are released in .bin and WFDB format. They included 24 unipolar abdominal signals, three bipolar thoracic ECG leads, and a maternal respiration signal.

The electrode positioning is depicted in Fig. 8. Specifically, the 24 unipolar abdominal channels have been collected with respect to their common average by placing 22 electrodes (i.e., 1–22 in Fig. 8) on the maternal abdomen and two on the mother's back (i.e., 23 and 24 in Fig. 8). Conversely, for the three non-coplanar thoracic ECG leads, six electrodes have been exploited (25, 26, and 27 in Fig. 8), along with a ground electrode on the right hip. Despite apparently

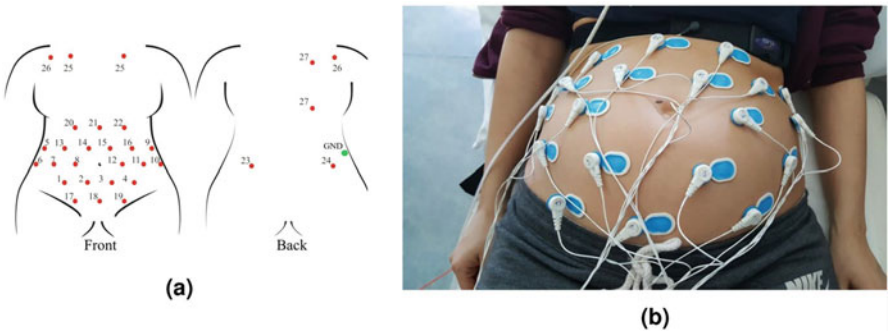

Fig. 8 Real and schematic electrode positioning for the signals in the NInFEA dataset; on the right, the respiration belt is also visible. (Adapted with permission from [37])

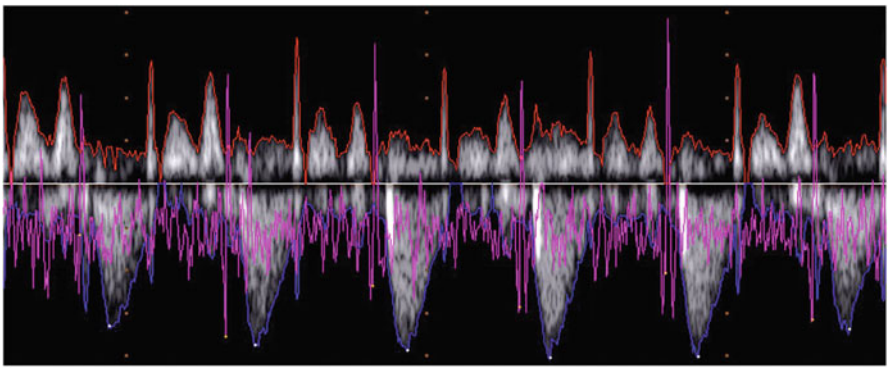

Fig. 9 Example of synchronous fECG trace (in pink) and PWD (in gray), with upper (in red) and lower (in blue) envelopes of the NInFEA dataset. (Adapted with permissions from [37])

redundant, this electrode configuration is particularly useful to reproduce most of the positioning schemes previously adopted in the literature [37]. Compared to other datasets, several acquisition details are provided for this one in the accompanying paper [37], including the electrode model, which was the BlueSensor N electrodes (Ambu, Denmark), selected because of its small size, offset connector for artifact reduction, and good skin-electrode contact impedance. Finally, maternal respiration was recorded by placing a piezo-resistive respiration belt (TMSi, The Netherlands) around the maternal chest, just below the breast (see Fig. 8). The duration of the NInFEA recordings varies from about 7 seconds to 2 minutes, which is limited with respect to other available datasets. Despite representing a limitation for some fECG extraction algorithms, or for fHR variability studies, this unavoidable disadvantage is strictly due to the need of a stable sample volume for the PWD recording, to provide clinically valuable representations of the fetal heart activity. An example of a synchronous recording involving both PWD and fECG is reported in Fig. 9.

5 Open Data for Fetal Cardiac Monitoring by CTG and fPCG

Beyond the fECG datasets, several other datasets have been released to enable studies on fetal cardiac monitoring. In particular, some relevant CTG and fPCG data collections will be introduced hereafter.

CTG is an ultrasound-based technology for the continuous monitoring of the fHR and uterine contractions. It represents the gold standard for fetal cardiac assessment in the antenatal period [40] and, particularly, during labor [41]. CTG can be performed from the 20th week of gestation by using an ultrasound transducer and a tocodynamometer [15]. These transducers are routinely applied noninvasively on the maternal abdomen. Although the advantages introduced by continuous CTG monitoring are still debated [42], many studies focused on the automatic analysis of CTG recordings in order to reduce inter- and intra-expert variability and enable the identification of risky or pathological conditions [43–50]. On these premises, several datasets have been made available to the researchers.

Among the most commonly adopted CTG datasets, the CTU-CHB Intrapartum Cardiotocography Database should be mentioned [51, 52]. It encloses 552 recordings of both fHR and tocogram, along with clinical information regarding maternal and fetal metadata, delivery, and its outcome. All recordings have been performed at University Hospital in Brno, Czech Republic, on singleton pregnancies with gestational age above 36th week of gestation, just before delivery, with a maximum duration of 90 minutes. Remarkably, the CTU-CHB has been recently provided with clinical expert annotations regarding important events in both fHR and uterine contraction signals, such as arrhythmias, acceleration, and deceleration episodes [53]. Another noteworthy CTG dataset is the UCI Machine Learning Repository [54, 55], which provides only features extracted from 2126 CTG recordings (including fHR baseline, number of accelerations and decelerations per second, number of uterine contractions per seconds, etc.), along with CTG trace classification labels concerning morphological patterns and fetal states. Similarly, also the Fetal Heart Rate Features of Healthy and Late Intra Uterine Growth Restricted (IUGR) Fetuses dataset has been recently released [56], releasing 31 fHR features derived from the time domain (e.g., mean and standard deviation of 1-min fHR, the short-term variability (STV), the long-term irregularity (LTI), etc.), the frequency domain (i.e., the spectral powers in low frequency (LF), movement frequency (MF) and high frequency (HF) bands), and the complexity domain (e.g., approximate entropy, the sample entropy, etc.). These features have been extracted from antepartum CTG recordings performed on 160 healthy and 102 late IUGR fetuses at the University Hospital Federico II (Napoli, Italy). Moreover, the same research group released a further dataset on linear and nonlinear indices for discriminating healthy and IUGR fetuses [45, 57, 58], where fHR parameters from time, frequency, and nonlinear domains (e.g., STV, LTI, spectral powers in LF, MF, HF bands, etc.) have been computed from CTG recording of 60 normal and 60 IUGR fetuses, and a larger database of labeled CTG recordings with useful clinical information is going to be issued [59].

Beyond CTG, *fPCG* also measures the fetal cardiac activity noninvasively, but it relies on the fetal heart sounds produced by the closure of the cardiac valves [60], and sensed by a piezoelectric or optical sensor placed on the maternal abdomen [61]. This technique can be used from the 20th week of gestation and can be exploited also during labor [17]. Nowadays, it is mainly used for the antenatal analysis of fHR and fetal breathing movements [62, 63] since considerable difficulties related to the signal acquisition and processing hamper its adoption in the clinical practice [64, 65]. Several datasets have been developed to support the conception and benchmarking of fPCG extraction and processing algorithms. Among them, the following four datasets should be mentioned. The Simulated Fetal Phonocardiograms [66, 67] consist of a set of 37 fPCGs, simulated during different physiological and external conditions. Conversely, the Fetal PCG database [68] consists of 26 real fPCG signals acquired by means of the Fetaphon Monitoring System (Pentavox, Hungary). It was recorded on healthy pregnant women between the 31st and the 40th week of gestation. Another dataset of real signals was released by the Shiraz University. The Fetal Heart Sounds database [69, 70] consists of 119 fPCG and 92 maternal PCG recordings, acquired from 109 pregnant women in single and twin pregnancies, by means of a digital JABES Electronic stethoscope (GS Technology Co. Ltd., South Korea) and the Audacity freeware tool for audio processing. Last but not least, the Indian Institute of Science Fetal Heart Sound database [71, 72] also presents real fPCG signals. In particular, it consists of 60 fPCGs from as many singleton pregnancies between the 30th and the 40th week of gestation, recorded with the SS30LA electronic stethoscope coupled with the MP36 acquisition system (Biopac Systems Inc., CA, USA).

6 Conclusions

In the last decades, the need for a trustworthy benchmark and comparison of signal processing algorithms for antenatal assessment has strongly called for the release of open datasets, which is currently only partially satisfied. Therefore, a lot of effort is still required from and to the scientific community in order to reduce the barriers hampering the entry of the largest number of scientists in the research arena, thus promoting the development of novel ideas and verifiable scientific results. Data are the first step toward the knowledge, so open data represent a way toward a faster and homogeneous development of knowledge. Open data philosophy is a required mindset shift for biomedical researchers, and we are all staring at the huge impact it is already having on the research world.

In this chapter, public open datasets fostering the scientific research on antenatal fetal surveillance, monitoring, and diagnosis have been analyzed, detailing their peculiar characteristics, with a special emphasis on noninvasive fECG. An important limitation of the available datasets is the reduced presence of pathological conditions and follow-up information. The former limits the possibility of assessing signal analysis and processing tools for diagnostic purposes, whereas the latter hampers

the studies on regression and classification analysis based on antenatal information. This is surely the next frontier of the development of new datasets, which must rigorously include metadata and detailed information on the (reproducible and homogeneous) recording setup. Moreover, by enriching the information provided to the users, multimodal sensing can allow studying the underpinnings of the observed phenomena and consequently lead to the optimization of the sensing features and sensors number. This will pave the way for the translational research and the development of effective and affordable devices for mass screening, which is a worldwide need, but it is especially important in low-income countries, where complex and expensive equipment cannot represent the standard of care.

References

1. M.D. Wilkinson et al., The FAIR guiding principles for scientific data management and stewardship. Sci. Data **3**(1), 160018 (2016)
2. C. Alvarez-Romero et al., FAIR4Health: Findable, accessible, interoperable and reusable data to foster health research [version 2; peer review: 1 approved, 2 approved with reservations]. Open Res. Eur. **2**(34) (2022)
3. A.L. Goldberger et al., PhysioBank, PhysioToolkit, and PhysioNet: Components of a new research resource for complex physiologic signals. Circulation **101**(23), e215–e220 (2000)
4. G. Moody, T. Pollard, B. Moody, WFDB Software Package (version 10.7.0). PhysioNet, 2022
5. I. Silva, B. Moody, G. Moody, Waveform Database Software Package (WFDB) for MATLAB and Octave (version 0.10.0), PhysioNet, 2021
6. I. Silva, G.B. Moody, An open-source toolbox for analysing and processing PhysioNet databases in MATLAB and octave. J. Open Res. Softw. **2**(1) (2014)
7. C. Xie, L. McCullum, A. Johnson, T. Pollard, B. Gow, B. Moody, Waveform Database Software Package (WFDB) for Python (version 4.0.0), PhysioNet, 2022
8. R. Sameni, The Open-Source Electrophysiological Toolbox (OSET), version 3.14 (2018)
9. F. Andreotti, J. Behar, S. Zaunseder, J. Oster, G.D. Clifford, An open-source framework for stress-testing non-invasive foetal ECG extraction algorithms. Physiol. Meas. **37**(5), 627–648 (2016)
10. J. Behar, F. Andreotti, S. Zaunseder, Q. Li, J. Oster, G.D. Clifford, An ECG simulator for generating maternal-foetal activity mixtures on abdominal ECG recordings. Physiol. Meas. **35**(8), 1537–1550 (2014)
11. E. Keenan, C.K. Karmakar, M. Palaniswami, The effects of asymmetric volume conductor modeling on non-invasive fetal ECG extraction. Physiol. Meas. **39**(10), 105013 (2018)
12. A. Agostinelli et al., Noninvasive fetal electrocardiography: An overview of the signal electrophysiological meaning, recording procedures, and processing techniques. Ann. Noninvasive Electrocardiol. **20**(4), 303–313 (2015)
13. R. Kahankova et al., A review of signal processing techniques for non-invasive fetal electrocardiography. IEEE Rev. Biomed. Eng. **13**, 51–73 (2020)
14. K.M.J. Verdurmen et al., A systematic review of prenatal screening for congenital heart disease by fetal electrocardiography. Int. J. Gynaecol. Obstet. **135**(2), 129–134 (2016)
15. R. Sameni, G.D. Clifford, A review of fetal ECG signal processing; issues and promising directions. Open Pacing Electrophysiol. Ther. J. **3**, 4–20 (2010)
16. M. Peters et al., Monitoring the fetal heart non-invasively: A review of methods. J. Perinat. Med. **29**(5), 408–416 (2001)
17. R. Jaros, R. Martinek, R. Kahankova, Non-adaptive methods for fetal ECG signal processing: A review and appraisal. Sensors **18**(11), 3648 (2018)

18. R. Sameni, Noninvasive Fetal Electrocardiography: Models, Technologies, and Algorithms, in *Innovative Technologies and Signal Processing in Perinatal Medicine*, ed. by D. Pani, C. Rabotti, M.G. Signorini, L. Burattini, vol. 1, (Springer, Cham, 2021), pp. 99–146
19. B. De Moor, P. De Gersem, B. De Schutter, W. Favoreel, DAISY: A database for identification of systems. J. A **38**(3), 4–5 (1997)
20. B. De Moor, Database for the Identification of Systems (DaISy), 1997. [Online]. https://homes.esat.kuleuven.be/~smc/daisy/daisydata.html
21. OB-1 Fetal ECG Database, PhysioNet, 2012. [Online]. https://physionet.org/content/ob1db/1.0.0/
22. Non-Invasive Fetal ECG Database, PhysioNet, 2007. [Online]. https://physionet.org/content/nifecgdb/1.0.0/
23. I. Silva, J. Behar, R. Sameni, T. Zhu, G.D. Clifford, and G. Moody, Noninvasive fetal ECG: The PhysioNet/computing in cardiology challenge 2013, PhysioNet, 2013. [Online]. https://physionet.org/content/challenge-2013/1.0.0/
24. I. Silva et al., Noninvasive Fetal ECG: the PhysioNet/Computing in Cardiology Challenge 2013. Comput. Cardiol. **40**, 149–152 (2013)
25. G.D. Clifford, I. Silva, J. Behar, G.B. Moody, Non-invasive fetal ECG analysis. Physiol. Meas. **35**(8), 1521 (2014)
26. F. Andreotti, J. Behar, G.D. Clifford, Fetal ECG synthetic database, PhysioNet, 2016. [Online]. https://physionet.org/content/fecgsyndb/1.0.0/
27. J. Jezewski, A. Matonia, T. Kupka, D. Roj, R. Czabanski, Determination of fetal heart rate from abdominal signals: Evaluation of beat-to-beat accuracy in relation to the direct fetal electrocardiogram. Biomed. Tech. Eng. **57**(5), 383–394 (2012)
28. Abdominal and direct fetal ECG database, PhysioNet, 2012. [Online]. https://physionet.org/content/adfecgdb/1.0.0/
29. A. Matonia et al., Fetal electrocardiograms, direct and abdominal with reference heartbeat annotations. Sci. Data **7**(1), 200 (2020)
30. A. Matonia, J. Jezewski, T. Kupka, M. Jezewski, K. Horoba, J. Wrobel, Fetal electrocardiograms, direct and abdominal with reference heart beats annotations, 2020. [Online]. https://doi.org/10.6084/m9.figshare.c.4740794.v1
31. J.A. Behar, L. Bonnemains, V. Shulgin, J. Oster, O. Ostras, I. Lakhno, Noninvasive fetal electrocardiography for the detection of fetal arrhythmias. Prenat. Diagn. **39**(3), 178–187 (2019)
32. J. Behar, Non-invasive fetal ECG arrhythmia database, PhysioNet, 2019. [Online]. https://physionet.org/content/nifeadb/1.0.0/
33. G. Baldazzi, E. Sulas, M. Urru, R. Tumbarello, L. Raffo, D. Pani, Annotated real and synthetic datasets for non-invasive foetal electrocardiography post-processing benchmarking. Data Br. **33**, 106399 (2020)
34. G. Baldazzi, M. Urru, D. Pani, E. Sulas, L. Raffo, T. Roberto, Annotated real and synthetic datasets for non-invasive foetal electrocardiography post-processing benchmarking, Mendeley Data, 2020. [Online]. https://data.mendeley.com/datasets/64zy9f2dkf/2
35. E. Sulas, M. Urru, R. Tumbarello, L. Raffo, D. Pani, Systematic analysis of single- and multi-reference adaptive filters for non-invasive fetal electrocardiography. Math. Biosci. Eng. **17**(1), 286–308 (2020)
36. G. Baldazzi, E. Sulas, M. Urru, R. Tumbarello, L. Raffo, D. Pani, Wavelet Denoising as a post-processing enhancement method for non-invasive Foetal electrocardiography. Comput. Methods Prog. Biomed. **195**, 105558 (2020)
37. E. Sulas, M. Urru, R. Tumbarello, L. Raffo, R. Sameni, D. Pani, A non-invasive multimodal foetal ECG–Doppler dataset for antenatal cardiology research. Sci. Data **8**(1), 30 (2021)
38. E. Sulas et al., A Novel Tool for Non-Invasive Fetal Electrocardiography Research: The NInFEA Dataset, in *2020 42nd Annual International Conference of the IEEE Engineering in Medicine & Biology Society (EMBC)*, 2020, pp. 5631–5634

39. D. Pani, E. Sulas, M. Urru, R. Sameni, L. Raffo, R. Tumbarello, NInFEA: Non-invasive multimodal Foetal ECG-Doppler dataset for antenatal cardiology research, PhysioNet, 2020. [Online]. https://physionet.org/content/ninfea/1.0.0/
40. R.M. Grivell, Z. Alfirevic, G.M. Gyte, D. Devane, Antenatal cardiotocography for fetal assessment. Cochrane Database Syst. Rev. **9**, CD007863 (2015)
41. D. Ayres-de-Campos, C.Y. Spong, E. Chandraharan, F.I.F.M.E.C. Panel, FIGO consensus guidelines on intrapartum fetal monitoring: Cardiotocography. Int. J. Gynecol. Obstet. **131**(1), 13–24 (2015)
42. D. Devane, J.G. Lalor, S. Daly, W. McGuire, A. Cuthbert, V. Smith, Cardiotocography versus intermittent auscultation of fetal heart on admission to labour ward for assessment of fetal wellbeing. Cochrane Database Syst. Rev. **1**, CD005122 (2017)
43. A. Georgieva et al., Computer-based intrapartum fetal monitoring and beyond: A review of the 2nd Workshop on Signal Processing and Monitoring in Labor (October 2017, Oxford, UK). Acta Obstet. Gynecol. Scand. **98**(9), 1207–1217 (2019)
44. M.G. Signorini, G. Magenes, S. Cerutti, D. Arduini, Linear and nonlinear parameters for the analysis of fetal heart rate signal from cardiotocographic recordings. IEEE Trans. Biomed. Eng. **50**(3), 365–374 (2003)
45. M.G. Signorini, N. Pini, A. Malovini, R. Bellazzi, G. Magenes, Integrating machine learning techniques and physiology based heart rate features for antepartum fetal monitoring. Comput. Methods Prog. Biomed. **185**, 105015 (2020)
46. P. Warrick, E.F. Hamilton, D. Precup, R.E. Kearney, Identification of the dynamic relationship between intrapartum uterine pressure and fetal heart rate for normal and hypoxic fetuses. IEEE Trans. Biomed. Eng. **56**(6), 1587–1597 (2009)
47. P. Warrick, E. Hamilton, R. Kearney, D. Precup, A machine learning approach to the detection of fetal hypoxia during labor and delivery. AI Mag. **33**, 79 (2012)
48. M. Cesarelli, M. Romano, P. Bifulco, F. Fedele, M. Bracale, An algorithm for the recovery of fetal heart rate series from CTG data. Comput. Biol. Med. **37**(5), 663–669 (2007)
49. M. Romano, P. Bifulco, M. Ruffo, G. Improta, F. Clemente, M. Cesarelli, Software for computerised analysis of cardiotocographic traces. Comput. Methods Prog. Biomed. **124**, 121–137 (2016)
50. M. Romano, P. Bifulco, A.M. Ponsiglione, G.D. Gargiulo, F. Amato, M. Cesarelli, Evaluation of floatingline and foetal heart rate variability. Biomed. Signal Process. Control **39**, 185–196 (2018)
51. V. Chudáček et al., Open access intrapartum CTG database. BMC Pregnancy Childbirth **14**, 16 (2014)
52. CTU-CHB Intrapartum Cardiotocography Database, PhysioNet, 2014. [Online]. https://physionet.org/content/ctu-uhb-ctgdb/1.0.0/
53. S. Romagnoli, A. Sbrollini, L. Burattini, I. Marcantoni, M. Morettini, L. Burattini, Annotation dataset of the cardiotocographic recordings constituting the 'CTU-CHB intra-partum CTG database'. Data Br. **31**, 105690 (2020)
54. K. Bache and M. Lichman, UCI Machine Learning Repository, UC Irvine Machine Learning Repository, 2013. [Online]. https://archive.ics.uci.edu/ml/datasets/cardiotocography
55. D. Ayres-de-Campos, J. Bernardes, A. Garrido, J. Marques-de-Sá, L. Pereira-Leite, Sisporto 2.0: A program for automated analysis of cardiotocograms. J. Matern. Fetal Med. **9**(5), 311–318 (2000)
56. N. Pini, M. Lucchini, G. Esposito, M. Campanile, G. Magenes, M.G. Signorini, Fetal Heart Rate Features of Healthy and Late IUGR Fetuses. IEEE DataPort. (2020)
57. M.G. Signorini, N. Pini, A. Malovini, R. Bellazzi, G. Magenes, Dataset on linear and non-linear indices for discriminating healthy and IUGR fetuses. Data Br. **29**, 105164 (2020)
58. M.G. Signorini, M. Campanile, G. Magenes, Data for: Integrating Machine Learning Techniques and Physiology Based Heart Rate Features for Antepartum Fetal Monitoring, Mendeley Data, 2019. [Online]. https://data.mendeley.com/datasets/2953f8fgcy
59. E. Spairani, B. Daniele, G. Magenes, M.G. Signorini, A novel large structured cardiotocographic database. Annu. Int. Conf. IEEE Eng. Med. Biol. Soc. **2022**, 1375–1378 (2022)

60. F. Kovács, C. Horváth, Á.T. Balogh, G. Hosszú, Fetal phonocardiography—Past and future possibilities. Comput. Methods Prog. Biomed. **104**(1), 19–25 (2011)
61. C.E. Valderrama, N. Ketabi, F. Marzbanrad, P. Rohloff, G.D. Clifford, A review of fetal cardiac monitoring, with a focus on low- and middle-income countries. Physiol. Meas. **41**(11), 11TR01 (2020)
62. F. Kovács, M.Á. Goda, G. Hosszú, T. Telek, A Proposed Phonography-Based Measurement of Fetal Breathing Movement Using Segmented Structures with Frequency Splitting, in *2020 42nd Annual International Conference of the IEEE Engineering in Medicine & Biology Society (EMBC)*, 2020, pp. 4483–4486
63. M.Á. Goda, T. Telek, F. Kovács, Novel phonography-based measurement for fetal breathing movement in the third trimester. Sensors **21**(1), 211 (2021)
64. P. Chetlur Adithya, R. Sankar, W.A. Moreno, S. Hart, Trends in fetal monitoring through phonocardiography: Challenges and future directions. Biomed. Signal Process. Control **33**, 289–305 (2017)
65. M. Ruffo et al., Non-invasive foetal monitoring with combined ECG-PCG system. Biomed. Eng. Trends Electron. Commun. Softw. **25**, 347–366 (2011)
66. M. Cesarelli, M. Ruffo, M. Romano, P. Bifulco, Simulation of foetal phonocardiographic recordings for testing of FHR extraction algorithms. Comput. Methods Prog. Biomed. **107**(3), 513–523 (2012)
67. M. Cesarelli, M. Ruffo, P. Bifulco, Simulated fetal phonocardiograms, PhysioNet, 2014. [Online]. https://physionet.org/content/simfpcgdb/1.0.0/
68. M. Ruffo, Fetal PCG Database, PhysioNet, 2015. [Online]. https://physionet.org/content/fpcgdb/1.0.0/
69. M. Samieinasab, R. Sameni, Fetal phonocardiogram extraction using single channel blind source separation, in *2015 23rd Iranian Conference on Electrical Engineering*, 2015, pp. 78–83
70. R. Sameni, M. Samieinasab, Shiraz University Fetal Heart Sounds Database, PhysioNet, 2021. [Online]. https://physionet.org/content/sufhsdb/1.0.1/
71. A. Bhaskaran, M. Arora, Indian Institute of Science Fetal Heart Sound Database (IIScFHSDB), PhysioNet, 2022. [Online]. https://physionet.org/content/fetalheartsounddata/1.0/
72. A. Bhaskaran, S. Kumar, S. George, M. Arora, Heart rate estimation and validation algorithm for fetal phonocardiography. Physiol. Meas. **43**(7), 75008 (2022)

Index

A
Artificial agents, 31, 43, 51, 55–60, 62, 66, 68
Artificial intelligence, 31, 32, 42, 51–62, 66–68, 88, 122
Auditory and visual evoked responses, 82, 83

B
Biomarker, 21–29, 185
Brain development, 6, 7, 26, 71–92

C
Cardiotocography (CTG), 73, 75, 77, 84, 85, 88–91, 122, 130–140, 171, 194, 197–200, 207–219, 222, 235–236
Classification, 24, 74, 199–202, 209–217, 235
Clustering, 101, 107, 109, 201–204
Congenital heart diseases (CHD), 132, 142, 232

D
Dataset, 98, 192, 222, 224–237
Deep Gaussian processes, 192–194
Delivery room, 13, 14, 16
De-shape, 150–159
Doppler ultrasound, 2, 13, 90, 117, 130, 131, 138, 194

E
e-health, 46
Entropy, 73–75, 78, 79, 85, 86, 92, 171–179, 235

F
Facial expressions, 75, 76, 86–88, 90, 91
Fetal brain and autonomic nervous system maturation, 73
Fetal brain functional images, 81
Fetal electrocardiogram (fECG), 86, 97, 99, 103, 121, 122, 128–142, 149–167, 194
Fetal electrocardiography, 121–142
Fetal heart rate (FHR), 73, 76, 84, 85, 90, 92, 97–101, 117, 121, 122, 130–133, 135–139, 171, 172, 177, 185, 186, 189–204, 207–217, 219, 227
Fetal heart rate variability (fHRV), 71, 73, 74, 76, 78, 85, 86, 90–92, 171–186, 210, 215
Fetal monitoring, 86, 88, 132, 133, 140, 207, 223, 224
Fetal myocardial performance, 97–118

G
Gaussian processes (GPs), 177–179, 183, 185, 189–204
Gestational age, 4, 5, 7, 74, 78, 83, 85, 86, 91, 107, 110, 112, 113, 134, 173, 210, 226, 227, 235
Guidelines, 4, 11–17, 32, 35, 39–42, 46–48, 52, 54, 59, 61, 66, 129, 131, 195, 207

H
Heart rate variability (HRV), 73, 74, 76–79, 85, 89, 92, 100, 171, 177, 180, 199, 208, 210, 215, 219, 224

D. Pani (ed.), *Innovative Technologies and Signal Processing in Perinatal Medicine*, https://doi.org/10.1007/978-3-031-32625-7

Hypoxic-ischemic encephalopathy (HIE), 11, 21, 26–28, 207, 210

I
Information Theory, 171–186
Intrauterine growth restriction (IUGR), 3, 4, 88, 89, 110, 111, 116, 177, 185, 235

L
Law, 21, 24, 32, 35–39, 41, 43–45, 48, 49, 52–55, 57, 58, 63, 64, 67, 69
Liability, 22, 31–69, 202, 229

M
Machine learning, 199, 207–219, 235
Manifold denoise, 166
Medico-legal, 21–29, 39
Missing samples, 194–198, 200

N
Neonatal outcome, 12
Neonate, 11–13, 16, 17, 26, 27, 81, 199
Non-invasive recording, 130–139

O
Obstetrics, 1, 4, 207
Omics, 22–24, 28
Open data, 221–237
Optimal shrinkage (OS), 150–152, 159–163, 166

P
Perinatal asphyxia, 1, 11, 21–29
Phase-rectified signal averaging (PRSA), 92, 172, 179–186

R
Resuscitation, 11–17

S
Signal processing, 86, 135–139, 149–167, 207–219, 221–223
Simulators, 223, 227
Single channel blind source separation (scBSS), 149, 151
Stabilization, 14
System identification (SI), 209–216, 219

T
Tei index, 110

W
Wavelet, 86, 98, 102, 103, 105–107, 117, 136